U.S. DEPARTMENT OF COMMERCE
National Technical Information Service

PB-276 974

Supportive Studies in Fluidized-Bed Combustion

Argonne National Lab, Ill

Prepared for

Industrial Environmental Research Lab, Research Triangle Park, N C

Dec 77

PB 276 974

EPA
U.S. Environmental Protection Agency
Office of Research and Development

Industrial Environmental Research Laboratory
Research Triangle Park, North Carolina 27711

EPA-600/7-77-138
December 1977

SUPPORTIVE STUDIES IN FLUIDIZED-BED COMBUSTION

Interagency Energy-Environment Research and Development Program Report

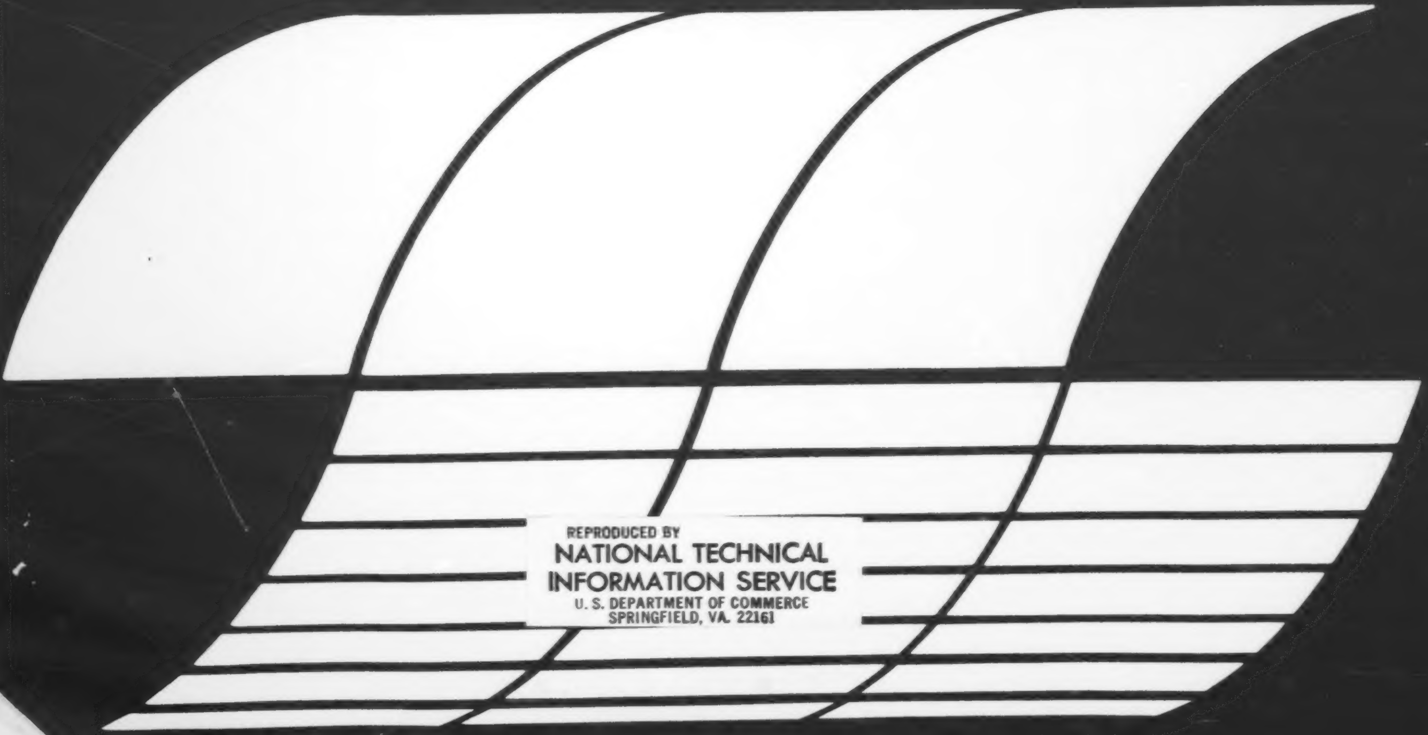

REPRODUCED BY
NATIONAL TECHNICAL INFORMATION SERVICE
U. S. DEPARTMENT OF COMMERCE
SPRINGFIELD, VA. 22161

RESEARCH REPORTING SERIES

Research reports of the Office of Research and Development, U.S. Environmental Protection Agency, have been grouped into seven series. These seven broad categories were established to facilitate further development and application of environmental technology. Elimination of traditional grouping was consciously planned to foster technology transfer and a maximum interface in related fields. The seven series are:

1. Environmental Health Effects Research
2. Environmental Protection Technology
3. Ecological Research
4. Environmental Monitoring
5. Socioeconomic Environmental Studies
6. Scientific and Technical Assessment Reports (STAR)
7. Interagency Energy-Environment Research and Development

This report has been assigned to the INTERAGENCY ENERGY-ENVIRONMENT RESEARCH AND DEVELOPMENT series. Reports in this series result from the effort funded under the 17-agency Federal Energy/Environment Research and Development Program. These studies relate to EPA's mission to protect the public health and welfare from adverse effects of pollutants associated with energy systems. The goal of the Program is to assure the rapid development of domestic energy supplies in an environmentally--compatible manner by providing the necessary environmental data and control technology. Investigations include analyses of the transport of energy-related pollutants and their health and ecological effects; assessments of, and development of, control technologies for energy systems; and integrated assessments of a wide range of energy-related environmental issues.

REVIEW NOTICE

This report has been reviewed by the participating Federal Agencies, and approved for publication. Approval does not signify that the contents necessarily reflect the views and policies of the Government, nor does mention of trade names or commercial products constitute endorsement or recommendation for use.

This document is available to the public through the National Technical Information Service, Springfield, Virginia 22161.

TECHNICAL REPORT DATA

(Please read Instructions on the reverse before completing)

1. REPORT NO. EPA-600/7-77-138	2.	3. RECIPIENT'S ACCESSION NO. PB276974
4. TITLE AND SUBTITLE Supportive Studies in Fluidized-Bed Combustion		5. REPORT DATE December 1977
		6. PERFORMING ORGANIZATION CODE
7. AUTHOR(S) A. Jonke, G. Vogel, I. Johnson, S. Lee, J. Lenc, A. Lescarret, J. Montagna, F. Nunes, J. Shearer, R. Snyder, G. Smith, W. Swift, F. Teats, C. Turner, I. Wilson		8. PERFORMING ORGANIZATION REPORT NO.
9. PERFORMING ORGANIZATION NAME AND ADDRESS Argonne National Laboratory 9700 South Cass Avenue Argonne, Illinois 60439		10. PROGRAM ELEMENT NO. EHE623A
		11. CONTRACT/GRANT NO. EPA Interagency Agreement IAG-D5-E681
12. SPONSORING AGENCY NAME AND ADDRESS EPA, Office of Research and Development Industrial Environmental Research Laboratory Research Triangle Park, NC 27711		13. TYPE OF REPORT AND PERIOD COVERED Annual; 7/76-6/77
		14. SPONSORING AGENCY CODE EPA/600/13

15. SUPPLEMENTARY NOTES IERL-RTP project officer is Walter B. Steen, Mail Drop 61, 919/541-2825. Previous report in this series was EPA-600/7-76-019.

16. ABSTRACT The report gives results of studies supporting the development of atmospheric and pressurized fluidized-bed combustion (FBC) of coal. It includes laboratory and bench-scale studies to provide needed information on combustion optimization, regeneration process development, solid waste disposal, synthetic SO2-sorbent studies, emission control and other tasks. It includes characterization of a variety of limestone and dolomites from various parts of the U.S. for suitability in FB combustors. Reduction in solid waste volumes to reduce the environmental impact of the waste sulfated limestone is a major goal of this program. These studies are to supply data essential for the application of FBC units to public utility and industrial systems. The report gives information on: 10-cycle combustion-regeneration PDU experiments using Greer limestone and Tymochtee dolomite, bed defluidization, flowsheet development, preparation of synthetic SO2-sorbents containing metal oxides, limestone characterization, coal combustion reactions, the enhancement of limestone sulfation by NaCl, evaluation of on-line particle size analyzers, and status of flue gas cleaning studies.

17. KEY WORDS AND DOCUMENT ANALYSIS

a. DESCRIPTORS		b. IDENTIFIERS/OPEN ENDED TERMS	c. COSATI Field/Group	
Air Pollution	Waste Disposal	Air Pollution Control	13B	
Coal	Sulfur Oxides	Stationary Sources	21D	07B
Combustion	Limestone	Fluidized-bed Combustion	21B	08G
Fluidized-bed Processing	Dolomite (Rock)			
	Sodium Chloride		13H, 07A	
Regeneration				

18. DISTRIBUTION STATEMENT RELEASE TO PUBLIC	19. SECURITY CLASS *(This Report)* Unclassified	21. NO. OF PAGES 212
	20. SECURITY CLASS *(This page)* Unclassified	22. PRICE A10- A01

EPA Form 2220-1 (9-73)

EPA-600/7-77-138
December 1977

SUPPORTIVE STUDIES IN FLUIDIZED-BED COMBUSTION

by

A. Jonke, G. Vogel, I. Johnson, S. Lee,
J. Lenc, A. Lescarret, J. Montagna, F. Nunes,
J. Shearer, R. Snyder, G. Smith, W. Swift,
F. Teats, C. Turner, and I. Wilson

Argonne National Laboratory
9700 South Cass Avenue
Argonne, Illinois 60439

EPA Interagency Agreement No. IAG-D5-E681
Program Element No. EHE623A

EPA Project Officer: Walter B. Steen

Industrial Environmental Research Laboratory
Office of Energy, Minerals, and Industry
Research Triangle Park, N.C. 27711

Prepared for

U.S. ENVIRONMENTAL PROTECTION AGENCY
Office of Research and Development
Washington, D.C. 20460

TABLE OF CONTENTS

Page

ABSTRACT 1

SUMMARY. 1

TASK A. REGENERATION PROCESS DEVELOPMENT. 11

1. Experimental 13
    - a. Materials--Sorbents. 13
    - b. Materials-Coals. 13
    - c. PDU--Combustion System and Procedure 13
    - d. PDU--Regeneration System and Procedure 16

2. PDU Regeneration Rate Experiments with Tymochtee Dolomite. . 17
    - a. Effect of Solids Residence Time and Temperature on Extent of CaO Regeneration. 18
    - b. Regression Analysis of Regeneration Data 20
    - c. Effect of Solids Residence Time and Temperature on SO_2 Concentration in the Off-Gas. 22
    - d. Effect of System Pressure on Extent of CaO Regeneration and Off-Gas SO_2 Concentration 25
    - e. Formation of CaS 27

3. PDU Regeneration Rate Experiments with Greer Limestone . . . 27
    - a. Effects of Solids Residence Time and Temperature on Extent of CaO Regeneration. 27
    - b. Effect of Solids Residence Time and Temperature on SO_2 Concentration in the Off-Gas. 30
    - c. Effect of System Pressure during Sulfation on the Reactivity of Greer Limestone. 31

4. Characterization of Causes of Defluidization during Regeneration 31
    - a. Experimental Design and Procedure. 33
    - b. Effect of Operating Variables on Defluidization Velocity 34
    - c. Analysis of Variance for Defluidization Velocity 35
    - d. Regression Analysis for Defluidization Velocity. 35

5. Cyclic Sorbent Life Studies with Tymochtee Dolomite. 37
    - a. Experimental Conditions. 38
    - b. Sulfur Acceptance during Combustion. 38
    - c. Sulfur Release during Regeneration 38
    - d. TGA Sulfation Experiments. 38
    - e. Estimate of Sorbent Makeup Requirements to Meet EPA Sulfur Emission Limit. 43

TABLE OF CONTENTS (Contd.)

Page

f. Porosity of Dolomite as a Function of Utilization Cycle. 49
g. Coal Ash Buildup during Utilization Cycles 49
h. Electron Microprobe Analysis of Tymochtee Dolomite from Tenth Utilization Cycle 59
i. Carbonate Levels of Sorbent Samples. 66
j. Attrition and Elutriation Losses during Regeneration and Combustion 67
k. Amount of Sorbent Processed per Cycle. 70

6. Cyclic Sorbent Life Study with Greer Limestone 71

a. Combustion Step Results. 71
b. Cyclic and Total Calcium Utilization 72
c. Porosity of Limestone as a Function of Utilization Cycles 74
d. Limestone Reactivity as a Function of Cyclic Utilization. 74
e. Regeneration Step Results. 75
f. Coal Ash Buildup during Cyclic Utilization 76
g. Attrition and Elutriation of Limestone Particles during Regeneration and Sulfation. 79
h. Total Cyclic Limestone Inventory 82

7. Regeneration Process Scale-up and Flowsheet Determination. . 82

8. Regeneration System Modifications. 86

TASK B. REGENERATION PROCESS ALTERNATIVES. 88

TASK C. SYNTHETIC SORBENTS FOR SO_2 EMISSION CONTROL. 88

1. Introduction 88

2. Attrition Resistance 88

3. Bauxite Support. 89

4. Cost 93

5. Conclusions. 96

TASK D. LIMESTONE CHARACTERIZATION 97

1. Limestone Properties Affecting SO_2 Reactivity. 97

2. Effects of Precalcination and Heat Treatment 101

TABLE OF CONTENTS (Contd.)

Page

3. Limestone Attrition. 104

4. Conclusions. 108

TASK E. TRACE ELEMENTS AND COMBUSTION EMISSION STUDIES 111

1. The Effect of Additives on the Calcination/Sulfation of Limestone/Dolomite. 111

a. Mechanism of Enhancement by Sodium Chloride. 111
b. Evaluation of Seven Additives. 117
c. Effect of NaCl Additive on Several Limestones. 126
d. Porosities of Limestones 130

2. The Determination of Inorganic Constituents in the Effluent Gas from Coal Combustion. 139

a. Coal Combustion Experiments. 140
b. Charcoal Combustion Experiments. 148
c. Lignite Combustion Experiments 152
d. Relation of Coal Ash Content to Sodium Vaporization. . . 154

TASK F: FLUE-GAS CLEANING STUDIES. 156

1. Evaluation of On-Line Light-Scattering Particle Analyzers. . 156

a. Principles of the SDL Particle Morphokinetometer 156
b. Procedure for Comparative Flue-Gas Particle Measurements 159
c. Experimental Evaluation of the PM Particle Analyzer. . . 161
d. The Effect of the PM Particle Analyzer Calibration on Particle Measurements 167

2. Particle Removal from Flue Gas 171

a. Granular-Bed Filter. 172
b. Acoustic Agglomeration 180
c. High Efficiency Cyclones 184

ACKNOWLEDGMENTS. 184

REFERENCES 185

APPENDIX A: Physical and Chemical Properties of Coals and Sorbents used in Sorbent Regeneration Studies. 189

LIST OF FIGURES

No.	Title	Page
1.	Conceptual Fluidized Bed Coal Combustion Power-Generating Facility Having Sorbent-Regeneration and Sulfur-Recovery Capabilities.	12
2.	Simplified Equipment Flowsheet of PDU Fluidized-Bed Combustor and Associated Equipment.	14
3.	Six-Inch-Diameter Pressurized, Fluidized-Bed Combustor.	15
4.	Experimental Sorbent Regeneration System.	17
5.	Regeneration of CaO in Tymochtee Dolomite as a Function of Solids Residence Time	20
6.	The Extent of CaO Regeneration for Tymochtee Dolomite as a Function of Temperature and Residence Time as Represented by the Model Equation, Equation 1	21
7.	Predicted and Experimental SO_2 Concentration as a Function of Solids Residence Time at Three Regeneration Temperatures	22
8.	Predicted SO_2 Concentration in the Dry Off-Gas as a Function of Solids Residence Time, Regeneration Temperature, and System Pressure	24
9.	Regeneration of CaO in Greer Limestone as a Function of Solids Residence Time and Regeneration Temperature.	29
10.	Experimental SO_2 Concentration for the Regeneration of Greer Limestone as a Function of Solids Residence Time and Temperature	30
11.	Qualitative Plot of Bed Temperature and Pressure Drop as a Function of Fluidizing-Gas Velocity for a Defluidization Experiment.	33
12.	Sulfur Retention in Bed and SO_2 Concentration in Flue Gas as a Function of Cycle Number	40
13.	Conversion of CaO to $CaSO_4$ as a Function of Time and Sulfation Cycle as Determined by TGA Sulfation Experiments.	42
14.	Percent Calcium as $CaSO_4$ as a Function of Time and Sulfation Cycle as Determined by TGA Sulfation Experiments.	42
15.	CaO/S Ratio Required to Achieve 75% Sulfur Retention as a Function of Cycle	44

LIST OF FIGURES (Contd.)

No.	Title	Page
16.	CaO Utilization at 75% Sulfur Retention as a Function of Sulfation Cycle	47
17.	Recycle Mechanism to Approximate the Steady-State Distribution of Sorbent for a Continuous Combustion-Regeneration Process . . .	47
18.	Calculated Makeup and Total CaO/S Ratios Required to Achieve 75% Sulfur Retention as a Function of the Makeup CaO to Total CaO Ratio	48
19.	Pore Distributions of Dolomite Samples from Cycles Two and Ten	50
20.	Coal Ash Buildup as a Function of Utilization Cycle	52
21.	Coal Ash Buildup as a Function of Particle Diameter in Tenth Cycle Regenerated Particles	52
22.	Photomicrographs of Sulfated and Regenerated Tymochtee Dolomite Particles from the First and Fifth Utilization Cycles.	53
23.	Photomicrographs of Sulfated and Regenerated Tymochtee Dolomite Particles from the Tenth Utilization Cycle	54
24.	Photomicrograph of Cross Section of a Tymochtee Dolomite Particle from the First Combustion Cycle.	56
25.	Photomicrograph of Cross Section of a Tymochtee Dolomite Particle from the First Regeneration Cycle.	56
26.	Photomicrograph of a Cross Section of a Tymochtee Dolomite Particle from the Tenth Combustion Cycle.	57
27.	Photomicrograph of Cross Section of a Tymochtee Dolomite Particle from the Tenth Regeneration Cycle	57
28.	Photomicrograph of Cross Section of a Tymochtee Dolomite Particle from the Tenth Regeneration Cycle.	58
29.	Photomicrograph of Cross Section of an Unreacted Tymochtee Dolomite Particle	58
30.	Electron Microprobe Analysis of a Typical Regenerated Dolomite Particle (P-1) from the Tenth Cycle.	60
31.	Electron Microprobe Analysis of a Typical Regenerated Dolomite Particle (P-2) from the Tenth Cycle.	61

LIST OF FIGURES (Contd.)

No.	Title	Page
32.	Electron Microprobe Analysis of a Typical Regenerated Dolomite Particle (P-3) from the Tenth Cycle.	62
33.	Electron Microprobe Analysis of a Typical Partially Sulfated Dolomite Particle (PS-1) from the Tenth Cycle.	63
34.	Electron Microprobe Analysis of a Typical Partially Sulfated Dolomite Particle (PS-2) from the Tenth Cycle.	64
35.	Electron Microprobe Analysis of a Typical Partially Sulfated Dolomite Particle (PS-3) from the Tenth Cycle.	65
36.	Comparison of the Reactivity of Tenth Cycle Regenerated Dolomite (-14 +30 mesh) to that of a Crushed (-30 +100 mesh) Sample from the Same Experiment	66
37.	Weight Fraction of Unsulfated Calcium as Calcium Carbonate in Sulfated and Regenerated Dolomite Samples as a Function of Utilization Cycle.	67
38.	Cyclic Calcium Utilization for Greer Limestone for 84% Sulfur Retention.	73
39.	Pore Distributions of Limestone Samples from Cycles Two and Ten	74
40.	Cyclic CaO/S Molar Feed Ratio Required to Retain 84% of the Sulfur.	75
41.	Conversion of Available Calcium to $CaSO_4$ as a Function of Time.	76
42.	Coal Ash Buildup as a Function of Greer Limestone Utilization Cycle	79
43.	Photomicrographs of Sulfated and Regenerated Greer Limestone Particles	80
44.	Process Flowsheet for a 10-MWe FBC Boiler with Sorbent Regeneration, Using Tymochtee Dolomite.	84
45.	Schematic of Regeneration System with Sorbent Preheater	87
46.	Particle Size Distribution of α-Al_2O_3 (heat-treated at 1100°C) Before and After Attrition Test	89
47.	Particle Size Distributions of Sulfated Dolomite from First Cycle of Ten-Cycle Experiment Before and After Attrition.	91

LIST OF FIGURES (Contd.)

No.	Title	Page
48.	Particle Size Distributions of Regenerated Dolomite, Before and After Attrition Test	91
49.	Porosity of Bauxite	92
50.	Calcium Utilization of Synthetic Sorbents	92
51.	Rate of SO_3 Capture by Sorbents	93
52.	Calcium Utilization at 900°C for Ten Precalcined (at 900°C) Limestones in a Thermogravimetric Analyzer.	97
53.	Cumulative Pore Volume as a Function of Pore Diameter for Ten Limestones.	100
54.	Calcium Utilization as a Function of Surface Area of Pores having Diameters Larger than MPD for Ten Limestones	101
55.	Calcium Utilization as a Function of Various Pretreatments. . . .	102
56.	Increased Energy Cost for Pretreatment Required to Reduce the Environmental Impact of Mining and Disposal of Sorbents . . .	104
57.	Laboratory-Scale Fluidized-Bed Apparatus for Attrition Experiments	105
58.	Attrition Rate of Calcined Tymochtee Dolomite as a Function of Superficial Gas Velocity; L/D = 1.39	107
59.	Attrition Rate of Calcined Tymochtee Dolomite as a Function of Bed Depth.	107
60.	Material Loss from Beds of Precalcined Limestones, Superficial Gas Velocity: 1.46 m/s; L/D: 1.38.	108
61.	Material Loss at 1.46 m/s Gas Velocity, Room Temperature.	109
62.	Effect of Impurity Concentration on Attrition	110
63.	Sulfation of Partially Sulfated Limestone Particle.	114
64.	Sulfation of Crystalline Calcite.	116
65.	Enhanced Sulfation in 4% SO_2 at 850°C of Greer Limestone by Pretreatment	120

LIST OF FIGURES (Contd.)

No.	Title	Page
66.	Enhanced Sulfation in 0.4% SO_2 at 850°C of Greer Limestone by Precalcination	120
67.	Effect of NaCl Concentration on Sulfation of Greer Limestone at 850°C in 0.3% SO_2.	122
68.	Enhancement of Greer Limestone Sulfation with Na_2SO_4 at 850°C in 0.3% SO_2	123
69.	Enhancement of Greer Limestone Sulfation with Na_2CO_3 at 850°C in 0.3% SO_2	124
70.	Enhancement of Greer Limestone Sulfation with $CaCl_2$ at 850°C in 0.3% SO_2	125
71.	Enhancement of Greer Limestone Sulfation with KCl at 850°C in 0.3% SO_2	126
72.	Weight of SO_3 Captured as a Function of Time for Eleven Untreated Limestones.	127
73.	Weight of SO_3 Captured as a Function of Time for Eleven Limestones with 2 wt % NaCl	128
74.	Effect of NaCl on Sulfation of Limestones at 850°C in 0.3% SO_2 after 7 Hours.	129
75.	Porosimetry Curves for Eleven Limestones Calcined One Hour at 850°C in 20% CO_2	131
76.	Porosimetry Curves for Eleven Limestones Plus 2% NaCl, Calcined 1 Hour at 850°C in 20% CO_2	132
77.	Porosimetry Curves for Greer Limestone plus NaCl Calcined at 1 Hour at 850°C in 20% CO_2	133
78.	Effect of NaCl on Sulfation of Limestones (Both Precalcined and Simultaneous Calcination/Sulfation) at 850°C in 0.3% SO_2 After Seven Hours	134
79.	Sulfation at 805°C of Limestones as a Function of Total Inerts Content in Precalcined Stones Treated with 2% NaCl	135
80.	Average Pore Diameter as a Function of Total Inerts Content of Limestones	136
81.	Sulfation at 850°C of Limestone as a Function of Average Pore Diameter in Precalcined Stones Treated with 2% NaCl.	137

LIST OF FIGURES (Contd.)

No.	Title	Page
82.	Average Pore Diameter as a Function of Percent NaCl Added	139
83.	Bed Temperature and Effluent Composition in a Typical Continuous Two-Batch Coal Combustion Experiment	142
84.	Bed Temperature and Effluent Composition in a Typical Continuous Two-Batch Coal Combustion Experiment	143
85.	Relationship of O_2 Content of Inlet Combustion Mixture to O_2 Consumption and CO_2 Formation in Combustion of Coal	144
86.	Relationship between Ash Content of Coal and Sodium Vaporized during Combustion at 900°C of Coal Impregnated with 0.5% NaCl	155
87.	Spectron Development Laboratory's PM Analyzer System for Velocity and Particle Size Measurement	157
88.	Visibility as a Function of Particle Size and Fringe Period for Two Particle Shapes	159
89.	Schematic of FBC System with Modified Flue-Gas System	160
90.	Sampling System for Flue Gas Particles	161
91.	Partial (1.5-23 μm) Cumulative Mass Distribution Obtained On-Line with the Spectron PM Analyzer Compared with that Obtained with a Coulter Counter (SGL-1)	163
92.	Partial (5-74 μm) Cumulative Mass Distribution Obtained On-Line with the Spectron PM Analyzer Compared with that Obtained with a Coulter Counter (SGL-1)	163
93.	Fractional Mass Distribution of All Elutriated Particles from the ANL PDU Combustor During a Combustion Experiment (SGL-1)	165
94.	Cumulative Mass Distribution of All Elutriated Particles from the ANL PDU Combustor During a Combustion Experiment (SGL-1)	165
95.	Comparison of the Partial (1.5-23.9 μm) Cumulative Distribution Obtained On-Line with the Spectron PM Analyzer with that Obtained by Coulter Counter Analysis of a Particle Sample (SGL-2C)	166
96.	Fractional Mass Distribution of Particles Contained in the Flue Gas Between the Secondary Cyclone and the Filter (SGL-2C) Obtained by Coulter Counter Analysis	167

LIST OF FIGURES (Contd.)

No.	Title	Page
97.	Cumulative Mass Distribution of Particles in the Flue Gas Between the Secondary Cyclone and Metal Filter (SGL-2C)	168
98.	Comparison of the Partial (5-73 μm) Cumulative Mass Distribution Obtained On-Line with the Spectron PM Analyzer with that Obtained with a Coulter Counter (SGL-1)	169
99.	Comparison of the Partial (1.5-23 μm) Cumulative Mass Distribution Obtained On-Line with the Spectron PM Analyzer with that Obtained with a Coulter Counter (SGL-1)	170
100.	Comparison of the Partial (1.5-23.8 μm) Cumulative Mass Distribution Obtained On-Line with the Spectron PM Analyzer to that Obtained by Coulter Counter Analysis of a Particle Sample (SGL-2C)	171
101.	Granular-Bed Filter Assembly	174
102.	Pressure Drop Across a Fixed Bed of -6 +14 Mesh Tymochtee Dolomite as a Function of Mass Flow Rate Through the Bed	176
103.	Pressure Drop Across a Fixed Bed of -14 +30 Mesh Tymochtee Dolomite as a Function of Mass Flow Rate Through the Bed	176
104.	Test Arrangement for the Determination of Particulate Loadings in the Effluent Gas from the Granular-Bed Filter. . . .	178
105.	Modified Flue-Gas System for Granular-Bed Filter Tests	180
106.	Schematic of Resonant Manifold System.	183

LIST OF TABLES

No.	Title	Page
1.	Experimental Conditions and Results for the Regeneration of Sulfated Tymochtee Dolomite by the Incomplete Combustion of Triangle Coal in a Fluidized Bed	19
2.	Effect of Regeneration Pressure on the Regeneration of Tymochtee Dolomite and the SO_2 Concentration in the Off-Gas	26
3.	Experimental Conditions and Results for the Regeneration of Greer Limestone by the Incomplete Combustion of Sewickley Coal in a Fluidized Bed	28
4.	Operating Conditions and Flue-Gas Compositions during the Sulfation of Greer Limestone with Sewickley Coal. Combustion at Two Operating Pressures	32
5.	Defluidization during Regeneration--Experimental Conditions and Results of the Full 2^3 Factorial Experiment	34
6.	Analysis of Variance for Defluidization Velocity Data from the AGL Series of Experiments	36
7.	Calculated Defluidization Velocities (V_d, m/s) at Different Bed Temperatures, Reducing Gas Concentrations, and Bed Particle Sizes for the Regeneration Process	37
8.	Operating Conditions and Flue-Gas Compositions for Combustion Step of Cyclic Experiments	39
9.	Experimental Conditions and Results for the Regeneration Step of the Ten Utilization Cycles with Tymochtee Dolomite	41
10.	Comparison of the Experimental Cyclic Sulfation Results Obtained at ANL with those reported by Zielke *et al*	45
11.	Porosity (cm^3/g) of Tymochtee Dolomite as a Function of Utilization Cycle	50
12.	Calculated Coal Ash Buildup during Sulfation and Regeneration of Tymochtee Dolomite, Based on Enrichment of Silcion	51
13.	Attrition and Elutriation Losses for Tymochtee Dolomite during Regeneration in the Cyclic Utilization Study	68
14.	Decrepitation and Entrainment Losses and Calcium Material Balances for the Ten Combustion Experiments in the Cyclic Sorbent Utilization Study	69
15.	Gross Amounts of Sorbent Processed and Calcium Balances for Each Half-Cycle in the Cyclic Combustion/Regeneration Study	70

LIST OF TABLES (Contd.)

No.	Title	Page
16.	Operating Conditions and Flue-Gas Compositions for Combustion Steps of Cyclic Experiments with Greer Limestone and Sewickley Coal	72
17.	Experimental Conditions and Results for the Regeneration Step of Ten Utilization Cycles with Greer Limestone	88
18.	Calculated Ash Buildup during Sulfation and Regeneration of Greer Limestone	78
19.	Losses of Greer Limestone Caused by Attrition and Elutriation during Sulfation and Regeneration Steps in the Cyclic Utilization Study	81
20.	Total Reacted Limestone Inventory as a Function of Cycle and Stage	82
21.	Effect of Makeup CaO/S Mole Feed Ratio for Tymochtee Dolomite in Boiler on Regeneration System	85
22.	Fluidized-Bed Attrition Experiments	90
23.	Chemical Compositions of Limestones	98
24.	Eutectics and Double Salts Formed in the System, NaCl-$CaCO_3$-$MgCO_3$-$CaSO_4$-$MgSO_4$	112
25.	Effect of NaCl on Reactions of Calcite	118
26.	Effect of Additives on Simultaneous Calcination-Sulfation of Crystalline Calcite at 900°C	121
27.	A Material Balance of Sodium from Combustion of Illinois Herrin No. 6 Coal Impregnated with 0.5 wt % NaCl	147
28.	A Material Balance of Potassium from Combustion of Illinois Herrin No. 6 Coal Impregnated with 0.5% NaCl	148
29.	Material Balance of Sodium from Combustion of Activated Coconut Charcoal Impregnated with 0.5 wt % NaCl	150
30.	Material Balance of Potassium from Combustion of Activated Coconut Charcoal Impregnated with 0.5 wt % NaCl	151
31.	Material Balance of Sodium from Combustion of Glen harold Lignite, North Dakota	153
32.	Selected Interference Fringe Spacings and the Corresponding Measurable Spherical Particle Size Ranges	158

LIST OF TABLES (Contd.)

No.	Title	Page
33.	Experimental Conditions for a Combustion Experiment in the Evaluation of the SDL Particle Morphokinetometer (PM)	162
34.	Experimental Determinations of ε and ϕ_s in the Ergun Correlation for the Flow of Gas Through a Fixed Bed of Tymochtee Dolomite.	177
35.	Measured Particulate Loadings in Effluent Gas from Granular-Bed Filter when Passing a "Clean" Gas through the Filter.	179

SUPPORTIVE STUDIES IN FLUIDIZED-BED COMBUSTION

Annual Report
July 1976—June 1977

by

G. J. Vogel, I. Johnson, S. Lee, J. Lenc, A. S. Lescarret,
J. Montagna, F. Nunes, J. Shearer, R. Snyder, G. Smith,
W. Swift, F. G. Teats, C. Turner, I. Wilson, and A. A. Jonke

ABSTRACT

These studies support the development studies for atmospheric and pressurized fluidized-bed coal combustion. Laboratory and bench-scale studies aimed at providing needed information on combustion optimization, regeneration process development, solid waste disposal, synthetic SO_2-sorbent studies, emission control, and other tasks are included. Characterization of a variety of limestones and dolomites from various parts of the country for suitability in fluidized-bed combustors is also included. Reduction in solid waste volumes to reduce the environmental impact of the waste sulfated limestone is one of the major goals of this program. These studies are designed to supply data essential for the application of fluidized-bed combustion units to public utility and industrial systems.

This report presents information on: 10-cycle combustion-regeneration PDU experiments using Greer limestone and Tymochtee dolomite, bed defluidization, flowsheet development, preparation of synthetic SO_2-sorbents containing metal oxides, limestone characterization, coal combustion reactions, the enhancement of the sulfation of limestone by NaCl, evaluation of on-line particle size analyzers, and status of the flue-gas cleaning studies.

SUMMARY

Task A. Regeneration Process Development

The feasibility of a sorbent regeneration process will depend on (1) the ability to regenerate the stones and to generate an SO_2-rich off-gas which can be treated in a sulfur recovery process, (2) the reactivity of the regenerated sorbent during subsequent sulfation (coal combustion) cycles, and (3) the availability of a sorbent that will not decrepitate beyond acceptable levels.

In the sorbent regeneration process being investigated, $CaSO_4$ is reductively decomposed in a fluidized bed at ∿1100°C. The heat and the reductants required are produced by incomplete combustion of coal in a fluidized bed of sulfated stone. A solid-gas reaction by which regeneration occurs is:

$$CaSO_4 + CO \rightarrow CaO + CO_2 + SO_2 \qquad (1)$$

The ability of the reductive decomposition process to fulfill the above requirements of a sorbent regeneration process for FBC boilers is being investigated.

PDU[*] Regeneration Rate Experiments with Tymochtee Dolomite. A series of regeneration experiments using once-sulfated Tymochtee dolomite and Triangle coal has now been completed, and the effects of regeneration temperature, solids residence time, and regeneration pressure on (1) the regeneration of CaO and (2) the SO_2 concentration in the dry off-gas have been evaluated. These data are being used in a model for the one-step regeneration process to find process conditions that are optimum from technical and economic points of view.

In experiments made at bed temperatures of 1000, 1050, and 1100°C, in which the solids residence time was varied from 35 min to 7 min, the extent of CaO regeneration decreased with decreasing solids residence time at all temperatures. Nevertheless, at 1100°C the extent of regeneration remained quite high (∿75%), even at the lowest investigated solids residence time.

At 1000°C, the SO_2 concentration in the dry off-gas was relatively unaffected (remaining at ∿2%) as the solids residence time was decreased from 37 min to 11 min. At 1050°C, the concentration of SO_2 in the dry off-gas increased from 3.0% to 4.8% when the solids residence time was decreased from 34 min to 12 min. At 1100°C, the SO_2 concentration increased to a greater extent than at 1050°C as the solids residence time was decreased. It was predicted that the SO_2 concentration at 1050°C and 1100°C would be at a maximum for a solids residence time of ∿2.5 min. At 1100°C, the maximum predicted SO_2 concentration in the dry off-gas would be 11.5%.

Also, the experimental regeneration data were statistically analyzed to obtain an equation for the extent of CaO regeneration as a function of (1) sorbent residence time in the reactor and (2) regeneration temperature. This equation was used in the mass and energy constrained regeneration process model to predict expected SO_2 concentrations in the off-gas in and beyond the experimentally investigated temperature range (*i.e.*, at temperatures up to 1200°C). At 1100°C the SO_2 concentration in the off-gas from a pressurized (1000 kPa) regeneration process was estimated to be ∿2%, and ∿12% at atmospheric pressure (101.3 kPa).

In still another series of experiments, the regeneration pressure was decreased by ∿25%, from ∿150 kPa to 115 kPa. The extent of regeneration was not affected by pressure; the dependence of extent of regeneration on solids residence time was equivalent at the two pressures. Regeneration pressure did, however, affect SO_2 concentration in the off-gas via the extent of dilution. At the lower pressure, higher SO_2 concentrations, up to 10.4%, were obtained.

---

[*] Process development unit.

Temperature, solids residence time, and pressure had no significant effect on the CaS content of the bed, which was low in all experiments.

PDU Regeneration Rate Experiments with Greer Limestone. A series of regeneration experiments was performed to obtain CaO regeneration rate data for Greer limestone. The dependence of CaO regeneration on regeneration temperature and solids residence time in the reactor was determined. The regeneration rate of Greer limestone was found to be equal to that of Tymochtee dolomite. The experimental results were used to obtain a "best fit" model equation for the dependence of CaO regeneration on temperature and solids residence time in the reactor. This relationship will be used in a process computer model to optimize the design process conditions for a pilot plant.

The effects of bed temperature, 1050 or 1100°C, and solids residence time, ∿20, 11, and 7 1/2 minutes, in the regenerator on SO_2 concentrations in the off-gas were determined using sulfated Greer limestone as the feed material. At the longest residence time little effect of temperature was found, but at the shortest residence time the SO_2 concentration was twice as high at the higher temperature. To obtain the highest SO_2 concentrations, a short residence time and a high bed temperature are required.

Two experiments were performed to test the effect of combustion system pressure on the reactivity of Greer limestone, one at a system pressure of 308 kPa (3 atm) and the other at 610 kPa (6 atm); both were at a bed temperature of 855°C. It was found that, although the extent of calcination was much lower in the higher pressure experiment, the reactivity of the stone was approximately the same in both experiments.

Characterization of Defluidization Causes during Regeneration. The effects of experimental variables on the defluidization characteristics (agglomeration) of the regenerator fluid bed are being investigated in the PDU regenerator. Sulfated Greer limestone obtained from PER and Sewickley coal are being used. A statistical experiment has been completed (a full 2^3 factorial experiment plus two replicate experiments) in which the effects of bed temperature (1050 and 1100°C), total reducing gas concentration in the off-gas (2.5 and 5.0%), and feed sorbent particle size (-10 +30 mesh and -14 +30 mesh) on the defluidization velocity (minimum velocity required to prevent agglomeration) were determined. Regeneration temperature and total reducing gas concentration in the off-gas were found to have the greatest statistical influence on the defluidization velocity. A model equation was obtained that can be used to predict the minimum operable fluidizing-gas velocity at which an industrial regenerator can be operated without agglomeration of the fluid bed.

Cyclic Sorbent Life Studies with Tymochtee Dolomite. The effect of repeated utilization cycles on the performance of Tymochtee dolomite as an

SO_2-acceptor was evaluated in a ten-cycle combustion-regeneration experiment. Combustion in each cycle was performed at a 900°C bed temperature, 810 kPa pressure, 1.5 CaO/S mole ratio (ratio of unsulfated calcium in sorbent to sulfur in coal), ∿17% excess combustion air, 0.9 m/s fluidizing-gas velocity, and a 0.9 m bed height. Regeneration in each cycle was at a nominal system pressure of 158 kPa, a bed temperature of 1100°C, and a fluidized-bed height of ∿46 cm. The required heat and reductants for regeneration were provided by incomplete combustion of Triangle coal.

During sulfation, the sorbent exhibited a steady loss in reactivity with increasing utilization cycle. The results of TGA sulfation experiments on samples of regenerated sorbent from the ten regeneration half-cycle experiments are presented. They show that both the rate of sulfation and the extent of sulfation decreased with utilization cycle. The TGA results indicate a leveling-off of the loss of reactivity after the eighth sulfation cycle which was not apparent from sulfation results obtained in the PDU cyclic study.

The extent of regeneration remained at acceptable levels (∿70%) for all ten cycles, and SO_2 concentrations in the dry off-gas measured ∿8.5% up through cycle 7. In the three final cycles, the SO_2 concentration upon regeneration was <7% because of a lower sulfur content of the sulfated sorbent fed to the regenerator.

Based on the results of the cyclic study, an analysis was made of the effect of makeup rate (ratio of makeup CaO to total CaO entering combustor) on the total CaO/S ratio required during continuous recycle operation for a sulfur retention of 75%. For example, a makeup rate of 0.18 requires a projected makeup CaO/S ratio of ∿0.27 and a total CaO/S ratio of ∿1.5 for a sulfur retention of 75%. Decreasing the makeup rate to 0.1 reduces the required makeup CaO/S ratio to ∿0.2 but increases the total CaO/S required to 2.0 because of the lower reactivity of the recycled CaO.

The porosity of regenerated dolomite decreased with cyclic use, as did its capacity to act as an SO_2-acceptor during combustion. The loss of porosity and loss of reactivity towards SO_2 could be due to either or both of the following: (1) the buildup of an ash layer around the particles or (2) high-temperature (1100°C) exposure during regeneration. Sintering, which begins to occur at the regeneration temperature, decreases the reactivity by decreasing the beneficial effect of porosity.

It was found that after ten utilization cycles, ∿13 g of coal ash had accumulated with the sorbent for every 100 g of starting virgin dolomite. Photomicrographs of particle surface and cross-section features revealed the formation of shells on the dolomite particles. Electron microprobe analyses were performed on cross sections of sulfated and regenerated dolomite samples from the tenth utilization cycle to determine the composition along cross sections of the particles and the role of the constituents during sulfation reactions. The analyses confirmed the existence of the ash shell. It was found that the coal ash shell was enriched in iron and calcium (relative to the silica concentrations in the pure coal ash). The sulfur concentration profiles in the tenth-cycle sulfated particles suggested that diffusion through the ash shell is not the limiting factor during sulfation and that the loss of reactivity was within the dolomite particles--perhaps due to sintering and loss of local porosity.

The carbonate level of sulfated and regenerated samples is also given. It further indicates the decrease in reactivity of the sorbent during combustion with increasing utilization cycle. The extent of recarbonation steadily decreases, as does the extent of sulfation.

Over ten cycles, sorbent losses during each regeneration cycle have averaged a relatively low 2% of the material fed. The combined losses due to attrition and/or elutriation have been found to be ∿8% per complete cycle of combustion and regeneration. This is the minimum expected makeup rate for Tymochtee dolomite in an FBC process utilizing sorbent regeneration at the operating conditions used in these tests. A still higher makeup rate may be required to maintain sufficient reactivity in the recycled sorbent.

Cyclic Sorbent Life Study with Greer Limestone. A cyclic sorbent utilization experiment was performed with Greer limestone, which is the stone that will be used by Pope, Evans and Robbins (PER) in the Rivesville pilot plant, and Sewickley coal. All ten combustion/regeneration cycles have been completed. The regenerability of the sulfated limestone was not affected by cyclic utilization and ranged from 49 to 71%; this appears to be acceptable. The SO_2 concentrations in the regenerator off-gas ranged from 8.6% in an early cycle to 6.1% in a later cycle.

The reactivity of the regenerated limestone with SO_2 decreased with cyclic use. The CaO/S mole feed ratio required to maintain a 84% sulfur retention increased from ∿2.9 in the first cycle to ∿8.2 in the tenth cycle. TGA sulfation experiments confirmed the reactivity loss as a function of cyclic use. The porosity of the regenerated stones decreased with cyclic usage due to sintering in the high-temperature reducing environment of the regenerator reactor. The loss of beneficial porosity is believed to be the primary cause of reactivity losses.

The total and cyclic calcium utilization in the regenerated stones decreased with cyclic usage. Calcium utilization decreased from ∿30% in the first cycle to ∿9% in the tenth cycle. These results on reactivity and utilization of Greer limestone as a function of cyclic usage will be used to predict fresh limestone makeup rates and to make flowsheet calculations optimizing FBC processes which include sorbent regeneration.

It has been found that after ten utilization cycles ∿25 g of coal ash had accumulated for every 100 g of starting virgin limestone. Photomicrographs of utilized limestone particles revealed ash adherence but no ash encapsulation.

The averaged combined loss of limestone per cycle due to attrition and elutriation is ∿10%--8% during the combustion steps and 2% during the regeneration steps. This is the minimum fresh limestone makeup required for a FBC process with sorbent regeneration. Higher makeup rates may be required to maintain the reactivity of the stone in the fluid bed of the boiler.

Regeneration Process Scale-up and Flowsheet Determination. A process flowsheet for a FBC process with sorbent regeneration is presented in which a fresh dolomite makeup CaO/S mole feed ratio of 0.2 is used. A 10-MWe FBC boiler module is used as the basis and Tymochtee dolomite is the sorbent. The calculations in the flowsheet are based on the performance of Tymochtee dolomite as a function of utilization cycle, which was established in a previously completed cyclic experiment. The effect of varying the fresh sorbent makeup rate to the boiler on the regeneration system performance and size was also evaluated. However, the results confirm that a final flowsheet can be established only after economic evaluations are performed.

Regeneration System Modifications. Installation of a fluidized-bed sorbent preheater for the regeneration system has been completed. The preheater will be used to evaluate the effect of sulfated sorbent feed temperature on the regeneration process.

Task B. Regeneration Process Alternatives

No report for this period.

Task C. Synthetic Sorbents for SO_2 Emission Control

Synthetic sorbents for SO_2 emission control in FBC have been under development as replacements for limestones. It was hoped that these synthetic sorbents would result in a significant reduction in the environmental impact that would occur if large amounts of limestone for SO_2 concentration were quarried and disposed of. In this final report on this topic, data are presented which indicate that the attrition resistance of $CaO-Al_2O_3$ type sorbent is superior to that of natural stones.

The results of a brief study of the use of unpurified bauxite as an alumina source for the preparation of synthetic sorbents are reported. The sorbents had about half the SO_2 capacity of synthetic sorbents prepared from purified alumina.

The probable cost of synthetic sorbents developed in these studies has been estimated. It is shown that the anticipated reduction in environmental impact which might be achieved by using these sorbents is not great enough to justify their additional cost.

Task D. Limestone Characterization

A study is under way of the characteristics of limestones which influence their utility as SO_2 sorbents in fluidized-bed combustion systems. Results are reported on the SO_2 capacity of ten different limestones as measured using a TGA method. Conversions of CaO to $CaSO_4$ varied from about 12% to 96% for the ten stones. It was found that the calcium utilization can be correlated with the internal surface area of the calcined limestone if the pore area is measured only down to a minimum pore diameter. The minimum pore diameter is a linear function of the $CaCO_3$ content of the stone. Stones having lower $CaCO_3$ contents can utilize smaller pores.

Precalcination and heat treatment were studied as a possible way of enhancing the SO_2 capacity of limestones. The energy cost for a precalcination process (in mills per kWh) has been estimated.

The attrition of limestones is being studied using a small room-temperature fluidized-bed test rig. Results are reported on the effect of fluidization velocity, the L/D ratio of the bed, and the compositions of ten different stones. It was found that the impurity content had a large effect on the attrition characteristics of the stone. Stones with high impurity contents had lower attrition rates.

Task E. Trace Elements and Combustion Emission Studies

The Effect of Additives on the Calcination/Sulfation of Limestone. The objective of these studies is to investigate the application of chemical additives for enhancing the SO_2 reactivity of limestone. These studies are based on the discovery made by Pope, Evans and Robbins that addition of common salt to a spent partially sulfated limestone bed rejuvenated its ability to capture SO_2 from the hot flue gas. In present work the mechanism of action is being investigated, other substances are being tested for their enhancement activity, and the practical aspects of the application to AFBC systems are being studied.

To study the mechanism of the action of NaCl on sulfation, large crystals of pure calcite were exposed to a SO_2-air gas mixture at 900°C both with and without treatment with NaCl. It was found that the NaCl treatment markedly increased the extent of the calcination and the sulfation reactions. Highly crystalline forms of both CaO and $CaSO_4$ were formed as a result of NaCl treatment. It was concluded that NaCl aids these reactions by facilitating the crystallization process, thereby leading to a product (CaO or $CaSO_4$) composed of larger crystals. The system is therefore more porous, and diffusion of the reactive gases into the limestone particle is facilitated. It has been hypothesized that the NaCl acts by forming a surficial liquid film which provides a ready path for recrystallization.

Results are reported on the effect of the concentrations of NaCl, Na_2SO_4, Na_2CO_3, $CaCl_2$, and KCl on the sulfation of Greer limestone. These salts are shown to decrease in effectiveness in the order $KCl > NaCl \approx CaCl_2 > Na_2CO_3 > Na_2SO_4$. Results are reported on the change in SO_2 capacity produced by a 2% NaCl addition to eleven different limestones or dolomites. It was found that limestones with the lowest SO_2 reactivities in the natural state were most affected by NaCl addition.

To gain an understanding of the reasons for the large differences in the effect of NaCl on different stones, porosity measurements were made on each stone after calcination, both with and without prior NaCl treatment. It was found that the NaCl treatment increased the mean pore diameter. The increase, found to depend on the amount of salt added, is specific for each stone. The magnitude of the effect of NaCl on the mean pore diameter depends on the impurity content of the stone, the effect being greater the smaller a stone's impurity content. For stones treated with 2% NaCl, the conversion of CaO to $CaSO_4$ was inversely proportional to the average pore diameter.

The Determination of Inorganic Constituents in the Effluent Gas from Coal Combustion. Some chemical elements carried by combustion gases are known to cause severe metal corrosion (for example, to turbine blades). A study is under way to quantitatively determine which elements and chemical compounds are present in the hot combustion gas of coal that may be important to metal corrosion. A laboratory-scale batch fixed-bed combustor has been designed and constructed for these studies. In this combustor, a sample of coal can be burned under controlled conditions and the combustion gases hot filtered and then cold trapped.

The results are reported for a series of experiments in which the vaporization of sodium and potassium was studied. The sodium content of the fuel was increased by the addition of 0.5 wt % NaCl prior to the combustion. Experiments were done using, in different experiments, a bituminous coal, a lignite, and charcoal as fuel. These three fuels had high, medium, and low ash contents. The fraction of the sodium in the fuel which was vaporized varied from about 20% for the low-ash (2%) charcoal to 1% for the high-ash (16%) bituminous coal.) Analysis of the ash residue indicated that the sodium was found as a complex silicate. When the hot (800°C) alumina filter was used, between 80 and 95% of the sodium vaporized from the fuel was captured by the filter. It is believed that the silicious binder of the filter reacted with the vaporized sodium compound (probably NaCl) to form a silicate. In runs in which the hot filter was not used, both NaCl and KCl were detected by X-ray diffraction analyses of the residue deposited on the cold trap, which suggests that sodium and potassium are carried as their chlorides in the hot flue gas.

Task F. Flue-Gas Cleaning Studies

Evaluation of On-Line Light-Scattering Particle Analyzers. In a pressurized FBC, a continuous on-line analyzer capable of instantly measuring the efficiency of particulate-removal equipment would be useful since such an analyzer could be incorporated into a flue-gas control and alarm system that would prevent gas turbine damage from high particulate loadings. Two on-line particle size analyzers, each using a laser light source, are being evaluated--a Spectron Development Laboratory split laser beam particle morphokinetometer and a Leeds and Northrup single laser beam particle analyzer.

The experiments with the Spectron Development Laboratory particle morphokinetometer (PM) have been completed, and the instrument has been returned to the manufacturer. Preliminary results are reported. Spectron's PM analyzer measurements are compared with those obtained on steady-state particle samples with an Anderson cascade impactor and with a Coulter counter. The results obtained with the Anderson cascade impactor and Coulter counter were in good agreement, whereas the results obtained with the Spectron PM analyzer diverged from Anderson/Coulter results for the larger diameters.

An empirical calibration curve has been developed for the Spectron PM which is based on comparative measurements obtained with the Spectron PM and those obtained by Coulter counter and cascade impactor analysis. The empirical calibration improved the agreement of the different measuring methods, especially in the 1.5-23 μm measuring range.

Delivery of the Leeds and Northrup (L&N) analyzer has been postponed because final tests by L&N revealed that the laser unit was not performing satisfactorily. This analyzer is now being tested by Leeds and Northrup.

Particle Removal from Flue Gas. In pressurized fluidized-bed combustion, the hot flue gas from the combustor must be expanded through a gas turbine. To prevent erosion (and possibly corrosion) of the turbine blades by particulate matter entrained in the flue gas, the particulate loading must be reduced to very low levels. A program has been initiated at ANL to test and evaluate promising flue gas cleaning methods for application in the off-gas system of the ANL, 6-in.-dia fluidized-bed combustor. The techniques which have been identified for investigation are acoustic conditioning of the flue gas, granular-bed filters using the limestone or dolomite sorbent as the granular bed material, and a Donaldson TAN-JET cyclone.

A small granular bed filter has been fabricated to study the use of either fresh limestone or sulfated sorbent as the filter medium. Using these materials, the filter cake would not have to be removed by blowback. Instead the entire bed would be replaced when it has become loaded. With sulfated sorbent, the discharged bed including the cake would be discarded. With fresh stone, the stone plus cake would be fed to the combustor bed where agglomeration of the particles in the cake could occur. Or the cake could be separated from the stone prior to adding the stone to the combustor.

Initially, testing of the granular bed filter was performed at ambient conditions to determine the pressure drop characteristics of the sorbent and the possible contribution of dust from the sorbent to the effluent gas from the filter. The pressure drop data was correlated with the Ergun equation for fluid flow through a packed bed, and the values for ϵ, bed void volume fraction, and ϕ_s, particle sphericity factor, were determined. When a clean gas was passed through the granular-bed filter, dust loadings exiting from the filter ranged from 0.0016 to <0.0001 grain/scf (0.0037 to <0.0002 g/m^3).

Acoustic conditioning of the flue gas is a technique to enhance the natural tendency of polydispersed particulates to impact upon each other. Thereby, the mean size of the particulate matter is increased (and the number of particles is decreased). The process is designed to increase the collection efficiency of downstream dust collectors.

A suggested procedure has been prepared by a consultant for developing a resonant manifold system for the evaluation of acoustic conditioning in the FBC system at ANL. The principal components of the proposed system are (1) a pulse-jet sound generator, (2) a resonant manifold for "splitting" the resultant acoustic power, and (3) an acoustic treatment section where agglomeration of the aerosol occurs.

A high-efficiency Donaldson TAN-JET cyclone would provide a means of evaluating how effective upstream acoustic agglomeration is in increasing the collection of dust in high efficiency collection devices. It is planned, therefore, to proceed with the design, procurement, and installation of a Donaldson TAN-JET cyclone as a part of the flue-gas cleaning studies.

TASK A. REGENERATION PROCESS DEVELOPMENT

In support of ERDA's national program for the development and implementation of FBC technology, the feasibility of regenerating and recycling the SO_2-accepting sorbents from the FBC boilers is being investigated.

Natural calcium-based stones such as limestones and dolomites are receiving primary consideration as sulfur-accepting sorbents (sulfur reacts with calcium to form $CaSO_4$) in FBC boilers. The primary reasons are their acceptable reactivity and low costs and the bountiful supply throughout the United States. Approximately one tonne of natural stone will be sulfated for every four tonnes of coal (∿3 wt % S) combusted. In a 1000-MW electric power plant (70% capacity factor), ∿2000 tonnes of stone per day will be sulfated. Using the stone only once would generate large amounts of sulfated stone for disposal. Regeneration of the CaO in the stone and recycling is a potential solution to the waste disposal problem.

A conceptual power-generating facility utilizing fluidized bed coal combustion and sorbent regeneration systems is schematically represented in Fig. 1. Steam is removed from the boiler and is expanded in turbines to generate power. The flue gas from the boiler meets EPA chemical emission requirements. The partially sulfated sorbent from the boiler is transferred to the regenerator, where it is regenerated, and then it is combined with fresh sorbent (to compensate for losses due to attrition and changes in reactivity) and is recycled to the boiler. The SO_2-rich off-gas from the regenerator is treated in a sulfur recovery plant.

For sulfur recovery, a process using coal as reductant, such as the Foster Wheeler RESOX process[1] is recommended. Since the volume of the off-gas from the regenerator and sulfur recovery system is much less than that from the boiler, it is proposed that the off-gas from the sulfur recovery process be recycled to the boiler. In this manner, the gas emission stream from the regenerator which could contain some trace elements due to volatilization from the sorbent during regeneration (not yet investigated) will be eliminated, and the tail gas from the sulfur recovery system will not have to be processed.

In the sorbent regeneration process being investigated, $CaSO_4$ is reductively decomposed in a fluidized bed at temperatures of ∿1100°C. The heat and the reductants required are produced by incomplete combustion of coal in the fluidized bed of sulfated stone. Two solid-gas reactions by which regeneration occurs are:

$$CaSO_4 + CO \rightarrow CaO + CO_2 + SO_2 \qquad (1)$$

$$CaSO_4 + H_2 \rightarrow CaO + H_2O + SO_2 \qquad (2)$$

At lower temperatures and under more highly reducing conditions, the formation of CaS is favored:

$$CaSO_4 + 4CO \rightarrow CaS + 4CO_2 \qquad (3)$$

$$CaSO_4 + 4H_2 \rightarrow CaS + 4H_2O \qquad (4)$$

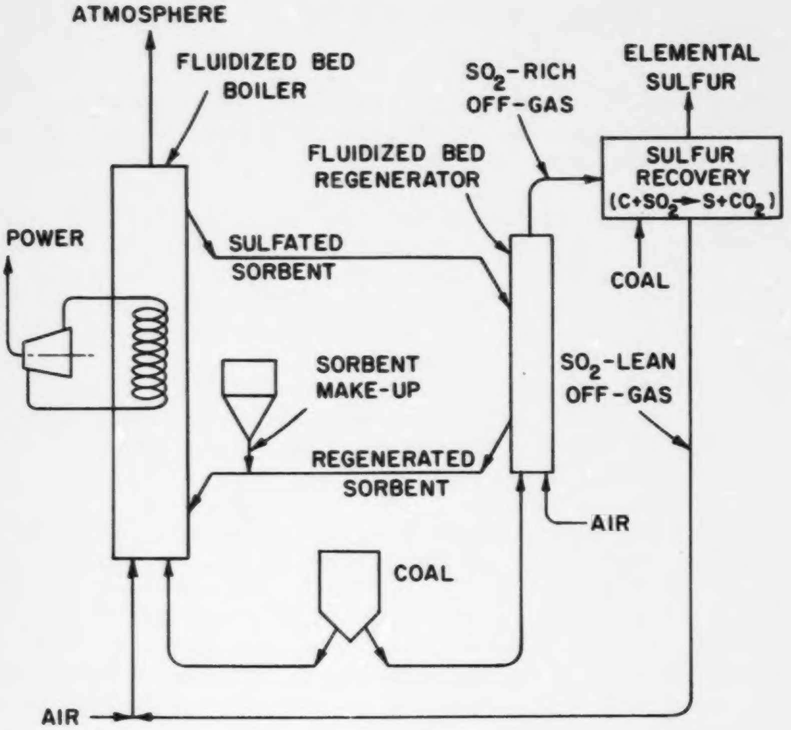
ATMOSPHERE
FLUIDIZED BED BOILER
SO_2-RICH OFF-GAS
ELEMENTAL SULFUR
FLUIDIZED BED REGENERATOR
SULFUR RECOVERY
$(C+SO_2 \rightarrow S+CO_2)$
POWER
SULFATED SORBENT
COAL
SORBENT MAKE-UP
SO_2-LEAN OFF-GAS
REGENERATED SORBENT
AIR
COAL
AIR

Fig. 1. Conceptual Fluidized-Bed, Coal Combustion, Power-Generating Facility Having Sorbent-Regeneration and Sulfur-Recovery Capabilities

An oxidizing zone which forms at the bottom of the fluidized bed, where the fluidizing gas (O_2 and N_2) is introduced, minimizes the buildup of CaS.

The feasibility of a sorbent regeneration process will depend on (1) the ability to regenerate the stones and to generate an SO_2-rich off-gas which can be treated in a sulfur recovery process, (2) the reactivity of the regenerated sorbent during subsequent sulfation (coal combustion) cycles, and (3) the availability of a sorbent that will not decrepitate above acceptable levels.

In this section of this report, (1) regeneration rate results (process development unit-scale) for Tymochtee dolomite and Greer limestone are presented in which the effects of key variables on regeneration of the sorbents were evaluated; (2) the effects of process operating variables on the tendency of the fluid bed in the regenerator reactor to defluidize and agglomerate have also been evaluated; (3) for Tymochtee dolomite and for Greer limestone, the effects of repeated utilization cycles on the reactivity and the resistance to decrepitation were evaluated in ten combustion (sulfation)/regeneration cycles which were performed without fresh sorbent makeup; and (4) some process flowsheet calculations for a FBC process with sorbent regeneration are presented and discussed.

1. Experimental

a. Materials--Sorbents

Tymochtee dolomite which had been sulfated during coal combustion experiments (using Arkwright coal) at ∿900°C and 810 kPa was regenerated. Also, some Greer limestone which had been sulfated by ANL and some by Pope, Evans and Robbins (PER) at 840-900°C and atmospheric pressure during combustion of Sewickley coal was regenerated.

The sulfated Tymochtee dolomite contained ∿9 wt % S as $CaSO_4$ (no $MgSO_4$ present), 26 wt % Ca, 9.5 wt % CO_2, and had a nominal size distribution of -14 +30 mesh before regeneration. In its virgin state, its main constituents were $CaCO_3$ (50 wt %) and $MgCO_3$ (39 wt %). The virgin Tymochtee dolomite had been obtained from C. E. Duff and Sons, Huntsville, Ohio.

The virgin Greer limestone used for this study contained 41.2 wt % CaO, 32 wt % CO_2, and 4.3 wt % Si, and its size was (nominally) -14 +30 mesh. When sulfated, it contained 5-9 wt % S in the cyclic experiment and ∿8 wt % in the remaining experiments.

b. Materials--Coals

The coal used in the sulfation of Tymochtee dolomite was a Pittsburgh seam coal obtained from the Consolidation Coal Company Arkwright mine. As received, the coal contained ∿2.8 wt % sulfur, ∿7.7 wt % ash, and ∿2.9 wt % moisture and had a heating value of 7,610 kcal/kg and an average particle size of 320 μm. Triangle coal was combusted under reducing conditions during the regeneration of Tymochtee dolomite. It is a bituminous high-volatile coal (32.6% volatile matter, dry) and has a high ash fusion temperature (1390°C, initial deformation under reducing conditions). As received, it contains 73.5 wt % C, 9.4 wt % ash, and 0.98 wt % S.

The coal used in the sulfation of Greer limestone was a bituminous coal, Sewickley. As received, it contains 4.3 wt % S, 12.7 wt % ash, and 1.1 wt % moisture and has a heating value of 7,220 kcal/kg; sizes were (nominally) -6 +14 mesh during ANL sulfation and -1/4 in. during PER sulfation. This same coal was combusted under reducing conditions in the regeneration step of each cycle. It does not have a high ash fusion temperature (initial deformation is at ∿1120°C under reducing conditions).

Additional data on the above sorbents and coals are presented in Appendix A.

c. PDU--Combustion System and Procedure

The experimental equipment and instrumentation of the PDU (process development unit) at Argonne consist of a 6-in.-dia, fluidized-bed combustor that can be operated at pressures up to 1014 kPa, a compressor to provide fluidizing-combustion air, a preheater for the fluidizing-combustion air, peripheral-sealed rotary feeders for metering solids into an air stream fed into the combustor, two cyclone separators and two filters in series for solids removal from the flue gas, associated heating and cooling arrangements and controls, and temperature- and pressure-sensing and display devices. A simplified schematic flowsheet of the combustion equipment is presented in Fig. 2.

Details of the PDU combustor are presented in Fig. 3. The reactor vessel consists of a 15-cm-dia, Schedule 40 pipe (Type 316 SS), approximately 3.4 m (11 ft) long. The reactor is centrally contained inside a 2.7-m (9-ft) section of 12-in.-dia, Schedule 10 pipe (Type 304 SS). A bubble-cap type gas distributor is flanged to the bottom of the inner vessel. Fluidizing air inlets, thermocouples for monitoring bed temperatures, solids feed line, and solids removal lines are accommodated by the bubble cap gas distributor. The coal and sorbent are fed in a common line which extends 2 in. above the top surface of the gas distributor plate and is angled 20° from the vertical. A constant bed height is maintained in the combustor by use of a 36-in.-high standpipe. The 6-in.-dia pipe is alternately wrapped with resistance-type heating elements and cooling coils onto which a layer of heat-conducting copper and then an overlay of oxidation-resistant stainless steel have been applied. Additional cooling capacity is provided by three internal, hairpin-shaped coils that extend down from the flanged top of the combustor to within 12 in. of the top surface of the gas distributor. The coolant is water entrained in air.

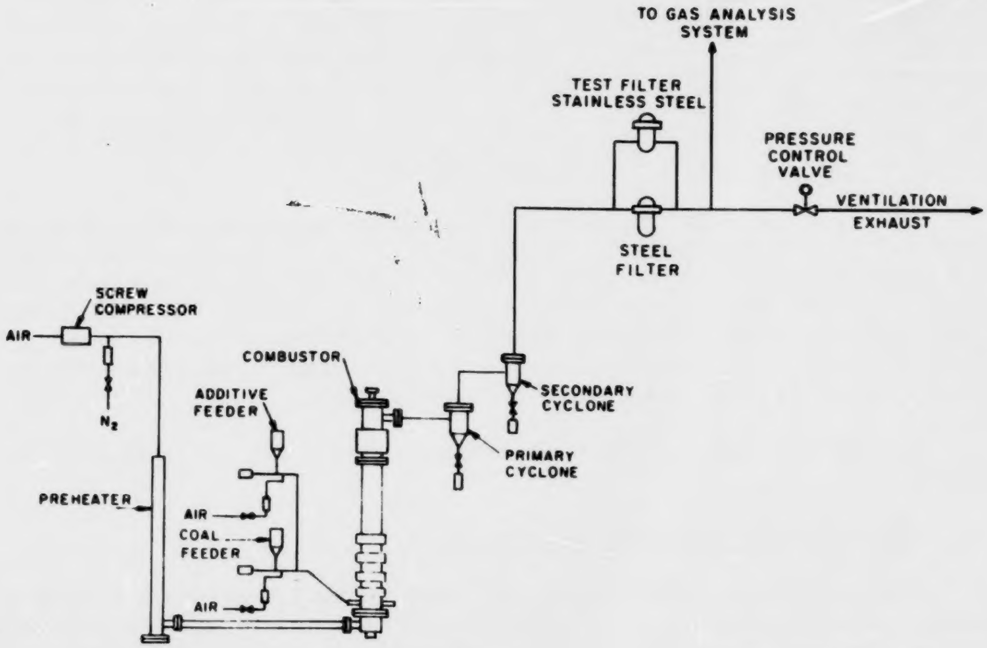
TO GAS ANALYSIS SYSTEM
TEST FILTER STAINLESS STEEL
PRESSURE CONTROL VALVE
VENTILATION EXHAUST
STEEL FILTER
SCREW COMPRESSOR
AIR
N_2
COMBUSTOR
ADDITIVE FEEDER
SECONDARY CYCLONE
PRIMARY CYCLONE
PREHEATER
AIR
COAL FEEDER
AIR

Fig. 2. Simplified Equipment Flowsheet of PDU Fluidized-Bed Combustor and Associated Equipment. The "additive feeder" is actually a "sorbent feeder."

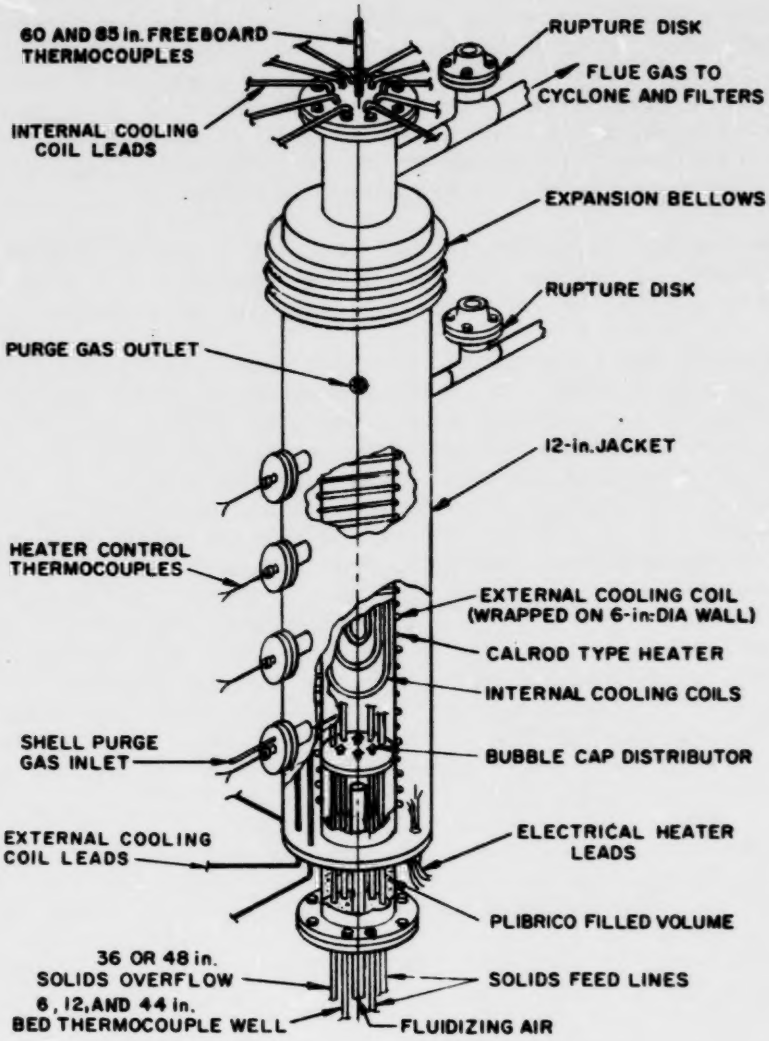
60 AND 85 in. FREEBOARD THERMOCOUPLES
RUPTURE DISK
FLUE GAS TO CYCLONE AND FILTERS
INTERNAL COOLING COIL LEADS
EXPANSION BELLOWS
RUPTURE DISK
PURGE GAS OUTLET
12-in. JACKET
HEATER CONTROL THERMOCOUPLES
EXTERNAL COOLING COIL (WRAPPED ON 6-in. DIA WALL)
CALROD TYPE HEATER
INTERNAL COOLING COILS
SHELL PURGE GAS INLET
BUBBLE CAP DISTRIBUTOR
EXTERNAL COOLING COIL LEADS
ELECTRICAL HEATER LEADS
PLIBRICO FILLED VOLUME
36 OR 48 in. SOLIDS OVERFLOW
SOLIDS FEED LINES
6, 12, AND 44 in. BED THERMOCOUPLE WELL
FLUIDIZING AIR

Fig. 3. Six-Inch-Diameter Pressurized, Fluidized-Bed Combustor

Fluidizing-combustion air is supplied by a 75-hp, screw-type compressor capable of delivering 100 cfm at 150 psig. The air can be heated to approximately 540°C in a 6-in.-dia, 10-ft-tall preheater containing eight 2700W, clamshell-type heaters.

Coal and either dolomite or limestone are pneumatically fed from hoppers to the combustor, using two 6-in.-dia rotary valve feeders. The feeders and hoppers are mounted on platform-type scales.

The flue gas (off-gas) is sampled continuously and is analyzed for the components of primary importance. Nitrogen oxide and total NO_x are analyzed using a chemiluminescent analyzer; sulfur dioxide, methane, carbon monoxide, and carbon dioxide determinations are made using infrared analyzers; oxygen is monitored using a paramagnetic analyzer; and total hydrocarbons are analyzed by flame ionization. Prior to and during each experiment, the response of each analytical instrument is checked, using standard gas mixtures of flue-gas constituents in nitrogen. Batch samples of flue gas can be taken and analyzed for constituents of secondary importance.

The combustion system is equipped with a Hewlett-Packard 2010C data acquisition system to monitor and record the temperature, pressure, gas flow, and flue-gas concentration for subsequent data handling and analysis.

Although the experimental procedure was subject to minor variations, it was basically as follows: a preweighed amount (∿15 kg) of (1) partially sulfated sorbent from a previous experiment, (2) fresh unsulfated sorbent, or (3) regenerated sorbent was charged to the reactor to provide an initial bed of material. The starting bed temperature was then raised to about 430°C by passing fluidizing air (preheated to 430-480°C) through the combustor and simultaneously employing the resistance heaters on the combustor wall. Once the bed temperature reached 430°C, the system was brought to the desired operating pressure, and coal (entrained in a transport air stream) was injected into the bed. To prevent carbon accumulation in the fluidized bed during startup, coal was initially injected in small amounts intermittently until a rapidly increasing temperature and a changing flue-gas composition confirmed ignition and sustained combustion. Continuous injection of coal was then initiated, and the bed temperature was raised to a selected combustion temperature. The desired temperature was maintained by the use of external and internal cooling coils.

Injection of the sulfur-accepting sorbent (virgin or regenerated) was begun when the bed reached operating temperatures. The air, coal, and sorbent feed rates were adjusted to give a specified mole ratio of calcium in the sorbent to sulfur in the coal, a specified superficial gas velocity, and a specified level of oxygen in the flue gas leaving the combustor. Sulfated sorbent was removed from the combustor by means of a standpipe to maintain a constant fluidized-bed level.

d. PDU--Regeneration System and Procedure

Figure 4 is a schematic diagram of the regeneration system used in this work. The reactor ID is 10.8 cm (4.25 in.), and the height of the fluidized bed (∿46 cm) is regulated by an overflow pipe that is external to the fluidized bed. The pressurized, fluidized-bed reactor is lined with a 4.8-cm-thick castable refractory. The coal and the sulfated sorbent are metered separately (for independent control) to a common pneumatic transport line which discharges into the fluidized bed above the gas distributor.

Other components of the experimental system are an electrically heated pipe heat exchanger for preheating some of the fluidizing gas and for preheating air (used in startup only) to ∿400°C and a solids-cleanup system for the off-gas. Continuous analyses of pertinent constituents (SO_2,

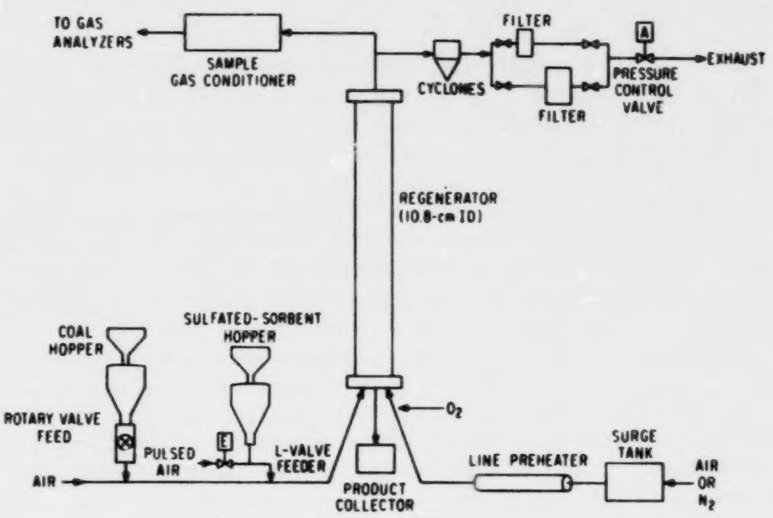
TO GAS ANALYZERS
SAMPLE GAS CONDITIONER
FILTER
A
EXHAUST
CYCLONES
PRESSURE CONTROL VALVE
FILTER
REGENERATOR (10.8-cm ID)
COAL HOPPER
SULFATED-SORBENT HOPPER
ROTARY VALVE FEED
E
PULSED AIR
L-VALVE FEEDER
O_2
SURGE TANK
LINE PREHEATER
AIR
PRODUCT COLLECTOR
AIR OR N_2

Fig. 4. Experimental Sorbent Regeneration System

O_2, CO, H_2, CH_4, and NO) in the off-gas was performed. Solids transport air constituted ∿40% of the total fluidizing gas in the reactor. The remaining fluidizing gas was a mixture of pure nitrogen and oxygen. Oxygen and nitrogen were metered separately and mixed to produce the required oxygen environment in the reactor. Thus the oxygen requirement at different experimental conditions could be satisfied without changing the fluidizing gas velocity. Oxygen concentrations in excess of that in air were used in the feed gas for most of the reported regeneration experiments. Large amounts of heat (per unit capacity) were required to compensate for (1) the heat losses in the relatively small experimental system and (2) the heat load imposed by feeding cold sulfated sorbent to the system. In a large-scale industrial regeneration system, such heat requirements would be absent and oxygen enrichment of the fluidizing air would not be needed.

2. PDU Regeneration Rate Experiments with Tymochtee Dolomite

[J. Montagna (Principal Investigator), G. Smith, C. Schoffstoll, R. Mowry, and J. Stockbar]

A requirement of a sorbent regeneration process is that CaO (SO_2 acceptor) be regenerated sufficiently while an SO_2-rich off-gas is generated which can be treated in a sulfur recovery process. The dependence of (1) regeneration of CaO and (2) SO_2 concentration in the dry off-gas on key variables (such as regeneration temperature, solids residence time in the reactor, and system pressure) has been determined for the regeneration of once-sulfated Tymochtee dolomite sorbent. This data is being used in a model for the reductive decomposition regeneration process to find the optimum process conditions from technical and economic points of view.

a. Effect of Solids Residence Time and Temperature on Extent of CaO Regeneration

The experimental conditions and results for thirteen experiments are given in Table 1. Data on six of these experiments were reported earlier in ANL/ES-CEN-1016. The experiments were performed at three temperatures: 1000°C, 1050°C, and 1100°C. Solids residence times ranged from ∿7 to ∿35 min.

Regeneration of CaO was calculated from chemical analyses of the steady-state products. It was based on the sulfur to calcium ratios in (1) the sulfated dolomite feed and (2) the steady-state product after regeneration. These calculated regeneration values are compared in Table 1 with values based on off-gas analyses. The latter values are the ratios of the total sulfur released into the off-gas stream to the total sulfur contained in the sulfated dolomite feed. The off-gas flow rate was calculated using the feed gas rate and the model of the regeneration process (discussed in a later section) in which the gas volumetric expansion in the reactor is predicted. The CaO regeneration values obtained by chemical analyses of the regenerated products generally agree within analytical accuracy with the values calculated from off-gas analyses. The extents of regeneration (based on off-gas and regenerated solids analyses) are plotted in Fig. 5 as a function of solids residence time for the three temperature levels. The solids residence time was varied by changing the solids feed rate and not by changing the reactor volume.

At 1000°C, as the solids residence time was varied from 37 min to 11 min, the extent of regeneration decreased drastically from 77% to 11% (based on solids analyses). The SO_2 concentration in the dry off-gas decreased from 2.5% to 1.4%. At this relatively low temperature, the rate of regeneration of CaO is low, and therefore long solids residence times are required to obtain acceptable ($\geq$50%) regeneration levels.

At 1050°C, decreasing the solids residence time from 34 min to 12 min decreased the extent of CaO regeneration from 90% to 56%. The SO_2 concentration in the dry off-gas increased from 3.0% to 4.8%. At 1100°C, the highest temperature level investigated, decreasing the solids residence time from 37 min to 7.0 min caused the extent of CaO regeneration to decrease from 95% to 75% and the SO_2 concentration to increase from 2% to 8.7%. (The SO_2 concentration for Exp CCS-1 for which the solids residence time was 7 min, was adjusted from 6.5% to 8.7% to compensate for the dilution due to the higher fluidizing-gas velocity.) Because the rate of regeneration of CaO is high at 1100°C, the extent of regeneration remained relatively high when the solids residence time was as low as 7 min.

An improved rate of $CaSO_4$ decomposition at higher temperatures ($\geq$1100°C) for the reductive decomposition of gypsum has also been reported by numerous workers, including Martin *et al.*[2] who used carbon as the reductant and Wheelock *et al.*[3] who used CO as the reductant. As expected, the oxygen required in the feed gas increased with sulfated sorbent feed rate and with total amount of reductive decomposition, which is represented by the SO_2 concentration in the off-gas.

Table 1. Experimental Conditions and Results for the Regeneration of Sulfated Tymochtee Dolomite by the Incomplete Combustion of Triangle Coal in a Fluidized Bed.

Nominal Fluidized-Bed Height: 46 cm Pressure: 153 kPa
Reactor ID: 10.8 cm
Coal: Triangle coal (0.98 wt % S) Ash fusion temp. under reducing conditions, 1390°C (initial deformation)
Sorbent: (1) -14 +50 mesh, 9.0 wt % S (CS-6, -7, -8)
(2) -14 +50 mesh, 9.4 wt % S (CS-10, -11, -12)
8.5 wt % S (CC-13 through -18 and CCS-1)

Exp. No.	Bed Temperature, °C	Fluidizing-Gas Velocity, m/s	O_2 Conc in Feed Gas, %	Feed Rate, kg/hr	Solids Residence Time, min	Reducing Gas Concentration in Effluent, %	Measured SO_2 in Dry Effluent Gas, %	CaO Regeneration, %[a] / %[b]
CS-6	1000	0.98	18	5.0	37	1.4	2.5	83/77
CS-8	1000	0.92	22	10.0	18	2.2	2.5	39/30
CS-17	1000	1.04	24	16.1	11	2.4	1.4	18/11
CS-7	1050	0.92	21	5.4	34	1.9	3.0	84/90
CS-16	1050	1.0	26	11.1	16	2.2	3.3	53/53
CS-10	1050	0.98	29	15.0	12	2.5	4.8	53/56
CS-15	1100	1.02	22	5.0	37	1.5	2	82/95
CS-14	1100	1.05	28	10.0	18	2.2	4.8	94/82
CS-11	1100	1.07	33	14.3	13	2.9	6.4	80/85
CSS-13	1100	1.09	33	31.6	13	2.2	6.1	89/72
CSS-18	1100	1.07	33	13.2	14	2.4	6.3	93/80
CS-12	1100	1.16	36	19.5	9.4	2.9	7.8	79/77
CCS-1	1100	1.43	27	26.4	7.0	2.7	6.5[c]	67/75

[a] Based on off-gas analysis.

[b] Based on chemical analysis of dolomite samples.

[c] The SO_2 concentration adjusted for a 1.08 m/s fluidizing gas velocity is ∿8.7%.

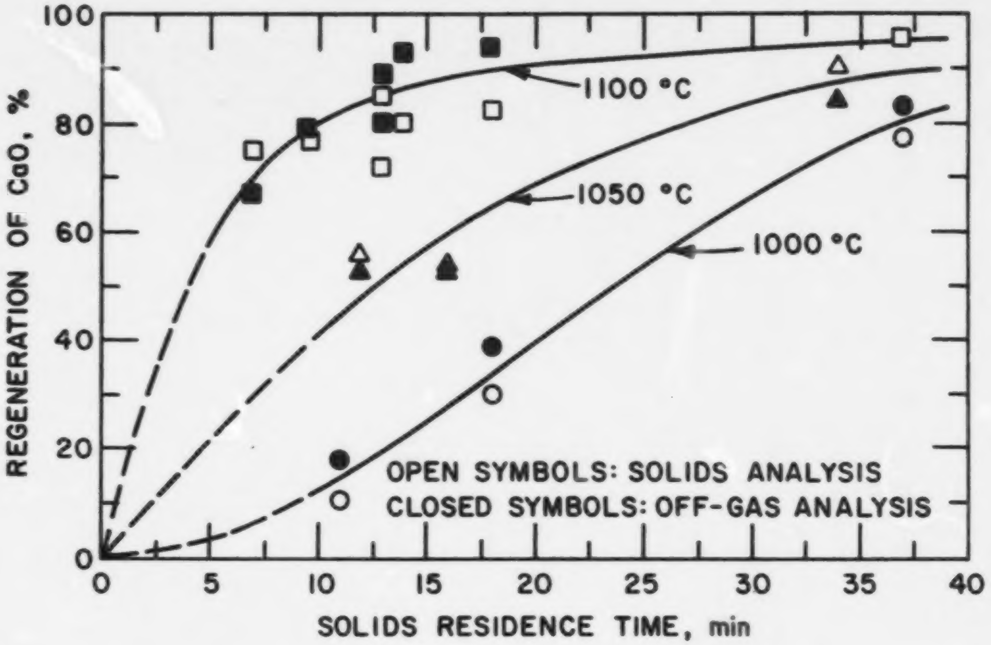

Fig. 5. Regeneration of CaO in Tymochtee Dolomite as a Function of Solids Residence Time (pressure: 153 kPa)

b. Regression Analysis of Regeneration Data

A best fit has been obtained for the experimental extent of CaO regeneration as a function of regeneration temperature and solids residence time by regression analysis. The equation is

$$\ln(1 - R) = A \cdot \tau + B \cdot \tau^2 \qquad (1)$$

where R = extent of CaO regeneration (*i.e.*, at complete regeneration, $R = 1$)
τ = particle residence time in the reactor, min
A, B = functions of temperature.

The temperature-dependent constants A and B were evaluated at the three regeneration temperature levels investigated (1000, 1050, and 1100°C) by a least squares technique. From these values, a quadratic equation was obtained to represent the functional dependence of A and B on regeneration temperature, as given below.

$$A \times 10^2 = -5.05 - 8.72T - 4.00T^2 \qquad (2)$$

$$B \times 10^4 = -2.94 + 18.64T + 10.65T^2 \qquad (3)$$

$$T = (t - 1050)/50$$

where t = regeneration temperature, °C

The values calculated by the model equation, equation 1, compare well with the experimental results. A correlation coefficient ranging from 0.96 to 0.99 was obtained for the experimental data and the results calculated from the model equation. Equation 1 with the calculated coefficients was found to be a good mathematical model of the dependence of the extent of CaO regeneration on regeneration temperature and solids residence time in the reactor for the investigated experimental range. This relationship for the rate of CaO regeneration is being used in a mass and energy-constrained model for the regeneration process to predict sorbent behavior within and outside the investigated operating range.

The extent of CaO regeneration as a function of temperature and sorbent residence time as calculated by equation 1 has been plotted in Fig. 6. The plot has been extrapolated to 1200°C, which is beyond the experimentally investigated temperature range of 1000-1100°C. On the basis of these predictions, it is expected that the extent of CaO regeneration would increase considerably (by ∿1/3) if the temperature were increased from 1100°C to 1150°C at a solids residence time of 5 to 7.5 min. At yet higher temperatures, the extent of regeneration increases more slowly.

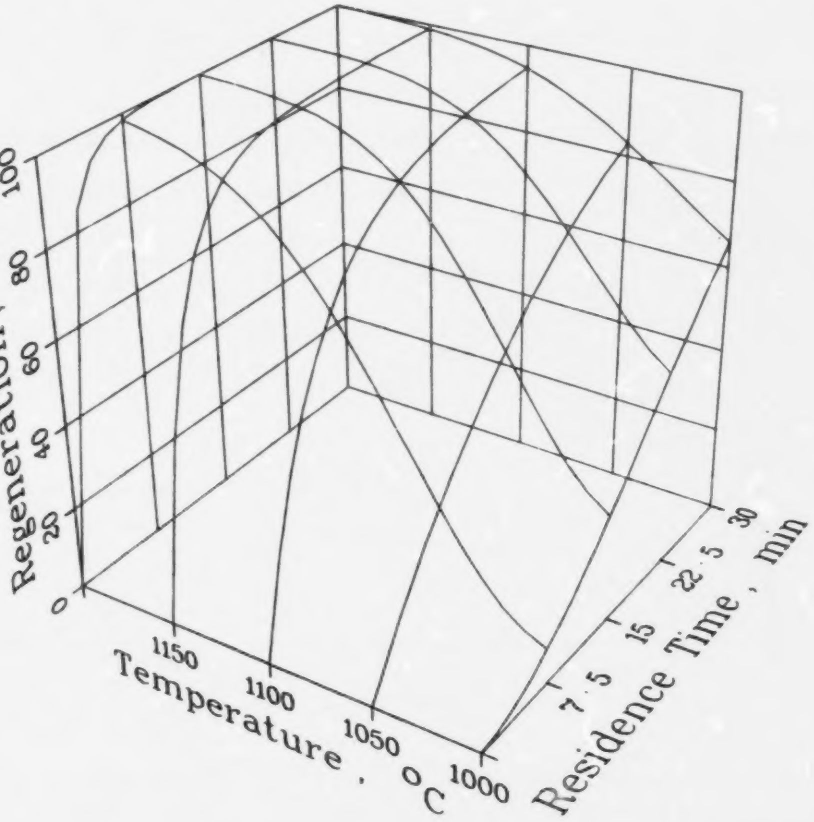

Fig. 6. The Extent of CaO Regeneration for Tymochtee Dolomite as a Function of Temperature and Residence Time as Represented by the Model Equation, Equation 1

c. Effect of Solids Residence Time and Temperature on SO_2 Concentration in the Off-Gas

A least-squares best-fit relationship was obtained from the experimental regeneration data for the functional dependence of CaO regeneration on solids residence time and regeneration temperature. It was used in a mass and energy constrained model for the regeneration process (equation and model are described in a following section). The SO_2 concentration in the dry off-gas was predicted with the process model for solids residence times ranging from 40 min to $\sim$2.5 min. In the model, gas volumetric changes due to combustion and decomposition reactions (which affect the extent of dilution) are included in the off-gas composition predictions. The predictions were made for the three investigated temperature levels, a pressure of 153 kPa, and a fluidizing-gas velocity of 1.07 m/s. A sulfur content of 9.5 wt % was assumed for dolomite. The predicted SO_2 concentrations in the dry off-gas (the curves) are plotted in Fig. 7, together with the experimentally obtained concentrations.

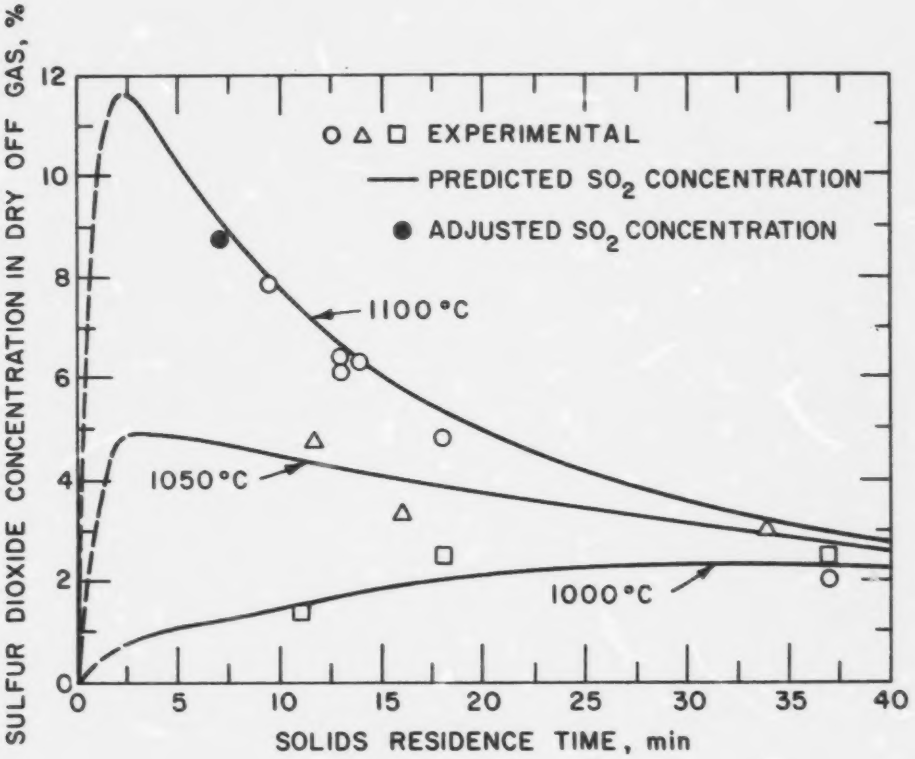

Fig. 7. Predicted and Experimental SO_2 Concentration as a Function of Solids Residence Time at Three Regeneration Temperatures (pressure: 153 kPa)

At 1000°C, the SO_2 concentration in the dry off-gas was predicted to continually decrease as the solids residence time decreased, in agreement with the experimental data. At this temperature, the regeneration rate was low. At 1050°C and higher temperatures, the maximum SO_2 concentrations were predicted at the lowest permissible solids residence time of $\sim$2.5 min, at which point oxygen that would be required would be greater than the total fluidizing gas.

At 1100°C much higher SO_2 concentrations were obtained. Based on the experimental data obtained for the extent of regeneration, an SO_2 concentration in excess of 10% is predicted for a 5-min solids residence time (realistic). The experimental and predicted SO_2 concentrations in the dry off-gas for all three temperature levels were in good agreement. These experimental results show that for temperatures $\geq$1050°C, as the solids residence time in the reactor decreased (*i.e.*, at higher rates of sulfated sorbent throughput) extent of regeneration is sacrificed but SO_2 concentration in the dry off-gas is increased. The effect of introducing room temperature sorbent in the reactor for very short solids residence times, $<$7 min, has not yet been evaluated.

Using equation 1 for the functional dependence of extent of CaO regeneration on temperature and solids residence time in the above-mentioned model for the regeneration process, the SO_2 concentrations in the dry off-gas at three different system pressures are predicted in Fig. 8 for the experimental conditions given. These predictions, also, were extrapolated beyond the experimentally investigated temperature range of 1000-1100°C. The effect of pressure on SO_2 concentration is very great, as discussed below. It is predicted that with a system pressure of 1000 kPa (10 atm), SO_2 concentrations no greater than 4% can be obtained, even with regeneration temperatures as high as 1200°C and solids residence times as low as 5 min. At a pressure of 100 kPa (1 atm), SO_2 concentrations as high as 20% are predicted at regeneration temperatures up to 1200°C. However, based on the experience to date with the regeneration process, it is expected that regeneration temperatures in excess of 1100°C will not be feasible because of the increased tendency of the sulfated sorbent (a mixture of sorbent and residual coal ash) to agglomerate at high temperatures.

High temperatures were found to increase both the extent of CaO regeneration and the SO_2 concentration in the off-gas. This effect of temperature agrees with previous results presented by Montagna *et al.*[4] in which methane was used as the fuel for the regeneration of dolomite by reductive decomposition. Higher SO_2 concentrations in the off-gas at higher regeneration temperatures have also been reported by Hoke *et al.*[5] for the reductive decomposition of pure $CaSO_4$ in a fluidized-bed batch reactor. Although at higher temperatures (above 1100°C), the regenerability of the sorbent would be further improved, the probability of agglomerating the sorbent and residual coal ash would be increased, as reported by Skopp *et al.*[6] Based on the above results with Tymochtee dolomite, an industrial regeneration process should be operated at 1100°C and a solids residence time of $\sim$5-8 min.

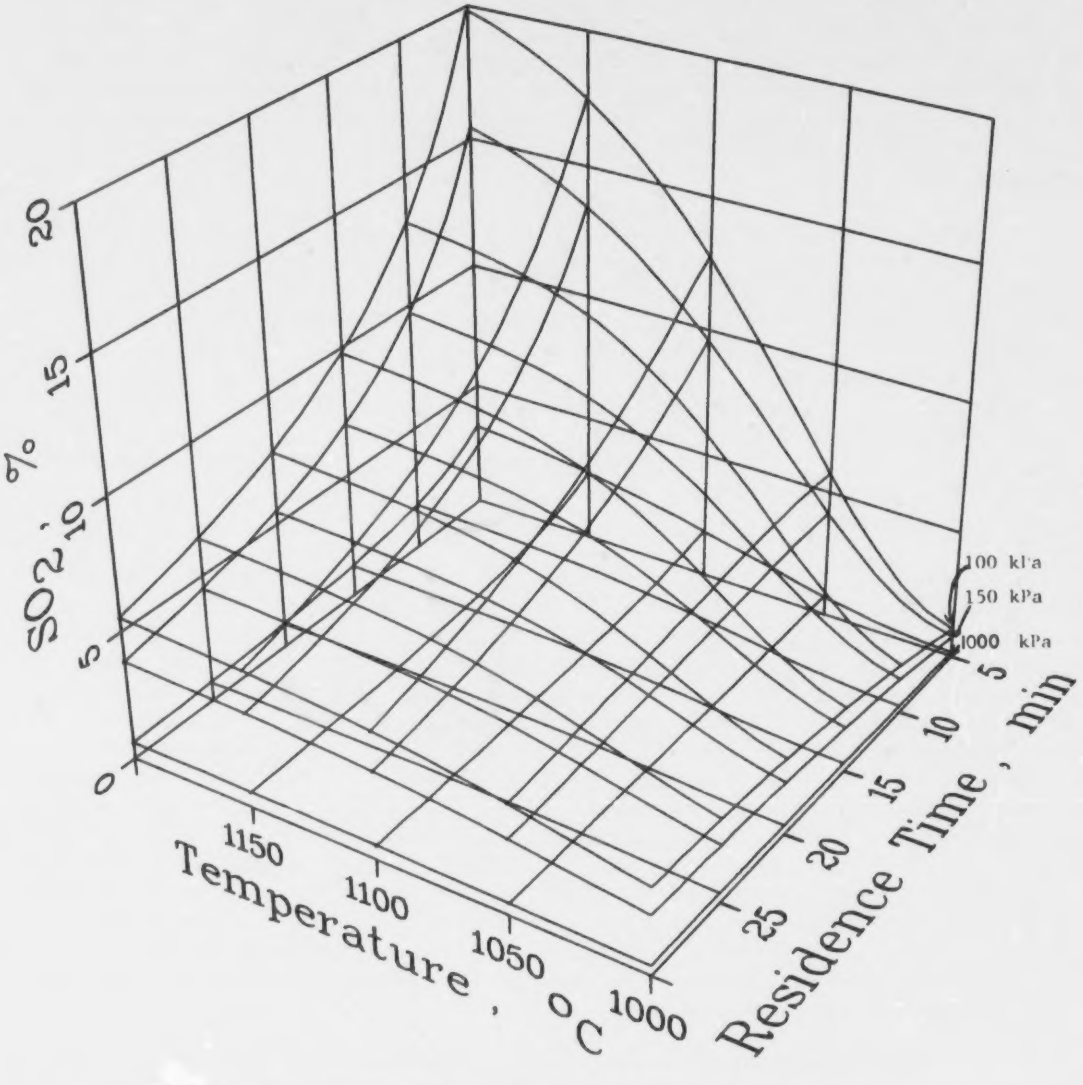

Fig 8. Predicted SO_2 Concentration in the Dry Off-Gas as a Function of Solids Residence Time, Regeneration Temperature, and System Pressure (Experimental Conditions: Solid Feed Temp, °C, 815; Fluidizing-Gas Velocity, m/s, 1.07; Fluidizing-Gas Feed Temp, °C, 650; Sulfur Concentration in Sorbent, %, 9.5)

d. Effect of System Pressure on Extent of CaO Regeneration and Off-Gas SO_2 Concentration

Thermodynamically, from an equilibrium standpoint, when the system pressure is lowered, the SO_2 concentration in the off-gas will increase. In the fluidized-bed process, the SO_2 concentration in the off-gas is determined by the rate of total gas flow through the reactor and the rate of CaO regeneration in the reactor. Because of high air (fluidizing gas and/or combustion oxygen) and energy (sensible heats of gas and solids, and the heats for the decomposition reactions) requirements of the process, equilibrium SO_2 concentrations in the off-gas cannot be achieved practically. At lower pressures, less fluidizing gas is required and thus the extent of dilution is reduced.

The effect of system pressure on the extent of regeneration of CaO and SO_2 concentration in the dry off-gas has been evaluated in six experiments in which sulfated Tymochtee dolomite from the second and sixth regeneration cycles of a ten-cycle experiment (discussed in a following section) was regenerated. The experimental conditions and results are given in Table 2. In experiments CCS-2A, -2B, and -2C, the pressure was ∿115 kPa or ∿75% of that in CCS-2. In the experiments at the lower pressure, decreasing the solids residence time from 8.8 min to 5.3 min caused the extent of CaO regeneration to decrease from 80% to 60% (based on solids analysis). These results on extent of regeneration are in agreement with those obtained at the higher pressure of 153 kPa (see Fig. 5) and equivalent solids residence times. Specifically, results for CCS-2B and CCS-2 agree well.

At the lower pressure, the measured SO_2 concentration in the dry off-gas increased from 8.9% to 9.6% as the solids residence time was decreased from 8.8 min to 5.3 min. These concentrations are higher than those obtained in the higher pressure experiments (Table 1 and Exp. CCS-2). A larger difference, and a more accurate comparison of off-gas SO_2 concentrations from the lower and the higher pressure experiments, would be obtained by adjusting the concentrations for a common fluidizing-gas velocity of 1.07 m/s (velocity used for predictions in Fig. 8). The adjusted SO_2 concentrations could then be compared with the results in Fig. 8.

During the regeneration step of the sixth utilization cycle of the cyclic experiments (reported in a following section of this report), an additional experiment (CCS-6A) was performed at a reduced pressure, 125 kPa instead of 153 kPa (CCS-6). The experimental conditions and results for both of these experiments are also presented in Table 2. As a result of lowering the system pressure by ∿20% while maintaining the fluidizing-gas velocity almost constant (∿1.2 m/s), the SO_2 concentration in the dry off-gas increased by ∿20% from 8.7% to 10.4% (the highest SO_2 enrichment obtained to date). The SO_2 concentration in the off-gas increased because of less dilution at the reduced pressure.

Relatively high SO_2 concentrations (∿8%) have also been reported by Gordon *et al.*[7] for the regeneration of limestone at atmospheric pressure. Although the number of experiments in this evaluation was limited and the pressure variation was small, the system pressure was found to have a negligible effect on the rate of CaO regeneration because the SO_2 concentration in the

Table 2. Effect of Regeneration Pressure on the Regeneration of Tymochtee Dolomite and the SO_2 Concentration in the Off-Gas

Nominal fluidized-bed height: 46 cm
Reactor ID: 10.8 cm
Temperature: 1100°C
Reducing gas concentration in off-gas: 3.0-3.2%
Coal: Triangle coal (0.98 wt % S)
Sorbent: -14 +30 mesh, sulfated dolomite in the second (10.7 wt % S) and sixth (9.3 wt % S) utilization cycles.

Exp.	Pressure, kPa	Fluidizing Gas Velocity, m/s	Solids Residence Time, min	CaO Regeneration,[a] %	SO_2 Concentration in Dry Off-Gas, %[b] / %[c]	Minor Sulfur Compounds in Off-Gas, %		
						H_2S	COS	CS_2
CCS-2A	115	1.35	8.8	78	8.9/11.2	0.03	0.1	0.1
CCS-2B	115	1.41	7.4	69	9.5/12.5	0.04	0.1	0.1
CCS-2C	118	1.44	5.3	57	9.6/12.9	-	-	-
CCS-2	153	1.26	7.5	67	8.6/10.1	0.02	0.1	0.1
CCS-6A	125	1.22	7.5	73	10.4/11.9	0.03	0.1	0.1
CCS-6	153	1.18	7.8	75	8.7/ 9.6	0.03	0.2	0.1

[a] Based on chemical analysis of dolomite samples.
[b] Measured SO_2 concentration.
[c] Adjusted SO_2 concentration based on a constant fluidizing-gas velocity of 1.07 m/s.

off-gas was not near equilibrium. However, pressure has been found to affect the SO_2 concentration in the off-gas via the extent of dilution.

e. Formation of CaS

The sulfated dolomite, before regeneration, contained negligible amounts of CaS. The buildup of CaS during regeneration of Tymochtee dolomite for all experiments, including those performed at 1000°C, was found to be $\leq$0.1% wt % (S^{2-}). The investigated ranges of temperature, solids residence time, and system pressure had no significant effect on the buildup of CaS because of the existence of an oxidizing zone at the bottom of the fluidized bed, as discussed by Montagna *et al.*[4] The CaS formed in the reducing zone is oxidized in the oxidizing zone to either CaO or $CaSO_4$.

$$CaS + 2O_2 \rightarrow CaSO_4 \tag{5}$$

$$CaS + 3/2\ O_2 \rightarrow CaO + SO_2 \tag{6}$$

The beneficial effect of an oxidizing zone on minimizing the buildup of CaS has also been observed by Hoke *et al.*[5] and Swift and Wheelock.[8]

3. PDU Regeneration Rate Experiments with Greer Limestone

[J. Montagna (Principal Investigator), F. F. Nunes, G. Smith, R. Beaudry, and R. Mowry]

The dependence of (1) CaO regeneration and (2) SO_2 concentration in the regenerator off-gas on key variables such as regeneration temperature and solids residence time in the fluid bed reactor was studied for once-sulfated Greer limestone to aid in optimizing the regeneration process conditions for the limestone.

A series of regeneration experiments with Pope, Evans and Robbins (PER) sulfated Greer limestone was performed earlier at regeneration temperatures of 1050°C and 1100°C. Some of these results have been discussed and compared to similar results for Tymochtee dolomite in ANL/ES-CEN-1016. The rest have not been reported because of inconsistencies in the results which are believed to be due to (1) inconsistency (limestone type) in the (PER) delivered sulfated limestone batches and (2) the uncertainty of the history (*e.g.*, salt added or not) during sulfation.

Consistent regeneration rate data has been obtained in six new regeneration experiments in which the same batch of Greer limestone (which contained 7.7 wt % sulfur) was regenerated. This limestone has been sulfated during combustion of Sewickley coal in the ANL 6-in., PDU combustor (no salt added). The experiments were performed at 1050°C and 1100°C; solids residence time in the reactor ranged from 7 to 23 min.

a. Effects of Solids Residence Time and Temperature on Extent of CaO Regeneration

The six new experiments were performed as a part of the regeneration step of the first cycle in the cyclic experiment with Greer limestone (reported in a following section) to determine the effects of solids residence time and temperature on the extent of CaO regeneration. The experimental conditions and results for these experiments are given in Table 3.

Table 3. Experimental Conditions and Results for the Regeneration of Greer Limestone by the Incomplete Combustion of Sewickley Coal in a Fluidized Bed

Nominal fluidized-bed height: ∿46 cm
Reactor ID: 10.8 cm
Pressure: 129 kPa
Coal: Sewickley (4.3 wt % S); ash fusion temperature (initial deformation) under reducing conditions: 1119°C
Sorbent: -14 +30 mesh sulfated limestone (7.7 wt % S)

Exp. No.	Bed Temperature, °C	Fluidizing-Gas Velocity, m/s	Feed Rate, kg/hr	Solids Residence Time, min	Reducing Gas Concentration in Effluent, %	CaO Regener., %[a] / %[b]	Major Sulfur Compounds in Dry Off-Gas, %			
							SO_2	H_2S	COS	CS_2
RGL-1A	1050	1.23	8.2	22.54	3.2	72.2/83.0	3.3	0.09	0.07	0.06
RGL-1B	1050	1.21	15.4	11.93	2.9	43.1/53.3	3.7	0.09	0.08	0.05
RGL-1C	1050	1.21	26.3	6.99	3.4	28.3/27.3	4.3	0.05	0.1	0.05
RGL-1D	1100	1.23	9.1	20.28	3.2	79.5/92.0	3.9	0.2	0.1	0.05
RGL-1E	1100	1.23	15.9	11.59	3.3	72.3/82.8	6.0	0.1	0.1	0.03
RGL-1F	1100	1.29	25.9	7.12	2.9	66.9/70.9	8.4	0.06	0.09	0.02

[a] Based on flue-gas analysis.
[b] Based on chemical analyses of limestone samples.

The extent of regeneration values are plotted in Fig. 9 as a function of solids residence time for two temperatures, 1050°C and 1100°C. At 1050°C, when the solids residence time was decreased from 22.5 min to 7.0 min, the extent of regeneration decreased from 83% to 27% (based on solids analyses). At 1100°C, the extent of regeneration decreased from 92 to 71% when the solids residence time was decreased from 20 min to 7.1 min. The regeneration rate is higher at 1100°C, and therefore the conversion ratio of $CaSO_4$ to CaO was less affected by a decrease in reactor particle residence time. With a residence time of 7 min, the extent of regeneration was still considerable, ∿70%.

A "best fit" equation has been obtained by regression analysis for the experimental extent of CaO regeneration as a function of regeneration temperature and solids residence time. A similar analysis performed earlier on regeneration rate data for Tymochtee dolomite was reported above. The equation for the Greer limestone regeneration rate is

$$\ln (1 - R) = A \cdot \tau + B \cdot \tau^2 \qquad (1)$$

where

R = extent of CaO regeneration ($R = 1$ for complete regeneration)
τ = solids residence time (reactor particle contact time)
$A \times 10^2 = -12.4T - 3.98$ (2)
$B \times 10^3 = 3.25T - 1.24$ (3)
$T = (t - 1050)/50$
t = regeneration temperature, °C

The values calculated by the model equation (Eq. 1) compare favorably with the experimental results. A correlation coefficient of ∿0.97 was obtained for the experimental data and the results predicted from the model equation. Therefore, Equation 1 is a good mathematical model of the dependence of CaO regeneration in Greer limestone on temperature and solids residence time for the investigated experimental range. These best fit results for Greer limestone are compared with results for similar experiments with Tymochtee dolomite

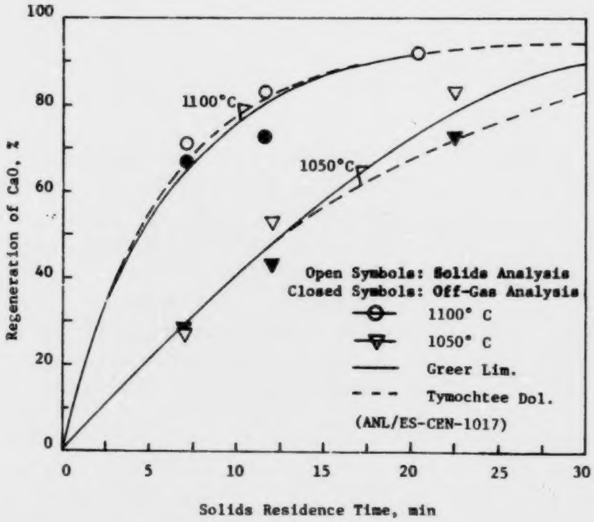

Fig. 9. Regeneration of CaO in Greer Limestone as a Function of Solids Residence Time and Regeneration Temperature

in Fig. 9. The regeneration rates for these two sorbents compare very favorably. This relationship for the rate of CaO regeneration will be used in the model for the regeneration process to optimize the design process conditions and to scale up sorbent regeneration systems.

b. Effect of Solids Residence Time and Temperature on SO_2 Concentration in the Off-Gas

In the fluidized-bed regeneration process, the SO_2 concentration in the off-gas is determined by (1) the feed rate of $CaSO_4$ to the regenerator reactor (solids residence time and sulfur content of sulfated sorbent), (2) the extent of regeneration of CaO, and (3) the gas flow rate through the reactor.

In this series of regeneration experiments, a single batch of sulfated limestone (containing 7.7 wt % sulfur) was used, and the fluidizing-gas velocity was varied from 1.21 to 1.29 m/s (a small variation). The gas flow rate through the reactor was not affected greatly by the fluidizing gas velocity in the experiments. Therefore, the variation of SO_2 concentration in the dry flue gas was due to the mass rate of CaO regeneration.

The experimentally obtained SO_2 concentrations in the dry off-gas are plotted in Fig. 10. At 1050°C, the SO_2 concentration increased from 3.3% to 4.3% as the solids residence time decreased from 22.5 min to 7.0 min (*i.e.*, as the sulfated-sorbent feed rate increased). At 1100°C, the SO_2 concentration in the dry off-gas increased from 3.9 to 8.4% as the solids residence time decreased from 20.3 min to 7.1 min. At the longest solids residence time (>20 min), the SO_2 concentration was found to be only slightly higher at the higher temperature. With this long reaction time, most of the CaO was regenerated at both temperature levels and hence the SO_2 concentration in the off-gas was dependent on the $CaSO_4$ feed rate. For the shorter reaction time (7 min), the SO_2 concentration was much higher at the higher temperature (1100°C) due to the higher rate of CaO regeneration.

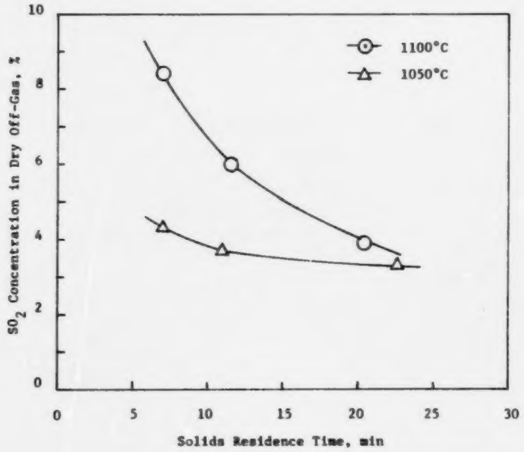

Fig. 10. Experimental SO_2 Concentration for the Regeneration of Greer Limestone as a Function of Solids Residence Time and Temperature. Pressure: 129 kPa; fluidizing-gas velocity: 1.21-1.29 m/s; limestone sulfur content: 7.7 wt %

c. Effect of System Pressure during Sulfation on the Reactivity of Greer Limestone

The effect of system pressure on the reactivity of Greer limestone has been evaluated using the ANL 6-in.-dia combustor. One experiment (SGL-1, the first cycle in the cyclic experiments discussed in a following section) was performed at a system pressure of 308 kPa and a bed temperature of 855°C, and the other (Greer-2C) at 610 kPa and 855°C. The results are given in Table 4.

In the 308-kPa experiment, at a Ca/S mole feed ratio of 2.9, a sulfur retention of ∿84% was obtained (656 ppm SO_2 in the dry flue gas). This is slightly higher than the 78% retention obtained at the same CaO/S mole feed ratio by Pope, Evans and Robbins[9] at 100 kPa (1 atm) and a higher fluidizing gas velocity (>3 m/s). The ratio of the CO_2 partial pressure (∿16% CO_2 in the dry flue gas) in the flue gas to the equilibrium CO_2 pressure at 855°C was 0.78. The ratio of moles of CO_2 to moles of CaO in the sulfated limestone product was 0.03, indicating that the limestone was fully calcined during this experiment.

At the Ca/S mole ratio of 3.2 used in the 610 kPa (6 atm) experiment, the sulfur retention was 85.5% (575 ppm of SO_2 in the dry flue gas). The ratio of CO_2 partial pressure in the flue gas to the equilibrium CO_2 pressure at 855°C was 1.5. Since the ratio of moles of CO_2 per mole CaO in the sulfated limestone product was 0.49, considerable calcination did occur. Although this extent of calcination was unexpected, the results are not surprising because the high CO_2 concentration in the flue gas is present only near the top of the fluid bed. Near the bottom of the fluidized bed, the CO_2 concentration in the gas bed is negligible and therefore calcination is expected to occur there. The CaO/S ratios required to achieve a constant sulfur retention in the two ANL experiments listed in Table 4 are very similar, which suggests that there was no noticeable effect of pressure on the reactivity of limestone. On the basis of findings reported by Westinghouse[10] on the effect of the ratio of CO_2 partial pressure to equilibrium CO_2 pressure during calcination at atmospheric pressure, it was expected that the reactivity in the lower-pressure experiment (SLG-1) would be higher. However, as mentioned above, the conditions are not constant throughout the fluidized bed, and hence the degree of calcination cannot be controlled. To enhance the reactivity of the limestones, calcination should be performed in a separate reactor where the optimum calcination conditions can be maintained.

4. Characterization of Causes of Defluidization during Regeneration

[J. Montagna (Principal Investigator), F. F. Nunes, G. Smith, R. Beaudry, and R. Mowry]

In the development of a sorbent regeneration process, an understanding of the process by which a fluid bed agglomerates is necessary so that agglomeration may be controlled. During sulfation of sorbent (combustion step), some coal ash is retained in the fluidized bed and is removed with the sulfated sorbent. It is believed that in agglomeration in the fluid bed during regeneration, coal ash is a contributor to initial coalescing of particles, which is followed by loss of fluidity in the fluidized bed and by

Table 4. Operating Conditions and Flue-Gas Compositions during the Sulfation of Greer Limestone with Sewickley Coal. Combustion at Two Operating Pressures

Combustor: ANL, 6-in. dia
Coal: Sewickley, -8 mesh, 4.3 wt % S
Sorbent: Greer limestone, -14 +30 mesh

Temperature: 855°C
Excess air: ∿17%
Nominal bed height: 0.9 m
Nominal gas velocity: 1.0 m/s

Combustion Exp.	System Pressure, kPa	Feed Rate, kg/hr		CaO/S Mole Ratio	Flue-Gas Analysis (avg. values)		Sulfur Retention, %[b] / %[c]	Calcium Utilization, %	Moles of CO_2/ Mole of CaO in spent limestone
		Coal	Sorbent		SO_2, ppm	O_2, %			
SGL-1	308	6.36	3.38	2.9	656	3.0	83.6/84.8	29.6	0.03
Greer-2C	610	12.68	6.42	3.2	575	3.0	85.5/87.3	31.7	0.49

[a] EPA standard for Sewickley coal is ∿635 ppm.

[b] Based on flue-gas analysis.

[c] Based on solids analysis.

increases in local temperatures. At these high local temperatures (>1100°C), the bed agglomerates; reactions occur that form calcium silicates and calcium-aluminum silicates.

A statistical experiment designed to study defluidization characteristics (agglomeration) has been carried out in the PDU regeneration system. Sulfated Greer limestone (from Pope, Evans and Robbins) and Sewickley coal were used in the investigation. The effects of (1) regeneration temperature, (2) particle size distribution of the sulfated sorbent, and (3) total reducing gas concentration (CO, H_2, and CH_4) in the off-gas on the defluidization velocity (minimum velocity required to prevent agglomeration) were determined.

a. Experimental Design and Procedure

The statistical experiment consisted of a full 2^3 factorial design. The three variables and their corresponding design levels were: regeneration temperature (1050°C and 1100°C), feed sorbent particle size (-10 +30 mesh and -14 +30 mesh), and total reducing gas concentration in the off-gas (2.5% and 5.0%). The effects of these variables on the minimum gas velocity required to prevent agglomeration (defluidization velocity, V_d) were studied. This velocity (V_d) is greater than the conventional minimum fluidization velocity of a similar nonsticky particle system. The effect of stickiness of bed material on the tendency of a fluidized bed to defluidize and agglomerate has been previously described by Gluckman *et al.*[11]

Each defluidization experiment was begun by starting with a fluidizing-gas velocity of ∿2.0 m/s. The other design conditions remained constant. The velocity was decreased in increments of ≤0.15 m/s every 30 min until the bed defluidized. Defluidization and agglomeration were indicated by a decrease in the pressure drop through the fluidized bed and the formation of a vertical temperature gradient in the fluid bed, as illustrated in Fig. 11. The regenerated sorbent samples taken just prior to agglomeration in each experiment were saved and are being sized.

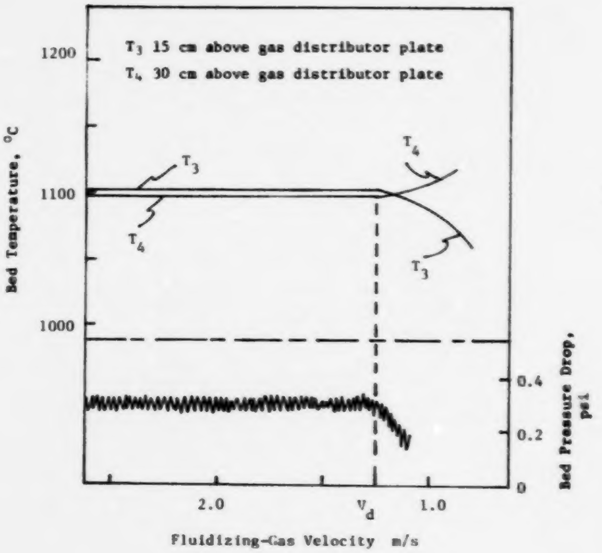

Fig. 11. Qualitative Plot of Bed Temperature and Pressure Drop as a Function of Fluidizing-Gas Velocity for a Defluidization Experiment. Bed height: 46 cm.

b. Effect of Operating Variables on Defluidization Velocity

The experimental conditions and results for this series of experiments are presented in Table 5. The lowest defluidization velocity (V_d = 0.88 m/s) was obtained in AGL-5, using the smaller feed particles (-14 +30 mesh), the lower temperature (1050°C), and the lower reducing gas concentration (2.5%) in the off-gas. The highest defluidization velocity (V_d = 1.56) was obtained in AGL-4 with the larger feed particles (-10 +30 mesh), the higher temperature (1100°C), and the higher reducing gas concentration (5.0%) in the off-gas. Higher temperature and higher reducing gas concentration probably cause the sulfated particles (containing 5-10% coal ash) to become sticky so that a higher fluidizing gas velocity is required to overcome the adhesive forces between particles and prevent defluidization. There are two possible reasons for particle size affecting the defluidization velocity: The minimum fluidization velocity of large particles is higher, and more kinetic energy must be imparted to larger particles to overcome their adhesive forces.

Table 5. Defluidization during Regeneration--Experimental Conditions and Results of the Full 2^3 Factorial Experiment

Nominal fluidized-bed height: ∿46 cm
Sorbent residence time: ∿25 min
Reactor ID: 10.8 cm
Pressure: 129 kPa (4 psig)
Coal: Sewickley (4.3 wt % S), nominal (-12 +100 mesh); ash fusion temperature (initial deformation) under reducing conditions: 1119°C
Sorbent: Regenerated Greer limestone

	Variables			Response
Exp.	Temp, °C	Mean Feed Sorbent Size, μm	Total Reducing[a] Gas Conc. in Off-Gas, %	Defluidization Velocity, m/s
AGL-1	1050	1271[b]	2.5	1.19
AGL-1-1R	1050	1271	2.5	1.02
AGL-1-2R	1050	1271	2.5	0.99
AGL-2	1100	1271	2.5	1.24
AGL-3	1050	1271	5.0	1.15
AGL-4	1100	1271	5.0	1.56
AGL-5	1050	969.2[c]	2.5	0.88
AGL-6	1100	969.2	2.5	0.96
AGL-7	1050	969.2	5.0	1.01
AGL-8	1100	969.2	5.0	1.51

[a] Combined concentrations of CO, H_2, and CH_4.
[b] Nominal -10 +30 mesh.
[c] Nominal -14 +30 mesh.

A requirement of a sorbent regeneration process is that an off-gas with a high SO_2 concentration ($\sim$10% SO_2) must be obtained to reduce the economic burden of a sulfur recovery system. The detrimental effect of a high fluidizing-gas velocity on the extent of SO_2 dilution has been discussed, along with previous ANL regeneration results.[12]

c. Analysis of Variance for Defluidization Velocity

An analysis of variance for the defluidization velocity is presented in Table 6. The regeneration temperature and the total reducing gas concentration were found to significantly affect the defluidization velocity (V_d) with the F-test for significance at the $\alpha = 0.1$ level (90% confidence level). The effect of the feed particle size on the defluidization velocity was found not to be significant at the $\alpha = 0.1$ level; however, it was significant at $\alpha = 0.15$.

The validity of this analysis depends upon the absence of interactions between the controlled variables. For a 2^3 factorial experimental design, the model equation is expressed by:

$$X_{ijk} = \mu + \alpha_i + \beta_j + \gamma_k + I_{ij} + I_{ik} + I_{jk} + I_{ijk} + \varepsilon_{ijk}$$

where X_{ijk} is the observed response; μ is the mean of all possible responses; α_i, β_j, and γ_k are the treatment effects for the three controlled variables; I_{ij}, I_{ik}, I_{jk}, and I_{ijk} are the interaction effects between the controlled variables; and ε_{ijk} is the error between the observed and the expected response.

The analysis of variance for a factorial experiment design with partial replication cannot estimate the separate effects of the interaction terms I_{ij}, I_{ik}, I_{jk}, and I_{ijk}. These interaction effects are included in the term ε_{ijk}. In addition to inflating the error mean square, the presence of interactions can give misleading results in F-tests for significance. Comparing the error mean square (0.01576) with the variance (0.004634) calculated from replicate experiments AGL-1, AGL-1-1R, and AGL-1-2R gives an indication of the extent to which interaction effects have inflated the error mean square. Since both of these values are estimators for σ^2 (the true variance of the response data), the difference tends to indicate the presence of interactions between the controlled variables. Thus, the lack of significance (at $\alpha = 0.1$) for feed particle size on the defluidization velocity (indicated above) is possibly in error. Experimental results (AGL-1 *vs* -5, AGL-2 *vs* -6, *etc.*) do suggest an effect of feed particle size on the defluidization velocity.

d. Regression Analysis for Defluidization Velocity

A best fit relation for defluidization velocity (V_d) as a function of regeneration temperature, mean feed sorbent particle size, and total reducing gas concentration in the effluent from the regeneration fluid-bed reactor was obtained by using least-squares techniques

$$V = 4.05 - 3.61 \times 10^{-3}T - 2.62R + 2.54 \times 10^{-3}TR + 5.26 \times 10^{-4}F \quad (4)$$

Table 6. Analysis of Variance for Defluidization Velocity Data from the AGL Series of Experiments

Source of Variation	Degrees of Freedom	Sum of Squares	Mean Square	Calculated F_e[a]	$F_{1-\alpha}$[b]
Temperature	1	0.17701	0.17701	11.23	4.54
Feed Particle Size	1	0.04961	0.04961	3.15	4.54[c]
Reducing Gas	1	0.15401	0.15401	9.77	4.54
Error	4	0.06305	0.01576		
Corrected Total	7	0.44368			

[a] The term F_e = ratio of variable mean square to error mean square
[b] For $\alpha = 0.1$ (90% confidence level).
[c] For $\alpha = 0.15$, the value of $F_{1-\alpha}$ is 3.15.

where V_d = defluidization velocity, m/s
T = operating temperature, °C
R = total reducing gas concentration, %
F = mean particle size of feed sorbent, μm

Based on the analysis of variance and examination of scatter plots of the data, it was decided to include a term (TR) for the interaction between temperature and reducing gas concentration in the regression model. This greatly improved the agreement of the model equation, Equation 4, with the experimental results. In the absence of the interaction term, TR, a comparison of regression model results with observed experimental values shows that the coefficient of determination (R^2) is only 0.83. Equation 4, in contrast, has a coefficient of determination of 0.95.

By use of the model equation obtained (Eq. 4) for defluidization velocity, the minimum operable fluidizing gas velocity ($>V_d$) at which industrial (or Rivesville) sorbent regeneration process reactors can be operated without defluidization and agglomeration of the fluid bed can be predicted. Predicted defluidization velocities for a reductive decomposition regeneration process are given in Table 7. (The predictions for a 1500-μm mean feed sorbent particle size are applicable to a regeneration process at Rivesville.) The effect of predicted minimum operable fluidizing-gas velocity on the maximum expected concentration of SO_2 in a regeneration process off-gas and its effect on the economic burden of a sulfur recovery system will also be evaluated and reported.

Additional agglomeration experiments will be performed to evaluate the effects on defluidization velocity of (1) using different coals (including one with a high ash fusion temperature), (2) using a higher regeneration temperature (1150°C), and (3) extensive buildup of an ash layer on the sorbent particles (dolomite from the tenth utilization cycle).

Table 7. Calculated Defluidization Velocities (V_d, m/s) at Different Bed Temperatures, Reducing Gas Concentrations, and Bed Particle Sizes for the Regeneration Process

Reducing Gas Concentration, %	V_d, Defluidization Velocity, m/s 1050°C	1075°C	1100°C
Mass Mean Particle Diameter, 1500 μm[a]			
2	1.14	1.18	1.22
3	1.19	1.29	1.39
4	1.24	1.40	1.56
5	1.28	1.51	1.74
Mass Mean Particle Diameter, 1000 μm			
2	0.88	0.92	0.95
3	0.93	1.03	1.13
4	0.97	1.14	1.30
5	1.02	1.25	1.47

[a] Approximate mean particle size of feed limestone that will be used at the Rivesville pilot plant.

5. Cyclic Sorbent Life Studies with Tymochtee Dolomite

[J. Montagna and W. Swift (Principal Investigators), F. F. Nunes, G. Smith, G. Teats, H. Lautermilch, R. Mowry, S. Smith, C. Schoffstoll, and J. Stockbar]

The feasibility of sorbent regeneration technology will depend on the ability to recycle the sorbent a sufficient number of times (1) without loss of its reactivity for either sulfation or regeneration and (2) without severe decrepitation. Unless both of these requirements are met, the sorbent makeup rate will be so high that in comparison with the fresh sorbent requirements and spent sorbent waste disposal for a once-through FBC process, regeneration may not be economically justified.

Two ten-cycle sorbent utilization experiments were performed, therefore, with no fresh sorbent makeup to evaluate: the changes in reactivity (sulfur acceptance during combustion), the changes in regenerability (sulfur release during regeneration), the extent of decrepitation, and the extent of coal ash buildup as a function of utilization cycle. This section presents the results of the ten-cycle sorbent-life study performed with Arkwright coal and Tymochtee dolomite. (The results of the ten-cycle sorbent life study performed with Sewickley coal and Greer limestone at 308 kPa pressure during the combustion steps are presented in the following section.)

Since the processing capacity of the ANL PDU regenerator is much greater than that of the combustor (by almost a factor of ten), the sorbent could not be continuously recycled between the reactors. Thus, the sulfation and regeneration experiments were performed batchwise.

a. Experimental Conditions

The combustion experiments in each utilization cycle were performed at a 900°C bed temperature, 810 kPa pressure, 1.5 CaO/S mole ratio (ratio of unsulfated calcium in sorbent to sulfur in coal), ∿17% excess combustion air, 0.9 m/s fluidizing-gas velocity, and a 0.9 m bed height.

The operating conditions during the regeneration step of each cycle were a nominal system pressure of 158 kPa, a bed temperature of 1100°C, and a fluidized-bed height of ∿46 cm. The required heat and reductants for regeneration were provided by incomplete combustion of Triangle coal.

b. Sulfur Acceptance during Combustion

Representative steady state operating conditions and flue-gas composition data for the ten combustion cycle experiments are presented in Table 8. The level of sulfur dioxide in the flue gas and the corresponding sulfur retention based on the flue gas analysis for all ten combustion cycles are graphically presented in Fig. 12.

Sulfur dioxide levels in the gas increased from ∿300 ppm in cycle 1 to ∿950 ppm in cycle 10. This represents a decrease in sulfur retention from ∿88% in cycle 1 to ∿55% in cycle 10. Although there is some scatter in the data, it appears that the reactivity of the sorbent for sulfur retention decreased linearly with combustion cycle over the 10-cycle experiment.

c. Sulfur Release during Regeneration

The experimental conditions and results for a representative segment of each regeneration step are given in Table 9.

In the ten regeneration experiments, solids residence times ranged from 6.8 to 8.1 min. The extent of CaO regeneration based on solids analysis varied from 67 to 80%, with no apparent loss in regenerability over the ten utilization cycles.

The SO_2 concentration in the dry off-gas from the regenerator varied from 8.8% to 6.1%. In the first cyclic regeneration experiment (CCS-1), the SO_2 was diluted by gas used to obtain the fluidizing-gas velocity of 1.43 m/s (other experiments were done at <1.26 m/s). In the three final cyclic regeneration experiments, the lower SO_2 concentrations in the regeneration reactor off-gas were a result of the lower sulfur concentration in the sulfated sorbent (7.1-7.9 wt % S instead of ∿10% S). Although the combustion steps of these cyclic experiments were performed with a constant CaO/S mole ratio of ∿1.5 with no virgin sorbent makeup, the total sulfur content of the sulfated sorbent decreased in each cycle due to lowered sulfation reactivity of the sorbent.

d. TGA Sulfation Experiments

To further test the reactivity of the sorbent for sulfation, samples of the sorbent from each regeneration half-cycle experiment were sulfated in a TGA apparatus at 900°C, using a reactant gas containing 0.3% SO_2, 5% O_2, and

Table 8. Operating Conditions and Flue-Gas Compositions for Combustion Step of Cyclic Experiments

Combustor: ANL, 6-in. dia
Coal: Arkwright, -14 mesh, 2.8 wt % S
Sorbent: Cycle 1, Tymochtee dolomite, -14 +30 mesh
Cycles 2-10, Regenerated Tymochtee dolomite

Temperature: 900°C
Pressure: 810 kPa
Excess air: ∿17%
Nominal bed height: 0.9 m
Nominal gas velocity: 0.9 m/s

Combustion Cycle REC-	Additive Feed Analysis, wt %		Feed Rate, kg/hr		CaO/S Mole Ratio[a]	Flue-Gas Analysis (avg values)						Sulfur Retention, %[b] / %[c]
	Ca	S	Coal	Sorbent		SO_2, ppm	NO, ppm	CH_4, ppm	CO, ppm	CO_2, %	O_2, %	
1	20	-	14.6	4.1	1.6	290	200	32	90	16.0	3.4	88/81
2	30.7	4.7	13.3	2.8	1.5	400	120	30	40	15.5	3.1	82/79
3	29.7	4.6	13.5	2.9	1.5	490	130	(d)	20	16.0	3.2	78/86
4	29.6	6.0	13.3	3.2	1.5	450	120	30	45	16.0	3.2	79/66
5	29.0	5.2	13.3	3.4	1.6	600	100	31	55	16.6	3.3	72/64
6	28.3	4.2	13.2	3.0	1.5	600	105	21	40	17.0	3.0	72/66
7	28.8	3.1	13.4	2.6	1.4	680	97	47	59	16.1	2.7	69/61
8	28.7	3.2	12.6	2.6	1.5	810	94	43	40	16.2	2.8	61/57
9	27.0	3.0	13.0	3.1	1.6	770	104	49	56	16.5	3.1	63/52
10	25.8	3.4	13.3	3.0	1.4	950	94	49	64	15.9	2.9	55/50

[a] Ratio of unsulfated calcium in dolomite feed to sulfur in coal.
[b] Based on flue-gas analysis.
[c] Based on solids analysis.
[d] Analyzer inoperative.

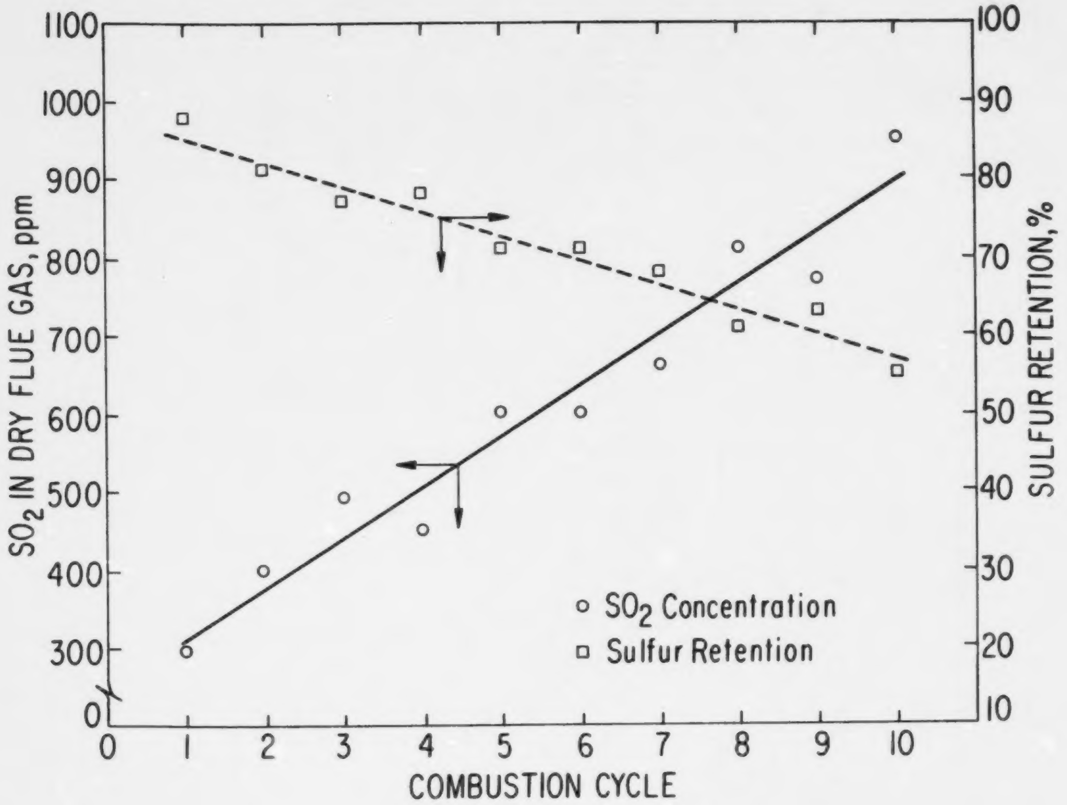

Fig. 12. Sulfur Retention in Bed and SO_2 Concentration in Flue Gas as a Function of Cycle Number

the balance N_2. The results of the experiments are shown in Figs. 13 and 14. Figure 13 gives the percent of the CaO in the regenerated samples converted to $CaSO_4$ as a function of time (*i.e.*, the rate of conversion) for all ten regeneration half-cycles. The numbers of the curves (2 through 10) correspond to the numbers of the corresponding combustion half-cycles, and curve 11 represents sulfation of regenerated material from cycle 10. With the exception of the curve corresponding to the fourth combustion cycle, the rate of conversion decreased from the second through the eleventh sulfation.

An interesting observation is that after the eighth sulfation cycle, the loss in reactivity with succeeding sulfation cycles is quite small. This indicates that the reactivity of the sorbent may level off in the higher sulfation cycles. This potential leveling-off of reactivity was not detected in the cyclic combustion-regeneration experiments performed in the PDU.

Figure 14 plots the utilization of the stones for each sulfation cycle as a function of time for the TGA experiments--*i.e.*, the extent of conversion. The starting point for each sulfation experiment is determined by the extent of regeneration during the preceding regeneration half cycle.

Table 9. Experimental Conditions and Results for the Regeneration Step of the Ten Utilization Cycles with Tymochtee Dolomite

Nominal fluidized-bed height: 46 cm
Reactor ID: 10.8 cm
Pressure: 153 kPa
Temperature: 1100°C
Coal: Triangle (0.98 wt % S), ash fusion temperature
(initial deformation under reducing conditions): 1390°C
Sorbent: -14 +30 mesh sulfated Tymochtee dolomite

Cycle No.	Expt. No.	Fluidizing Gas Velocity, m/s	Solids Residence Time, min	O_2 Conc in Feed Gas, %	Reducing Gas Concentration in Off-Gas, %	Sulfur Conc in Sulfated Sorbent, %	CaO Regeneration, %[a]/%[b]	Major Sulfur Compounds in Dry Off-Gas, %			
								SO_2	H_2S	COS	CS_2
1	CCS-1	1.43	7.0	26.7	2.8	9.0	73/71	6.5	0.04	0.06	0.04
2	CCS-2	1.26	7.5	37.9	3.0	10.7	67/67	8.6	0.02	0.1	0.1
3	CCS-3	1.22	7.2	36.7	3.4	10.3	63/76	8.4	0.07	0.1	0.1
4	CCS-4	1.17	7.8	36.5	2.9	9.9	67/69	8.1	0.04	0.1	0.1
5	CCS-5	1.17	7.4	36.1	3.0	9.5	69/75	8.8	--[c]	--[c]	--[c]
6	CCS-6	1.18	7.8	41.8	2.6	9.3	66/75	8.7	0.03	0.2	0.1
7	CCS-7	1.16	7.3	38.2	2.9	8.5	69/77	8.2	0.07	0.1	0.1
8	CCS-8	1.18	8.1	35.9	3.0	7.8	64/80	6.3	0.06	0.07	0.07
9	CCS-9	1.09	7.3	36.4	3.0	7.9	53/67	6.1	0.1	0.1	0.1
10	CCS-10	1.24	6.8	38.0	3.0	7.1	63/68	6.7	0.05	0.08	0.09

[a] Based on off-gas analysis.
[b] Based on chemical analysis of dolomite samples.
[c] Analysis not performed.

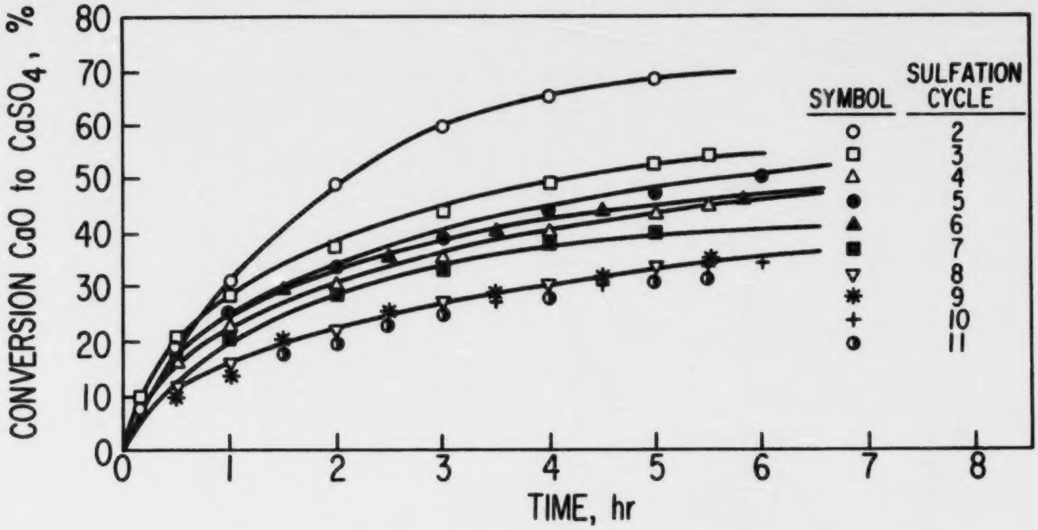

Fig. 13. Conversion of CaO to CaSO$_4$ as a Function of Time and Sulfation Cycle as Determined by TGA Sulfation Experiments. Temperature: 900°C; reaction gas: 0.3% S, 5.0% O$_2$, balance nitrogen.

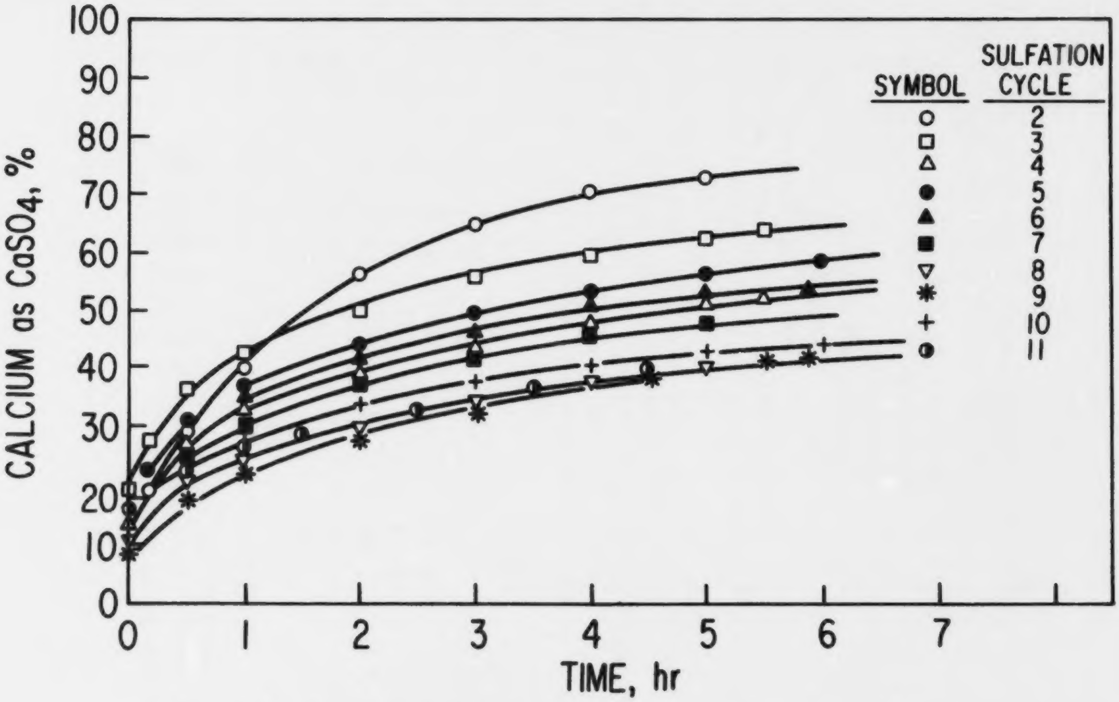

Fig. 14. Percent Calcium as CaSO$_4$ as a Function of Time and Sulfation Cycle as Determined by TGA Sulfation Experiments. Temperature: 900°C; reaction gas: 0.3% S, 5.0% O$_2$, balance nitrogen.

However, after sulfation for a period of several hours, the utilization of the stone decreases with sulfation cycle except for the inconsistency in the fourth-cycle sulfation data. Again, the attainable sorbent utilization appears to stabilize and become fairly constant at about the eighth combustion cycle.

e. Estimate of Sorbent Makeup Requirements to Meet EPA Sulfur Emission Limit

Based on the results of the cyclic combustion/regeneration experiments, an analysis was made to estimate the sorbent makeup rate which would be required in a continuous recycle operation to meet the EPA sulfur emission limit. The makeup rate is essentially determined by three factors: (1) the level of sulfur retention required, (2) the sorbent loss of reactivity with increasing number of utilization cycles, and (3) the sorbent recycle rate, which establishes the total CaO/S mole ratio during the combustion cycle. In this discussion, the term CaO/S mole ratio is used to emphasize that the mole ratio refers to the ratio of the available (unsulfated) calcium in the sorbent feed to the sulfur in the coal feed.

The analysis was based on the results obtained during the ten combustion experiments (REC-series experiments) in the cyclic combustion-regeneration study. Conditions assumed for the analysis were, therefore, a 900°C bed temperature, 810 kPa pressure, and a 0.9 m/s fluidizing-gas velocity. The analysis was also based on maintaining a sulfur retention of 75%, which is slightly above the ∿70% required to meet the EPA sulfur emission limit.

The two requirements for the analysis were: (1) to determine the utilization ("activity") of the sorbent at 75% sulfur retention as a function of sulfation cycle and (2) to derive an analytical expression for the age distribution (that is, the cycle number distribution) of the reactor charge at steady state as a function of makeup rate.

In order to establish the first requirement in the analysis, it was first necessary to determine the CaO/S mole ratio required as a function of utilization cycle to maintain a constant sulfur retention of 75%. During two of the combustion experiments (REC-7 and REC-8) in the cyclic combustion-regeneration study, the CaO/S ratio was intentionally increased sufficiently above 1.5 near the end of each experiment to bring sulfur retention to ∿75%. With this additional data, it was possible to determine the required CaO/S ratio as a function of cycle to maintain a constant sulfur retention of 75%. These results are illustrated in Fig. 15.

From the correlation of VAR-series* experimental results, the CaO/S ratio which would be required to achieve ∿75% retention during the first combustion cycle was calculated to be 1.0. From the correlation of the REC-series cyclic combustion experiments at a CaO/S ratio of 1.5, a sulfur

---

*A series of PDU experiments to study the effects of experimental conditions on SO_2 retention.

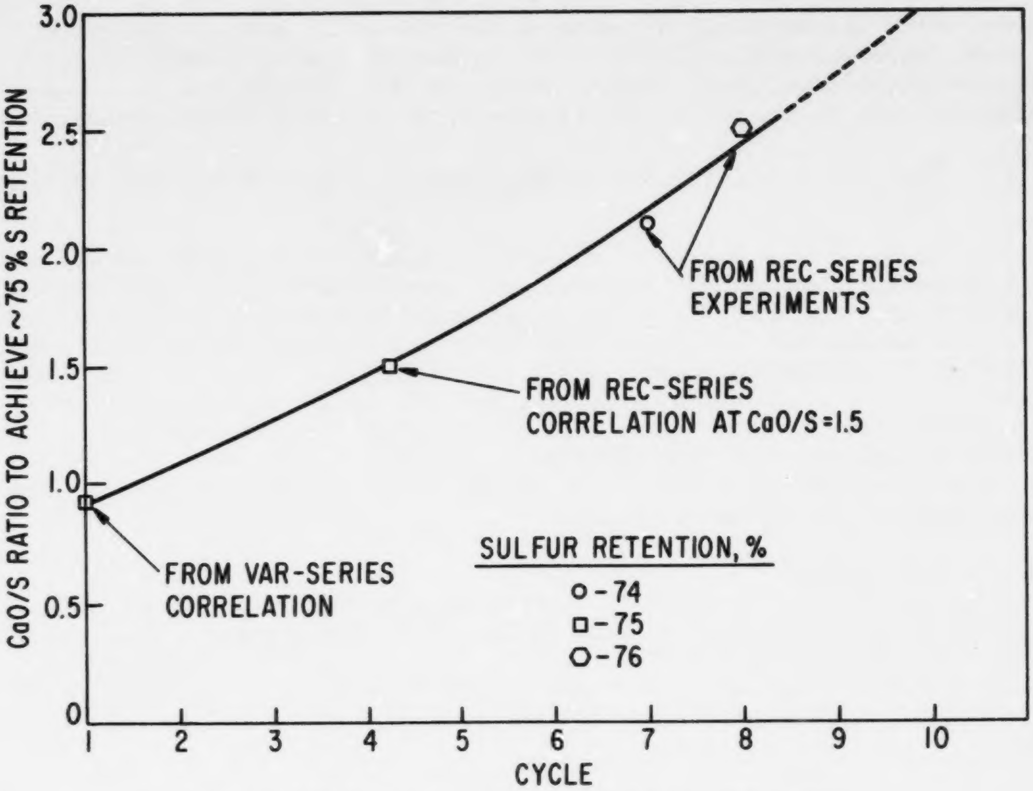

Fig. 15. CaO/S Ratio Required to Achieve 75% Sulfur Retention as a Function of Cycle

retention of 75% occurs during combustion cycle 4.2.[*] It was then experimentally determined that during combustion cycles 7 and 8, CaO/S ratios of 2.1 and 2.5 were required to achieve sulfur retentions of ~74 and ~76%, respectively. The resulting curve indicates that the CaO/S ratio required in the eighth cycle to maintain a constant sulfur retention of 75% was approximately two and one-half times that in the first cycle.

Zielke *et al.*[13] performed a similar cyclic combustion-regeneration study using Tymochtee dolomite at ~155 kPa. A comparison of the results of the two studies is given in Table 10. The results are obviously in very good agreement; CaO/S ratios reported by Zielke *et al.* to achieve ~80% sulfur retention were slightly higher than the ANL values of CaO/S to achieve ~75% retention.

---

[*] For purposes of correlation, a fractional combustion cycle such as 4.2 can be used to indicate a material which is less reactive than sorbent being sulfated for the fourth time and more reactive than sorbent being sulfated for the fifth time.

Table 10. Comparison of the Experimental Cyclic Sulfation Results Obtained at ANL with Those Reported by Zielke *et al.*[a] Tymochtee dolomite used in both studies.

Conditions	ANL	Zielke *et al.*[a]
Combustion		
Pressure, kPa	∿810	∿155
Temperature, °C	900	980
Excess Air, %	17	20
Gas Velocity, m/s	0.91	0.91
Sorbent Size, mesh	-14 +30	-14 +28
Solids Residence Time, hr	∿5	∿1.1
Regeneration		
Pressure, kPa	153	155
Temperature, °C	1100	1065
Gas Velocity, m/s	∿1.3	∿0.6
Solids Residence Time, min	∿7	108

Results	Cycle No. 1	2	3	4	5	6	7	8
ANL[b]								
Sulfur Retention, %	75	75	75	75	75	75	75	75
CaO/S Ratio	0.93	1.1	1.3	1.5	1.7	1.9	2.2	2.5
Zielke *et al.*[a]								
Sulfur Retention, %	79.3	80.4	80.2	78.7	77.6	79.3	80.6	N.D.[c]
CaO/S Ratio	0.95	1.4	1.9	1.9	2.2	2.3	2.6	N.D.

[a] Reference 13.

[b] Values obtained from Fig. 16.

[c] No data.

By the use of the correlation of Fig. 15, it was possible to calculate the utilization ("activity") of the sorbent at 75% sulfur retention as a function of sulfation cycle using the equation

$$U_n = \frac{0.75}{(CaO/S)_n} \tag{5}$$

where U_n = CaO utilization at 75% S retention for n*th* sulfation

$(CaO/S)_n$ = CaO/S mole ratio required for 75% sulfur retention during n*th* sulfation

The resulting correlation of the sorbent utilization at 75% sulfur retention with the sulfation cycle is graphically presented in Fig. 18. Utilization for a given sulfation cycle can be estimated from the equation for the straight line in Fig. 16,

$$U_n = 0.92e^{-0.14n} \tag{6}$$

where n is the sulfation cycle number.

The second requirement in the analysis was to develop an expression for the age distribution of the sorbent feed (recycle plus makeup) so that the fractional amount of the feed being sulfated for the n*th* time can be estimated. The approach taken was adapted from a procedure developed by Nagier[14] and is illustrated in Fig. 17.

In Fig. 17,

w_o = constant CaO makeup charged to each cycle
w_n = total CaO charged to the n*th* cycle, n = 1,2,...n
α = constant fraction of total charge rejected after each cycle (includes decrepitation losses, incomplete regeneration, and sorbent drawdown)

Therefore, $(1 - \alpha)$ represents the fraction of the CaO charged to each stage which is recycled (via the regeneration process) to the next stage. It can be easily shown that as $n \to \infty$, w_n converges to

$$\begin{aligned} w_n &= [1 + (1 - \alpha) + (1 - \alpha)^2 + \dots + (1 - \alpha)^{n-1}]w_o \\ &= w_o/\alpha \end{aligned} \tag{7}$$

where the fraction, g_n, of the total charge, w_n, being sulfated for the n*th* time is expressed as follows:

$$g_n = \alpha(1 - \alpha)^{n-1}, \; n = 1, 2, \dots, \infty \tag{8}$$

An equilibrium CaO utilization, U_{eq}, can then be calculated for 75% sulfur retention at steady state as

$$U_{eq} = \sum_{n=1}^{\infty} U_n g_n \tag{9}$$

From this result, the total CaO/S ratio at equilibrium can be calculated as

$$\text{Total CaO/S} = 0.75/U_{eq} \tag{10}$$

and the makeup CaO/S ratio as

$$\text{Makeup CaO/S Ratic} = (\text{Total CaO/S})\cdot\alpha \tag{11}$$

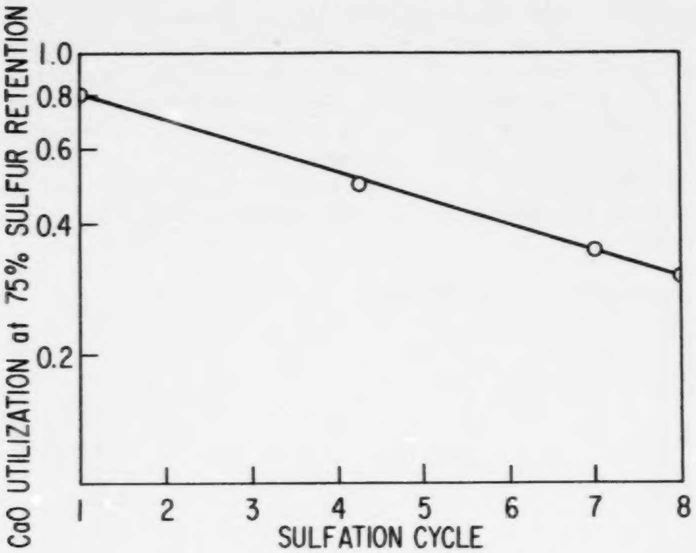

Fig. 16. CaO Utilization at 75% Sulfur Retention as a Function of Sulfation Cycle

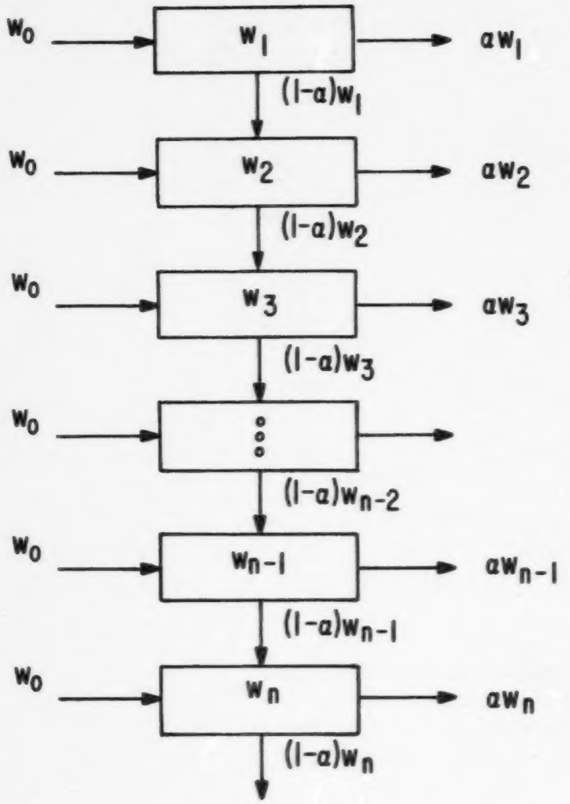
w_0
w_1
aw_1
$(1-a)w_1$
w_0
w_2
aw_2
$(1-a)w_2$
w_0
w_3
aw_3
$(1-a)w_3$
w_0
$(1-a)w_{n-2}$
w_0
w_{n-1}
aw_{n-1}
$(1-a)w_{n-1}$
w_0
w_n
aw_n
$(1-a)w_n$

Fig. 17. Recycle Mechanism to Approximate the Steady-State Distribution of Sorbent for a Continuous Combustion-Regeneration Process

The results of the analysis for U_n as given by Eq. 6 are presented in Fig. 18. As an example of using Fig. 18, if α (makeup CaO/total CaO) is 0.18, a makeup CaO/S ratio of ∿0.27 and a total CaO/S ratio of ∿1.5 are required for a sulfur retention of 75%. Decreasing α to 0.1 (10% makeup) reduces the makeup CaO/S ratio to ∿0.2 (a reduction of 25%) but increases the total CaO/S required to 2.0 (an increase of 33%). In comparison to the once-through CaO/S ratio of ∿1.0 for 75% sulfur retention, the makeup of 0.2 for a cyclic process corresponds to an estimated savings in quantity of limestone needed of ∿80%.

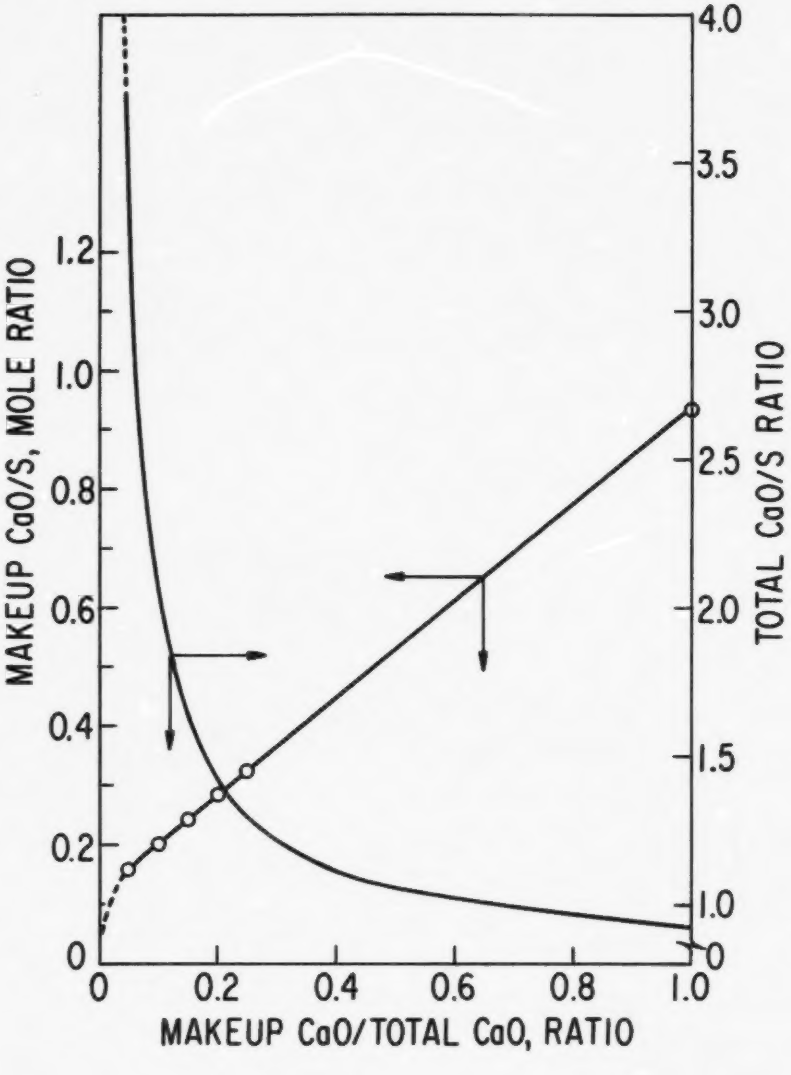

Fig. 18. Calculated Makeup and Total CaO/S Ratios Required to Achieve 75% Sulfur Retention as a Function of the Makeup CaO to Total CaO Ratio. Sulfation conditions: Temp, 900°C; Pressure, 810 kPa; Sorbent, Tymochtee Dolomite; Sulfur retention, 75%.

It should be emphasized, however, that the choice of α is not arbitrary. The value of α will affect both the process flow sheet and the system economics. For a thorough discussion of the effect of recycle rate, the reader is referred to a following section, "Regeneration Process Scale-up and Flowsheet Determination."

f. Porosity of Dolomite as a Function of Utilization Cycle

The porosity of -25 +30 mesh particles was measured by the mercury penetration method. The pore distributions of samples from cycles 2 and 10 are given in Fig. 19. The cumulative pore volume for pores $\geq$0.4 μm and also for pores $\geq$0.04 μm in sulfated and regenerated Tymochtee dolomite are given in Table 11. It has been reported by Hartman and Coughlin[15] that most sulfation takes place in larger pores ($\geq$0.4 μm) and that pores smaller than 0.4 μm are relatively easy to plug. During sulfation of CaO, the pores shrink as a result of molecular volume changes.

The porosity of sulfated dolomite was relatively unaffected by utilization cycle, although the sulfur content decreased from ∿10 wt % to ∿7 wt % (Fig. 19). However, the porosity of the regenerated dolomite consistently decreased with utilization, as did the sulfur content in the regenerated stones. The difference in porosity of the sulfated and regenerated samples decreased from ∿0.15 cm^3/g (pores $\geq$0.4 μm) after the first cycle to ∿0.07 cm^3/g after the tenth cycle. The porosity of regenerated dolomite decreased with cyclic use, and thus its effectiveness as an SO_2 acceptor decreased.

The loss of porosity in the dolomite could be due to (1) buildup of an ash layer around the particle or (2) high-temperature (1100°C) exposure during regeneration. At the regeneration temperature used, sintering begins, decreasing the reactivity by decreasing the beneficial porosity of the particles. This limits local diffusion and reaction of SO_2. The effect of porosity and reactivity of high-temperature exposure as a function of time is being evaluated for Tymochtee dolomite and will be reported.

g. Coal Ash Buildup during Utilization Cycles

The extent of coal ash buildup in the fluidized bed during coal combustion is of particular importance in evaluating its effect on (1) the SO_2-accepting capability of the sorbent in the subsequent combustion step and (2) the ash-sorbent agglomerating tendency in the regenerator reactor.

The ash buildups during all ten sulfation and regeneration steps have been calculated from wet chemical analyses (Si and Ca) of the sorbent product samples and are given in Table 12. As a basis for calculation, 100 g of virgin dolomite was used. The ash buildup was based on bulk silicon enrichment. The concentrations of silicon and the calculated coal ash buildups are plotted in Fig. 20. After ten utilization cycles with no fresh sorbent makeup, it has been found that for every 100 g of starting virgin dolomite, ∿13 g of coal ash accumulated in the sorbent. The silicon concentration increased from 2.1% in the virgin dolomite to 6.1% in the regenerated sorbent from the tenth cycle. The differences in the concentration of silicon

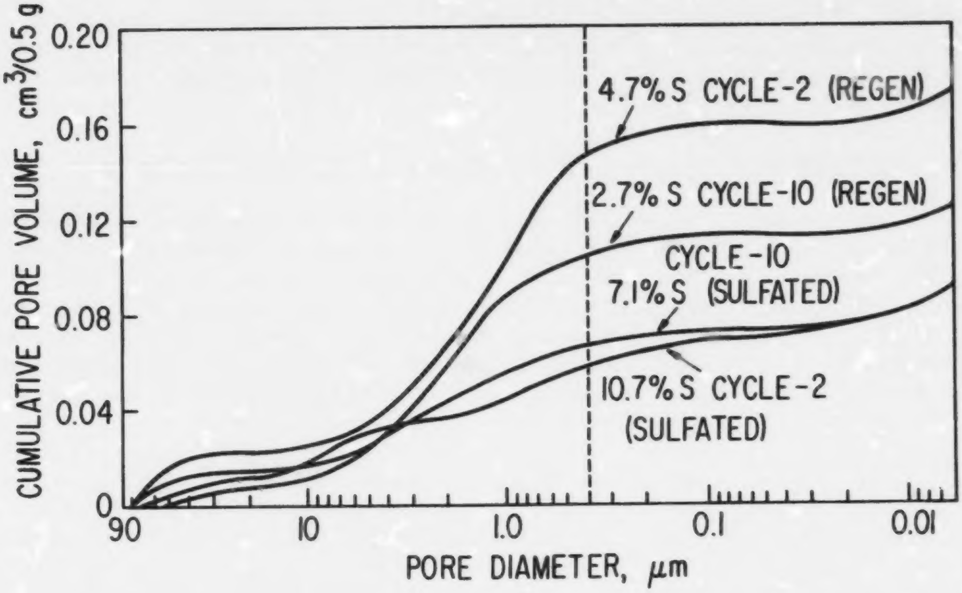

Fig. 19. Pore Distributions of Dolomite Samples from Cycles Two and Ten

Table 11. Porosity (cm^3/g) of Tymochtee Dolomite as a Function of Utilization Cycle

Cycle No.	Sulfated	Regenerated	Change, Δ
1	0.120[a]/0.164[b]	0.268[a]/0.340[b]	0.148[a]/0.176[b]
2	0.120 /0.212	0.288 /0.308	0.168 /0.096
4	0.120 /0.140	0.252 /0.276	0.132 /0.136
6	0.156 /0.164	0.244 /0.258	0.088 /0.094
8	0.144 /0.156	0.238 /0.260	0.094 /0.104
10	0.132 /0.140	0.204 /0.220	0.072 /0.080

[a] Pores ≥0.4 μm.
[b] Pores ≥0.04 μm.

in sulfated and regenerated samples are due to the weight loss of the sorbent during regeneration ($CaSO_4 \rightarrow CaO$). The calculations for ash buildups do not identify in which of the two process steps (sulfation or regeneration) most of the ash buildup occurred. However, it is believed that most of the ash buildup occurred during the sulfation step because the feed rate of fresh ash (in the coal) was ∿1 kg for every 3 kg of regenerated sorbent feed. In contrast, during regeneration, the feed rate of fresh ash (in the coal) was ∿1 kg for every 70 kg of sulfated sorbent feed.

Table 12. Calculated Coal Ash Buildup during Sulfation and Regeneration of Tymochtee Dolomite, Based on Enrichment of Silicon

Mass Basis: 100 g virgin Tymochtee dolomite
(20.0 wt % Ca and 2.14 wt % Si)

Cycle No.	Cycle Step	Si Conc., %	Ash Buildup wt %	Ash Buildup g ash / 100 g virgin dolomite
1	S[a]	2.68	0	0
1	R[a]	3.64	0	0
2	S	2.88	2.4	2.1
2	R	3.98	4.0	2.7
3	S	3.19	3.3	2.8
3	R	4.35	7.7	4.8
4	S	3.43	4.1	3.4
4	R	4.51	7.0	4.9
5	S	3.70	6.0	5.2
5	R	4.60	7.4	5.2
6	S	3.68	5.9	5.1
6	R	5.38	11.5	8.1
7	S	4.19	8.2	7.0
7	R	5.39	11.2	7.8
8	S	4.72	11.0	9.6
8	R	6.41	17.0	12.5
9	S	4.69	11.0	9.7
9	R	6.05	15.8	12.2
10	S	5.42	14.7	13.3
10	R	6.13	16.3	12.7

[a] S = sulfation step, R = regeneration step.

The coal ash buildup was also evaluated as a function of particle diameter in a regenerated dolomite sample from the tenth cycle. The results are plotted in Fig. 21. It was found that ash accumulation increased with the particle diameter of the sorbent. The (nominal) 1700 μm particles (+14 mesh) were made up of agglomerates of smaller particles which are each coated with coal ash. Thus the larger (+14 mesh) particles had more ash-coated surface than did the smaller particles.

Sulfated and regenerated dolomite particles from the first, fifth, and tenth utilization cycles were examined for macrofeatures under a low-magnification microscope. Photomicrographs of these samples are given in Figs. 22 and 23. The photomicrographs reveal that even the once-sulfated stones were beginning to be coated with what is believed to be coal ash. Particles from the tenth cycle (Fig. 23) appear to be completely coated with ash. The coating can be more readily seen in color photographs. The cause of the ash blisters is uncertain; however, their presence is probably beneficial in that they expose reactive CaO in the particles.

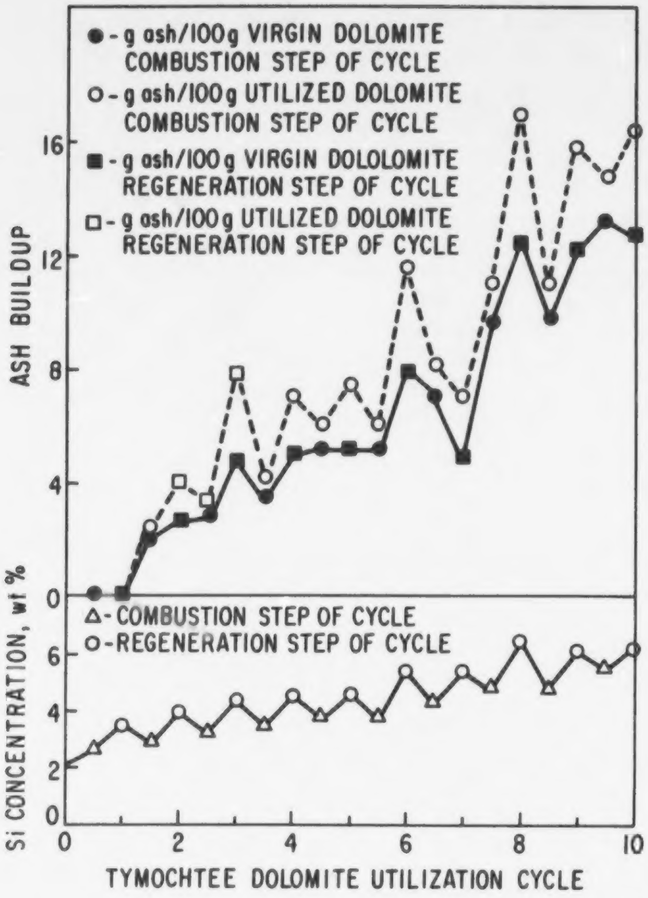

Fig. 20. Coal Ash Buildup as a Function of Utilization Cycle

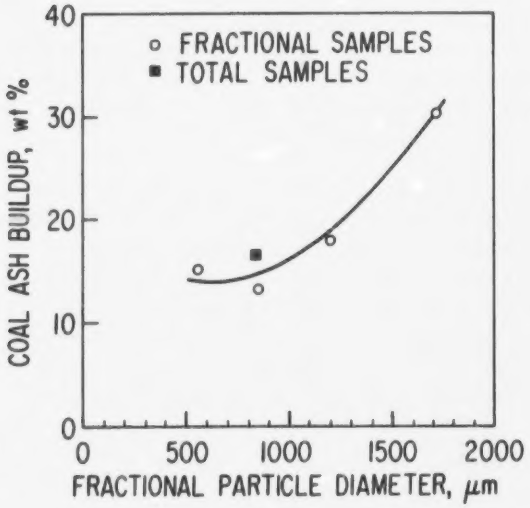

Fig. 21. Coal Ash Buildup as a Function of Particle Diameter in Tenth Cycle Regenerated Particles

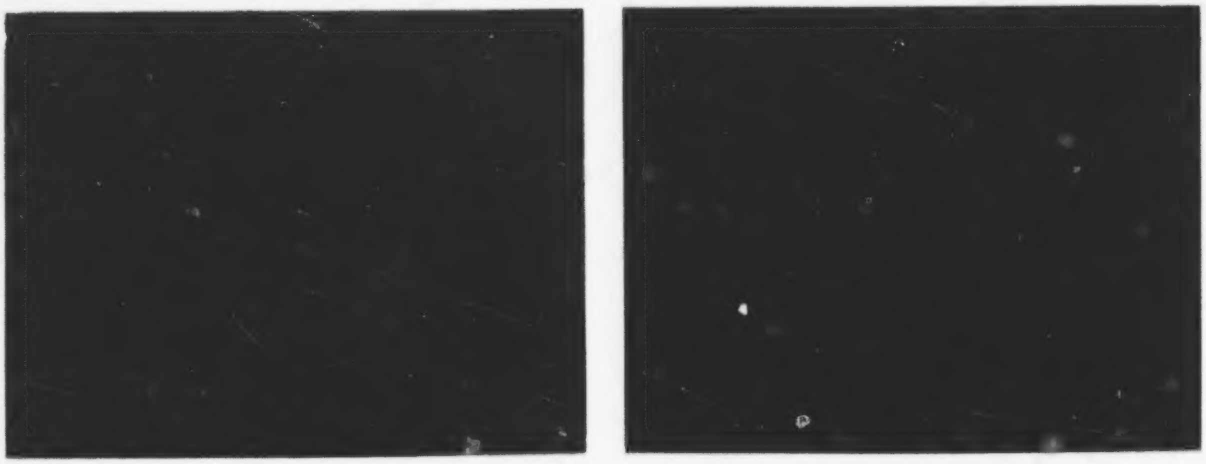

a. Cycle One, Sulfated (12.5 X) b. Cycle One, Regenerated (12.5 X)

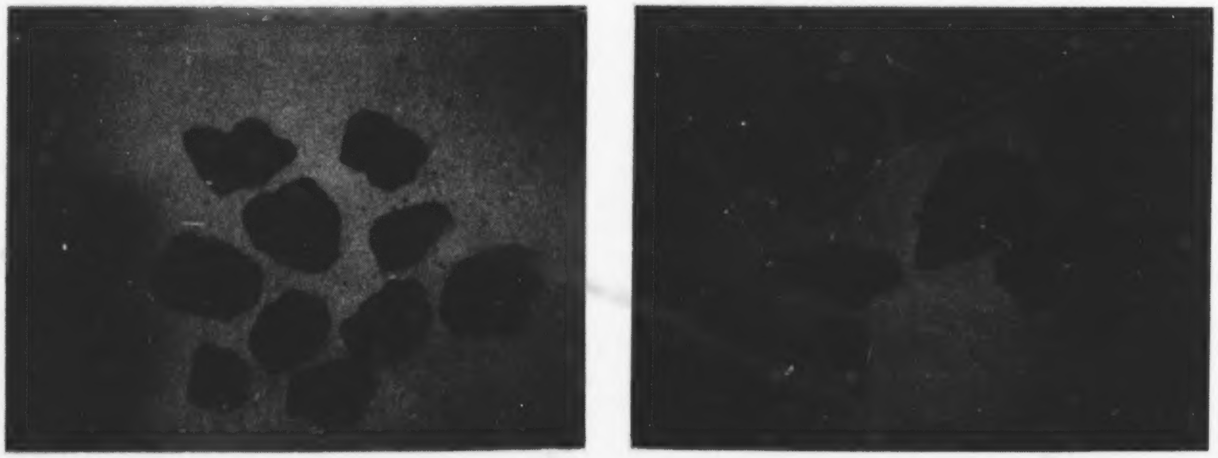

c. Cycle Five, Sulfated (12.5 X) d. Cycle Five, Regenerated (12.5 X)

Fig. 22. Photomicrographs of Sulfated and Regenerated Tymochtee Dolomite Particles from the First and Fifth Utilization Cycles

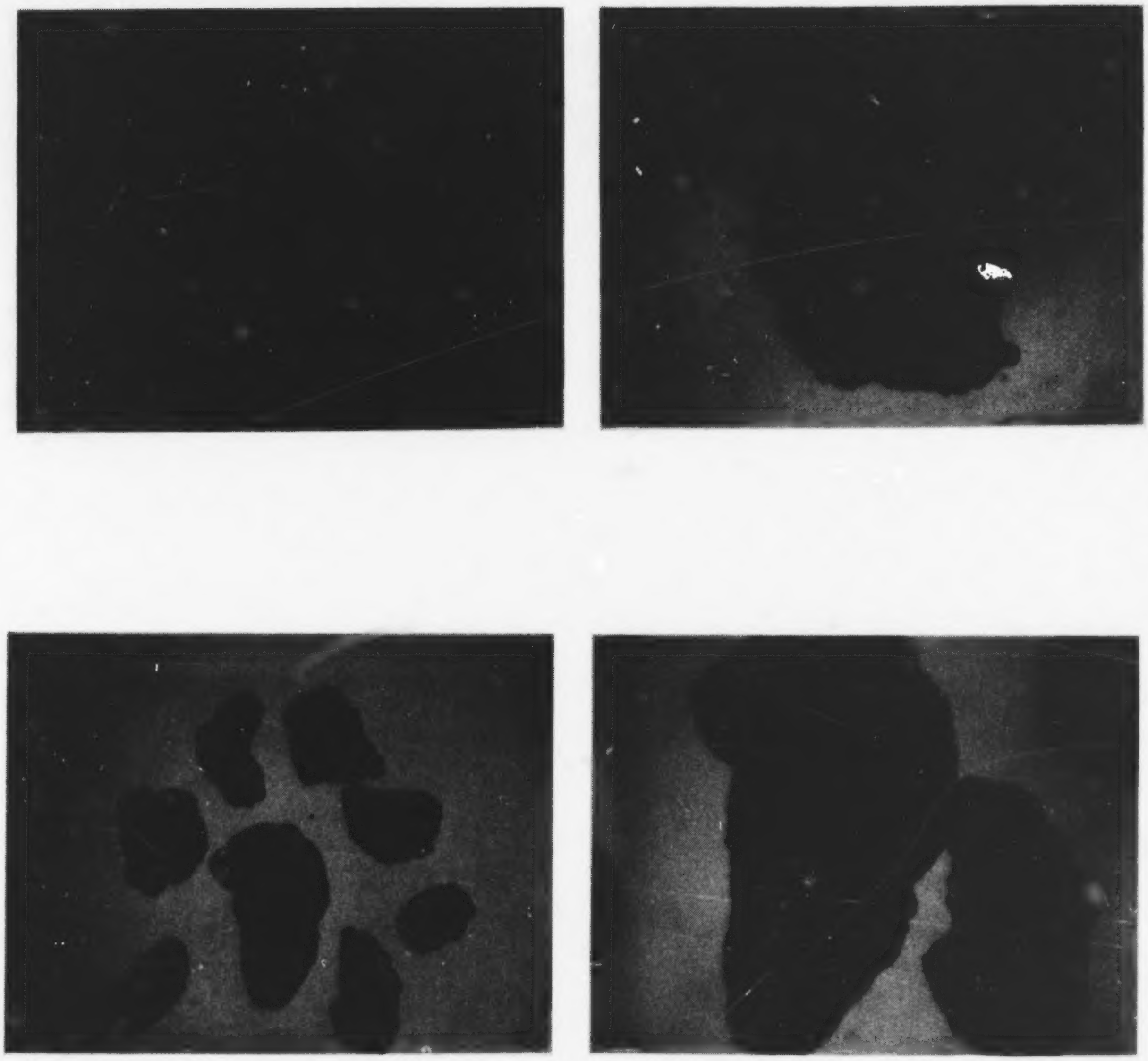

Fig. 23. Photomicrographs of Sulfated and Regenerated Tymochtee Dolomite Particles from the Tenth Utilization Cycle

A petrographic examination was also made of the unreacted dolomite and of samples of the dolomite after the first and tenth sulfation and regeneration half-cycles.[*] As was observed in the above examination of the macrofeatures, progressive buildup of a vitreous crust surrounding most of the particles over the ten cycles was observed. The spotty beginnings of crust formation during the first cycle are shown in Figs. 24 and 25. Representative encrusted particles from the tenth cycle are shown in Figs. 26 and 27.

Where the crust is well developed (as in Figs. 26 and 27), it is red with some black areas when viewed in ordinary light. Under the microscope, a polished section viewed in reflected light shows that the black parts have higher reflectivity and are magnetite (Fe_3O_4). The less reflective red parts resemble a silicate or silicate glass. The red coloration is probably due to finely dispersed hematite (Fe_2O_3) and is free of magnetite. The contrast between these two parts is indicated in Fig. 27.

X-ray diffraction analyses were made of the surfaces of particles from the first and tenth cycles. On the surface of first-cycle regenerated particles, the presence (very minor) of $Ca(Al_{0.7}Fe_{0.3})_2O_5$ was detected. On the surface of tenth-cycle regenerated particles, evidence for the presence of this compound was more pronounced. The tenth-cycle sulfated particle surface contained a high concentration of α-Fe_2O_3.

Although the two predominant crystalline phases in the crust are magnetite and MgO, it is very likely that they are dispersed phases in a vitreous matrix (of unknown composition), as evidenced by the vesicular character shown in Fig. 28. In this respect, this material is similar to the fusion crust of stony meteorites. No silicon-based compound was found by X-ray diffraction (glassy silicate compounds would not be detected).

The iron and aluminum compounds on the surface of these particles are probably present in adhering coal ash. Specifically, the iron content of the crust is much greater than the iron content of the average dolomite particle. The unreacted dolomite particle shown in Fig. 29 contains the highest visible amount of iron oxide and iron sulfide of some 24 particles randomly selected and polished.

It is reasonable to speculate that ash particles stick to the surfaces of dolomite particles during combustion. A glassy crust may form by fusion at the combustion temperatures in the combustor (there is evidence of crust formation during the first combustion cycle, Fig. 25) and later when the particles are regenerated at 1100°C.

The presence of coal ash shells on the dolomite particles did not cause routine defluidization during regeneration, although it is thought that in the regeneration reactor (at 1100°C under reducing conditions) this shell is soft. The absence of agglomeration in the fluid bed during regeneration

---

[*] Analysis performed by L. H. Fuchs, Chemistry Division, Argonne National Laboratory.

Fig. 24. Photomicrograph of Cross Section of a Tymochtee Dolomite Particle from the First Combustion Cycle (X75)

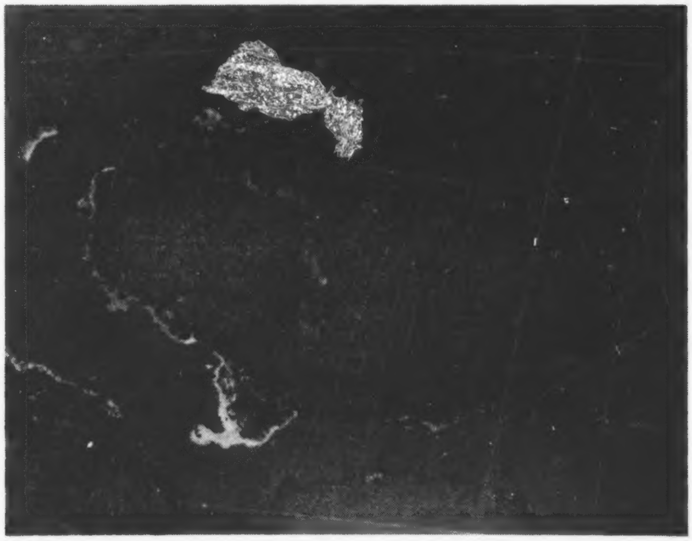

Fig. 25. Photomicrograph of Cross Section of a Tymochtee Dolomite Particle from the First Regeneration Cycle (X75)

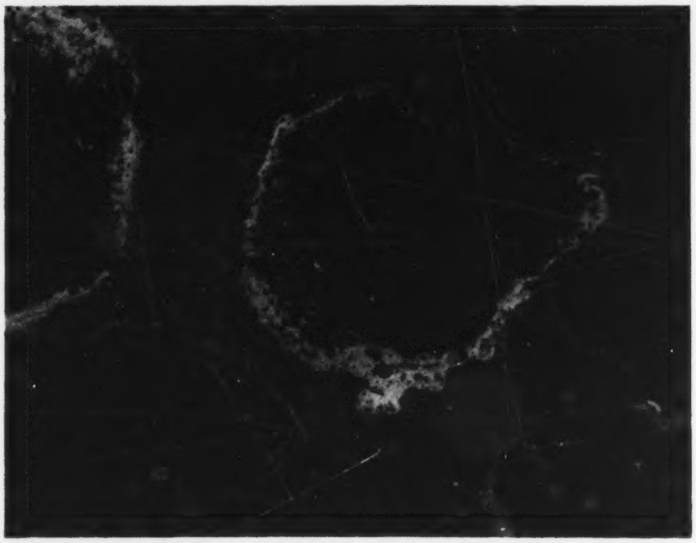

Fig. 26. Photomicrograph of a Cross Section of a Tymochtee Dolomite Particle from the Tenth Combustion Cycle (X75)

Fig. 27. Photomicrograph of Cross Section of a Tymochtee Dolomite Particle from the Tenth Regeneration Cycle (X75). Arrows indicate magnetite concentrations in crust; bracket = magnetite-free area.

Fig. 28. Photomicrograph of Cross Section of a Tymochtee Dolomite Particle from the Tenth Regeneration Cycle. The arrows point to vesicles (X150)

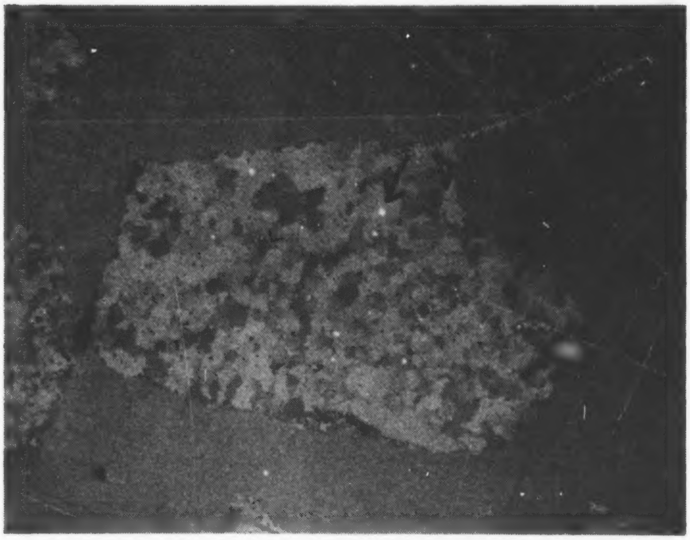

Fig. 29. Photomicrograph of Cross Section of an Unreacted Tymochtee Dolomite Particle. The arrow points to a pyrite inclusion (X75)

was probably due to the fluidizing velocity which was >1.0 m/sec and high enough to maintain stable fluidization for the -14 mesh particles used in these experiments. The beneficial effects of high fluidization velocities in "sticky" beds have been described by Gluckman *et al.*[11]

Evidence that the crust may be an effective sealant against gas diffusion is an observation pertaining to samples from the tenth regeneration cycle which contain a few particles having no crust. (The crust was probably broken off prior to reduction.) An X-ray pattern of the interiors of these crust-free regenerated particles showed strong CaO and MgO and weak $Ca(OH)_2$; in contrast, a pattern of the interiors of encrusted particles in the same sample showed strong MgO, medium $CaSO_4$, and only weak CaO.

h. Electron Microprobe Analysis of Tymochtee Dolomite from Tenth Utilization Cycle

Electron microprobe analyses were performed on cross sections of sulfated and regenerated dolomite samples from the tenth utilization cycle to confirm the existence of the coal ash shell and to determine its composition and its role during sulfation reactions.

Steady state samples of dolomite particles were screened (-20 +25 mesh), mounted in epoxy, and machined to remove the equivalent of one-half of the nominal diameter (∿400 μm). A thin carbon layer was applied to the machined surface by vapor deposition to enhance the conductivity of the mounts. Apatite (38.94% CaO), MgO (60.31% Mg), SiO_2 (49.88% Si), Al_2O_3 (52.93% Al), and FeS_2 (46.55% Fe and 53.45% S) were used as standards to obtain a quantitative estimate of local component concentrations. The measured local concentrations of constituents were probably biased on the low side due to surface irregularities (absent from the standards) which scatter the characteristic emitted X-rays.

The radial component concentration profiles for three typical regenerated particles (P-1, P-2, P-3) after ten cycles are given in Figs. 30, 31, and 32. The particle sections, when viewed with an optical microscope, revealed a well-developed crust. Particle 1 (P-1), which is shown in Fig. 30, has a shell which is thicker on the side where the scan was initiated. The electron microprobe scan of P-1 confirms the existence of the ash crust on the particle. Peak concentrations of Si ∿12 wt %, Fe ∿25 wt %, and Al ∿7 wt % were found in the crust. The concentrations of these components in Arkwright coal ash, which was used during the combustion step of the experiments, are: 12 wt % Si, 14 wt % Fe, and 12 wt % Al. The above-measured concentrations of relatively major components in the particle crust were not in the same proportion as in the coal ash; Fe/Si was ∿2 in the crust and ∿0.7 in the coal ash. The coal ash which encapsulated the particle was strongly enriched with iron. The sulfur concentration profile shows that this particle (P-1) had not been completely regenerated and that very little sulfur was present in the particle crust.

The electron probe scans for two additional tenth-cycle regenerated dolomite particles (P-2 and P-3) are given in Figs. 31 and 32. Both of these particles also were encrusted with ash, as the scans for Si, Fe, and Al

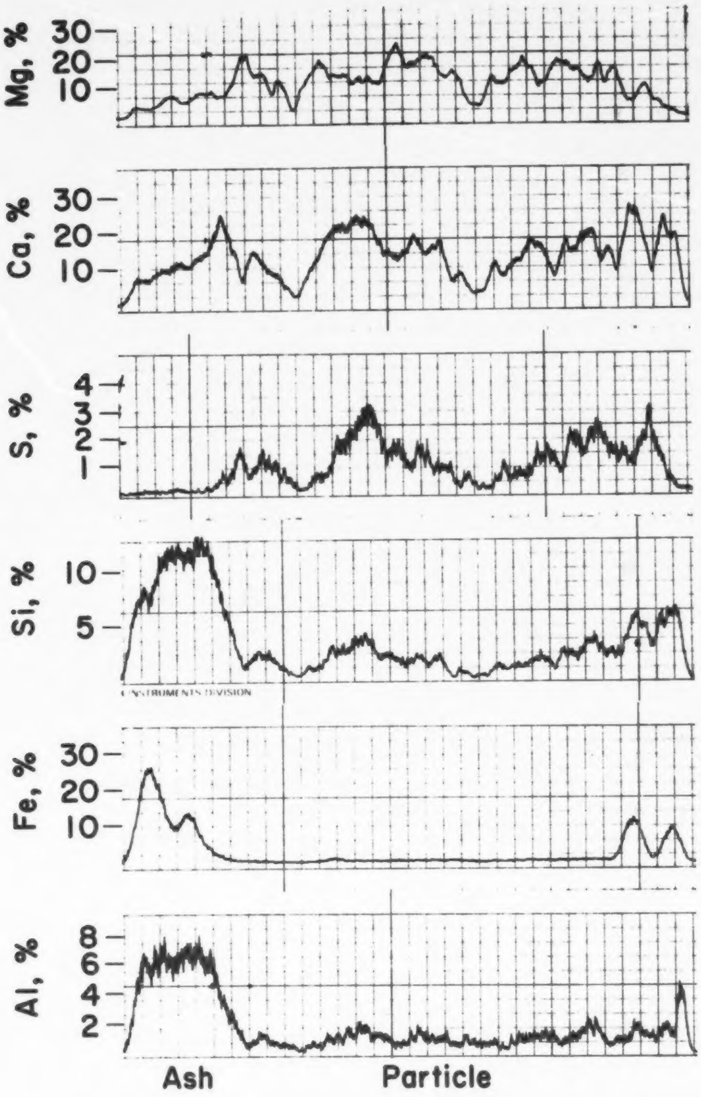

Fig. 30. Electron Microprobe Analysis of a Typical Regenerated Dolomite Particle (P-1) from the Tenth Cycle

reveal. In these particles also, a relative elemental enrichment of the ash crust with iron was found. The calcium concentration in the crusts is as high or higher than that in the particle interiors, which suggest the possibility of calcium enrichment in the ash crust by diffusion from the particle interior. The calcium concentration in the Arkwright coal ash, 3.5 wt %, is much lower than in the crust. The sulfur concentration profiles show that these particles have been nearly completely regenerated, with peak concentrations of <0.5% S. The bulk concentration of sulfur in the dolomite

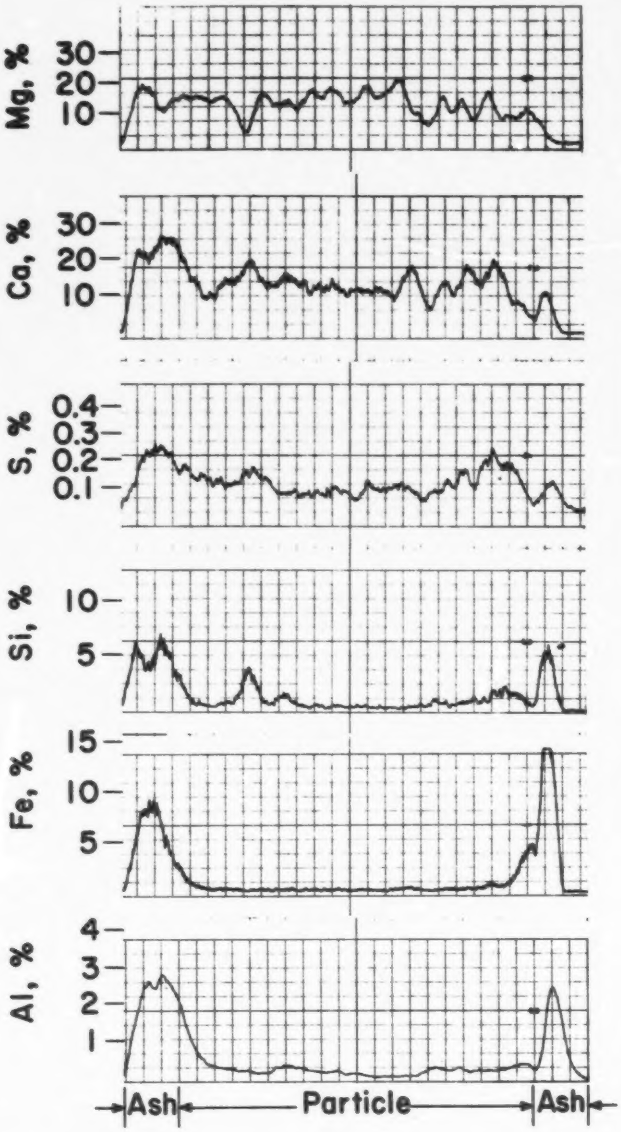

Fig. 31. Electron Microprobe Analysis of a Typical Regenerated Dolomite Particle (P-2) from the Tenth Cycle.

before regeneration was 7.1 wt % (determined by chemical analysis). The presence of the coal ash shell apparently does not prevent sulfur in the particles from escaping during regeneration. Possibly, cracks and voids in the ash crust could be major routes for gas transport during regeneration.

Sulfated particles from the tenth cycle (sulfated ten times and regenerated nine times) were also analyzed with the electron microprobe.

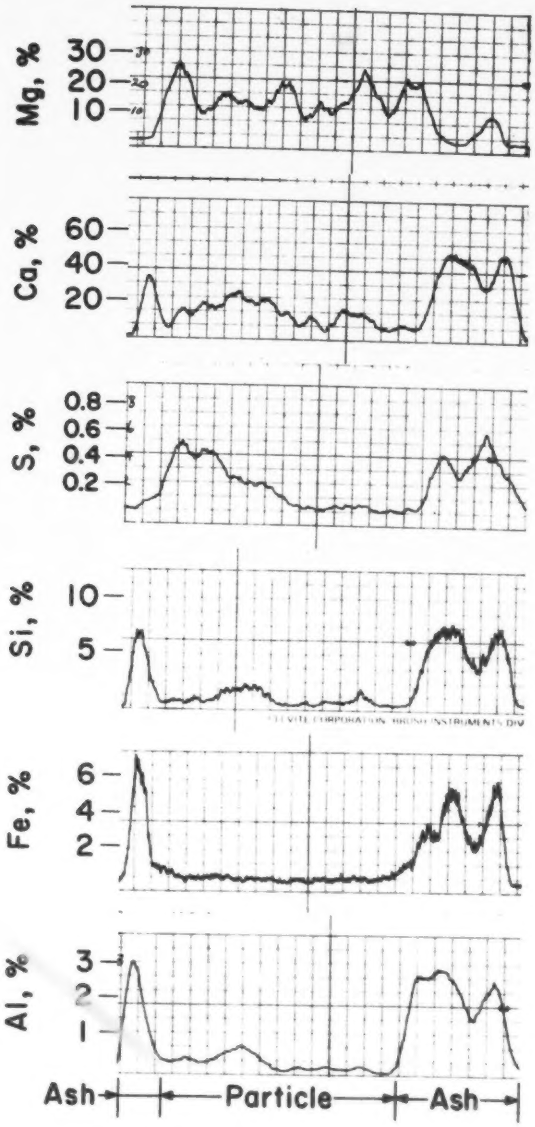

Fig. 32. Electron Microprobe Analysis of a Typical Regenerated Dolomite Particle (P-3) from the Tenth Cycle

The analyses for three typical sulfated particles are given in Figs. 33, 34, and 35. In all three particles, the formation of an ash crust (high concentrations of Si, Fe, and Al) is again verified. Enrichment of iron (in relation to Si and Al) in the crust was again observed, particularly in the second and third particles. As was also found in the regenerated

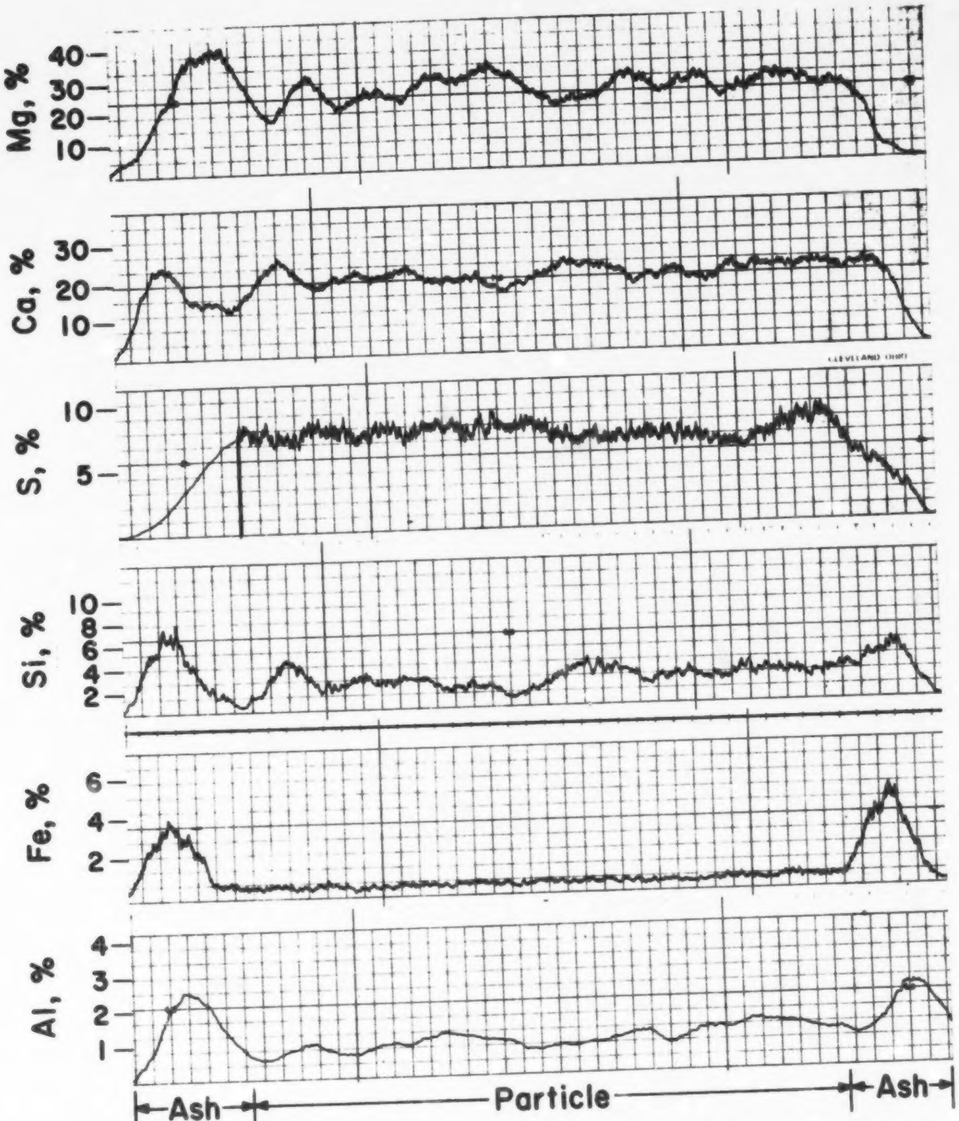

Fig. 33. Electron Microprobe Analysis of a Typical Partially Sulfated Dolomite Particle (PS-1) from the Tenth Cycle.

particles, the ash crust was enriched in calcium, reaching concentrations equivalent to those in the particle interiors.

The sulfur concentration profiles in the first two particles (PS-1, PS-2) revealed uniform sulfation of the particle interiors, with local sulfur concentrations ranging from 7.5 to 10%. (The bulk sulfur content of the sulfated dolomite samples was 7.1 wt %.) The calcium in the ash crust does not appear to have reacted with sulfur. It could be present as a

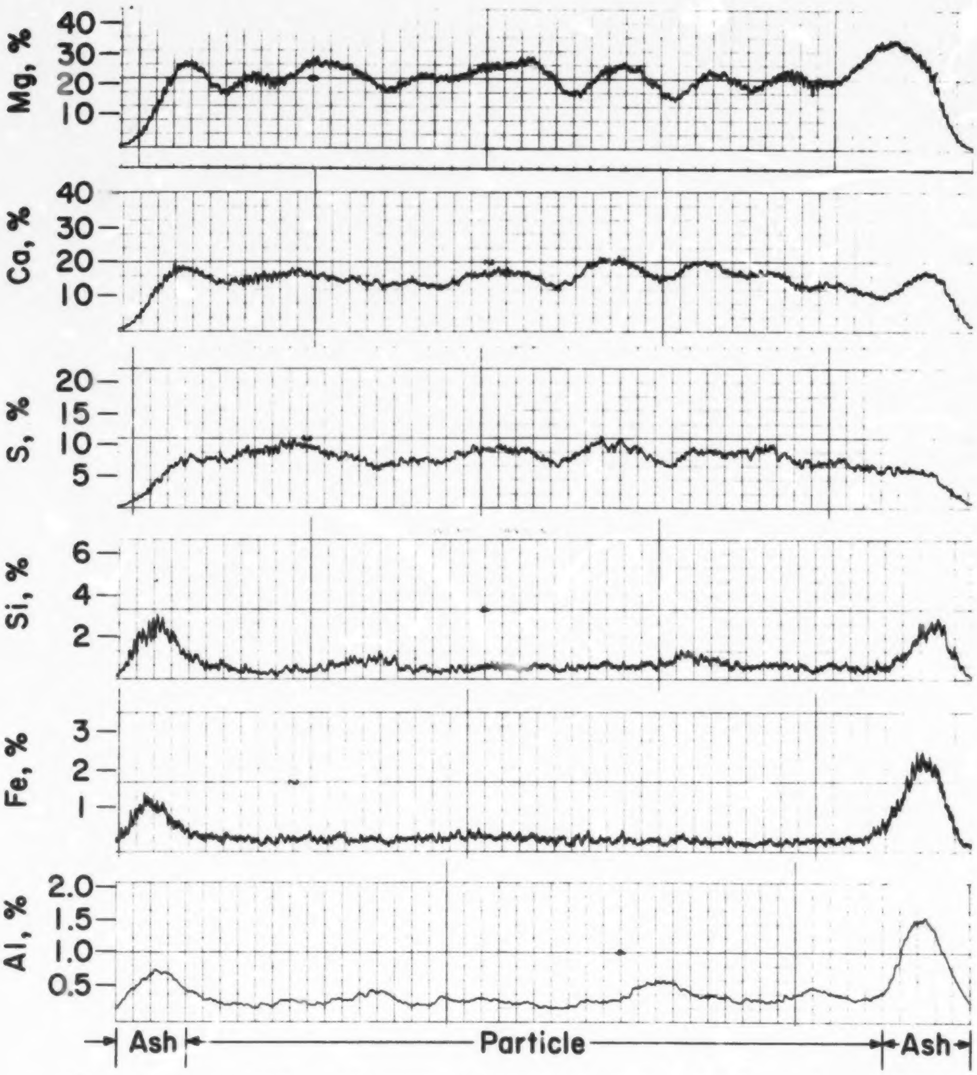

Fig. 34. Electron Microprobe Analysis of a Typical Partially Sulfated Dolomite Particle (PS-2) from the Tenth Cycle

silicate. The sulfur concentration profile in the third partially sulfated particle also shows that the calcium in the ash shell is not in a reactive form. The sulfur concentration below the ash crust is highest near the crust and decreases with penetration towards the center of the particle. If diffusion through the ash crust or sulfated shell controlled the sulfation reaction, the calcium adjacent to the crust would be expected to be more fully sulfated (∿10 wt % S) in a partially reacted particle. Also, a sharper radial sulfur concentration gradient would be expected at the reaction front. The electron microprobe analysis of sulfur concentration in tenth cycle partially sulfated dolomite suggests a resistance at the reaction front.

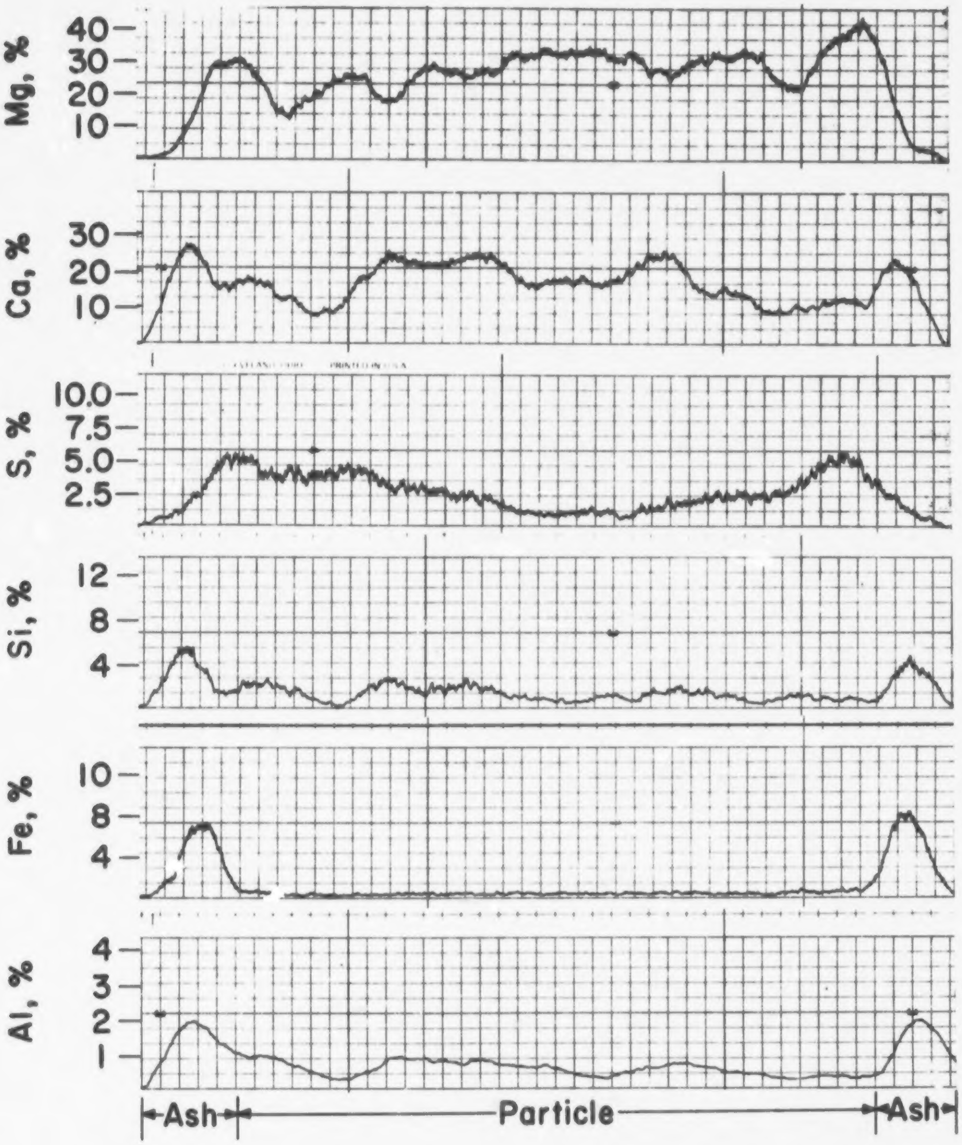

Fig. 35. Electron Microprobe Analysis of a Typical Partially Sulfated Particle (PS-3) from the Tenth Cycle

The loss of reactivity could be due to a loss of local microporosity caused by sintering within the dolomite particles.

Electron microprobe analyses performed on once-sulfated Tymochtee dolomite particles were reported previously (ANL/ES-CEN-1016). In those results, it was observed that a sulfated shell had formed on the particles and that the shell moved toward the center of the particles with increasing extent of sulfation. There were sharp sulfur concentration gradients between the sulfated shell edges and the unsulfated particle interiors. The local sulfur content in the sulfated shell (for the incompletely reacted particles) was as high (∿10 wt % S) as that in the completely reacted particles. The above observations suggest that diffusion through the sulfated shell was the controlling step during sulfation in the first cycle and that the reaction of sulfur (SO_2) occurred in a well-defined reaction front.

A sample of tenth-cycle regenerated dolomite particles was crushed and screened. The crushed (-30 +100 mesh) particles were sulfated in a TGA, and the results are compared in Fig. 36 with TGA reactivity results for uncrushed tenth-cycle dolomite. No notable difference in reactivity was found, further suggesting that formation of an ash shell on the particles is not responsible for the loss of sulfation reactivity in the dolomite during cyclic utilization.

i. Carbonate Levels of Sorbent Samples

The weight fraction of the unsulfated calcium present as calcium carbonate was derived for the sorbent at each half-cycle in the utilization study up to the end of the sixth full cycle. The results are shown in Fig. 37. Initially, all of the calcium was present as $CaCO_3$ in the virgin dolomite feed to the first combustion cycle. After the first combustion half-cycle, the unsulfated calcium was still predominantly (∿68%) $CaCO_3$. Following the first regeneration, however, only 4% of the unsulfated calcium was present as $CaCO_3$. Although the carbonate fraction remained essentially constant during succeeding regeneration cycles, the carbonate fraction steadily

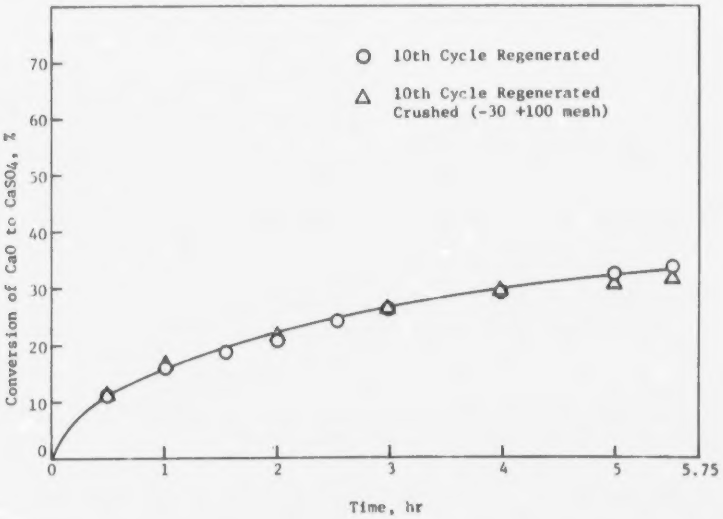

Fig. 36. Comparison of the Reactivity of Tenth Cycle Regenerated Dolomite (-14 +30 mesh) to that of a Crushed (-30 +100 mesh) Sample from the Same Experiment

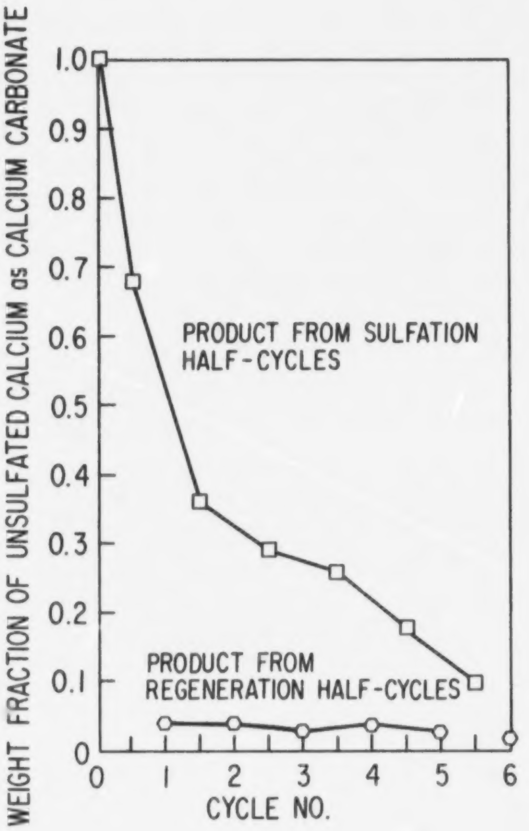

Fig. 37. Weight Fraction of Unsulfated Calcium as Calcium Carbonate in Sulfated and Regenerated Dolomite Samples as a Function of Utilization Cycle

decreased following successive combustion cycles. These results further emphasize the increasing blockage to gas penetration (for carbonation as well as sulfation) with increasing combustion cycle. Neither calcination nor regeneration appears to diminish or to be adversely affected with increasing utilization cycle, however.

j. Attrition and Elutriation Losses during Regeneration and Combustion

The extent of sorbent losses during the regeneration steps of the ten cycles was determined. The losses were estimated using three different approaches, all based on the mass of calcium present in the particulate streams. In the first method, the sorbent loss for an entire regeneration step was calculated from the difference in calcium weight of the sulfated dolomite fed and of the regenerated dolomite. In the second method, the sorbent losses were calculated for a steady-state segment of the experiment. The results obtained from both of these methods were inconclusive because the calcium balances were greater than 100% (generally <5% high) in most experiments. The high calcium balances may be explained by the accuracy of the calcium analysis being ∿5%. The calcium loss from the entire regenerated product stream is less than 5%.

In the third approach, the losses were predicted by evaluating the percentage of the calcium in the sulfated dolomite fed to the regeneration reactor that was elutriated and subsequently removed from the off-gas by the cyclones and filter. (The calcium contribution of the coal ash from the Triangle coal used for regeneration was found to be insignificant.) The losses, based on calcium content of particulates removed from the off-gas stream, averaged 2.0% (see Table 13). Because the off-gas particles were -30 mesh and the feed sulfated dolomite was normally -14 +30 mesh, it can be assumed that the off-gas particles were attrited fragments of the regenerated dolomite. No apparent trend in the extent of attrition was found for the ten cycles.

Table 13. Attrition and Elutriation Losses for Tymochtee Dolomite during Regeneration in the Cyclic Utilization Study

S.D. = Ca in sulfated dolomite (feed), kg/hr
O.P. = Ca in particulate collected from off-gas, kg/hr

Regeneration Cycle CCS-	Loss for Steady-State Experiment Segment, $\left(\frac{\text{O.P.}}{\text{S.D.}}\right) \times 100$
1	1.9
2	1.7
3	3.0
4	1.2
5	3.5
6	3.7
7	2.0
8	2.6
9	0.9
10	1.3
Avg	2.2

The extent of sorbent losses by decrepitation and/or entrainment during the ten combustion half-cycles was also determined, based on the steady-state calcium material balances around the combustor, which accounted for the calcium in both the dolomite and the coal. The assumption was made that all calcium entering the combustor in the coal was entrained in the flue gas as fly ash with no correction for ash buildup in the fluidized bed. Based on the rates involved and the relatively low calcium concentration of the ash as compared with the calcium concentration of dolomite, such a correction would then be very minor. The sorbent loss by decrepitation and/or entrainment was then calculated as follows:

$$\text{Sorbent Loss (\%)} = \frac{\left(\begin{array}{c}\text{Calcium in Entrained}\\ \text{Particulate Matter}\end{array} - \begin{array}{c}\text{Calcium in}\\ \text{Coal Feed}\end{array}\right) \times (100\%)}{(\text{Calcium in Sorbent Feed})} \qquad (12)$$

The results are presented in Table 14 along with the calcium material balances for the ten combustion experiments.

Table 14. Decrepitation and Entrainment Losses and Calcium Material Balances for the Ten Combustion Experiments in the Cyclic Sorbent Utilization Study

Sulfation Cycle	Sorbent Loss by Decrepitation and Entrainment, %	Calcium Material Balance, (In/Out) x 100
REC-1	16	108
REC-2	4	94
REC-3	5	104
REC-4	3	96
REC-5	3	99
REC-6	6	102
REC-7	4	100
REC-8	7	101
REC-9	6	91
REC-10	4	96

The 16% loss reported for experiment REC-1 is a revision of the previously reported value of 20-25% (ANL/ES-CEN-1016). Although the first-cycle loss was still quite large, losses during the remaining nine combustion cycles were reasonably small, averaging about 5% per cycle. It is quite likely that after the first combustion cycle, the resistance of the sorbent to decrepitation is increased by (1) residual sulfate in the sorbent following regeneration and (2) the presence of the vitreous crust on the particles. It is also possible that the rapid calcination of $MgCO_3$ during the first combustion cycle contributed to the large sorbent loss during the cycle. On the basis of these results, the loss of sorbent reactivity may be more significant in affecting cyclic performance adversely than is the loss of sorbent by decrepitation.

Although the thermal cycling is more extreme and the reactions are more rapid (decomposition) during regeneration than during sulfation, the extent of attrition during regeneration was lower. The lower sorbent losses during regeneration can be attributed to the very short solids residence time ($\sim$7.5 min) in the reactor in each regeneration step as compared with the much longer solids residence time ($\sim$5 hr) in the combustor reactor for each sulfation step. The effect of introducing solids that were at room temperature into a hot reactor environment in each half-cycle cannot be estimated. In an industrial process, the solids would be cycled between the combustor and the regenerator reactor at the temperature of the reactors, and hence the thermal shock would be lessened. It is believed that lower sorbent losses would be obtained with a continuous sorbent cycling system.

The combined losses due to attrition and/or elutriation per cycle (sulfation and regeneration) have been found to be ∿8%. In an FBC process utilizing sorbent regeneration, it is expected that the makeup rate for Tymochtee dolomite would have to be at least this high because of attrition. An even higher makeup rate may be required to maintain sufficient SO_2-sorption reactivity in the fluidized bed of the combustor.

k. Amount of Sorbent Processed per Cycle

Table 15 presents the amounts of sorbent processed during each phase of the cyclic utilization study along with calcium balances. It should be emphasized that losses of materials between cycles included handling losses (spills, *etc.*), sampling losses, and (in the case of combustion) losses during startup.

Table 15. Gross Amounts of Sorbent Processed and Calcium Balances for Each Half-Cycle in the Cyclic Combustion/Regeneration Study

Cycle	Gross wt in, kg	Ca in, wt %	Ca in, kg	Gross wt out, kg	Ca out, wt %	Ca out, kg	Calcium Balance, %
Combustion							
1	620	20.0	124.0	359	26.3	94.4	76
2	268	33.9	90.9	328	22.4	73.5	81
3	282	29.7	83.8	285	23.4	66.7	80
4	146	29.4	42.8	169	24.1	40.7	95
5	144	29.0	41.7	143	22.9	32.8	79
6	115	28.3	32.5	108	22.9	24.8	76
7	88.5	28.8	25.5	97.5	23.3	22.7	89
8	80.3	28.7	23.0	85.3	22.8	19.4	85
9	76.6	27.1	20.7	75.3	22.6	17.0	82
10	66.7	65.9	17.3	71.7	22.1	15.8	92
Regeneration							
1	359	26.3	94.4	268	33.9	90.9	96
2	328	22.3	73.5	282	29.7	83.8	114
3	181	23.4	42.5	146	29.4	42.8	101
4	169	24.1	40.7	144	29.0	41.7	102
5	143	22.9	32.8	115	28.3	32.5	99
6	108	22.9	24.8	88.5	28.8	25.5	103
7	97.5	23.3	22.7	80.3	28.7	23.0	102
8	85.3	22.8	19.4	76.6	27.1	20.7	107
9	75.3	22.6	17.0	66.7	25.9	17.3	102
10	71.7	22.1	15.8	62.1	25.6	15.9	101

6. Cyclic Sorbent Life Study with Greer Limestone

[J. Montagna (Principal Investigator), F. F. Nunes, G. Teats, R. Beaudry, R. Mowry, S. Smith, and J. Stockbar]

A cyclic sorbent utilization experiment was performed with Greer limestone and Sewickley coal (this coal is used in both the combustion and the regeneration steps). This limestone and coal are being used by Pope, Evans and Robbins (PER) in the atmospheric pilot plant at Rivesville.

Evaluated as a function of utilization cycle (with no sorbent makeup) were (1) the changes in reactivity (sulfur acceptance during combustion), (2) the changes in regenerability (sulfur release during regeneration), (3) the extent of decrepitation, and (4) the extent of ash buildup. In addition, a balance for the trace elements of interest will be made for the combined combustion/regeneration system.

The processing capacity of the ANL PDU regenerator is much greater than that of the combustor (by almost a factor of ten), and the sorbent cannot be cycled continuously between these reactors. This limitation was overcome by performing the sulfation and regeneration experiments batchwise with no fresh sorbent make-up. The results (as a function of utilization cycle) are being incorporated in the regeneration process model and will be used to predict the performance of the sorbent system in a boiler with continuous regeneration--specifically, to evaluate the effect of fresh sorbent make-up rates on the overall process.

a. Combustion Step Results

The combustion steps of the experiments were performed at 308 kPa (∿3 atm), ∿855°C (∿1570°F), a nominal fluidizing-gas velocity of 1.0 m/s and a constant sulfur retention of ∿84% by the sorbent. This corresponds to a sulfur concentration of ∿640 ppm in the dry flue gas, which is the EPA emission limit for Sewickley coal (which contains 4.3 wt % S).

Data for the combustion step of the ten cycles are presented in Table 16. Sulfur retention was maintained at ∿84% by adjusting the regenerated sorbent feed rate so that the SO_2 concentration in the off-gas was maintained at ∿640 ppm. Therefore, the flue-gas-based sulfur retentions reported in Table 16 are indicative of the ability to maintain the experimental design conditions. The other reported values of sulfur retention were based on the steady-state ratio of the amount of sulfur retained by the limestone to that released by the coal. The differences between these values and the designed retention are indicative of experimental errors. The largest deviations (∿27%) occurred in cycles four and five.

b. Cyclic and Total Calcium Utilization

The cyclic calcium utilizations and the calcium present as $CaSO_4$ in the combustor feed and product streams are given in Table 16. The percent calcium present as $CaSO_4$ in the combustor feed stream is dependent on the extent of regeneration and the extent of sulfation in previous cycles. The percentage generally decreases with utilization cycle as the stone becomes

Table 16. Operating Conditions and Flue-Gas Compositions for Combustion Steps of Cyclic Experiments with Greer Limestone and Sewickley Coal

Combustor: ANL, 6-in.-dia
Coal: Sewickley, -6 +100 mesh, 4.3 wt % S
Sorbent: Cycle 1, Greer limestone, -14 +30 mesh
Cycles 2-10, regenerated Greer limestone

Temperature: 855°C
Pressure: 308 kPa
Excess air: ∿17%
Nominal bed height: 0.9 m
Nominal gas velocity: 1.0 m/s

Combustion Cycle No.	Sorbent Total Ca, wt %	Feed Rate, kg/hr		CaO/S Mole Ratio[a]	Flue Gas Analysis, avg values		Sulfur Retention, %[b] / %[c]	Calcium Present as $CaSO_4$ in the Combustor Streams		Calcium Utilization,[d] %
		Coal	Sorbent		SO_2, ppm	O_2, ppm		Feed, %	Product, %	
1	29.4	6.27	3.41	2.87	628	3.2	83.6/84.8	0	30	30
2	41.1	6.73	3.14	3.13	636	3.0	84.3/68	13	32	22
3	40.0	6.73	5.09	4.75	674	3.0	83.7/65.3	15	26	14
4	39.7	6.59	5.14	4.67	598	3.1	85.5/57.4	18	28	12
5	39.5	6.36	4.95	4.88	630	2.9	84.2/57.4	15	25	12
6	39.9	6.93	6.02	5.54	696	3.0	84.0/63.5	14	23	11
7	40.8	6.46	6.24	6.64	580	3.0	86.6/78	9	20	12
8	40.4	6.14	6.36	7.05	620	3.3	84.1/86.3	8	20	12
9	39.6	6.14	5.80	7.35	615	2.9	84.9/85.1	9	19	12
10	39.8	6.36	7.61	8.21	642	2.8	84.0/71.4	7	15	9

[a] Ratio of unsulfated calcium in dolomite feed to sulfur in coal.

[b] Based on flue-gas analysis.

[c] Based on solids analysis.

[d] Utilization of available calcium during cycle. Utilization is defined as the percentage of the available CaO that is converted to $CaSO_4$ in the combustion step.

less reactive. The cyclic utilization value, *i.e.*, the percent of CaO that is sulfated in each step, is plotted in Fig. 38. Calcium as $CaSO_4$ in the product decreased from ∿30% in the first cycle to ∿15% in the tenth cycle. The cyclic calcium utilization, also plotted in Fig. 38, decreased from ∿30% in the first cycle to ∿12% in the 10th cycle.

Hammond and Skopp[16] also reported cyclic limestone reactivity data for a series of batch sulfation/regeneration experiments. A sulfur retention of 80% was maintained in their sulfation steps. Using particles having an average diameter of ∿930 μm (equivalent to the size of the Greer limestone used in this study), they found that calcium utilization decreased from ∿20% to ∿15% in seven cycles.

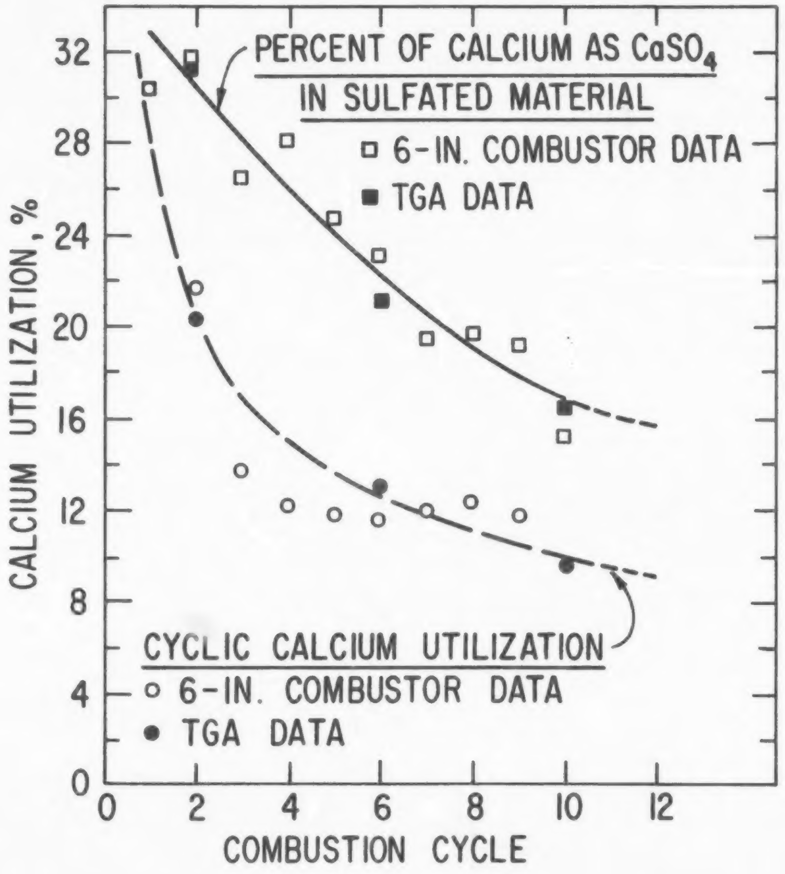

Fig. 38. Cyclic Calcium Utilization for Greer Limestone for 84% Sulfur Retention

c. Porosity of Limestone as a Function of Utilization Cycle

The porosity of -25 +30 mesh particles was measured by the mercury penetration method. The pore distributions of samples from cycles 2 and 10 are given in Fig. 39. It has been reported by Hartman and Coughlin[15] that most sulfation takes place in larger pores ($\geq$0.4 μm) and that pores smaller than 0.4 μm are relatively easy to plug. During sulfation of CaO, pores shrink as a result of molecular volume changes.

The porosity of sulfated limestone was relatively unaffected by utilization cycle (Fig. 39), although the sulfur content (or total calcium utilization) decreased from ∿8.9 wt % to ∿4.1 wt %. The porosity of the regenerated limestone decreased with utilization cycle. Simultaneously, the sulfur content of the regenerated stones decreased. The difference in porosity of the sulfated and regenerated stones decreased from ∿0.084 cm^3/g (pores $\geq$0.4 μm) after the second cycle to ∿0.055 cm^3/g after the tenth cycle. Most of the porosity loss was experienced in the first six cycles. The loss in porosity decreased the reactivity of the limestone with SO_2. This loss can be attributed to high-temperature (1100°C) exposure in the reducing environment of the regenerator. Loss of beneficial porosity limits internal particle diffusion and reaction with SO_2.

d. Limestone Reactivity as a Function of Cyclic Utilization

As the reactivity of the limestone decreased with cyclic use, the molar feed rate of CaO/S required to achieve 84% sulfur retention with no virgin limestone makeup increased from 2.9 to 8.2 in ten cycles (see Fig. 40). These results and those on cyclic calcium utilization will be used to predict fresh limestone makeup rates and flowsheets for FBC processes with sorbent regeneration.

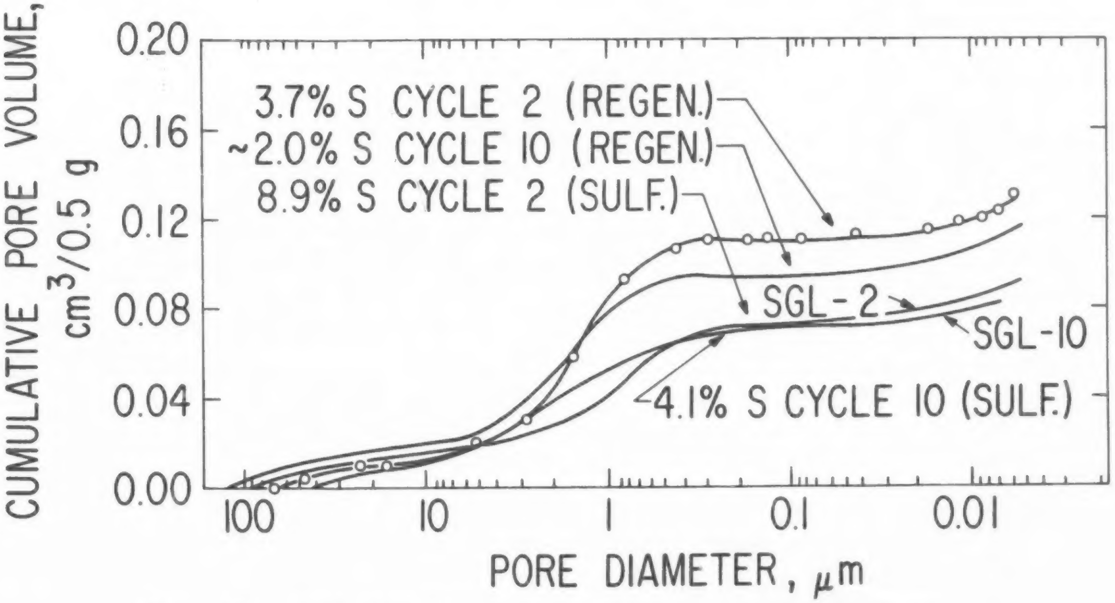

Fig. 39. Pore Distributions of Limestone Samples from Cycles Two and Ten

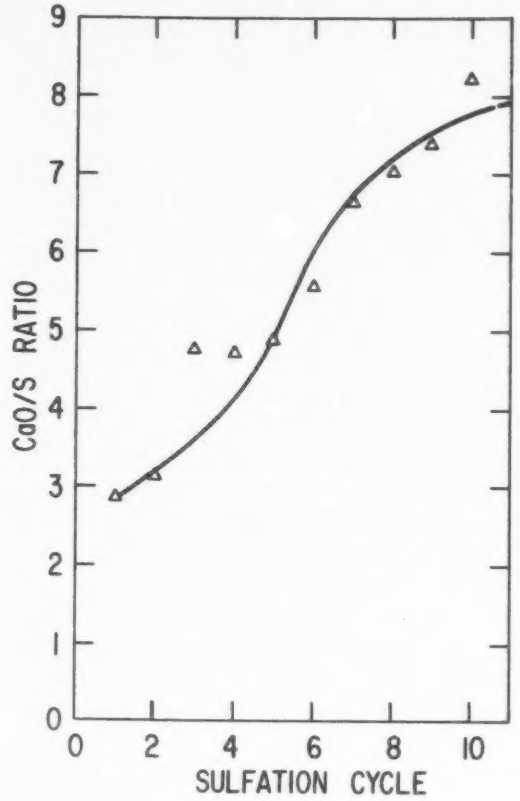

Fig. 40. Cyclic CaO/S Molar Feed Ratio Required to Retain 84% of the Sulfur

TGA sulfation experiments were performed on regenerated samples from this cyclic experiment. They were performed at 855°C and atmospheric pressure, using a simulated flue gas containing 0.3% SO_2, 3% O_2, and the balance N_2. The results obtained are shown in Fig. 41. These results confirmed the PDU results in that the rate of sulfation decreased with cyclic use of the limestone.

In the PDU sulfation steps of the cyclic experiments, as the reactivity of the limestone decreased with cyclic use, the CaO/S mole feed ratio was increased to maintain 84% sulfur retention. Increasing the CaO/S feed ratio caused the limestone residence time in the combustor to decrease. This, together with decreasing reactivity, lowered cyclic stone utilization. The TGA results and the PDU combustor limestone residence times in the corresponding cycles were used as a basis for very crude predictions of calcium utilization. The results (*i.e.*, TGA data points) are given in Fig. 38, together with data obtained in the 6-in.-dia PDU combustor. Good agreement was obtained between the PDU and the TGA data.

e. Regeneration Step Results

The operating conditions during the regeneration step of each cycle were: a nominal system pressure of 129 kPa (∿4 psig), a bed temperature of

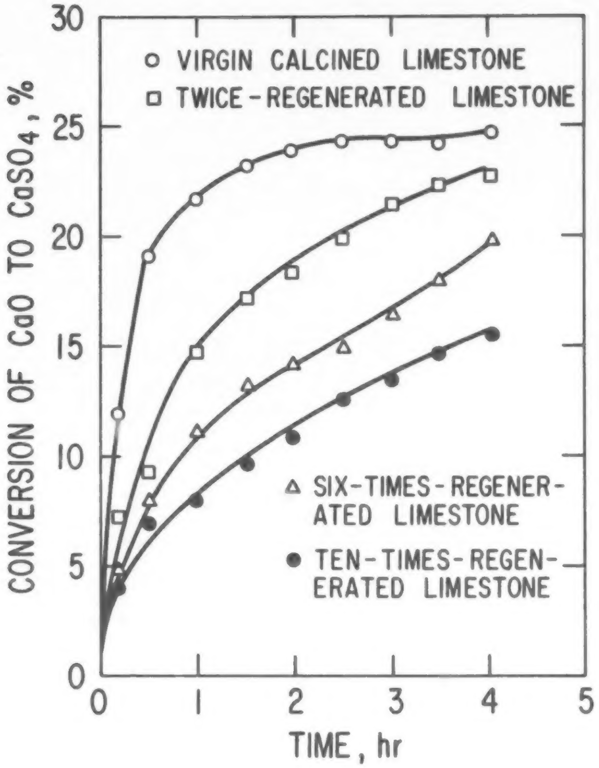

Fig. 41. Conversion of Available Calcium to $CaSO_4$ as a Function of Time. Obtained with TGA at 855°C and atmospheric pressure

1100°C, a fluidizing-gas velocity of ∿1.2 m/s, a total reducing gas concentration of ∿3.0% in the dry off-gas, and a fluidized-bed height of ∿46 cm. The residence time of the sorbent was ∿7 min.

Results for the regeneration step of the ten cycles are given in Table 17. The SO_2 concentration in the dry off-gas in the ten cycles ranged from 6.1 to 8.6%. The extent of CaO regeneration ranged from 49 to 81% during the ten cycles. The lowest extent of regeneration was obtained in the third cycle, in which the solids residence time was low. After ten cycles, the regenerability of the limestone remained acceptable.

f. Coal Ash Buildup during Cyclic Utilization

Sewickley coal, which contains 12.7% ash, was combusted in the sulfation and regeneration steps of the ten-cycle experiment. The extent of coal ash buildup has been calculated based on wet-chemical analysis (Si and Ca) of samples from each half-cycle of the experiment. The basis for calculations was 100 g of virgin Greer limestone. Coal ash buildup was based on silicon enrichment. The results are given in Table 18 and are plotted in Fig. 42.

It was found that every 100 g of starting virgin limestone accumulated 25 g of coal ash in ten cycles. The silicon concentration increased from

Table 17. Experimental Conditions and Results for the Regeneration Step of Ten Utilization Cycles with Greer Limestone

Nominal fluidized-bed height: ∿46 cm
Reactor ID: 10.8 cm
Pressure: 129 kPa
Temperature: 1100°C
Coal: Sewickley (4.3 wt % S), ash fusion temperature (initial deformation) under reducing conditions: 1119°C
Sorbent: -14 +30 mesh sulfated limestone

Regeneration Cycle No.	Sulfur Conc. in Sulfated Sorbent, %	O_2 Conc in Feed Gas, %	Fluidizing-Gas Velocity, m/s	Solids Residence Time, min	Reducing Gas Concentration in Dry Off Gas, %	CaO Regeneration, %[a] / %[b]	Major Sulfur Compounds in Dry Off-Gas, %			
							SO_2	H_2S	COS	CS_2
1	7.7	44.1	1.29	7.1	2.9	67/71	8.4	0.06	0.09	0.02
2	8.6	44.1	1.20	6.8	3.7	55/63	8.6	0.1	0.1	0.07
3	8.1	42.9	1.23	6.3	3.2	50/49	7.5	0.2	0.1	0.2
4	7.9	41.1	1.18	7.0	3.4	58/58	8.2	0.05	0.1	0.1
5	7.5	39.9	1.32	7.0	2.9	59/65	7.3	0.06	0.07	0.09
6	6.0	39.5	1.25	7.2	3.1	79/62	8.1	0.08	0.08	0.1
7	5.5	38.5	1.25	6.8	3.0	63/60	6.6	0.06	0.07	0.07
8	6.0	40.8	1.28	6.5	2.8	54/60	6.3	0.04	0.04	0.08
9	5.6	40.3	1.29	6.2	3.0	54/73	6.2	0.08	0.06	0.06
10	5.1	37.9	1.24	7.0	3.1	64/81	6.1	0.06	0.06	0.1

[a] Based on off-gas analysis.
[b] Based on chemical analysis of limestone samples.

Table 18. Calculated Ash Buildup during Sulfation and Regeneration of Greer Limestone. Based on the Enrichment of Silicon.

Mass Basis: 100 g virgin limestone (29.4 wt % Ca and 4.27 wt % Si)

Cycle No.	Cycle Step	Si Conc, wt %	Ash Buildup	
			wt %	g Ash / 100 g Virgin Sorbent
1	S[a]	7.52	13.98	15.4
1	R[b]	3.94	0	0
2	S	6.70	10.46	12.3
2	R	7.79	15.58	21.2
3	S	7.08	12.09	14.35
3	R	7.63	14.46	19.67
4	S	6.50	9.50	11.88
4	R	7.56	14.16	19.01
5	S	7.40	13.47	15.9
5	R	8.25	17.12	23.24
6	S	9.22	21.3	25.28
6	R	8.87	19.79	27.47
7	S	8.50	18.20	22.04
7	R	9.04	20.52	28.20
8	S	8.59	18.59	22.88
8	R	9.28	21.56	29.0
9	S	8.10	16.48	19.73
9	R	10.25	25.73	34.83
10	S	8.58	18.54	22.77
10	R			

[a] S = sulfation step.
[b] R = regeneration step.

4.3 wt % in the virgin limestone to 8.6 wt % in the product of the tenth sulfation step. In the Tymochtee dolomite cyclic experiment, 13 g of coal ash were accumulated for every 100 g of starting virgin dolomite. Arkwright coal, which was used in the combustion (sulfation) steps of that cyclic experiment, contained considerably less ash, 7.7 wt %, than did the Sewickley coal, 12.7%. In both cyclic experiments, most of the ash was probably accumulated during the combustion step (where the sorbent is exposed to much more coal) rather than in the regeneration step.

Sulfated and regenerated limestone particles from the first and tenth utilization cycles were examined with a low magnification microscope for macrofeatures. Photomicrographs of these samples are given in Fig. 43. Limestone particles from the first cycle contain some adhering coal ash. The regenerated particles appear to contain more ash, but this is probably caused by the sharper color contrasts in the regenerated particles. (This is more apparent in color photographs.) Also, the surface of the once-regenerated

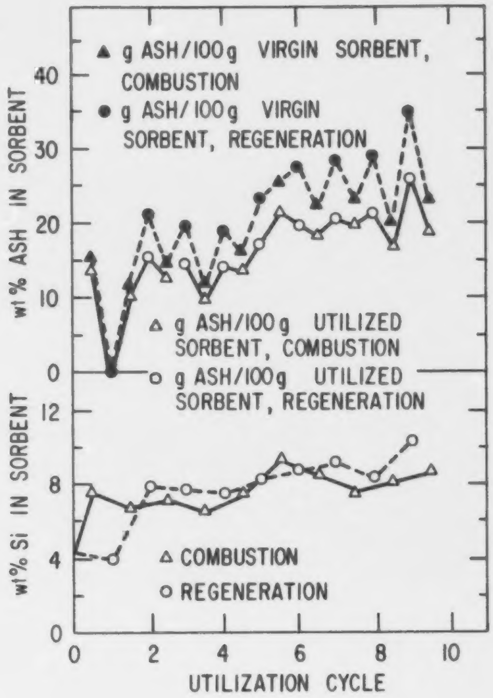

Fig. 42. Coal Ash Buildup as a Function of Greer Limestone Utilization Cycle

limestone particles is glossier and whiter than the surface of the once-sulfated particles. This is probably due to the sintering effect of the regenerator environment (1100°C and reducing) on the silicon-rich Greer limestone. Particles from the tenth utilization cycle sample appear to contain more ash than do the first-cycle particles. However, the particles are not all encapsulated with coal ash, as was the case for particles from the cyclic dolomite experiments. Many of the tenth-cycle Greer limestone particles are visually identical to first-cycle particles (unlike the results from the cyclic dolomite experiments), which would indicate that the ash layer thickness is not increasing and that much of the coal ash is present as individual particles in the bulk utilized limestone. The results in Fig. 43 suggest that the maxmimum ash buildup to be expected when using Greer limestone and Sewickley coal is $\sim$20 wt % in the utilized stone.

g. Attrition and Elutriation of Limestone Particles during Regeneration and Sulfation

The fresh limestone makeup rate into an FBC boiler will depend on the losses of limestone caused by attrition and subsequent elutriation of particles from the boiler and the regenerator, and on the amount of sulfated limestone drawn off to maintain the reactivity of the bed in the boiler. The sorbent losses from attrition and elutriation of particles have been determined for the sulfation and regeneration steps and the data are given in Table 19. Losses were based on the ratio of sorbent-attributable calcium in off-gas particles to calcium in the feed sorbent. The limestone losses caused by

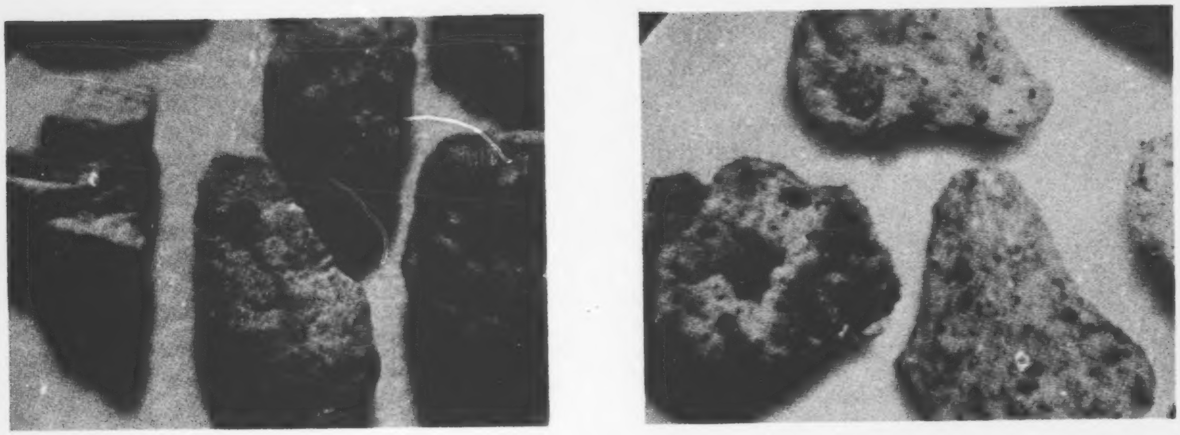

a. Cycle One, Sulfated Particles b. Cycle One, Regenerated Particles

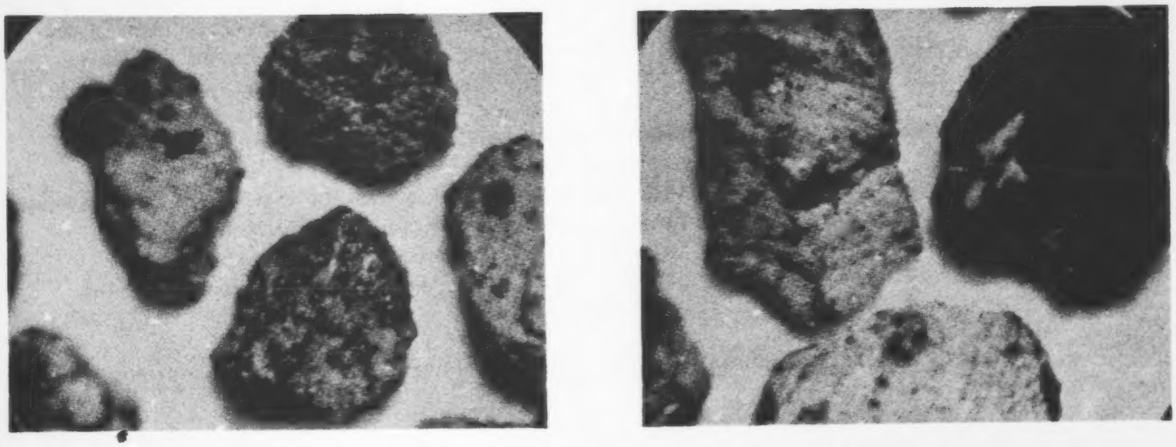

c. Cycle Ten, Sulfated Particles d. Cycle Ten, Regenerated Particles

Fig. 43. Photomicrographs of Sulfated and Regenerated Greer Limestone Particles (X24)

Table 19. Losses of Greer Limestone Caused by Attrition and Elutriation during Sulfation and Regeneration Steps in the Cyclic Utilization Study

A = Ca in feed limestone (sulfated or regenerated), kg/hr
B = Ca in particles collected from off-gas, kg/hr

Loss = $100 \times \frac{B}{A}$

		Limestone Loss, % during	
Cycle No.		Sulfation	Regeneration
1		20.0	2.9
2		12.0	0.6
3		9.2	-
4		7.4	1.3
5		8.6	-
6		8.6	2.9
7		4.3	2.0
8		3.8	1.6
9		2.6	2.4
10		4.9	1.5
	Avg	8.2	1.9

attrition were ∿2.0% during each regeneration step. During sulfation, the losses were ∿20% in the first cycle and steadily decreased to ∿4% in the final cycles. During the first sulfation cycle, the limestone calcined. The sulfated product contained 0.9 wt % CO_2 in sulfated limestone; ∿3% of the available calcium was carbonate. No recarbonation occurred in the entire cyclic experiment. The heavier attrition losses in the first sulfation step can be attributed to calcination. In subsequent cycles, the resistance of the particles to attrition increased because of (1) sulfated hardening and (2) partial sintering which occurs at the regeneration temperature.

The losses during sulfation were slightly higher for the Greer limestone cyclic experiment than for the Tymochtee dolomite experiment (Table 14). However, combustion operating conditions were different in these experiments. The Greer limestone was fully calcined at the system pressure of 308 kPa and a bed temperature of 855°C whereas the $CaCO_3$ in the Tymochtee dolomite was not at 810 kPa and 900°C.

The combined average losses caused by attrition and elutriation per cycle were ∿10%. Therefore, the fresh Greer limestone makeup rate is expected to be at least ∿10% to replenish losses. A higher makeup rate may be required to maintain the SO_2-sorption reactivity in the fluidized bed of the boiler.

h. Total Cyclic Limestone Inventory

A total cyclic inventory history for the Greer limestone is contained in Table 20. The total loss per cycle was ∿12--∿9.0% during sulfation and ∿3.0% during regeneration. These losses, based on total inventory (∿12%), are higher than those reported in the preceding section (∿10%) which were based on steady-state mass balances. The total losses include all losses during cyclic handling (spills, *etc.*).

Table 20. Total Reacted Limestone Inventory as a Function of Cycle and Stage

Cycle	Stage	Total wt, lb	Ca, %	Ca, lb-moles	Loss, %
1	S[a]	468	32.4	3.783	
	R[b]	374.0	41.1	3.835	1.4
2	S	393	34.6	3.440	10.3
	R	328.0	40.0	3.273	4.9
3	S	325	34.9	2.830	13.5
	R	280.0	39.7	2.773	2.01
4	S	280.1	36.4	2.544	8.3
	R	204	39.5	2.010	21.0
5	S	245	34.7	2.117	5.3[c]
	R	203	39.9	2.023	4.4
6	S	204	34.9	1.776	12.2
	R	192	40.8	1.954	10.02[c]
7	S	186	35.6	1.652	15.5
	R	164	40.4	1.657	3.0
8	S	166	36.2	1.499	9.5
	R	143	39.6	1.413	5.7
9	S	149	35.2	1.309	7.4
	R	132	39.8	1.311	0.2
10	S	136	36.1	1.225	6.6
	R	124	39.0	1.209	1.3

Avg S 8.7
Avg R 3.4

[a] S = sulfated.
[b] R = regenerated.
[c] Negative losses due to experimental inaccuracy.

7. Regeneration Process Scale-up and Flowsheet Determination

(J. Montagna and G. Smith)

The development of the fluid-bed, reductive decomposition regeneration process for sulfated limestones has been successful. A stage has been reached at which the potential integration of sorbent regeneration with a FBC boiler plant is being considered by ERDA. As the next step a 10-MWe boiler, equivalent in size to a cell in the Rivesville pilot plant, is being used as a basis for the calculations. The actual size and location of the "next stage" regeneration facility has not been determined by ERDA.

A process flowsheet for a FBC process with sorbent regeneration is discussed. Tymochtee dolomite is the sorbent used. The performance of Tymochtee dolomite as a function of cycle number was established in a ten-cycle experiment; most of those results are reported in a preceding section. Because the sulfation step in those experiments was performed at 8 atm instead of 1 atm used in Rivesville, the obtained sulfation reactivity function may be high for atmospheric boiler predictions. Those results on reactivity, calcium utilization, ash buildup, and elutriation as a function of cycle number have been incorporated into the ANL-developed regeneration process model (ANL/ES-CEN-1016).

Flow diagrams containing mass and energy flow streams have been obtained for different process conditions. These calculations are intended to evaluate the effect of makeup CaO/S feed rates (feed rate of virgin dolomite into the system) to the boiler on the size of the regeneration system, on the SO_2 concentration in the regenerator off-gas, and on the fuel burden of the sorbent regenerator on the boiler or power plant.

The following base conditions are assumed for the boiler: $\sim$12.1 m^2 (130 ft^2) gas distributor plate area, 3.05 m/s (10 ft/sec) fluidizing-gas velocity, 3% excess oxygen in the flue gas, and combustion of 90.8 tonnes/day (100 tons/day or T/D) of Sewickley coal, which contains 4.3 wt % sulfur and has a heating value of 7,220 kcal/kg (13,000 Btu/lb).

A process flowsheet for the above boiler conditions and a fresh sorbent feed CaO/S ratio of 0.2 is given in Fig. 44. The combined (virgin plus regenerated) dolomite CaO/S feed ratio is $\sim$2.0. In the absence of regeneration, a CaO/S feed ratio of $\sim$1.0 would be required for Tymochtee dolomite based on reactivity data that was obtained at 8 atm.

The sulfated dolomite ($\sim$50 T/D) is assumed to be introduced into the regenerator at 843°C (1550°F), the temperature in the fluid bed of the boiler. Boiler flue gas and air are mixed to provide the required oxygen concentration in the regenerator (17.2% O_2), and a fluidizing-gas velocity sufficiently high to prevent agglomeration of the fluidized bed of the reactor. The fluidizing gas velocity of 1.37 m/s is $\sim$12% above the velocity predicted to be required to prevent agglomeration of sorbent having a mean size of 1500 μm (-1/8 in.) and regenerated at 1100°C with 2% reducing gas in the regenerator off-gas. The fluidizing gas to the regenerator is assumed to be heated to 843°C by recovering waste heat from the regenerator off-gas and other process streams.

The coal consumption by the regenerator reactor with 843°C solids and gas feed streams was estimated to be 2.9 T/D. This includes an equivalent coal thermal credit of 0.55 T/D for the sensible heat which is carried by the hot regenerated sorbent to the boiler. The SO_2 concentration in the regenerator off-gas is predicted to be 9.5% (dry), and the gas distributor area for the regenerator is predicted to be 0.66 m^2 (7.1 ft^2).

The makeup (fresh sorbent) feed rate in a regenerative system is dependent on (1) the sorbent losses due to attrition and (2) losses in sorbent reactivity with usage. The total feed rate of sorbent (fresh sorbent

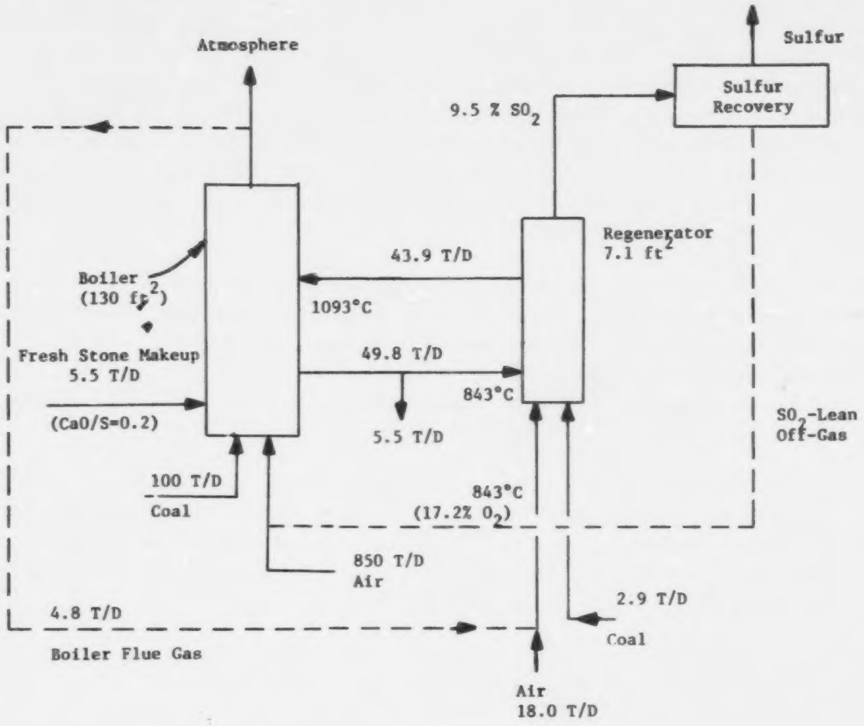
Atmosphere
Sulfur
Sulfur Recovery
9.5 % SO_2
Regenerator 7.1 ft^2
Boiler (130 ft^2)
43.9 T/D
1093°C
Fresh Stone Makeup 5.5 T/D
(CaO/S=0.2)
49.8 T/D
843°C
5.5 T/D
SO_2-Lean Off-Gas
100 T/D Coal
843°C (17.2% O_2)
850 T/D Air
2.9 T/D Coal
4.8 T/D
Boiler Flue Gas
Air 18.0 T/D

Fig. 44. Process Flowsheet for a 10-MWe FBC Boiler with Sorbent Regeneration, Using Tymochtee Dolomite. Regeneration Conditions: T = 1100°C, Sorbent residence time = 7 min, P = 1 atm, Extent of regeneration = 70%, V = 1.37 m/s, Bed depth = 0.46 m (1.5 ft)

and regenerated sorbent) into the boiler is dependent on the combined reactivity of the sorbent.

The effect of makeup (fresh sorbent) CaO/S mole feed ratio to the boiler on the regeneration system was evaluated and is shown in Table 21. Increasing the makeup CaO/S feed ratio from 0.16 (5% of total CaO/S feed) to 0.28 (20% of total CaO/S feed) would cause (1) the mass rate of sulfated stone that must be regenerated to decrease from 85 T/D to 32 T/D, (2) the sorbent waste stream (combined elutriated and draw-off sorbent) to increase from 4.5 T/D to 7.9 T/D, and (3) the size of the regeneration system to be decreased by a factor of ∿3. The coal required for the regeneration step would decrease from 4.6 T/D to 2.6 T/D. (Boiler coal consumption is 100 T/D.) The SO_2 concentration in the regenerator off-gas would increase from 6.6% to 12% over the same range of CaO/S makeup ratios (0.16 to 0.28). Reducing the power plant's fresh sorbent requirement (and its spent sorbent waste stream) would increase the size of the regeneration and sulfur recovery

Table 21. Effect of Makeup CaO/S Mole Feed Ratio for Tymochtee Dolomite in Boiler on Regeneration System (10-MWe FBC boiler)

Regeneration conditions: T = 1100°C, Extent of regeneration = 65%
P = 1 atm, Solids residence time = 7 min

Boiler CaO/S Mole Feed Ratio		Effluent Boiler Mass Rate, T/D		Coal[a] Required for Hot Regeneration, T/D[b]	Thermal Credit for Regen. Sorbent, T/D	Required O_2 in Regen. Feed Gas, %	Regenerator, Size, ft^2	SO_2 Conc. in Regen. Off-Gas, %
Makeup	Total	Waste Stream	Regenerator Feed					
0.16	3.2	4.5	85	4.6	1.0	14.1	12	6.6
0.2	2.0	5.5	50	2.9	0.55	17.2	7.1	9.5
0.28	1.4	7.9	32	2.6	0.32	20.3	4.5	12.0

[a] Boiler coal consumption is 100 T/D.

[b] Includes thermal credit for hot regenerated sorbent.

system, would decrease the SO_2 concentration of the regenerator off-gas (which would increase the cost of sulfur recovery), and would increase the fuel burden of the regeneration step on the boiler.

The above technical relationships must be combined with economic considerations in choosing a sorbent makeup rate. Economic evaluation is being performed at ANL.

8. Regeneration System Modifications

(J. Montagna and F. F. Nunes)

Installation of a fluidized-bed sorbent preheater in the PDU sorbent regeneration system has been completed. A new top flange for the regenerator designed to accommodate the sorbent preheater has also been installed. A schematic of the regeneration system with sorbent preheater is shown in Fig. 45.

In the absence of the preheater, the sensible heat required to raise the temperature of the sulfated sorbent from room temperature to ∿1100°C (normal operating temperature of regenerator reactor) was a large part of the total process thermal requirement. Since the sorbent would enter the regenerator reactor at ∿870°C or higher in an industrial process, this is unrealistic.

The fluidized-bed sorbent preheater will be used to evaluate the effect of sorbent feed temperature on the regeneration process. Then the results will be compared with predictions.

For startup, the sorbent preheater is electrically heated through the metal shell (6-in. pipe), which is lined with a castable refractory (3-in. ID) to permit high internal operating temperatures without exceeding the design metal wall temperature of the reactor (538°C). To provide the required heat during operation, kerosene is combusted under oxidizing conditions in the fluidized bed of the sorbent preheater.

The bed height in the sorbent preheater can be varied by allowing the sorbent to exit at any one of four vertically oriented overflow locations. This allows the sorbent residence time in the preheater to be varied while the sorbent feed rate into the fluidized-bed regenerator is kept constant.

These parameters can now be used to establish the experimental conditions for testing the filter in the ANL flue-gas system using the Ergun correlation. The correlation should also prove helpful in translating results obtained in the ANL flue-gas system at temperatures of 250-300°F and pressures of 8 atm to higher temperature (∿1600°F) conditions.

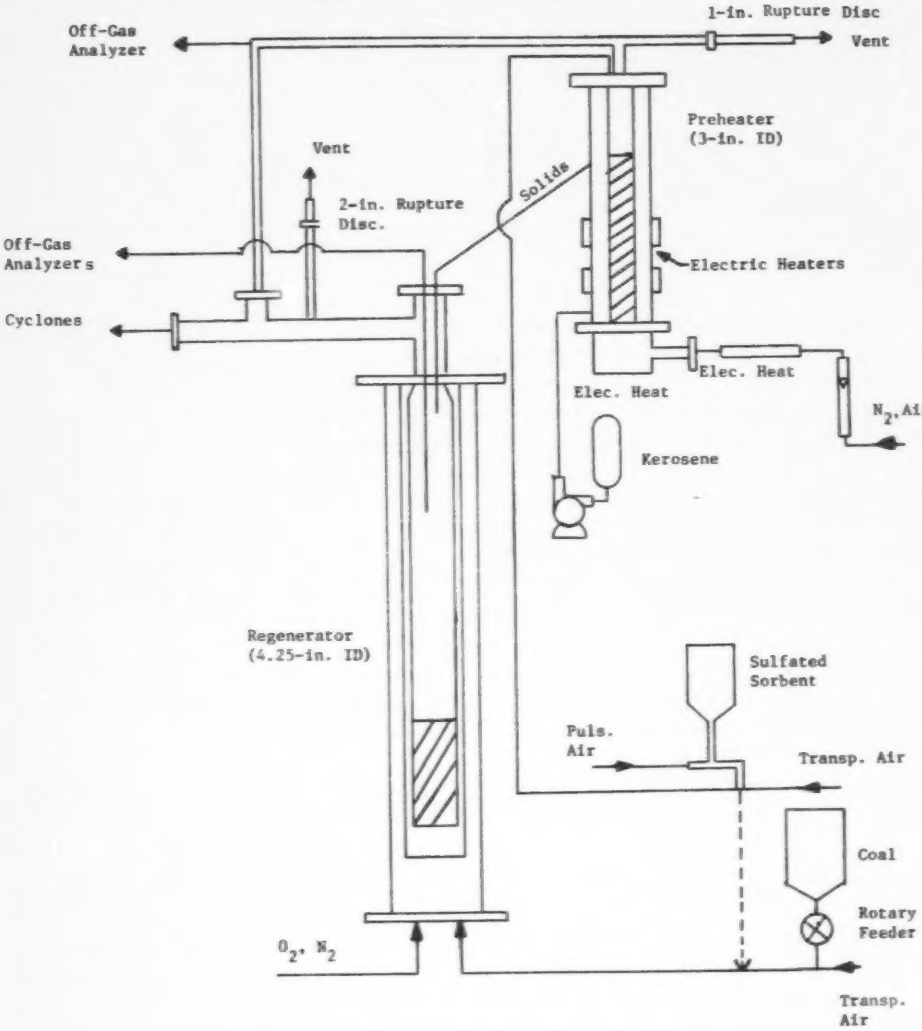
1-in. Rupture Disc
Off-Gas Analyzer
Vent
Preheater (3-in. ID)
Vent
2-in. Rupture Disc.
Solids
Off-Gas Analyzers
Electric Heaters
Cyclones
Elec. Heat
Elec. Heat
N_2,Air
Kerosene
Regenerator (4.25-in. ID)
Sulfated Sorbent
Puls. Air
Transp. Air
Coal
Rotary Feeder
O_2, N_2
Transp. Air

Fig. 45. Schematic of Regeneration System with Sorbent Preheater

TASK B. REGENERATION PROCESS ALTERNATIVES

No report for this period.

TASK C. SYNTHETIC SORBENTS FOR SO_2 EMISSION CONTROL

(R. B. Snyder, W. I. Wilson, and Irving Johnson)

1. Introduction

For fluidized-bed coal combustion, naturally occurring limestones and dolomites are the principal calcium-bearing materials being considered for the sorption of SO_2. This is primarily due to their low cost and vast reserves. However, these materials have some disadvantages. Attrition rates may be excessively high, especially at high superficial gas velocities of 4-5 m/s. Also, during cyclic sulfation and regeneration, the reactivity of the limestone sorbent with SO_2 will decrease. Finally, it may be determined that regeneration of these sulfated sorbents is not economical, in which case large quantities of limestones must be quarried and disposed of. Due to these potential disadvantages, synthetic SO_2-sorbent materials were investigated as an alternative to limestones.

It has been determined that CaO in α-Al_2O_3 is the most promising synthetic SO_2 sorbent.[17] The preparation method and reactivity of this synthetic sorbent[18] have been previously reported (ANL/ES/CEN-1016).

The three subjects studied and reported below are: (1) attrition resistance, (2) bauxite support material, and (3) cost.

2. Attrition Resistance

The attrition rate of a 10.4% CaO in α-Al_2O_3 synthetic SO_2 sorbent was compared with that of Tymochtee dolomite, half-calcined Tymochtee dolomite, sulfated Tymochtee dolomite, and 1100°C heat-treated (H.T.) α-Al_2O_3 support material for synthetic sorbents. All starting material for attrition tests was in the size range, -14 +30 mesh. The test materials were screened before and after each test to help determine the attrition mechanism. These attrition tests were performed in a 5.08-cm-dia fluidized bed at room temperature. The attrition rate was determined as the amount of material lost overhead in 10 hr. The attrition results are shown in Table 22. The synthetic sorbent had one-fifth the attrition rate of sulfated Tymochtee dolomite, only 0.6% being lost. The uncalcined and half-calcined dolomite had high attrition rates--23 and 47%, respectively. The α-Al_2O_3 support material had a 3% material loss in 10 hr; this indicates that impregnation with CaO to form calcium aluminates hardens the material, making it more attrition-resistant.

The results are shown in Figs. 46-48 for (1) granular α-Al_2O_3 that had been heat-treated (H.T.) at 1100°C, (2) sulfated dolomite, and (3) regenerated dolomite for which results are not shown in Table 22. The weight percent of material is given for various particle diameters (1410 to 30 μm).

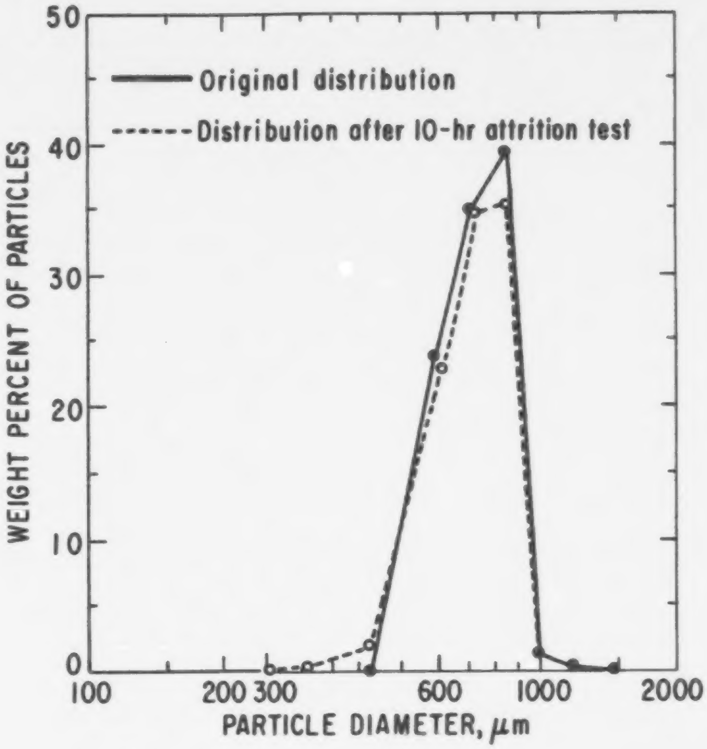

Fig. 46. Particle Size Distribution of α-Al_2O_3 (heat-treated at 1100°C) Before and After Attrition Test

3. Bauxite Support

Due to the high cost of synthetic sorbent, CaO in α-Al_2O_3 (see below), bauxite, a less expensive material, was tested as a support material. The bauxite used in these experiments was approximately 70% Al_2O_3-30% SiO_2 and was obtained from Harbinson-Walker Refractories, Chicago. The bauxite was heat-treated at 1100°C for 6 hr or at 1500°C for 8 hr in an attempt to enlarge the pore diameters in the support and to stabilize grain growth. The porosity curves for the bauxite heat-treated at the two temperatures are shown in Fig. 49, where they are compared with bauxite dried at 110°C for 2 hr. Heat-treating at 1100°C increased the total porosity and increased the average pore diameter. However, heat-treating at 1500°C caused particle shrinkage and a loss of porosity.

Two synthetic sorbents were prepared from the heat-treated bauxites and were tested for reactivity. The conversion of CaO to $CaSO_4$ for the 13.2% CaO in 1100°C H.T. bauxite and for the 14.2% CaO in 1500°C H.T. bauxite are shown in Fig. 50. The bauxite-supported sorbents are compared with a 14.8% CaO in α-Al_2O_3 sorbent and with Greer limestone. The bauxite sorbents had the poorest performance--only conversion of $\sim$31% of the calcium to $CaSO_4$.

Table 22. Fluidized-Bed Attrition Experiments L/D = 1.38; Fluidizing Gas Velocity = 0.6 m/s

Run	Sample	Particles in Bed after 10 hr, %	Percent Loss[a] in 10 hr
1	Tymochtee Dolomite (half-calcined) (-14 +30)	52.6	47
2	Sulfated Dolomite	96.7	3
3	Tymochtee Dolomite (uncalcined)	77	23
4	1100°C H.T. granular α-Al_2O_3 support	97.4	3
5	10.4% CaO in granular α-Al_2O_3 support	99.4	0.6

[a] The percent loss determined as grams of overhead material x 100/gram original material. All overhead material was smaller than 70 mesh.

The 1100°C H.T. α-Al_2O_3 had only a 3% materials loss in 10 hr of attrition, and therefore in Fig. 46, only a slight change in particle diameter distribution is seen. The amounts of original material between 18 and 16 mesh (1000 μm, 1.3%) and between 16 and 14 mesh (1190 μm, 0.4%) were small. In contrast, the sulfated dolomite distribution was skewed toward large particle diameters (Fig. 47). This material also had a 3% material loss (Table 22). In this graph, one can see the slight shift in distribution to smaller particles. Figures 46 and 47 tend to indicate that the mechanism for attrition is abrasion (the wearing away of surface material), in contrast to the breakup or splitting of particles due to particle-particle or particle-wall collision.

Figure 48 confirms that abrasion is the mechanism of material loss. This graph shows the particle size distributions for dolomite before and after a 10-hr attrition test. Material lost from the bed, which was collected on a filter, constituted 50% of the bed. This overhead material had very small particle diameters (37-74 μm). Very little overhead material was in the particle diameter range from 200 to 300 μm. There was no bed material left in the final bed with diameters below 400 μm. If there had been particle splitting, one would expect to find not a bimodal distribution, but a shift of all particles to smaller sizes. The bimodal distribution found indicates that abrasion was occurring and that the particles attrited had a diameter range of 30 to 80 μm. Figures 46 and 47 show no bimodal distribution for the material after attrition since only a very small quantity of material was lost.

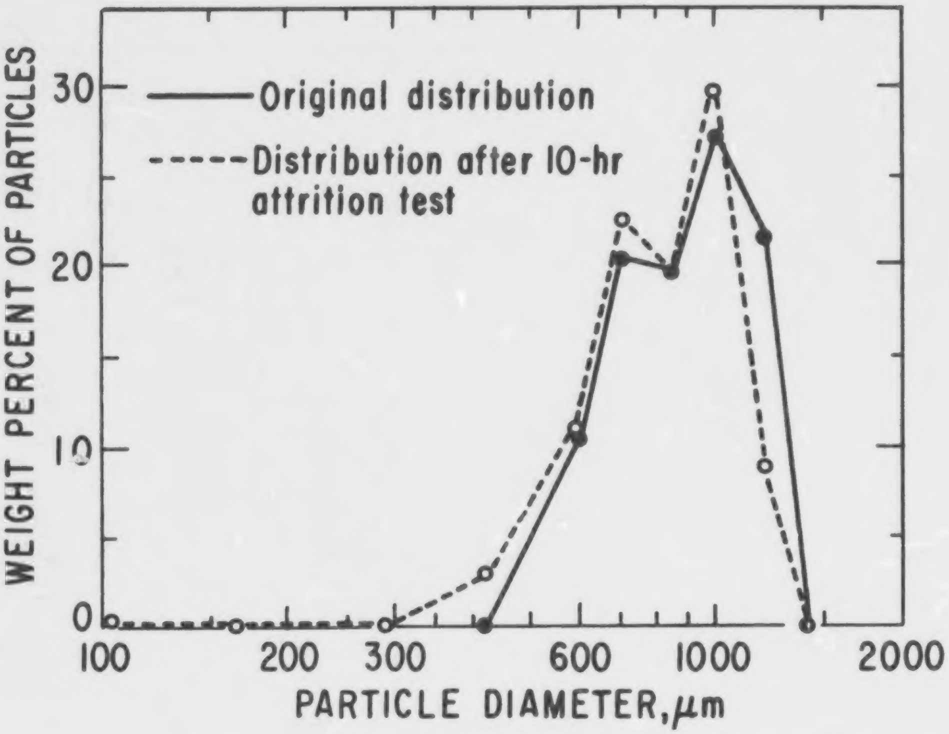

Fig. 47. Particle Size Distributions of Sulfated Dolomite from First Cycle of Ten-Cycle Experiment Before and After Attrition

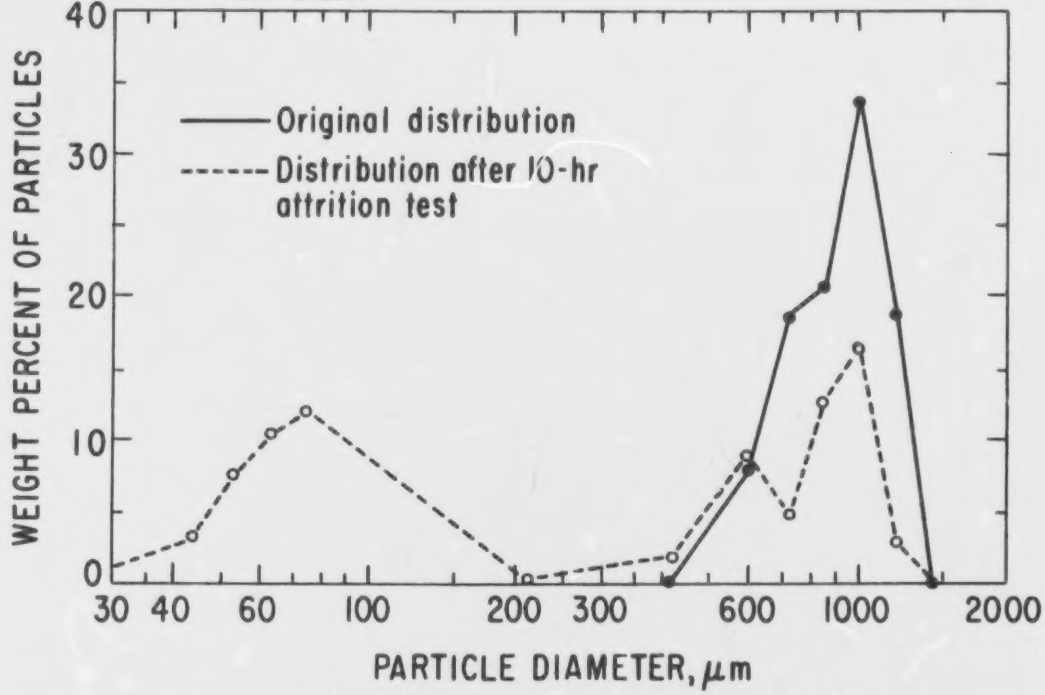

Fig. 48. Particle Size Distributions of Regenerated Dolomite, Before and After Attrition Test

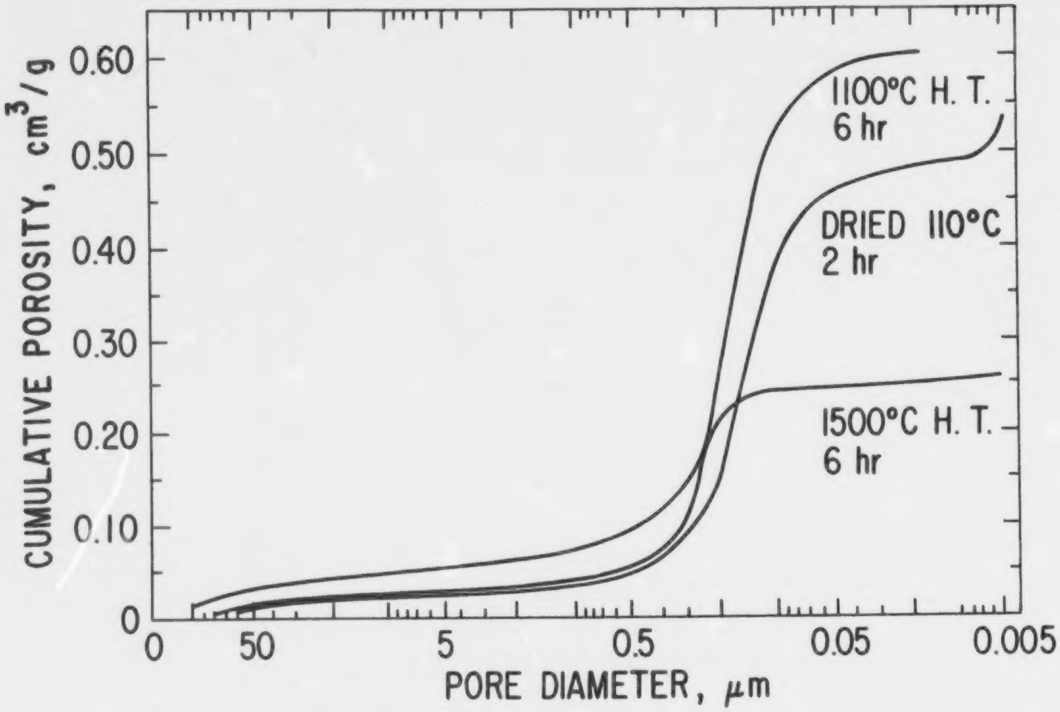

Fig. 49. Porosity of Bauxite

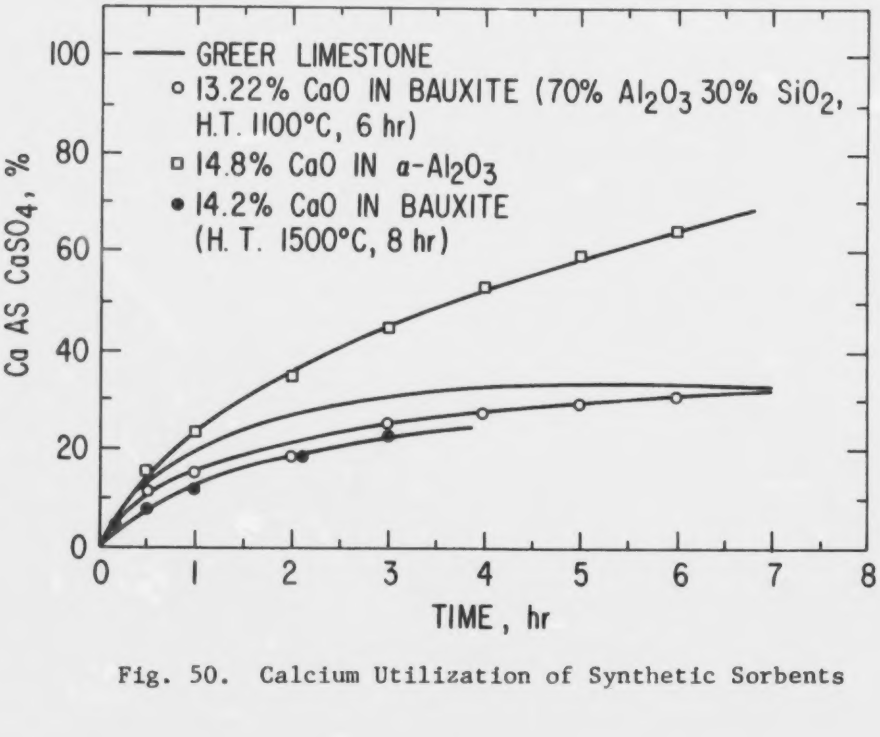

Fig. 50. Calcium Utilization of Synthetic Sorbents

In Fig. 51, the number of grams of SO_3 captured per kilogram of sorbent material is shown as a function of time. In 4 hr, the bauxite-supported sorbent captured only 50 g of SO_3--in comparison, Greer limestone captured 190 g, almost four times as much. The poor reactivity, compared with that of CaO in α-Al_2O_3 sorbent, is probably due to the low reactivity of calcium silicates in the bauxite.

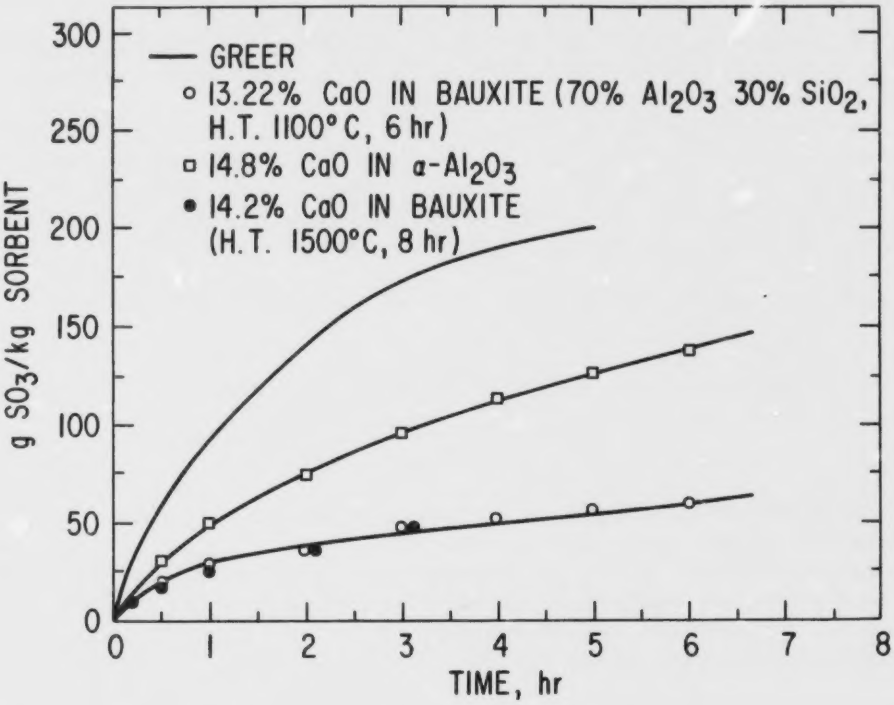

Fig. 51. Rate of SO_3 Capture by Sorbents

Because of the poor performance of sorbents prepared from bauxite and the loss of porosity upon heat treatment at 1500°C, these sorbents are concluded to be unacceptable.

4. Cost

The main incentive for developing synthetic sorbents is to reduce the environmental impact of the SO_2-emission control systems for fluidized-bed coal combustion systems. In this section, the cost of using synthetic sorbents will be compared with the cost of a once-through system using a natural limestone.

Synthetic sorbents of the type developed in this study will be more costly than natural limestones. No large-scale preparational method for synthetic sorbents has been devised and tested, and the laboratory method can be used as the basis for an estimation of the cost. If refined hydrated alumina ($Al_2O_3 \cdot H_2O$) is used as a source of the alumina, then to prepare one ton of a 20% $CaO \cdot Al_2O_3$ sorbent, about 0.94 ton of alumina would be needed which at \$118 per ton would cost \$111. Two-tenths of one ton of chemical lime at \$25 per ton would add \$5 to the cost. About 900 lb of nitric acid at \$4.50 per 100 lb would add another \$40 to the material cost, yielding a total material cost of \$156 per ton.

Hydrated alumina must be heat treated to form porous alumina support, treated with $Ca(NO_3)_2$ solution, dried, and given a final heat treatment. These steps are estimated to cost about \$100 per ton. Thus, the final synthetic sorbent would be about \$250 per ton. Since additional development of the process should lower the cost, a cost of about \$200 per ton does not seem to be unrealistic at the present time. This cost is about 20 times that of a natural limestone, which is assumed to be about \$10 per ton delivered to the FBC site and disposal after sulfation as landfill.

The total cost of SO_2 emission control may be computed using the equation:

$$\text{Total cost per kWh(e)} = \frac{RS}{C}\,[F\$ + (1 - F)G] \qquad (1)$$

where:

R = Ca/S (mole) ratio needed to achieve the EPA SO_2 emission level
S = moles of sulfur generated per kWh(e)
C = moles of calcium per kg of sorbent
F = fraction of new sorbent which must be fed per kWh(e)
\$ = cost of new sorbent, mills per kg
G = regeneration cost, mills per kg

The G factor will depend on the size of the regeneration plant, which will depend on the recycle rate and the size of the FBC. The numerical value of G is not known. An estimate for a pressurized fluidized-bed combustion system, made by Westinghouse in 1975,[19] indicated that the regeneration system would added about 3 mills per kWh(e) to the electrical power cost. The cost for an atmospheric FBC would be expected to be less than this--probably of the order of 1.5 to 2 mills per kWh(e).

To generate 1 kWh(e) of power requires about 0.8 lb of coal per hour. If this coal contains 4% sulfur and has a heating value of 12,200 Btu/lb, about 82% of the sulfur needs to be removed from the flue gas to meet the EPA standard of 0.6 lb of sulfur emission per 10^6 Btu. Thus for our system, 0.8 x 0.04 = 0.032 lb of sulfur will be produced for each kWh(e), or 0.45 mole per kWh(e), the value of S. If Greer limestone is used in an AFBC, a Ca/S ratio, R, of 3.1 is needed if the FBC is operated at 816-832°C with a 3.8-4.7 m/s superficial gas velocity. Greer limestone is a high SO_2 reactivity stone which has been used for many studies in large FBC test rigs. Greer limestone contains 80.4% $CaCO_3$ and hence the value of C is 8.04 moles of calcium per kg. The cost for a once-through system as obtained from Eq. 1 will be about 1.9 mills/ per kWh(e). Note that F = 1 in this case (*i.e.*, there is no recycle) and the cost of sorbent, $, is 11 mills per kg. The latter sorbent cost includes quarrying, shipping and disposal.

The Ca/S (R) ratio needed for a 20% $CaO-Al_2O_3$ synthetic sorbent must be estimated from a comparison of the TGA curves (Fig. 51) for the synthetic sorbent with a similar curve for Greer limestone. When this is done, it is estimated that an R value of 5 would be needed to achieve the 82% sulfur removal required to meet the EPA standard. This high value reflects the rather poor SO_2 capacity of the synthetic sorbent in comparison to a good natural limestone. Since the sorbent contains only 20% CaO, the value of C is 3.57 moles per kg.

Although the attrition rate measured for a synthetic sorbent would indicate that over 100 cycles would be possible, it seems best to assume a lower value. We have therefore assumed that 25 cycles can be achieved. On this basis, F is 0.04 and the sorbent cost when computed using Eq. 1 is 5.6 mills per kWh(e) or about three times the cost of one-through sorbent. To obtain the total cost of using the synthetic sorbent the regeneration cost must also be added. As noted above, this will probably add another 1.5 to 2 mills per kWh(e) to the cost, leading to a synthetic sorbent cost of about 7 mills per kWh(e) compared with about 2 mills/kWh(e) for once-through natural stone with the assumptions used above.

If one assumes that the environmental impact for the two systems may be taken to be proportional to the sum of the quantities of fresh sorbent feed and waste. In the case of the once-through system, the sum is 7.2 tonne/Mwd(e); for the synthetic sorbent, the sum is 1.2 tonne/Mwd(e). Thus a six-fold decrease in environmental impact would have an additional energy cost of about 5 mills/kWh(e). It is our opinion that this decrease in environmental impact is not sufficient to justify the additional energy cost.

Examination of Eq. 1 shows where any future work on synthetic sorbents should be concentrated. Two factors appear amenable to change, the SO_2-reactivity as represented by the Ca/S ratio, R, and the sorbent cost, $. It should be possible, by better control of the porosity and heat treatment, to obtain a synthetic sorbent at least as good as the best natural limestone. The cost of the synthetic sorbent is probably where the greatest improvement needs to be made. Although our limited experiments using a less expensive support material (the bauxite studies) did not yield high-reactivity sorbent, the results point to the direction where future studies should be concentrated. It is also clear from the results of this study that inexpensive starting materials must be used for synthetic sorbents since limestone is one of the least costly materials available.

5. Conclusions

The synthetic sorbent, CaO in $\alpha-Al_2O_3$, presently is the most promising synthetic sorbent for use in fluidized-bed coal combustors to minimize SO_2

emissions. K_2O and Na_2O in alumina have higher sulfation rates; however, their products (sulfates) decompose in the temperature range of interest for combustion and regeneration. These compounds contribute to corrosion of metals at high temperatures. Calcium oxide is the least expensive of the metal oxides tested. CaO sorbents capture more SO_2 per unit weight of sorbent than do barium oxide or strontium oxide; therefore, calcium oxide is the metal oxide of choice. The choice of α-Al_2O_3 as the support material was based on its stability in the temperature region being considered. The calcium aluminates also add to the mechanical strength of the sorbent, minimizing attrition.

The sulfation rate of CaO in α-Al_2O_3 sorbent is highly dependent on its physical properties, particularly the pore size distribution. Both pore diffusion and gas-solid diffusion control the rate of SO_2 capture by the sorbent; therefore, large pores in the support (with diameter larger than about 0.2 μm) are beneficial. Sorbents containing higher CaO concentrations are less porous. However, the optimum CaO concentration depends on the residence time required in the combustor and the CaO concentration effect on sorbent strength, since the quantity of SO_2 captured per unit weight of sorbents in a given time is independent of the sorbent's CaO concentration.

Natural sorbents (dolomite or limestone) contain higher concentrations of CaO than do the synthetic sorbents and therefore capture more SO_2 per unit weight of material. Thus, more synthetic sorbent material may be needed for each pass through the combustor (possibly twice as much). However, with regeneration of synthetic sorbent, the overall consumption of synthetic sorbent should be lower.

The estimated large increase in the cost of electricity to obtain the moderate decrease in environmental impact that would be achieved by using synthetic sorbents is considered to be unacceptable. Therefore, at this time, synthetic sorbents are not believed to be a viable option for reducing SO_2 emissions from a fluidized-bed coal combustor. A final topical report on these studies has been prepared (ANL/CEN/FE-77-4).

TASK D. LIMESTONE CHARACTERIZATION
(R. Snyder and I. Wilson)

A research program is under way to characterize limestone for fluidized-bed coal conversion plants. That is, the reactivity of limestone with SO_2 under various environmental conditions is being determined and correlated with limestone physical properties. Pretreatment (precalcination and heat treatment) is being investigated and the mechanism of SO_2 capture is being studied. Finally, the attrition rate of the various limestones in fluidized beds was determined.

1. Limestone Properties Affecting SO_2 Reactivity

Ten limestones and dolomites were fully calcined at 900°C in 20% CO_2-80% N_2 in a thermogravimetric analyzer (TGA), after which they were immediately reacted at 900°C with a 0.3% SO_2-5% O_2-20% CO_2-balance N_2 synthetic combustion gas mixture in the same apparatus. The results are shown in Fig. 52.

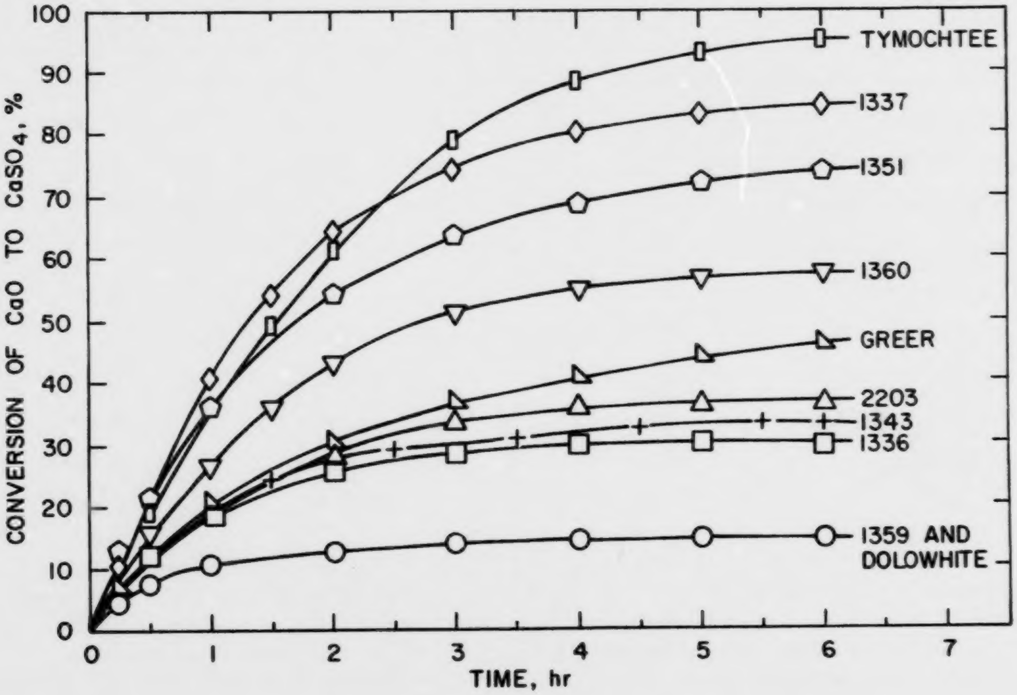

Fig. 52. Calcium Utilization at 900°C for Ten Precalcined (at 900°C) Limestones in a Thermogravimetric Analyzer. Sulfation gas composition: 0.3% SO_2, 5% O_2, 20% CO_2, and balance N_2.

Different stones vary greatly in (1) reactivity of the CaO with SO_2 and (2) calcium utilization. In 5 hr of sulfation, 95% of the calcium (as CaO) in Tymochtee dolomite was converted to $CaSO_4$, whereas for dolowhite and limestone 1359, only 15% of the calcium was utilized.

To be able to predict the rate of SO_2 capture or calcium utilization of a given limestone, one must determine which limestone physical properties affect SO_2 reactivity. Below (in Table 23), the chemical compositions of the limestones and dolomites studied are given. The stones are listed in order from highest to lowest calcium utilization after 5 hr of reaction. Since $MgCO_3$ converts to MgO on calcination, helping to make the material porous, one can also attempt to correlate $MgCO_3$ content with calcium utilization. There is a trend of greater calcium utilization with higher $MgCO_3$ concentration except for dolowhite, which has a high $MgCO_3$ concentration, 44.4% but has a low calcium utilization. Additional limestones with high magnesium contents will be tested to determine if dolowhite is an anomaly.

Table 23. Chemical Compositions of Limestones (listed in order of highest to lowest calcium utilization after 5-hr reaction time)

	Composition, wt %						
	$CaCO_3$	$MgCO_3$	SiO_2	Al_2O_3	Fe_2O_3	Na_2O	H_2O
Tymochtee dolomite	51.5	43.0	3.6	1.5	0.4	0.07	0
Limestone 1337	53.4	45.4	0.7	0.08	0.07	0.08	0.3
Limestone 1351	61.2	28.7	3.2	0.5	5.6	0.13	0.67
Limestone 1360	81.6	11.6	1.9	0.2	0.9	0.10	3.7
Greer limestone	80.4	3.5	10.3	3.2	1.2	0.23	1.17
Limestone 2203	96.0	3.6	0.2	0.01	0.2	0.04	0
Limestone 1343	89.8	2.2	4.0	1.0	0.7	0.1	2.2
Limestone 1336	92.6	5.3	1.3	0.4	0.2	0.1	0.1
Limestone 1359	95.3	1.3	0.8	0.3	0.1	0.03	2.2
Dolowhite	55.2	44.4	0.2	0.01	0.09	0.02	0.1

High silica content also may affect calcium utilization, possibly decreasing calcium utilization due to the formation of stable calcium silicates. However, Greer limestone does not seem to be strongly affected by its unusually high SiO_2 content of 10.3%. High sodium content would be expected to increase reactivity; however, no trend was observable from Table 23 data. Apparently, calcium utilization can not be predicted from chemical composition alone.

Unpublished data obtained at ANL indicate that calcium utilization is more likely to correlate with the surface area of CaO in "sufficiently large pores" than with chemical composition. Therefore, porosity measurements were performed on all of the limestones to determine what is a "sufficiently large pore." From a porosity measurement, one also obtains the cumulative volume of pores which have a maximum diameter between 100 μm and a specified smaller size. From this information, the internal surface area can be obtained as a function of decreasing pore diameter.

The environmental history of a limestone sample affects its porosity curve. The porosity curves were determined on natural limestone--18 to 20 mesh material which had been calcined at 900°C for 15 min in a 20% CO_2-80% N_2 atmosphere. Changing of any of the above conditions would produce different results which would most likely prevent meaningful interpretation.

The reasons for selecting the conditions used are as follows: Different sizes of particles have different reaction rates and different porosities. To minimize the effect of particle size distribution, a narrow size range was chosen--the starting material was virgin limestone which had been sieved to 18-20 mesh. Porosity determinations were made on calcined limestones prepared from the same lot as were the calcined 18-20 mesh limestones (sulfated on the TGA), and the porosities of these two materials were compared.

The calcining conditions prior to porosity measurements must exactly reproduce the calcining conditions used on the TGA because (as is well known) the rate of calcination is affected by temperature and CO_2 concentration. The rate of calcination affects the pore size distribution and the crystal structure of the limestone and hence its reactivity. Since the sulfation reactions (for which results are given in Fig. 52) included calcination at 900°C in 20% CO_2, these same conditions were chosen for calcining the limestones prior to porosity measurements. Porosity measurements were made immediately after a sample was calcined since CaO is an excellent desiccant and reacts with water to form calcium hydroxide, causing a loss in total porosity.

Figure 53 shows the porosity curves for the ten calcined limestones. Limestone 1360 had the greatest total porosity (0.75 cm^3/g), and it had more internal pore volume contributed by large pores (pore diameter, >0.2 μm) than did the other stones. Limestone 1336 had the least total porosity (0.31 cm^3/g). However, total porosity does not correlate with reactivity nor with calcium utilization. Most of these limestones are uni-modal, having only one major size cluster of pores. For example, the diameters of a majority of limestone 1337 pores range from 0.035 to 0.07 μm. Dolowhite has a low reactivity and its pore cluster occurs at pore diameters that are smaller (0.025-0.045 μm) than for the other stones. This implies that these small pores plug or close off quickly during sulfation due to the formation of $CaSO_4$.

It is concluded that there is a minimum size pore whose surface area of CaO is reactive with SO_2--that is, there is a minimum effective pore diameter. Below this size, pores will close off prematurely during sulfation since $CaSO_4$ has a larger molar volume than does CaO. The cumulative surface area was determined for all pores with diameters larger than each of several specified minimum diameters. Correlation of calcium utilization with this cumulative surface area was then attempted. A correlation was not observed

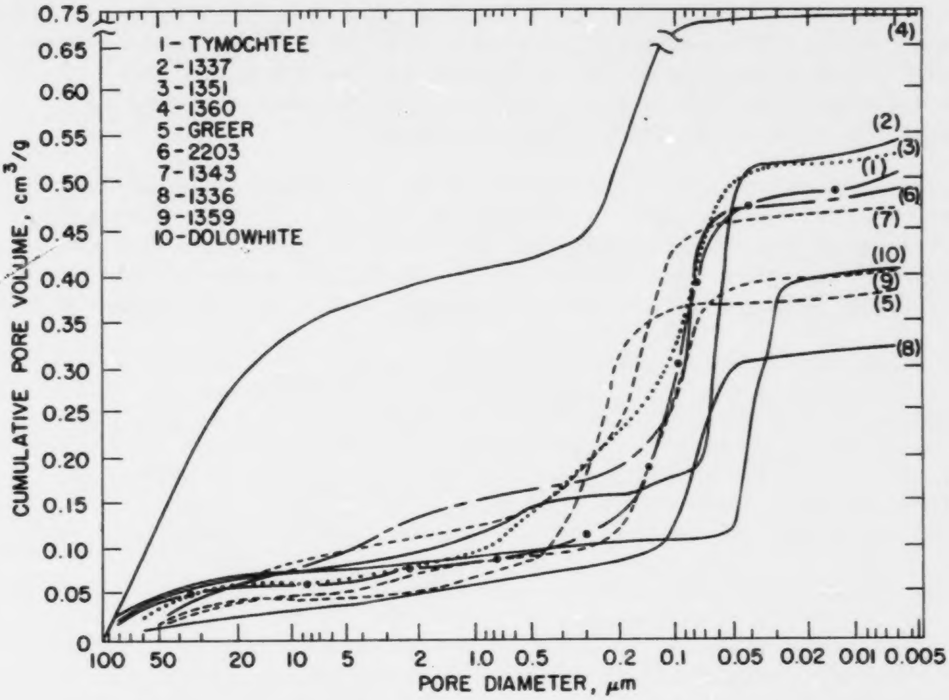

Fig. 53. Cumulative Pore Volume as a Function of Pore Diameter for Ten Limestones

when a specified minimum pore diameter was used for each limestone. It is highly unlikely that all limestones have the same minimum effective pore diameter. In fact, one would expect that the greater the calcium content of the limestone, the larger the pores would have to be in order not to prematurely plug with $CaSO_4$.

The inert materials (SiO_2, Al_2O_3, Fe_2O_3) probably do not affect plugging behavior since they are not part of the calcium-magnesium crystal structure. Therefore, a minimum pore diameter, MPD, was determined based on the Mg/Ca ratio in the limestone.

$$MPD = \frac{174}{5400\left(\frac{\%\ MgCO_3}{\%\ CaCO_3 + \%\ MgCO_3}\right) + 1000} \qquad (1)$$

where

MPD = minimum pore diameter, μm
$\%\ MgCO_3$ = wt % $MgCO_3$ in virgin limestone
$\%\ CaCO_3$ = wt % $CaCO_3$ in virgin limestone

The MPD was assumed to be linear with respect to the limestone's Mg/Ca ratio. It was also assumed that for a pure limestone, Mg/Ca = 0, the MPD is

0.174 μm, which is its value at 1000 psi during porosimeter measurements. Borgwardt and Harvey[20] have indicated that all calcined limestones with pores larger than 0.2 μm have high reactivity with SO_2.

Since dolowhite is nonreactive, it was assumed that the MPD for dolowhite is 0.05 μm, which reduces the effective surface area of dolowhite for reactivity to approximately 6500 cm^2/g.

By use of the above equation, the calcium utilization of various limestones was plotted against the surface area of pores having a diameter larger than the MPD. These results are shown in Fig. 54. This correlation applies reasonably well to all stones.

2. Effects of Precalcination and Heat Treatment

In atmospheric fluidized-bed coal combustion, large quantities of limestone sorbent (Ca/S ratio of 4/1 to 6/1) may be required so that the flue gas will meet EPA SO_2-emission standards. Pretreatment of limestones to enhance their reactivity and their calcium utilization may reduce limestone requirements. Therefore, the effect of calcination-heat treatment on calcium utilization of Greer limestone has been studied and a preliminary economic-environmental impact assessment made.

Greer limestone was precalcined at 900°C in a 20% CO_2-80% N_2 gas stream, then heat-treated at 900°C for 0, 2, 6, and 22.2 hr. The pretreated Greer limestones were then sulfated at 900°C on a TGA, using 0.3% SO_2-5% O_2 in N_2.

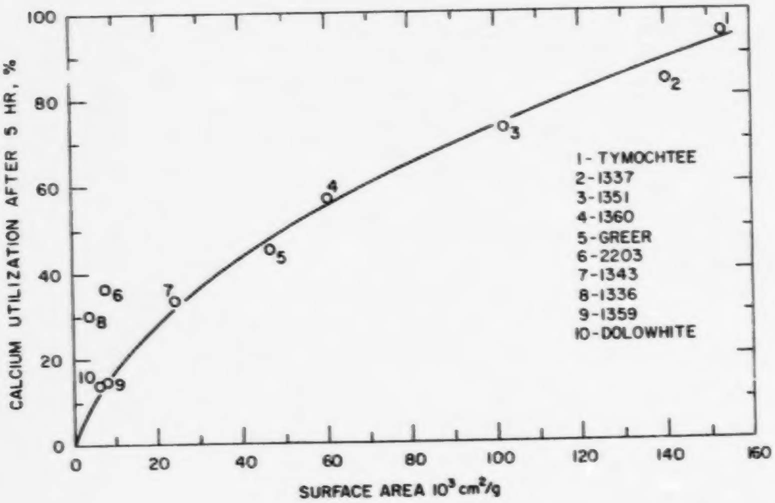

Fig. 54. Calcium Utilization as a Function of Surface Area of Pores having Diameters Larger than MPD for Ten Limestones

In Fig. 55, the percent conversion of CaO to $CaSO_4$ is given as a function of sulfation time for the various pretreated limestones. Their CaO conversions are compared with that of Greer limestone which was simultaneously calcined and sulfated with 0.3% SO_2-5% O_2-20% CO_2 in N_2 gas. The Greer limestone which was simultaneously calcined and sulfated had the poorest conversion--only 28% of the CaO was utilized to capture SO_2. This result is in excellent agreement with the data obtained on Greer limestone by Pope, Evans and Robbins[21] in a 9 ft^2 atmospheric combustor. They reported calcium utilizations of 25 to 28 percent with a limestone residence time of approximately 4 hr.

The Greer limestone tested in the TGA (Fig. 55) calcined completely in approximately 10 min. This was one-half the calcination time for the limestone which had been simultaneously calcined and sulfated. The lower calcination rate during simultaneous calcination-sulfation probably produces a limestone having smaller pores and thereby results in less calcium utilization.

Precalcination increased the calcium utilization from 28% to 43% for a 5-hr sulfation time. Heat treating the limestone for 2 hr after a 5-min precalcination further increased the calcium utilization from 43% to 48% (a residence time of 15 hr gave a 51% calcium utilization). Heat treating for 6 hr and 22.2 hr gave calcium utilizations of 52 and 55% in 5 hr. The precalcination and heat treatments definitely increased the sulfation rate and calcium utilization. However, after heat treating for 6 hr, additional heat treatment gave a minimal change in sorbent performance.

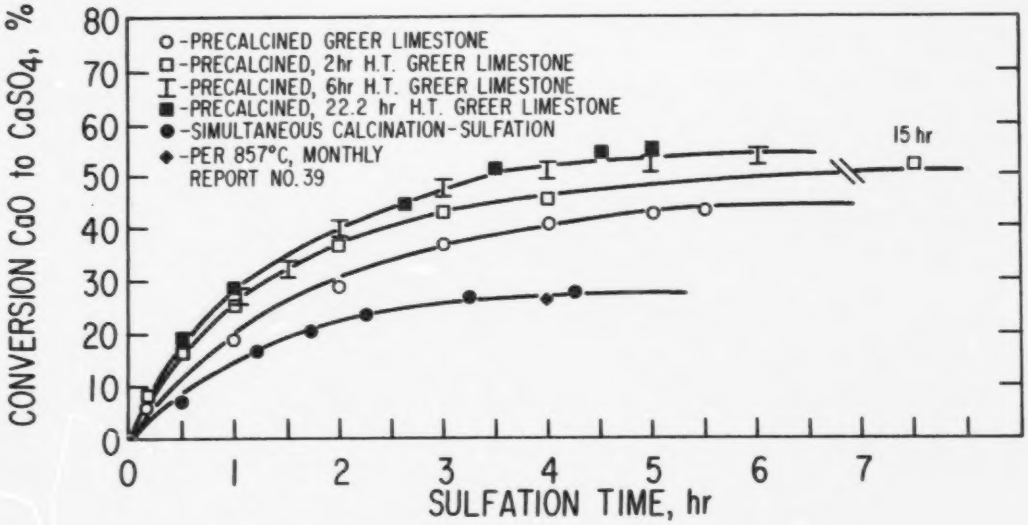

Fig. 55. Calcium Utilization as a Function of Various Pretreatments. Sulfation at 900°C with 0.3% SO_2-5% O_2 in N_2

To apply the results shown in Fig. 55 to a practical fluidized-bed combustion system, a preliminary economic analysis was performed to determine the cost of a precalcination-heat treatment step. The economic analysis was made for a 600-MW atmospheric fluidized-bed coal combustor.

The pretreatment costs were based on the costs quoted by the Kennedy Van Saun Corporation.[22] A kiln (calciner and heat treating unit) was estimated to cost $5 million/(1000 tons of calcined product per day). A limestone residence time of 178 min was assumed. This unit requires two operators per shift and also requires 5,000,000 Btu of energy per ton of product (calcined, heat-treated limestone). From this information, a first order economic analysis was performed to determine the cost of a pretreater for various limestone residence times and for various quantities of limestone per day.

Five costs were included in the analysis: capital, installation, operating, maintenance, and fuel costs. The capital cost was estimated to be a function of the limestone residence time and lime production rate to the 0.6 power. The installation cost was assumed to be twice the capital cost. On the basis of two men per shift, the operating cost was estimated to be 300,000 dollars per year. Maintenance cost and fuel cost are directly a function of the lime production rate. Limestone requirements were estimated to be 1720 tons/day for a plant using a Ca/S ratio of 4. For heat treatment times longer than 2 hr, the capital cost (installed) is the largest cost; the next largest is fuel cost.

From the above information, the increased energy cost can be estimated. If a 2-hr residence time and a Ca/S ratio of 4 are assumed, the increased energy cost of precalcination and heat treatment would be 0.85 mill/kWh. That is, it would cost 0.85 mill/kWh to decrease the environmental impact by 42 percent (Fig. 56).

Figure 56 illustrates the energy cost for reducing the environmental impact of Greer limestone. The environmental impact of Greer limestone with no precalcination treatment was arbitrarily set at 1.0. This can be converted to a given quantity of limestone that must be mined and disposed of. As shown in Fig. 56, the environmental impact can be reduced by increasing the energy cost (by means of pretreatment and thus greater calcium utilization). However, decreasing the limestone requirements further would require a large increase in energy cost. In fact, however much is spent, the environmental impact can not be reduced more than 50% by heat treating.

The above analysis is only for Greer limestone which has been tested at 900°C. Also, the cost analysis for pretreatment kilns is only a first approximation, and the effect of pretreatment on attrition has not yet been determined. Nevertheless, this is the type of cost *vs* environmental impact information needed for assessment of the viability of pretreatment.

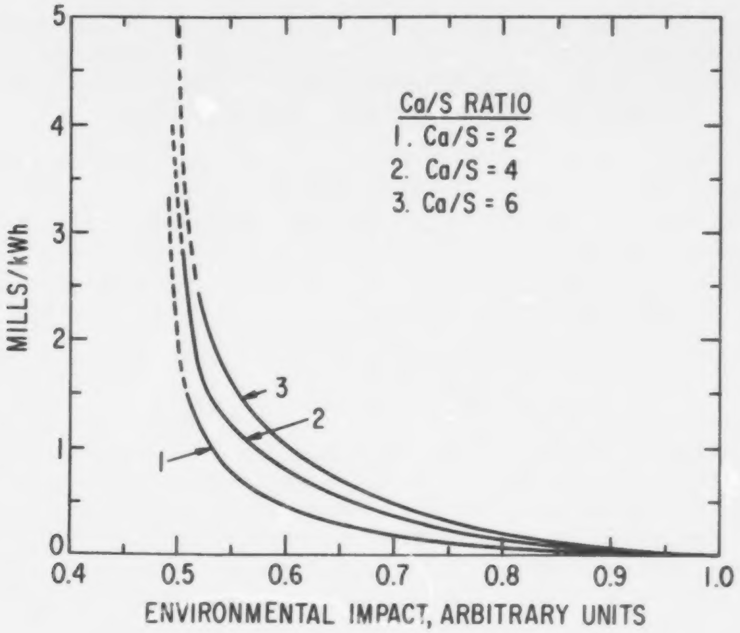

Fig. 56. Increased Energy Cost for Pretreatment Required to Reduce the Environmental Impact of Mining and Disposal of Sorbents

3. Limestone Attrition

The effects of fluidization velocity, the L/D ratio of the bed, and stone composition on limestone attrition rates are being studied in a room temperature (cold) fluidized bed. Attempts will be made to correlate the results with limestone attrition rates in fluidized-bed coal combustors. Also, the mechanism of attrition is being studied. In addition to the small room-temperature fluidized-bed test rig used in this work, a small 2-in.-dia high-temperature (850°C) fluidized-bed test unit is being constructed to determine the effects of calcination and continuous sulfation on the attrition rates of various limestones.

High attrition rates are undesirable since they may decrease SO_2 retention, require more or larger equipment to capture the higher dust loadings (in order to meet EPA emission standards), and necessitate an increase in the limestone fresh feed rate. In the case of pressurized fluidized-bed combustion, the dust loading must be low to meet turbine requirements.

The "cold" fluidized bed apparatus is schematically depicted in Fig. 57. The column has a 78.74-cm height which can be increased or decreased by adding or removing sections. In the present assembled apparatus, the bottom section is 30.48 cm high and has a 5.08-cm diameter. The top section

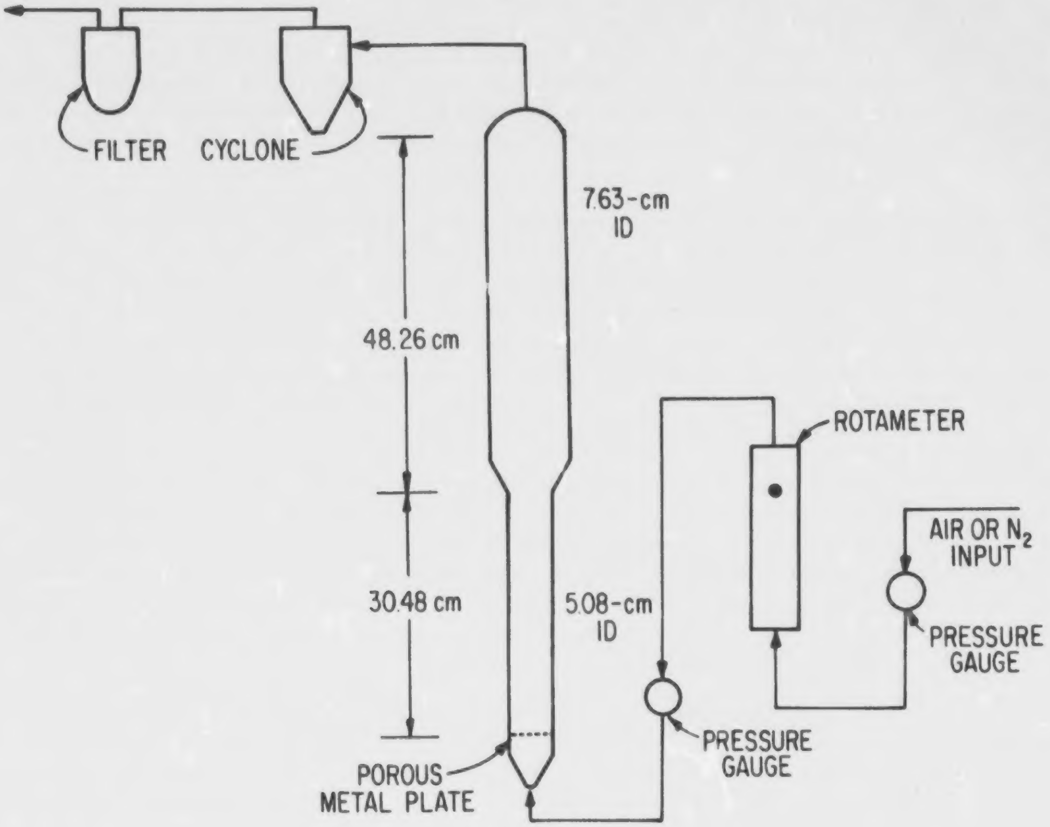
FILTER
CYCLONE
7.63-cm ID
48.26 cm
30.48 cm
5.08-cm ID
ROTAMETER
AIR OR N_2 INPUT
PRESSURE GAUGE
PRESSURE GAUGE
POROUS METAL PLATE

Fig. 57. Laboratory-Scale Fluidized-Bed Apparatus for Attrition Experiments

(removable) is 48.26 cm high and has a 7.63-cm diameter. The top portion of the bed is a disengagement section, which functions to decrease the velocity of the fluidizing gas and particles, minimizing particle entrainment.

At the bottom of the bed, there is a porous metal plate that functions as a gas distributor. A pressure regulator controls the fluidizing gas flow. A cyclone and a filter are located downstream from the bed to collect the overhead particles produced from particle-particle and particle-wall collisions (abrasion) during fluidization.

The sorbent is loaded into the apparatus after sections of the bed have been separated. The fluidizing gas fed into the bed is house air or nitrogen.

The percent of the bed material that is elutriated overhead is considered the material loss due to attrition. During each 10-hr attrition test, the bed material is periodically weighed to determine the quantity of material that has been lost overhead.

Many parameters affect the attrition rate of limestones (fluidization velocity, bed depth, tube arrangement, particle size, limestone composition, calcination rate, extent of sulfation, temperature). Although there is a number of variables involved in determining attrition rates, Tymochtee dolomite, fully calcined, -14 +30 mesh, was initially studied as a function of only three variables: fluidization velocity, bed depth, and tube arrangement.

The attrition rates for calcined Tymochtee dolomite (no tubes in the bed) are shown in Figs. 58 for a L/D of 1.38 and fluidization velocities of 0.88, 1.19, 1.46, and 2.13 m/s. As can be seen in the figure, as the superficial gas velocity increases, the attrition rate increases. At all gas velocities, the attrition rate is high initially, then decreases to a steady state rate in approximately 2-4 hr. The steady state attrition rate is approximately proportional to the superficial velocity squared; which is the theoretical attrition dependency on velocity. The results for L/D ratios of 0.28 and 0.55 are for well-mixed fluidized beds. For a L/D of 1.38, the fluidized bed is in the transition region between well-mixed and slugging; for a L/D of 2.2, the operates entirely in a slugging mode. The effect of bed depth on attrition is shown in Fig. 59 for a gas velocity of 1.46 m/s. In deeper beds, where there apparently are more particle-particle collisions per kg of limestone, attrition rates are higher. At 2.13 m/s, the attrition rate is independent of L/D since an entrained bed develops (for -14 +30 mesh particles), causing very high attrition rates.

The introduction of cooling coils (simulated by using copper tubing) was expected to decrease the limestone particle velocity, "quieting" the bed and thereby decreasing limestone attrition rates. There were six layers of horizontal tubes, six tubes at each level, and a 1.2-cm spacing between adjacent levels. The first layer of tubes was 1.2 cm above the gas distributor plate. At the lower velocities of 1.19 and 1.46 m/s, the attrition rates were decreased by a factor of 2.8 and 2, respectively. At 2.13 m/s, an entrained bed develops, and thus the attrition rate is the same in the presence and absence of simulated cooling coils.

The attrition rates of ten limestones (precalcined) were tested at room temperature, a superficial gas velocity of 1.46 m/s, and a L/D of 1.38 (expanded). Figure 60 shows the total material loss in 10 hr. The limestones are in the order of decreasing reactivity with SO_2 from left to right, as determined in a TGA. No relationship between SO_2 capacity and attrition is seen.

Figure 61 shows the amount of material lost overhead as a function of time. The attrition rate is high for the first 1/2 hr, then decreases rapidly. Of the ten limestones tested, limestone 1337 had the highest attrition rate--a loss of 55% of the bed material. Greer was the strongest, losing only 4.5%. The overhead material was finely powdered (smaller than 70 mesh), indicating that the material lost from the bed was due to attrition, not elutriation.

The wide variation in attrition resistance can be correlated with the impurity (Si, Fe, Al) concentrations of the limestones. In Fig. 62, the

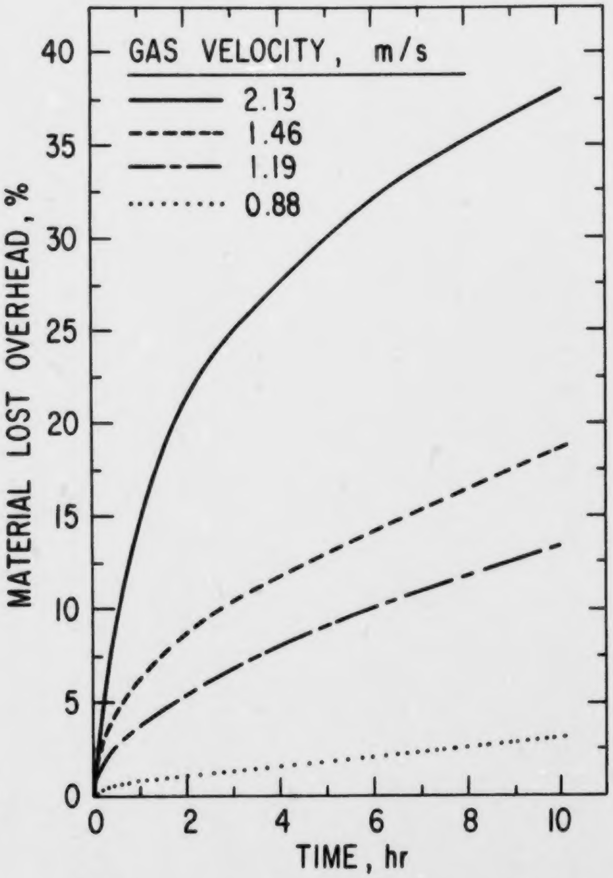

Fig. 58. Attrition Rate of Calcined Tymochtee Dolomite as a Function of Superficial Gas Velocity; L/D = 1.38

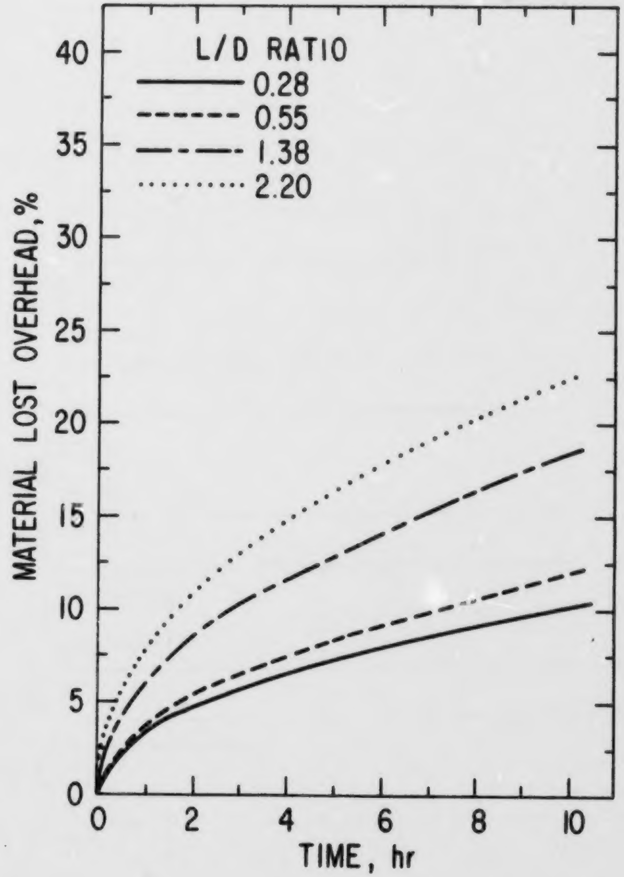

Fig. 59. Attrition Rate of Calcined Tymochtee Dolomite as a Function of Bed Depth. Superficial gas velocity, 1.46 m/s

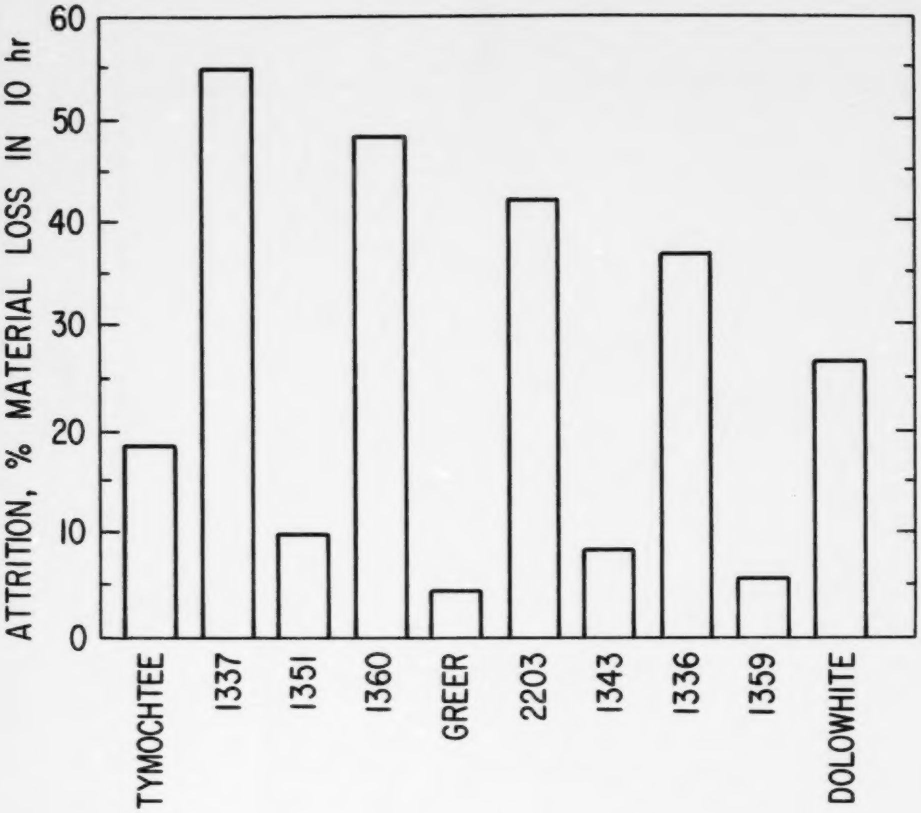

Fig. 60. Material Loss from Beds of Precalcined Limestones, Superficial Gas Velocity: 1.46 m/s; L/D: 1.38

material lost due to attrition is given as a function of impurity concentration. At high impurity levels (above 4%), the material loss is low (less than 20%); however, at low impurity levels, there is considerable scatter in the data, making it difficult to predict material losses due to attrition.

4. Conclusions

The calcium utilization of limestones with SO_2 can be correlated with composition (MgO content); however, more limestones samples must be tested to determine how accurate this correlation is.

The calcium utilization of limestones can also be correlated with the "accessible" internal surface area of the stone. Precalcination of limestones may increase the calcium utilization of the stone; however if residence times in a preheater are long, the capital cost of pretreatment equipment may become too high for the procedure to be considered.

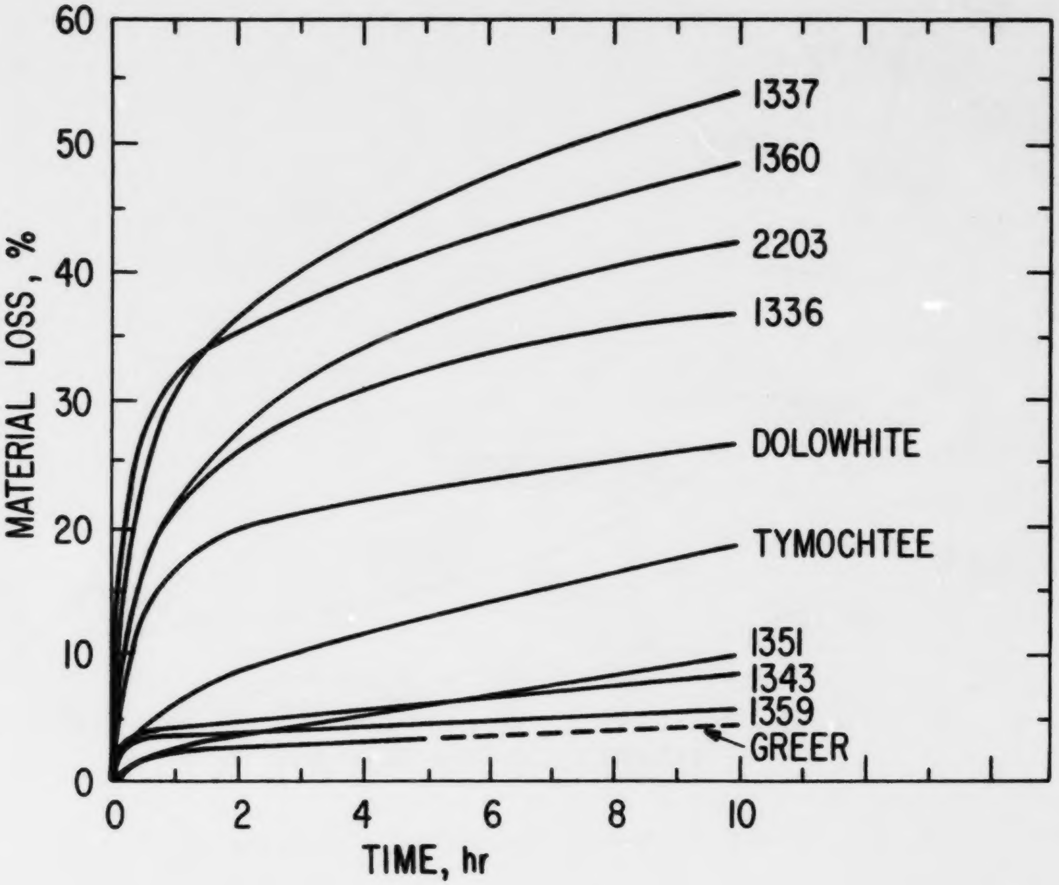

Fig. 61. Material Loss at 1.46 m/s Gas Velocity, Room Temperature.

Attrition rates of limestones can be correlated with the concentrations of impurities (Al, Si, Fe). High impurity concentration levels increase attrition resistance.

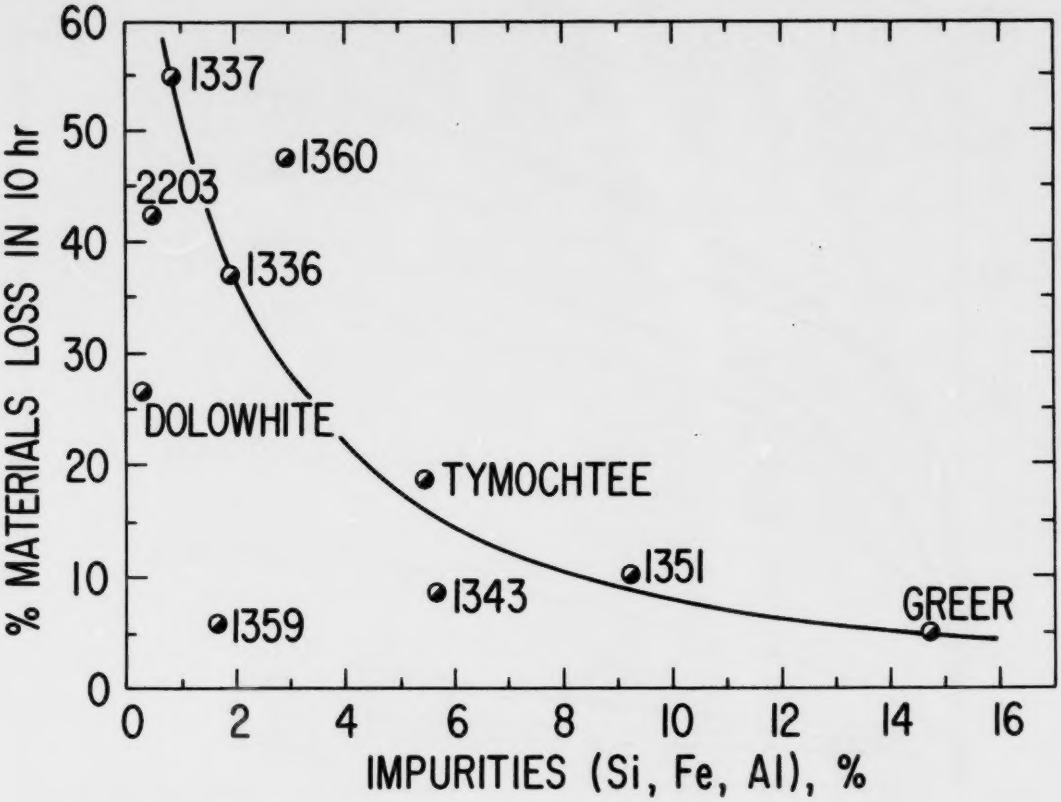

Fig. 62. Effect of Impurity Concentration on Attrition

TASK E. TRACE ELEMENTS AND COMBUSTION EMISSION STUDIES

1. The Effect of Additives on the Calcination/Sulfation of Limestone/Dolomite

(J. Shearer and C. Turner)

The use of additives in a fluidized-bed coal combustion system to increase the SO_2-sorption capabilities of limestone and dolomite has received considerable attention. In particular, the addition of small amounts of NaCl to enhance the SO_2 absorption characteristics of limestones has been used with success by Pope, Evans and Robbins[21] in atmospheric pressure fluidized-bed combustors.

In order to fully understand the role that the salt mixture plays, a clear picture of the reaction mechanism must be obtained. An extensive search of the literature (during the report period) has revealed a multiplicity of uses of NaCl (and of other salts) as a catalyst or mineralizer in related areas.[22a-29]

Apparently, no detailed theoretical study of the effect of catalysts on the calcination/sulfation system has been performed. Several researchers have looked at the individual systems of calcination and sulfation separately under laboratory conditions and have concluded that the sorption capacity is diffusion-controlled for the most part, depending greatly on the physical characteristics of the stone itself. Therefore, any effects of mineralizers must be directly related to diffusion and/or rearrangement in the limestone/dolomite matrix.

Pope, Evans, and Robbins[21] suggested that the addition of sodium chloride leads to a physical disruption of the pore structure of the limestone by the sodium ions, so that compounds form having sufficiently different lattice constants to strain the system during replacement. This concept was put forth on the basis of gross effects observed in a large fluidized-bed coal combustor with limestone additive and NaCl catalyst.

A review of various compound melting points and eutectic points in the system $NaCl$-$CaCO_3$-$MgCO_3$-$CaSO_4$-$MgSO_4$, as shown in Table 24, suggests a mechanism involving low-temperature melts and solid solutions for the enhancement of calcination and sulfation of limestone and dolomite.

DTA studies of dolomite have shown a depression of temperature of initial decomposition in the presence of NaCl[22a,30] similar to the effects on limestone.

a. Mechanism of Enhancement by Sodium Chloride

It is proposed that a liquid phase exists upon the dissolution of carbonate and/or sulfate into NaCl when these components are in contact at temperatures above 750°C. The enhancement of interaction is directly attributable to the presence of these molten salt films on particle surfaces.

The accelerating effect of NaCl on partially sulfated stone is due to the appearance of the above-mentioned liquid phase at high temperatures. The

Table 24. Eutectics and Double Salts Formed in the System, $NaCl-CaCO_3-MgCO_3-CaSO_4-MgSO_4$

Species	Decomposition (d) or m.p., °C	Eutectic	m.p., °C	Double Salt	Double Salt Decomposition (d) or m.p., °C
NaCl	801				
$CaCO_3$	d.825	$2NaCl - CaCO_3$	690	$Na_2Ca(CO_3)_2$ $Mg_3Ca(CO_3)_4$	770 d.817 d.<350
$MgCO_3$	d.350				
$CaSO_4$	1450	$4NaCl - CaSO_4$	721	$Na_2Ca(SO_4)_2$ $Mg_2Ca(SO_4)_4$	915 1201
$MgSO_4$	d.1124	$2NaCl - MgSO_4$	624	$Na_2Mg_3(SO_4)_4$	700
Na_2CO_3	850	$4NaCl - Na_2CO_3$	634	$Na_2(SO_2,CO_3)$	612
Na_2SO_4	844	$4NaCl - Na_2SO_4$	638		
$CaCl_2$	770			$CaCl_2 \cdot CaCO_3$	d.700
$MgCl_2$	712				

liquid phase greatly increases the area of contact of the reactants between the salt ions, and the calcium and carbonate ions may weaken the ionic strength of the crystal lattice--that is, the mobility of ions in the crystal lattice increases and some of the ions on the surface of the crystal separate and dissolve in the salt films.

Some of the salt ions may enter the crystal, causing the mobility of the ions in the crystal to be increased by the formation of a solid solution or a compound. When calcium ions or oxygen ions move in the salt layer, the mobilities of these ions may depend on the viscosity of the molten salt. The presence of carbon dioxide from the decomposition of the stone creates a highly mobile liquid with low viscosity, increasing the diffusion rate of migrating ions. As the diffusion rate increases, the rate of interaction of the components to form the new crystallization phase, $CaSO_4$, increases. Possibly, the formation of the new crystalline phase at high temperatures is preceded by removal of individual ions and molecules from the solid $CaCO_3$ lattice, which leads to the appearance of molecularly porous substances that form pseudomorphs of the original crystals and effectively lower the surface energy barrier to recrystallization. Ongoing crystallization of CaO to its normal lattice structure initially increases the specific surface with respect to SO_2 capture, allowing more complete sulfation to occur. The appearance of these molecularly porous structures has a considerable influence on the capture of SO_3 introduced into the system and on further penetration of the crystal by the melt, leading to considerable contact of the components.

Figure 63 is a sketch of a portion of a partially sulfated limestone particle undergoing sulfation in the presence of NaCl. The NaCl vapor dissolves SO_3 gas and small amounts of $CaSO_4$ on the surface of the particle, forming a liquid melt $[CaSO_4 + SO_3 + NaCl]_L$ which penetrates the shell of previously formed $CaSO_4$ (Zone I) along grain boundaries and imperfections. At the same time, the $CaSO_4$ dissolves and recrystallizes as the liquid moves into the interior until it contacts unreacted $CaCO_3$ (Zone II). At the reaction interface, the $NaCl-CaSO_4-SO_3$ melt provides a medium for the dissolution of small amounts of $CaCO_3$, incorporating it into a liquid phase $[CaCO_3]_L$. The $[CaCO_3]_L$ readily dissociates into Ca^{2+} and $CO_3{}^{2-}$ with the subsequent release of CO_2 gas and the simultaneous formation of CaO and/or $CaSO_4$ from interaction with the dissolved SO_3. The CO_2-saturated liquid is highly mobile and diffuses inward. As the CO_2 escapes outward, the liquid dissolves more $CaCO_3$, precipitates $CaSO_4$, and continues to penetrate the unreacted portion of the limestone lattice until the reaction is brought to a halt when the amount of $CaCO_3$ is too small to form a liquid with the NaCl, and diffusion barriers arise.

The effect of the additive is to enhance crystal growth by providing nucleation centers while simultaneously separating and dissolving the lattice structure of the original limestone. The ions of the incipient $CaSO_4$ and CaO crystal surfaces also undergo separation, redissolution, and recrystallization via the salt film, leading to a more open porous structure with little diffusional resistance. Diffusional barriers due to blockage of pore structures are removed by this continual dissolution and recrystallization in the NaCl-containing liquid phase. Rapid diffusion of ions and gases through a mobile liquid accounts for the effective lowering of the temperature of reaction at which these processes occur.

As part of this investigation of the mechanism of the catalytic effect of mineralizers and its relevance to coal combustion, a small laboratory reactor was built for controlled-atmosphere and -temperature experiments. The current experiments are concerned mainly with common salt, NaCl, and calcite ($CaCO_3$) in order to provide experimental verification of the proposed mechanism of interaction.

Large (0.6-cm) pseudocrystal rhombs of calcite spar were chosen for this study of sulfation and calcination because of (1) their low reactivity in these reactions, (2) their high purity, and (3) their extremely low porosity, which results in a layered effect in the reaction products. The reaction proceeds only from the crystal surface inward, not throughout the entire sample as in natural limestones and dolomites.

A horizontal tube furnace capable of achieving 1100°C was set up with a gas-mixing system for providing appropriate combinations of air, CO_2, and SO_2.

Preliminary experiments were performed in an air medium with a small flow of SO_2 at 900°C. The gas mixture passed for short time periods over calcite samples, which were in quartz boats in the furnace. In most runs, NaCl vapor was evaporated from a boat filled with fused NaCl in the upstream portion of the system. In a few runs performed with NaCl directly deposited

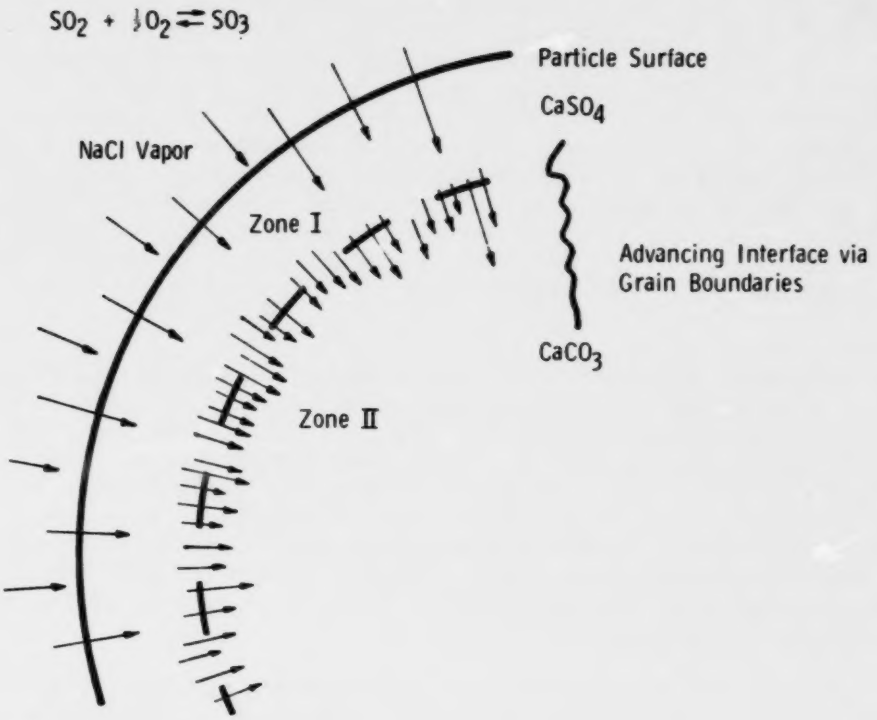
$SO_2 + \frac{1}{2}O_2 \rightleftharpoons SO_3$
Particle Surface
$CaSO_4$
NaCl Vapor
Zone I
Advancing Interface via Grain Boundaries
$CaCO_3$
Zone II

Zone I: $CaSO_4$ product layer

$$CaSO_4(s) + NaCl(g) + SO_3(g) \rightleftharpoons |CaSO_4 + SO_3 + NaCl|_L$$

$$|CaSO_4|_L \rightleftharpoons CaSO_4(s)$$

Interface: $|CaSO_4 + SO_3 + NaCl|_L + CaCO_3(s) \rightleftharpoons |CaCO_3 + CaSO_4 + SO_3 + NaCl|_L$

$$|CaCO_3|_L \rightleftharpoons |Ca^{++} + O^{=}|_L + CO_2(g)\uparrow$$

$$|Ca^{++} + O^{=}|_L \rightleftharpoons |CaO|_L$$

$$|Ca^{++} + O^{=}|_L + |SO_3|_L \rightleftharpoons |CaSO_4|_L$$

$$|CaSO_4|_L \rightleftharpoons CaSO_4(s)$$

Zone II: Unreacted $CaCO_3$

Fig. 63. Sulfation of Partially Sulfated Limestone Particle

on the crystal surface, most of the NaCl was lost by evaporation from the crystal surface before the length of time required for reaction elapsed, and only the crystal surface was affected. Blank runs with no salt present provided samples for comparison.

Figure 64 illustrates the dramatic results obtained upon salt addition. Photos I and II show calcite crystals exposed to SO_2 in air at 900°C for 15 min. There is a very thin reaction rim of $CaSO_4$ crystals, with some CaO microcrystals on the samples; the major part is unreacted $CaCO_3$. The reaction proceeds along existing fractures and crystal defects at the surface.

Photos III and IV show calcite crystals exposed at the identical conditions with NaCl vapor present. It can readily be seen that the amount of reacted material is much greater in both cases than for the no-salt cases and is more variable in extent. There is a highly crystalline layer of $CaSO_4$ on the outside over a thicker layer of CaO which surrounds the residual $CaCO_3$. An X-ray study shows the outer layer to be highly crystalline $CaSO_4$ with minor amounts of NaCl present, indicating that NaCl penetrated the sample at least to this depth.

That there is a gradation of sulfate in the CaO layer was indicated by some preliminary microprobe scans intended to determine the sodium distribution in the reaction layers. Due to problems with maintaining a polished surface, the results were ambiguous. The CaO is very finely crystalline, with little coherence, and is highly reactive with water vapor. In many cases, the outer layer of sulfate crystals had separated from the oxide as a thin coherent shell, making it difficult to mount the entire specimen.

From the relative thicknesses of the product layers, it can be seen that NaCl increases the extent of calcination more rapidly than it increases the extent of sulfation.

Several runs were performed without salt present and with CO_2 levels such that no calcination occurred during the experiments. Salt vapor was then added to the system, and calcination proceeded despite the high CO_2 levels in the furnace. It is hoped that by suitable adjustment of CO_2 levels, a much greater extent of sulfation than calcination can be achieved. Previous work[31] has shown the importance of the calcining conditions when calcined stones are reacted with SO_2.

In the sulfation experiment illustrated by the photographs of Fig. 64, the no-salt samples show a very thin layer of calcium sulfate and calcium oxide, with the sulfate predominating. The effectiveness of NaCl in promoting calcination and producing an initially porous product shows clearly in the very thick layers of CaO in the samples with additive. The sulfate layer in these samples is revealed under the microscope as consisting of fairly large crystals growing out of the CaO layer. Literature descriptions of alkali effects commonly refer to enhanced crystallization of the product phases and increased porosity.[25,29] It has been found that the reaction of SO_2 with limestone is greatly influenced by the reduction in porosity caused by the sulfation reaction.[32]

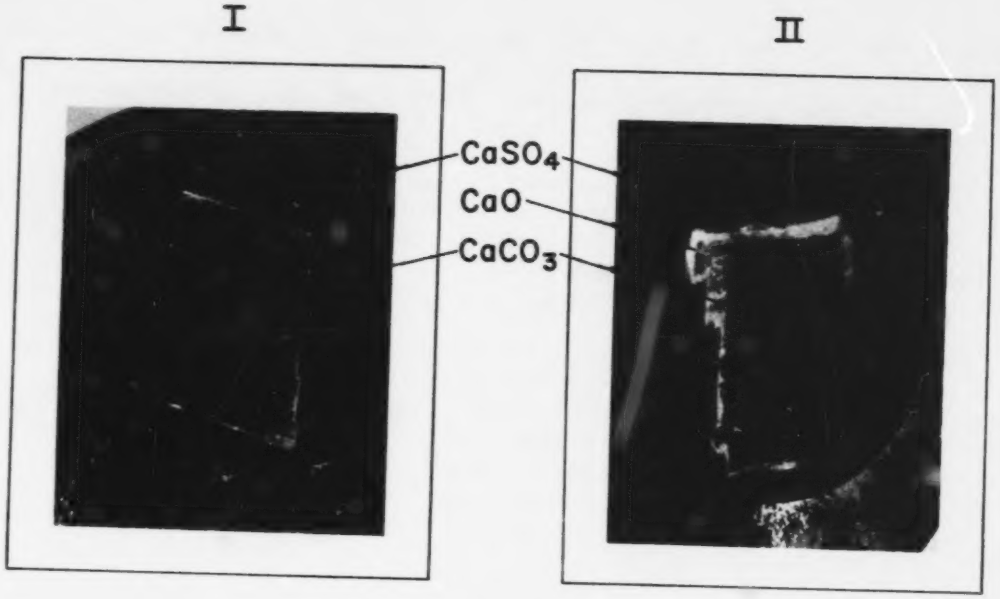
I
II
$CaSO_4$
CaO
$CaCO_3$

CRYSTALLINE CALCITE SULFATED AT 900°C IN AIR FOR 15 MINUTES

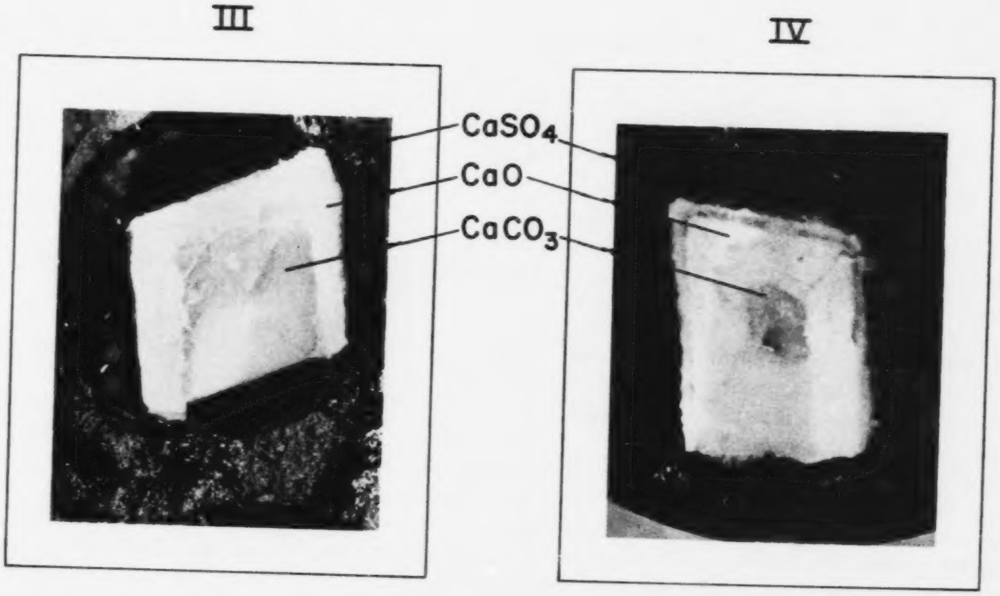
III
IV
$CaSO_4$
CaO
$CaCO_3$

CRYSTALLINE CALCITE SULFATED AT 900°C IN AIR IN PRESENCE OF NaCl FOR 15 MINUTES

Fig. 64. Sulfation of Crystalline Calcite

The microscopically observed penetration of NaCl along grain boundaries and fractures, with reaction occurring at crystal defects and pore surfaces, supports the mechanism that transient surficial melts form which increase the reactivity of the dissolved phases and lower the resistance to diffusion of gases. Scanning electron microscope photographs are being taken to determine if indeed the NaCl penetrated the reaction layers and to indicate the final disposition of the salt.

Preliminary calcination experiments were done, with no SO_2 present, on calcite spar samples to note any qualitiative changes as a result of the presence of NaCl. The sample exposed to air and CO_2 without salt was partially calcined for 30 min. The product was white and brittle and was finely crystalline under the microscope. When NaCl was added in similar experiments, the product was more completely calcined and had a more porous and crumbly texture. The outer surface, however, had begun to sinter into a rigid shell. This product was discolored, with brownish tones.

Table 25 summarizes the observations made during a series of diagnostic experiments performed in a horizontal furnace, which led to the design of thermogravimetric experiments to provide quantitative results. From the table, it can be seen that under simultaneous calcination and sulfation conditions, there is a marked decrease in the total amount of reacted material during a given period of time as compared with the amount of reaction under simple calcination conditions. The diffusional barrier of incoming SO_2 slows down the calcination of the $CaCO_3$. Addition of the mineralizer, NaCl, increases both the extent of calcination and the extent of sulfation by improving the porosity of the calcined stone. When simple calcination is performed under a high enough CO_2 pressure that calcination does not occur readily, the addition of NaCl vapor to this same system effectively overcomes the diffusional barriers, and calcination proceeds rapidly.

When a precalcined stone is reacted with SO_2, the amount of sulfation both with and without salt addition is increased in comparison to simultaneous calcination-sulfation. The addition of NaCl, however, increases the amount of sulfation and of interpenetration of CaO by the crystallizing $CaSO_4$, with a fluid phase following defects and grain boundaries within the crystal. This differs considerably from the sharply defined reaction front observed with no salt present.

b. Evaluation of Seven Additives

Compounds other than NaCl that have been found to be effective mineralizers[23-29] have been studied to evaluate their potential usage in coal combustion, as reported here. Among the compounds reported in the literature are NaOH, Na_2CO_3, KCl, $CaCl_2$, $MgCl_2$, Na_2SO_4, Na_3PO_4, and kaolin and other clays. The noncorrosive aspects of some of these compounds may make them more attractive than NaCl if all other considerations are favorable.

Most workers agree that the reaction mechanisms of both calcination and sulfation have rate-controlling diffusion-limited steps so that any mineralizing effects in calcination may have similar results in sulfation. Many

Table 25. Effect of NaCl on Reactions of Calcite

Experiment	Additive	NaCl Introduction Technique	Reaction Conditions[a]	Comments
NaCl-1a	None	-	Calcined at 900°C in air, 15 min	Reaction almost complete
NaCl-1b	NaCl	Vapor	Calcined at 900°C in air, 15 min	Complete reaction, salt gave a more porous product
NaCl-2a	None	-	Calcined at 900°C in high CO_2, 15 min	No reaction
NaCl-2b	NaCl	Vapor	Calcined at 900°C in high CO_2, 15 min	Almost complete reaction, porous product
NaCl-3b	None	-	Simultaneous 900°C calcination/sulfation, 15 min	Surficial reaction, white coating with thicker layer of CaO
NaCl-3B	NaCl	Vapor	Simultaneous 900°C calcination/sulfation, 15 min	Some $CaCO_3$ remains in center, a thick layer of CaO, outer thick layer of crystalline $CaSO_4$
NaCl-4a	None	-	Precalcined at 900°C 30 min, then exposed to SO_2 for 15 min	Thin layer of $CaSO_4$, flaky
NaCl-4b	NaCl	Vapor	Precalcined at 900°C 30 min, then exposed to SO_2 for 15 min	Thick layer of crystalline $CaSO_4$ intergrown with CaO
NaCl-5a	None	-	Partially sulfated stone further reacted, 15 min	No appreciable change
NaCl-5b	NaCl	Vapor	Partially sulfated stone further reacted, 15 min	Thicker shell developed having a more crystalline character

[a] Sulfation atmosphere was 20 vol % SO_2 in air.

salts have been shown to be effective in the calcination of limestone and are used routinely to promote the formation of reactive limes. Table 26 summarizes the results of qualitative experiments in which NaCl and several other additives were used. The only salts comparable to NaCl (in terms of magnitude of effect) are $CaCl_2$ and $MgCl_2$; NaOH, Na_2CO_3, and Na_2SO_4 all behave similarly; the first two salts sulfated readily during reaction and then effectively behave as Na_2SO_4 in the system. One set of experiments (vapor salt introduction mode) was done using open boats of salt introduced into the furnace to supply a vapor to interact with the calcite. If a porous limestone instead of calcite spar crystals were used, the salts could be directly deposited within the stone and thus could perhaps avoid the difficulties associated with subsequent sulfation of the additive.

The volatility of the Na_2SO_4 is low compared to that of NaCl and $CaCl_2$. Its melting point is fairly high compared to the reaction temperature, whereas NaCl and $CaCl_2$ are easily melted below 900°C. Sulfation with Na_2SO_4 and the other related salts (NaOH and Na_2CO_3) occurred only when the salts were placed directly on the calcite crystals. These effects support the view that a fluid phase is present during the reaction. The presence of low-melting eutectics of salt and matrix appears to open up the system to further sulfation. In porous stones, these salts may indeed have much greater effects due to more intimate surface contact of the salt with the stone.

These qualitative results indicated the desirability of pursuing quantitative experiments on a thermogravimetric apparatus to measure weight changes during sulfation and to deduce absolute values for sulfur capture when mineralizers are present. The effects on sulfur absorption of varying the concentration of the additives are reported below.

Figure 65 shows the effect of precalcination of Greer limestone (in the tube furnace) on sulfur retention and the enhancement by NaCl. The NaCl was introduced by immersion of the limestone in an aqueous solution. After the limestone was soaked in a 20% NaCl solution, it was dried at 150°C, leaving approximately 1% NaCl by weight in the stone. The sample was then calcined in the furnace assembly at 900°C in an atmosphere of 20% CO_2 in N_2, reweighed to verify the completion of calcination, and then exposed to a gas mixture containing 4% SO_2. Despite the loss by evaporation of most of the salt, the effects upon sulfation can be seen, with the stones' capacity for SO_2 increased by approximately 50%. The effect of simultaneous calcination/sulfation can also be seen—a substantially lower reactivity—although within the time period, the total amount of conversion eventually reaches the same level as does the precalcined stones at this concentration of SO_2. At lower concentrations of SO_2 (Fig. 66), as in a flue gas, the effect is much more apparent because the uncalcined stone does not reach the same level of sulfation as the precalcined stone in any reasonable time interval. Figure 66 shows experimental data points from the thermogravimetric analyzer with 0.4% SO_2.

The initial use of the horizontal tube furnace assembly instead of a thermogravimetric analyzer was prompted by the possibility of extensive corrosion when volatile alkali salts are used. Figure 67 gives the results

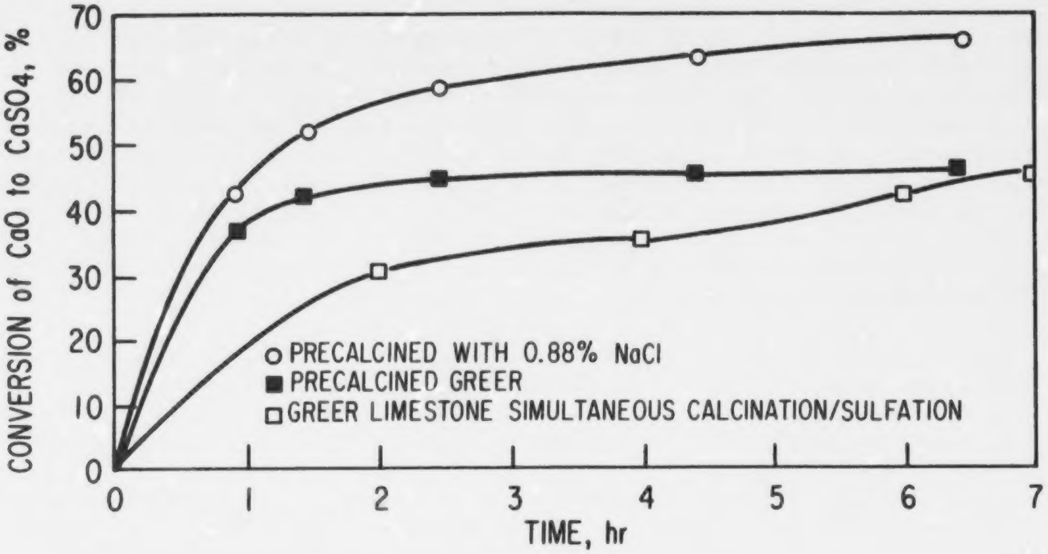

Fig. 65. Enhanced Sulfation in 4% SO_2 at 850°C of Greer Limestone by Pretreatment

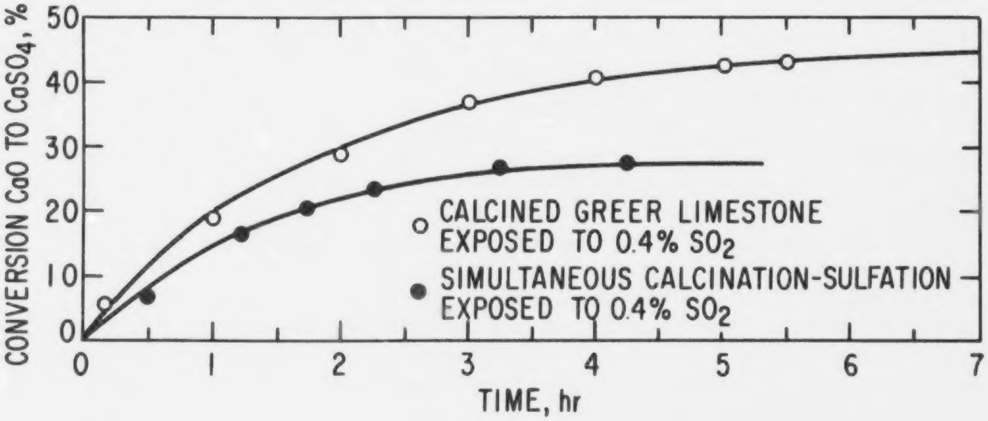

Fig. 66. Enhanced Sulfation in 0.4% SO_2 at 850°C of Greer Limestone by Precalcination

Table 26. Effect of Additives on Simultaneous Calcination-Sulfation of Crystalline Calcite at 900°C

Expt.	Additive	Salt Introduction Mode	Reaction Time, min	% SO_2 in Air	Extent of Reaction	Comments
CS 1	None	None	30	25	Minor	Surficial white deposit on $CaSO_4$ plus CaO
CS 2a	NaCl	Vapor[a]	30	25	Major	Highly crystalline $CaSO_4$ over a thick layer of CaO
CS 2b	NaCl	Solid[b]	30	25	Major	As in CS 2a, over entire crystal
CS 3a	$CaCl_2$	Vapor	30	25	Major	Similar to NaCl though less CaO formed
CS 3b	$CaCl_2$	Solid	30	25	Major	Similar to NaCl
CS 4a	Na_2CO_3	Vapor	30	25	Minor	Some surficial reaction
CS 4b	Na_2CO_3	Solid	30	25	Major	Reaction localized with small effects elsewhere
CS 5a	NaOH	Vapor	30	25	Minor	Very little (NaOH appears to boil away and sulfate)
CS 5b	NaOH	Solid	30	25	Major	Very localized (boils away)
CS 6a	Na_2SO_4	Vapor	30	25	Minor	Small amount of surface reaction
CS 6b	Na_2SO_4	Solid	30	25	Major	Entire crystal surface reacted
CS 7a	$MgCl_2$	Vapor	30	25	Major	Similar to $CaCl_2$, though less extensive reaction
CS 7b	$MgCl_2$	Solid	30	25	Major	Similar to $CaCl_2$

[a] Additive in a boat upstream.
[b] Additive on calcite surface as slurry.

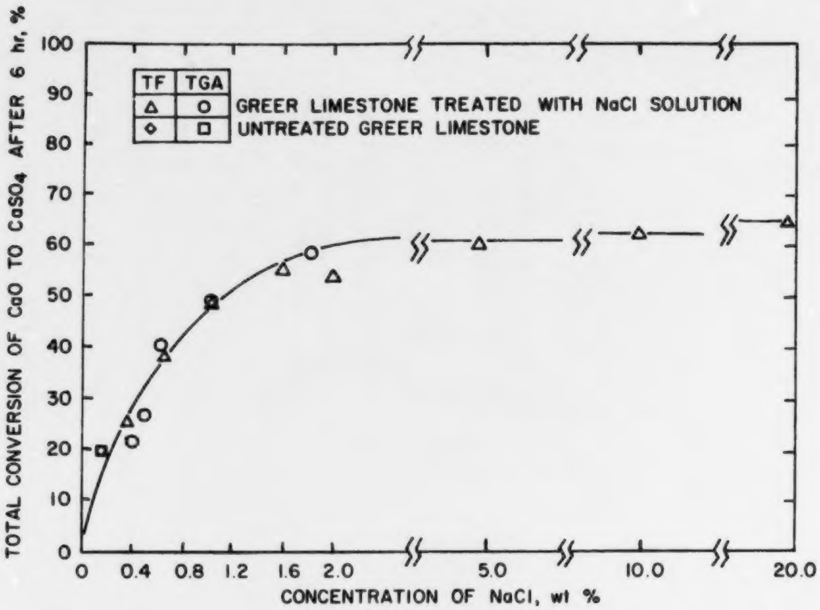

Fig. 67. Effect of NaCl Concentration on Sulfation of Greer Limestone at 850°C in 0.3% SO_2. A comparison of TGA with horizontal tube furnace (TF).

of two series of experiments at 850°C using Greer limestone with NaCl the mineralizing additive; these series were performed on the TGA and the tube furnace (TF) under simultaneous calcination/sulfation conditions. After six hours, the two methods are in excellent agreement for a given concentration of sodium chloride. Some samples were prepared by immersion in a near-boiling brine of NaCl and then drying in an oven at 100°C. The sodium chloride was thereby uniformly distributed throughout the sample—within pores and on particle surfaces. Samples used were all sieved to 18-20 mesh size. The maximum concentration of salt introduced in this way was 2% by weight.

High concentrations of NaCl were incorporated into samples of Greer limestone by evaporating a slurry of water and salt or by a dry mixing of finely ground salt with the Greer. Both of these methods yield salt particles unattached to the limestone; hence, to avoid corrosion of the TGA, no experiments with high-NaCl limestones were carried out in the TGA. The plot of the percentage conversion of CaO to $CaSO_4$ in Greer limestone versus the concentration of NaCl admixed with the stone in Fig. 67 shows that the data for both the TGA runs and the horizontal tube furnace runs are in excellent agreement. The lower value for the 2% run in the horizontal tube furnace compared with the 1.8% run in the TGA reflects the different methods of preparation; for the tube furnace, the method was slurry evaporation wherein some of the free salt (most of which had deposited on the surface of the particles during evaporation) evaporates without contributing to the reactivity of the stone. These higher concentration runs thus represent a lower value of salt concentration than was initially introduced. (Samples prepared by simple mixing of finely ground salt with the stone gave even lower values of conversion.)

As can be seen from the curve (Fig. 67), at low concentrations of salt, doubling the amount of NaCl added doubles the percent conversion. Conversion levels off near 2% NaCl, and there is very little increase in conversion with further addition of salt.

By adding NaCl to the original Greer limestone (which itself has a sodium content equivalent to 0.16 wt % NaCl), the amount of conversion is substantially increased (Fig. 67). The untreated stone levels off after 6 hours near 20% conversion; in the runs with the highest concentrations of NaCl (from 2% up to ∿20%), conversion levels off near 60-65%, a factor of three greater. The nonlinearity of the relation between salt content and amount of conversion illustrated in Fig. 67 suggests that at these high concentrations of salt, fusion of the sample and/or blockage of porosity may hinder further sulfation.

The effect of a series of salts (Na_2SO_4, Na_2CO_3, $CaCl_2$, and KCl) on Greer limestone reactivity is presented in Fig. 68, 69, 70, and 71, respectively. In each graph, the natural stone without additive is represented by a dashed curve.

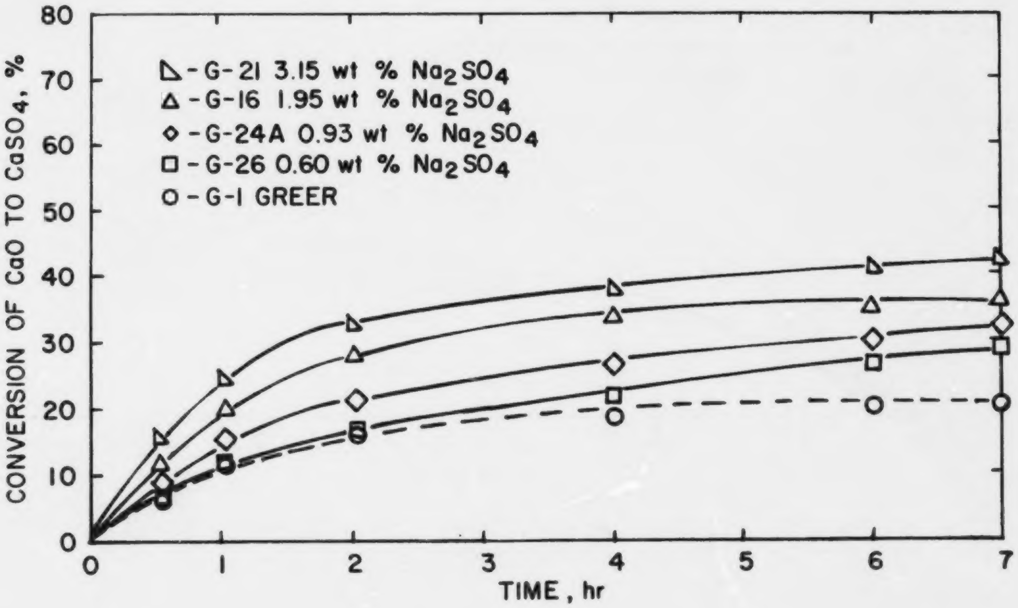

Fig. 68. Enhancement of Greer Limestone Sulfation with Na_2SO_4 at 850°C in 0.3% SO_2

Figure 68 contains plots of the percent conversion versus time for Greer limestone doped with Na_2SO_4. For this salt, the increase in SO_2 absorption is not as great as with NaCl. Comparison at 2% mineralizer concentration shows a 35% conversion for Na_2SO_4 and a 60% conversion for NaCl (Fig. 67). On the basis of formula weights, the salts have approximately equivalent concentrations of sodium. Increasing the concentration of Na_2SO_4 does not increase the conversion percentage as much as increasing the NaCl concentration does. In fact, when corrections are made for the amount of sulfate possibly exchanged with CaO, the increases in conversion versus concentration of Na_2SO_4 are barely noticeable. Results of analysis of the reaction products appear to agree with this conclusion; further checks will be made on all of the experiments performed.

Figure 69 is a plot of the percent CaO converted to $CaSO_4$ for Greer limestone containing Na_2CO_3 additive. Soaking the stone in a saturated Na_2CO_3 solution (thereby adding approximately 3% salt) increases the conversion to sulfate from 20% to 50%, *i.e.*, by more than a factor of two. Larger amounts of salt will be added in future experiments to obtain a complete picture of the relationship between conversion and concentration of salt.

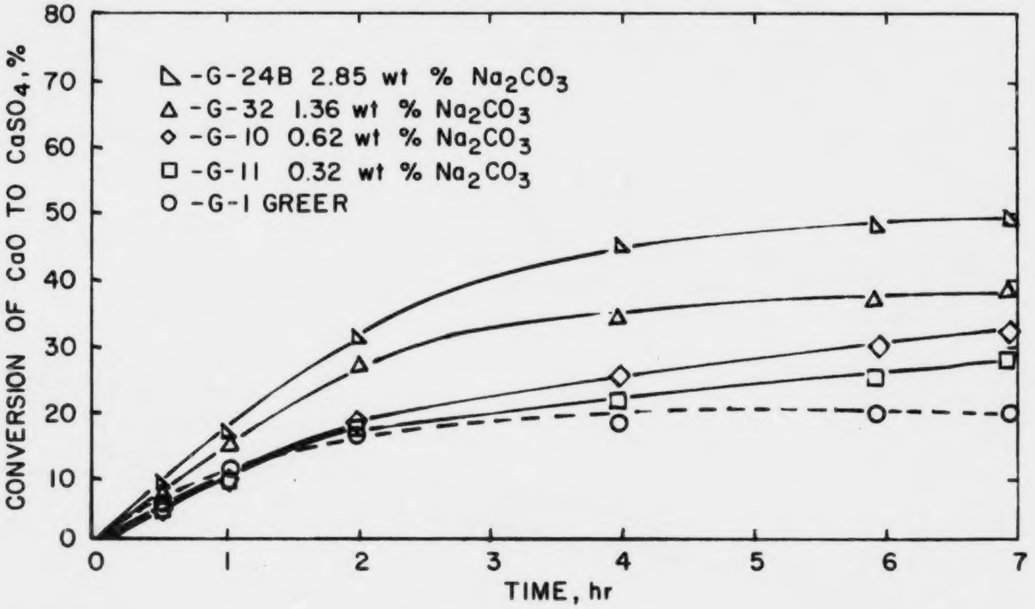

Fig. 69. Enhancement of Greer Limestone Sulfation with Na_2CO_3 at 850°C in 0.3% SO_2

Figure 70 shows conversion versus time for Greer limestone doped with $CaCl_2$ solutions. Conversion increases significantly at low concentrations of $CaCl_2$ but appears to level off rapidly above ∿1% $CaCl_2$, as indicated by the 50% conversion level reached; conversion with 5.5% $CaCl_2$ was only slightly higher than with 0.6% $CaCl_2$. These experiments indicate that sodium ion is not the only effective mineralizer in these systems. Chloride ion has an effect on limestone sulfation that is as large as the effect of sodium. This may partly explain the effectiveness of NaCl being greater than that of the other sodium salts.

The enhancement due to KCl is shown in Fig. 71. The percent conversion of Greer limestone, 20%, increased to over 50% with ∿2.5% KCl in the stone. The effectiveness of this salt is close to that of NaCl.

The weight percentages of salts present in the samples were compared, and the individual additives were arranged in decreasing order of effectiveness: $KCl \geq NaCl \approx CaCl_2 > Na_2CO_3 > Na_2SO_4$.

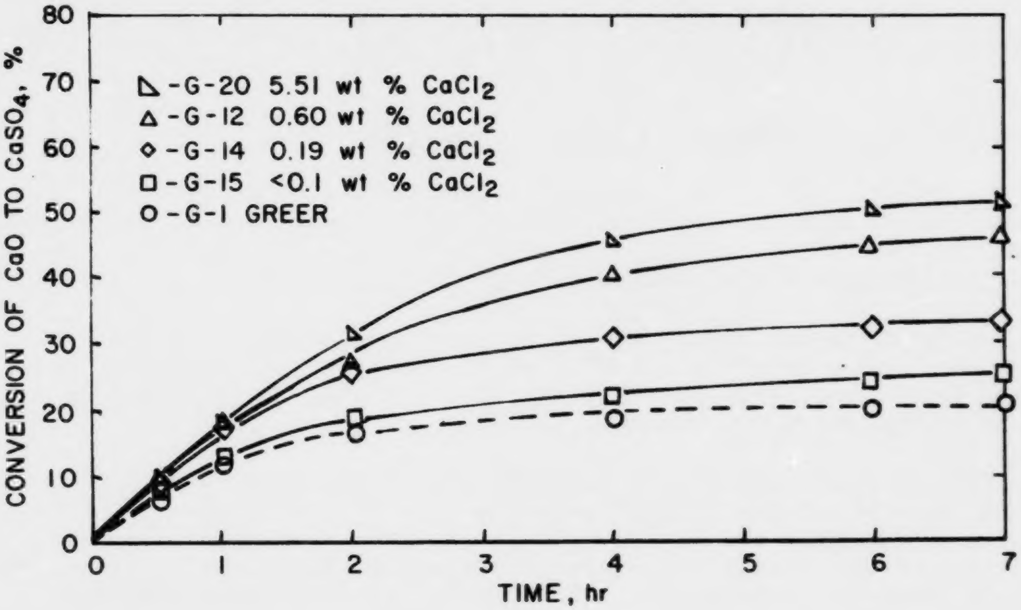

Fig. 70. Enhancement of Greer Limestone Sulfation with $CaCl_2$ at 850°C in 0.3% SO_2

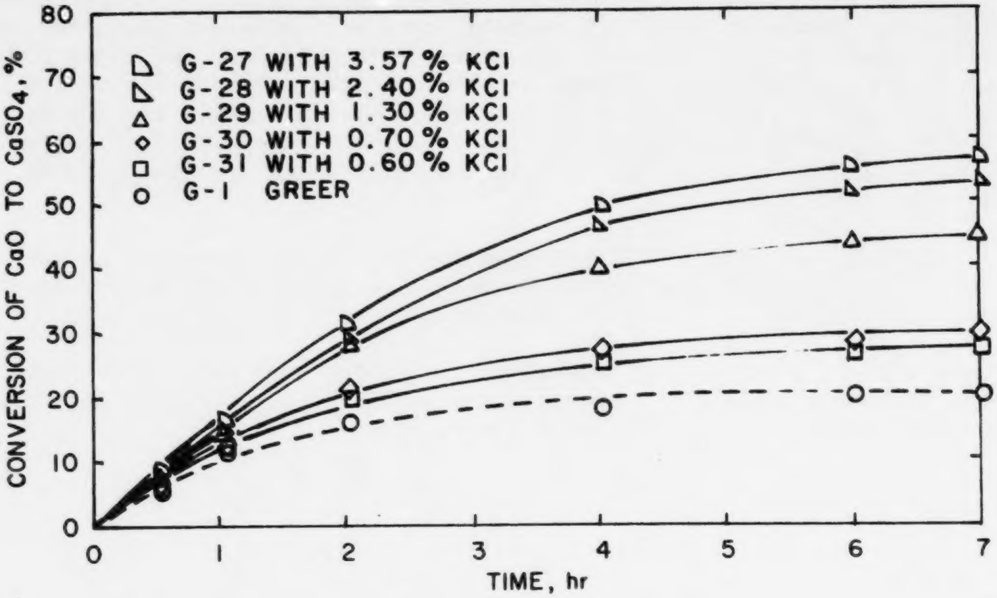

Fig. 71. Enhancement of Greer Limestone Sulfation with KCl at 850°C in 0.3% SO_2

c. Effect of NaCl Additive on Several Limestones

The greater part of this work so far has dealt with the reaction of Greer limestone with sulfur dioxide and several additive salts, namely, NaCl, Na_2SO_4, Na_2CO_3, $CaCl_2$, and KCl. The results of tests on a series of limestones having various compositions and morphologies are next discussed.

Eleven limestones and dolomites have been reacted for seven hours in a horizontal tube furnace assembly at 850°C with a 0.3% SO_2-5% O_2-20% CO_2-balance N_2 synthetic flue gas mixture. Figure 72 shows SO_3 captured/kg of sorbent for the untreated stones.

There is great variation in both the rate of reactivity of the stones with SO_2 and the calcium utilization among the different samples. Initial reaction rates differ considerably but do not necessarily correlate with total calcium utilization for the sulfation period. Comparison of limestone 1337 with Tymochtee dolomite shows that initial reaction rates are very similar; changes occur after 2 hr, 1337 having a steeper slope; later, Tymochtee picks up SO_2 faster than 1337 and has a steeper slope. After 7 hr of reaction time, the percentage of calcium (as CaO) in the stones converted to $CaSO_4$ ranges from 10% for 1359 up to 90% for Tymochtee. The plot is corrected for the amount of actual CaO present and available for reaction.

These data may be compared with results on limestone characterization by Snyder with several reservations. Snyder's work was performed at 900°C

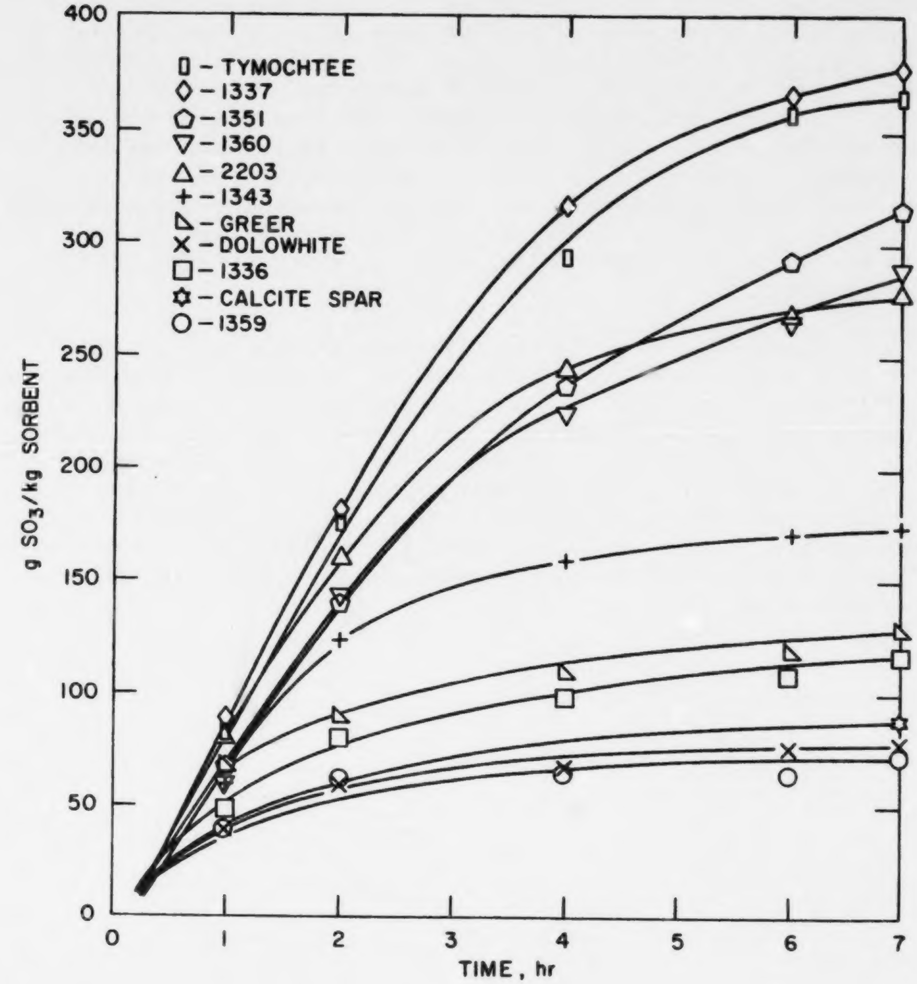

Fig. 72. Weight of SO_3 Captured as a Function of Time for Eleven Untreated Limestones.

using precalcined stones; the data reported here was collected at 850°C under conditions of simultaneous calcination/sulfation. The relative order of reactivity for the more reactive stones is the same for the two series. However, at 850°C there is considerable rearrangement of the low to medium reactive stones in comparison with their order at 900°C; this illustrates the large effects of reaction conditions. There is no comprehensive correlation between percent calcium utilization and composition. For example, Dolowhite, which has about the same composition as Tymochtee, is particularly unreactive. Porosity determinations are being made on stones calcined at 850°C to attempt to verify a correlation of porosity-composition-reactivity suggested by Snyder.

Figure 73 is a plot of the same series of limestones reacted under conditions similar to those used in earlier runs (Fig. 72) except that 2% by weight of pure sodium chloride was added. The sodium chloride was added by evaporating a water slurry of the stones and salt. This method was used since it yielded a more intimate mixture than does simple mixing of dry salt and stones. Preliminary experiments have shown that the loss of salt by evaporation is greater when salt has been added as a powder. Such evaporation leads to difficulties in evaluating the actual amount of salt present during reaction. Slurry evaporation deposits most of the salt on the surfaces of the limestone particles, where it interacts rapidly with the stone on heating.

The reaction curves in Fig. 73 clearly show changes in the rate of reaction for each stone with 2 wt % NaCl present, as compared with the case with no salt present (Fig. 72). For most of the samples, initial reaction rates are higher than in the absence of salt, exceptions being the highly reactive stones 1337 and Tymochtee whose initial rates are lowered by salt addition. Noticeable also is the tendency of the reactivity of several stones to continue at a high level during the entire 7-hr period with no sign of leveling off. Dolowhite has a significant slope--even after seven hours (Fig. 73)--whereas with no salt present this stone levels off at a much earlier time (Fig. 72).

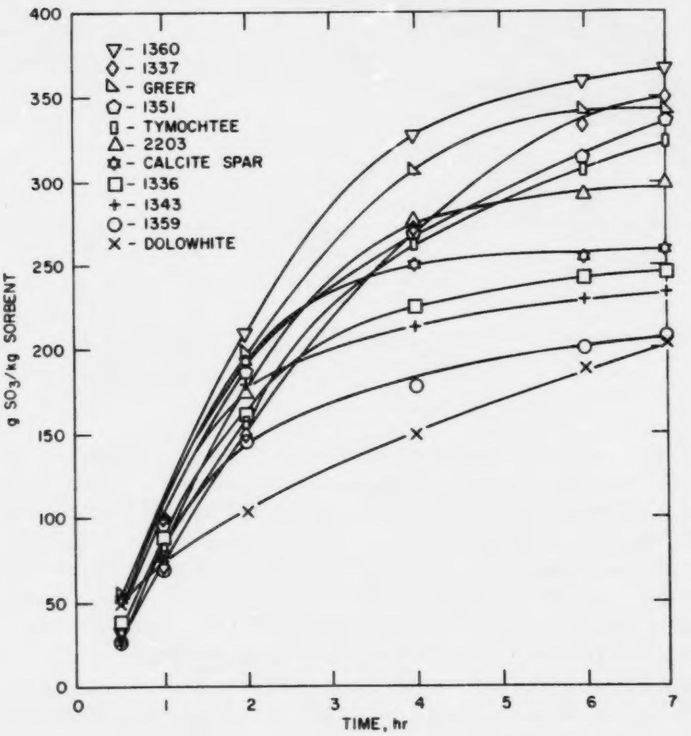

Fig. 73. Weight of SO_3 Captured as a Function of Time for Eleven Limestones with 2 wt % NaCl

For a clearer representation of the effect of NaCl on sulfation of limestone, Fig. 74 is presented as a bar graph to illustrate the results. It is arranged in order of increasing sulfation reactivity of the pure stones. The hatched bars represent the amounts of sulfation (in percent CaO converted to $CaSO_4$) occurring after seven hours in the absence of salt; the open bars represent the additional conversion of CaO to $CaSO_4$ due to the presence of 2 wt % NaCl.

In the case of calcite spar, the incomplete calcination of the raw stone in the absence of salt interferes with the measured reactivity. When salt is present, calcination is rapid and complete. If the entire calcium content of the raw calcite is considered available, rather than the partially calcined stone, conversion would amount to only 5% of the total stone.

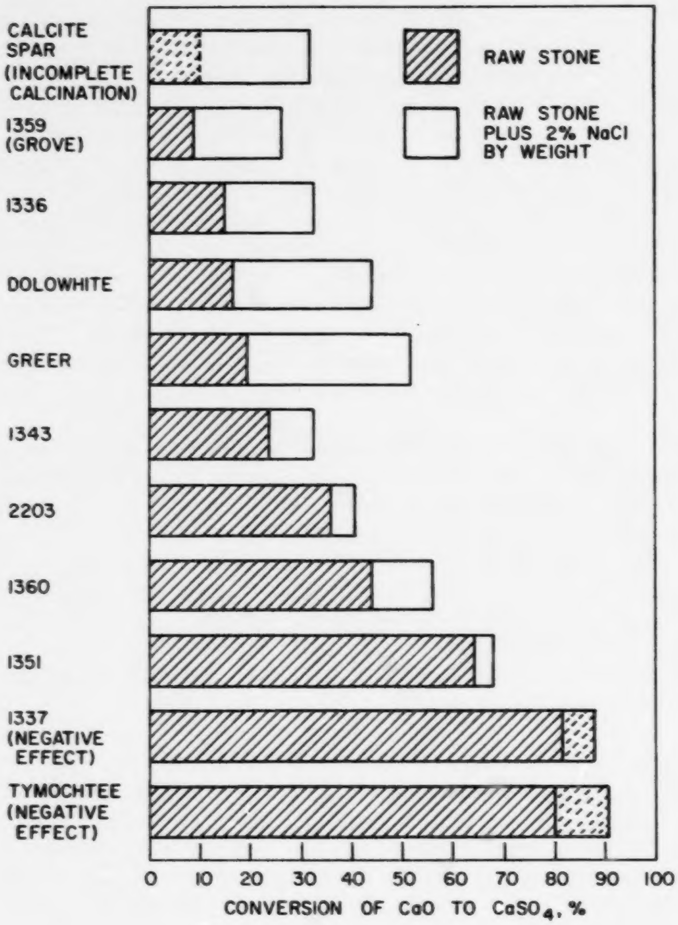

Fig. 74. Effect of NaCl on Sulfation of Limestones at 850°C in 0.3% SO_2 after 7 Hours. All stones except calcite spar were totally calcined.

From this graphic representation, it is readily apparent that the limestones with low reactivity show a greater effect of NaCl than do the rest of the samples. The highly reactive stones, 1337 and Tymochtee, are actually hindered by the presence of the salt. If, as has been suggested, the effect of the mineralizer is to change the crystallization characteristics of the calcining and sulfating stone with subsequent changes in the porosity, one might expect that any changes in stones normally undergoing nearly complete sulfation would be detrimental. Preliminary porosity measurements suggest that drastic changes in the pore size distribution occur during calcination when salt is present. Porosity tests have been completed for the entire series of limestones in both the calcined and the sulfated condition with and without NaCl present and are reported below.

d. Porosities of Limestones

The porosity curves of accumulated pore volume *vs* pore diameter for samples calcined in 20% CO_2 at 850°C for 1 hr are presented in Fig. 75. It can be readily seen that each stone has its own pore distribution and predominant pore size. Conditions of calcination being constant, what is reflected here are the differences in composition, morphology, and impurity level of the stones. Limestone 1360 decrepitates badly and the curve measures interparticle space for the powder produced, as well as intraparticle porosity. The eleven stones represent a wide range of limestones having various amounts of extraneous constituents. Enhancement of reactivity with SO_2 appears to depend a great deal on the formation of larger pores which can react more completely with large molecules such as sulfur trioxide. These curves represent the baseline calcines with no salt addition, *i.e.*, with only the small amount present naturally in the stone. The CO_2 level during calcination must be specified since the reactivity of a lime can be greatly affected by precalcination at high CO_2 levels.

Two weight percent sodium chloride was added to the stones, and calcination was carried out in a 20% CO_2 at 850°C for 1 hr. The resulting porosities of the eleven stones are shown in Fig. 76. The effect of the sodium chloride is to shift the curves to a larger average pore diameter. Each stone responds in a unique way. The different porosities appears to reflect the different compositions of the stones, but more analysis of the results is needed before the exact relations are defined. The effects are dramatic in every case, with the largest changes occurring in the more calcitic limestones. Correlations with SO_2 conversion of CaO to $CaSO_4$ are not readily discernible and await further analysis of the data.

For the present, one example from the eleven will serve to illustrate the effects of salt on limestone porosity. Greer limestone has been chosen as an example since there is a great deal of data on Greer's reactivity with SO_2. Figure 77 is a family of porosity curves for Greer limestone illustrating the effect of varying the concentration of NaCl added to the stone before calcination. The average pore diameter shifts to a higher size for every incremental addition of salt. The shape of the curves remains the same, with total porosity gradually rising, peaking at 1% NaCl, and falling with further addition. At concentrations higher than 1% NaCl, a

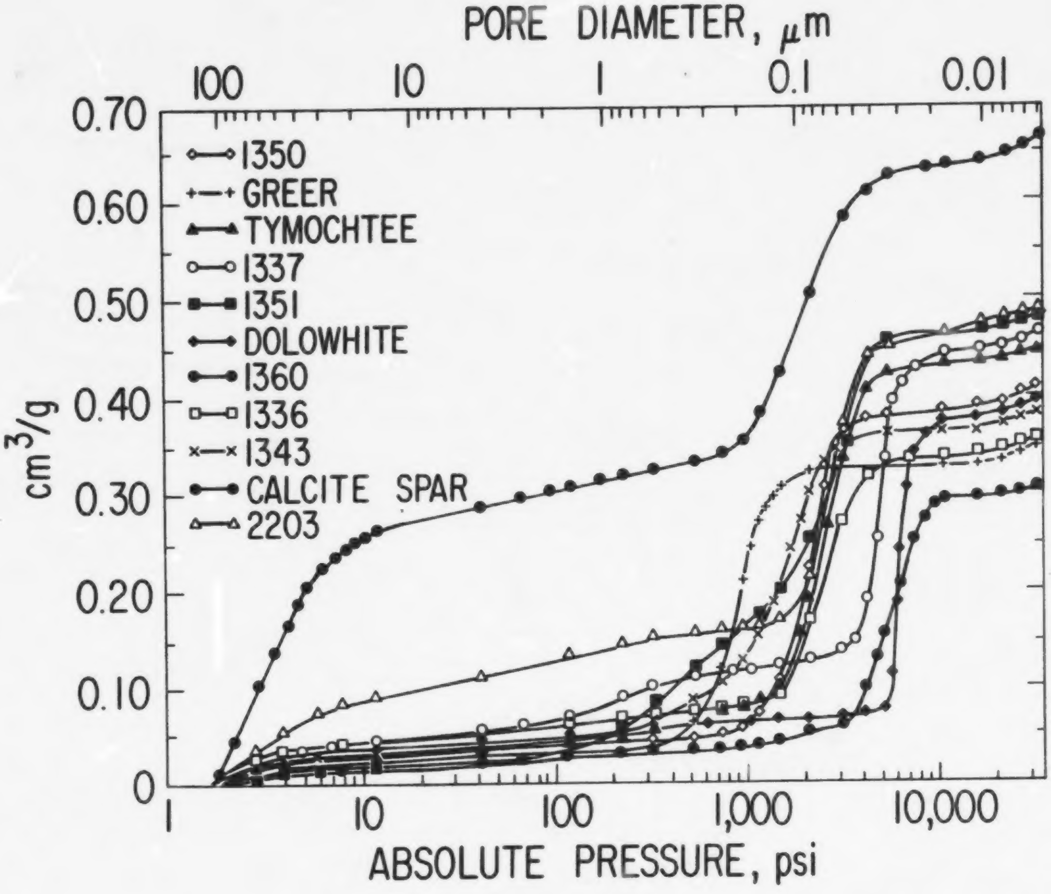

Fig. 75. Porosimetry Curves for Eleven Limestones Calcined One Hour at 850°C in 20% CO_2

great deal of the added salt vaporizes and has no contact with the stone; thus, the effect levels off rapidly. Data not reported here shows the effect of increased exposure time at the calcining conditions for Greer with 1% NaCl--only a slow growth of pores over a 6-hr timespan at 850°C. All of these porosimetry curves represent calcination without sulfation. For simultaneous calcination/sulfation, the resulting porosity is expected to differ, especially in the presence of NaCl. The salt particles act as centers of nucleation, causing rapid recrystallization and ionic diffusion. Surficial melts lower the energy barrier for ions to move from one structural lattice position to another, speeding the coalescence of grains within the crystallizing CaO and $CaSO_4$ and simultaneously maintaining an open-pore structure which counteracts the loss of surface area due to this increase in particle size. Further measurements are being made on other stones to attempt to define the effects of mineralizers on the porosity of the stones and how that affects the activity of the lime with respect to SO_2 capture.

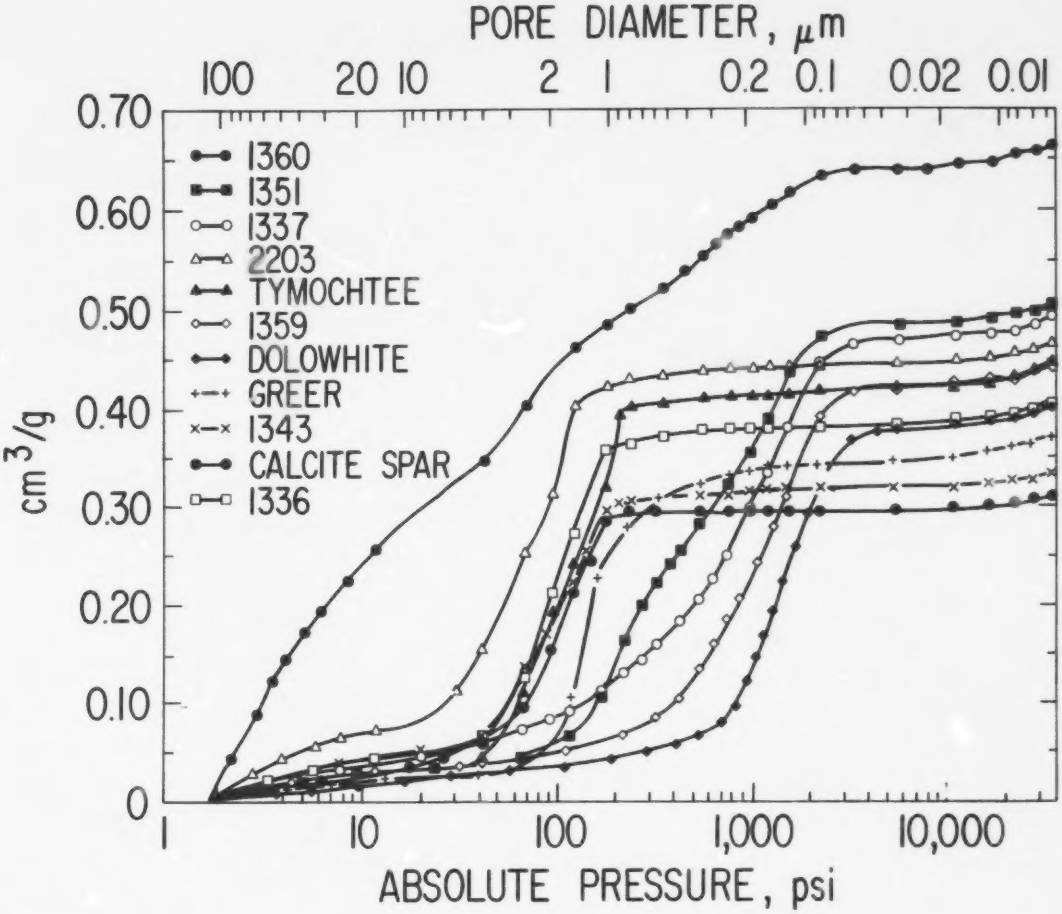

Fig. 76. Porosimetry Curves for Eleven Limestones Plus 2% NaCl, Calcined 1 Hour at 850°C in 20% CO_2

In order to relate the porosity measurements to reactivity, samples of the limestones were precalcined under identical conditions and then reacted with sulfur dioxide, thereby avoiding effects due to simultaneous calcination/sulfation. These sulfation runs were performed at 850°C in 0.3% SO_2, 5% O_2, 20% CO_2, and the balance N_2 with and without 2 wt % NaCl added.

The percent conversions to sulfate are presented in Fig. 78, along with calcination/sulfation data refined from earlier work. The bars represent the various modes of reaction with SO_2. The clear bars ("raw stone") are the percent conversions of CaO to $CaSO_4$, measured for simultaneous calcination/sulfation. Similarly, the shaded bars represent the total conversions under simultaneous calcination/sulfation with 2 wt % NaCl added. The widely spaced hatched bars are the conversions to sulfate for the precalcined raw stone, while the closely spaced hatched bars represent the

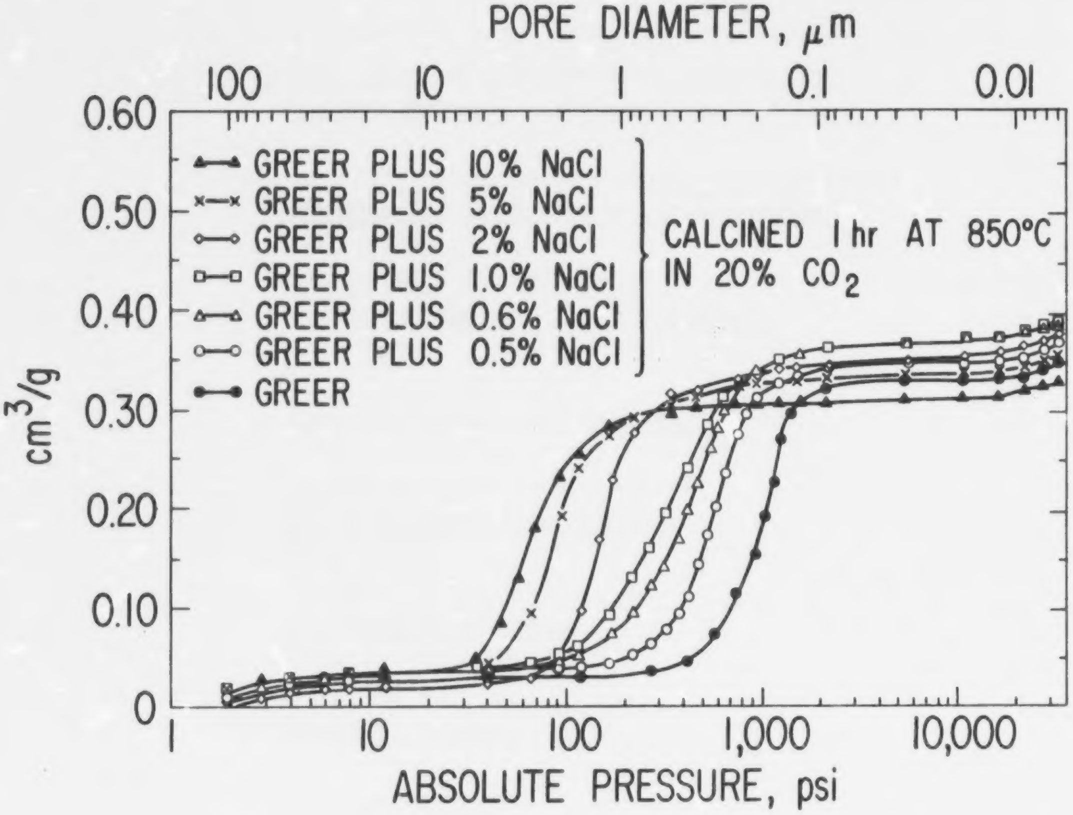

Fig. 77. Porosimetry Curves for Greer Limestone plus NaCl Calcined 1 Hour at 850°C in 20% CO_2

conversions to sulfate for precalcined stone that had been treated with 2 wt % NaCl. The graph is arranged in the order of increasing reactivity of the raw precalcined limestone, from "calcite spar" to Tymochtee. With a few exceptions, this order is also the order of increasing inerts content ("inerts" are constituents that do not react with SO_2, including MgO) of the calcined stone. There is a fair correlation between percent conversion and total inert content for untreated stones which is improved if one considers that stones 1360 and 2203 undergo considerable decrepitation and dusting when calcined; their anomalously high reactivities are due to the increased surface areas presented by the powders. The glaring exception to the general trend is the conversion of dolowhite, which is a highly crystalline pure dolomitic material and has very small pores. Its apparent unreactivity must be due to its initial low-porosity--perhaps constrained by its highly crystalline state.

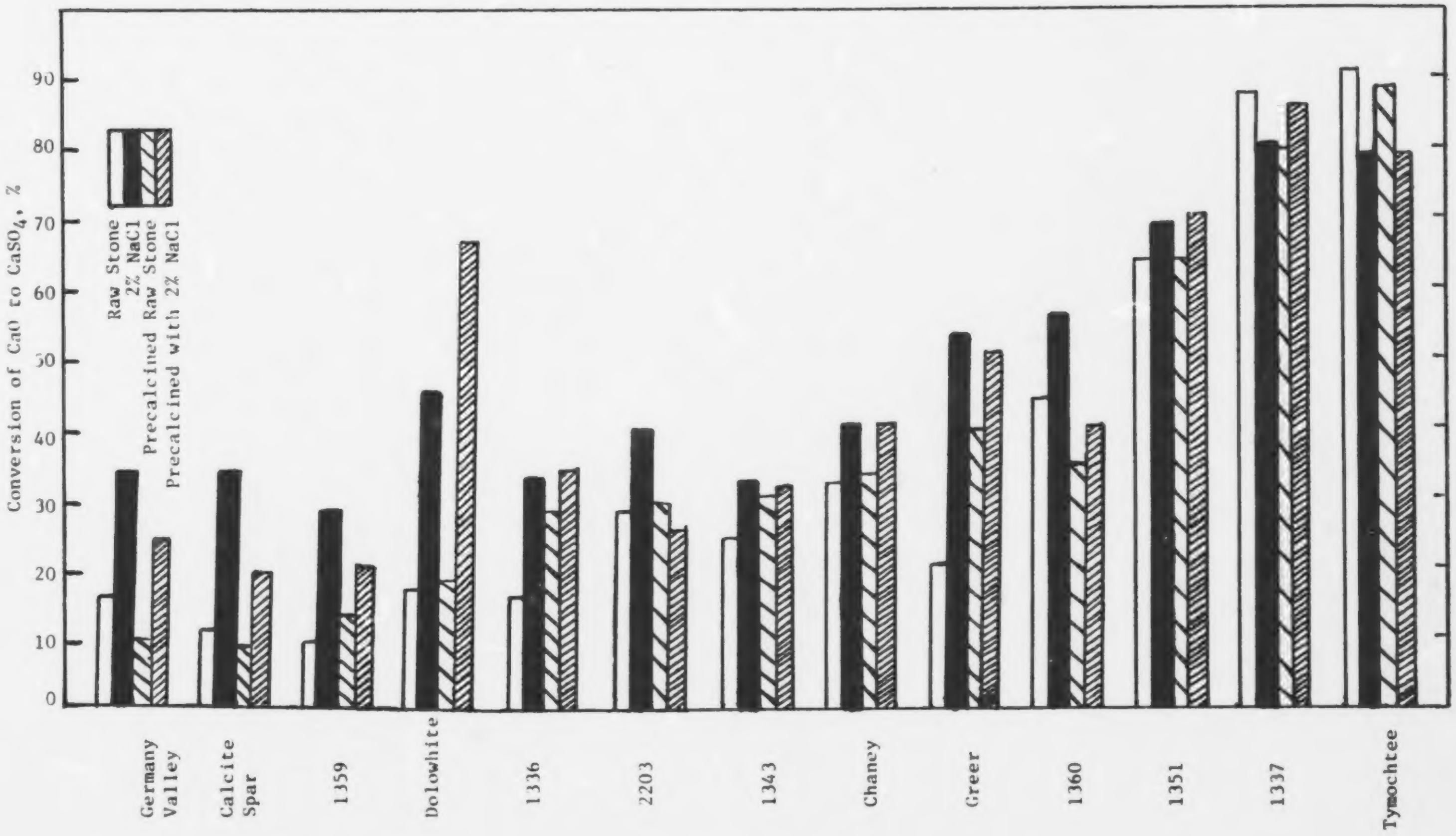

Fig. 78. Effect of NaCl on Sulfation of Limestones (Both Precalcined and Simultaneous Calcination/Sulfation) at 850°C in 0.3% SO$_2$ After Seven Hours.

The reactivity of precalcined limestones containing 2 wt % NaCl again shows the above relationship between inerts content and reactivity. Figure 79 is a plot of sulfur conversion versus total inerts content of the calcined stones treated with NaCl. Here, the correlation is excellent, including that for previouslv anomalous dolowhite, which here has a reactivity comparable to that of the other dolomitic stones studied. Apparently, the salt treatment opened up the structure to an extent, overcoming the restraints induced by the original crystallinity of this dolomite.

The porosity curves measured for these limestones have been used to obtain an "average" pore diameter by dividing the pore volume measured on the porosimeter by the calculated surface area. This gives one-half radius or, after multiplying by four, an "average" pore diameter for all pores that are larger than ≈0.02 μm. Smaller pores were not included since they play no important part in sulfur reactivity in the time period considered.

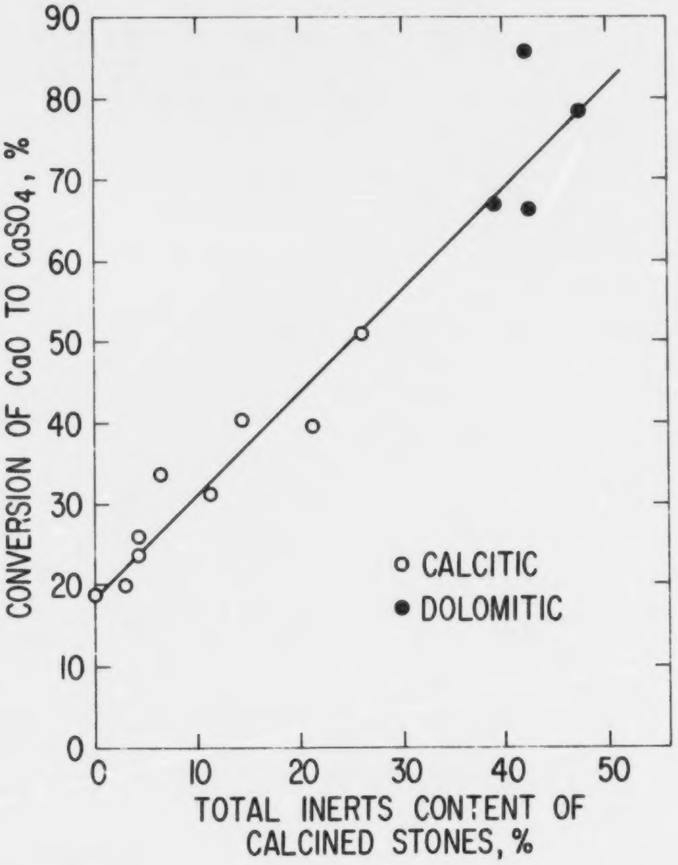

Fig. 79. Sulfation at 850°C of Limestones as a Function of Total Inerts Content in Precalcined Stones Treated with 2% NaCl.

Figure 80 is a plot of "average" pore diameter for precalcined stones (both raw stone and stones that had been treated with 2% NaCl) as a function of total inerts content of the calcines. There appears to be a strong correlation for the salt-treated stones that includes both the calcitic and the dolomitic limestones.

Of the untreated stones, the calcitic limestones form a straight line trend of increasing pore diameter with increasing inerts content. The dolomitic stones are in a separate cluster. Their high $MgCO_3$ content undoubtedly plays a major role in determining initial porosity and pore size distribution. The effect of NaCl on the pore diameter can be seen to increase as the inerts content of the stones decreases. Pure calcitic stones are affected to a much greater extent by the given amount of salt than are the impure limestones and highly magnesian dolomites.

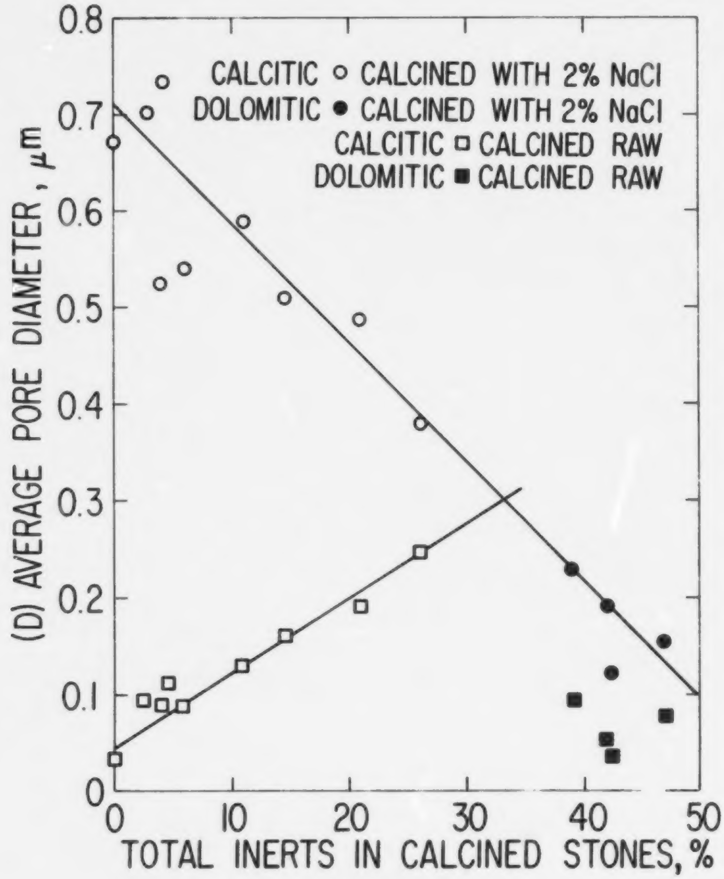

Fig. 80. Average Pore Diameter as a Function of Total Inerts Content of Limestones

The correlation between percent conversion of CaO to $CaSO_4$ and "average" pore diameter for the salt-treated precalcined stones is shown in Fig. 81. The larger the pore diameter, the lower the conversion of the salt-treated stones. In the case of untreated precalcined stones (no graph presented), no trend is clear (*i.e.*, the points scatter), but the relationship appears to be the inverse of that for treated stones--stones with large pores appear to have greater reactivity. This apparent contradiction can be resolved if pore size distribution is considered along with the known fact that pores smaller than a certain size do not react appreciably with SO_2 (as discussed below). The trend of increasing reactivity in the series of untreated precalcined stones with larger pores reflects the fact that most of the pores in these stones are too small to contribute to SO_2 reactivity. As a result, some stones with pores of a more favorable size distribution react more with SO_2. When NaCl is added, most of the pores in all stones now are larger than this lower limit, and now the controlling variable is surface area, which decreases dramatically as pore diameter increases.

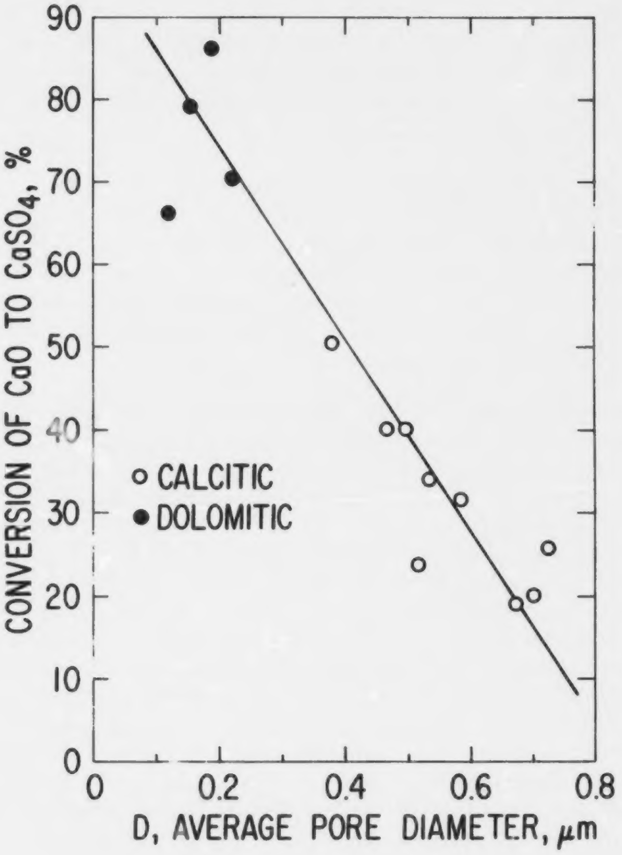

Fig. 81. Sulfation at 850°C of Limestone as a Function of Average Pore Diameter in Precalcined Stones Treated with 2% NaCl

In the case of the dolomitic stones, their inherent porosity is already at a near maximum with respect to sulfur capture due to the additional porosity contributed by $MgCO_3$ decarbonation; the porosity of dolowhite is anomalous since its pores are extremely small. When salt is added to dolomitic stones, the effect is that surface area is lost by growth of large pores at the expense of small pores; however, dolowhite's porosity is thereby shifted to a more favorable pore size distribution.

The selection of 2% as the NaCl concentration was arrived at on the following basis: (1) its favorable effect on one limestone (Greer) and (2) the fact that this concentration was used by Pope, Evans and Robbins to improve sulfur capture in their early atmopsheric fluidized-bed combustor. It is expected that by varying the amount of salt, an optimum reactivity for each stone should be achievable. Experiments are being done to study this.

Figure 82 illustrates how varying of the concentration of added NaCl affects the "average" pore diameter for a pure calcite spar and an impure (up to 24% inerts) limestone (Greer). As can be seen, the effect of NaCl addition on pore diameter is greater in the pure stone although the percent conversion of CaO to $CaSO_4$ with 2% NaCl addition is only 19% for calcite as compared with 50% for Greer (Fig. 78). Hence, reactivity is not a function of pore diameter alone. Surface area and direct effects of salt on the sulfation reaction must be considered.

It has been reported in the literature that the only property of limestone that reliably correlates with reactivity is the sodium content. This relationship holds true for this series of stone in a very loose way. The initial sodium contents of most of the samples are so low that comparisons would be unreliable. However, an overall trend exists, confirming the reported correlation. A larger number of stones must be considered before any definite relation can be observed.

One further point supports the concept that the effect of NaCl is related to the inerts content of the stones: The analyses of the products after sulfation for various limestones treated with 2% NaCl show a general increase in sodium content with an increase in the total inerts content of the calcined stone. This suggests that the inert materials are interfering with and tying up some of the effectiveness of the sodium. For the few dolomitic stones, no apparent differences due to the inert content appear. The formation of silicates, aluminates, *etc.* could effectively reduce the concentration of sodium available for interaction with the calcium and could hinder the recrystallization and growth of pores caused by salt. Thus, we find residual sodium in the impure limestones and dolomites, and we find that essentially no sodium is retained in the pure stones after 7 hr of sulfation. This point has consequences beyond this question of mechanistic effect. This loss of sodium in these experiments plays a role in determining the disposition of sodium in a fluidized-bed combustor and may be an important consideration in relation to corrosion, which appears to be related to alkali concentrations in the flue gas.

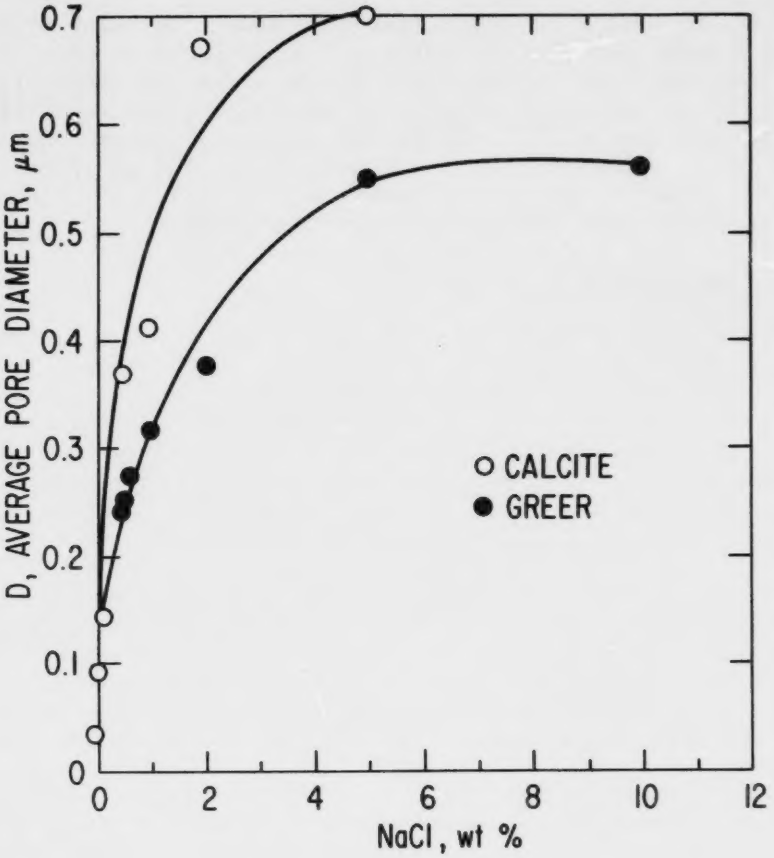

Fig. 82. Average Pore Diameter as a Function of Percent NaCl Added

In the above discussion, no attempt is made to evaluate those effects of the salt that may contribute to sulfation (such as continuous changes in porosity during reaction and surficial melts contributing to recrystallization and decomposition). As further analysis of the data is completed and scanning electron microscope photographs and elemental scans are correlated, the details of the mechanism will be formulated clearly.

2. The Determination of Inorganic Constituents in the Effluent Gas from Coal Combustion

(S. Lee)

Some chemical elements in combustion gases are known to cause severe metal corrosion. The objectives of this study are to determine quantitatively which elements are present in the hot combustion gas of coal, in either volatile or particulate form, and to differentiate between volatile and particulate species. It is desirable to identify which compounds are present as particulate species and their amounts and to determine the amounts of compounds present as condensable species.

Assembly of the laboratory-scale fixed-bed batch combustor system to be used for this study has been completed. A schematic diagram of this combustor system was presented and described in the preceding annual report (ANL/ES-CEN-1016). Several shakedown coal-combustion experiments have demonstrated satisfactory performance of the combustor system. During this period of reporting, systematic studies have been started to investigate the transport of alkali metals during the combustion of coal. The findings from these studies are discussed and presented in this report.

a. Coal Combustion Experiments

In initial coal combustion experiments, the problem was encountered that tar and/or soot condensed on the surface of the cold trap. This was found to be due to insufficient oxygen in the combustion air during the early stage of the experiment and was eliminated by introducing afterburning air downstream from the combustion section. The afterburning air was added to facilitate combustion of volatile matter evolved during the early stage of an experiment. With the combustion of coal successfully controlled, a standard experimental procedure was established and is described in the following:

After the alumina filter and the cold trap are installed in the combustor, the filtration section of the combustor is preheated to the desired temperature (800°C was used in all experiments), using external furnaces. When the temperature of the filtration section reaches a constant value, a sample is placed in the reactor and the entire system is flushed with nitrogen gas for a few minutes. The effluent gas analyzers are calibrated with calibration gases at this time. Prior to heatup of the combustion section, afterburning air is introduced into the combustor at a flow rate of 5.0 L/min. The coal sample is then heated indirectly by induction heating (applied to the combustor pipe at the combustion section of the combustor). When, during heatup of the coal sample, CO_2 gas is detected in the effluent by the effluent gas analyzer, the inlet gas mixture of O_2 and N_2 is introduced into the combustion section to burn the coal. During initial feeding of the inlet gas mixture (65% O_2 in N_2 at a flow rate of 6.4 L/min), volatile matter evolved during heatup of coal is completely combusted. This high-O_2-content gas mixture also burns coal at a high rate to heat the bed to the combustion temperatures rapidly. When the desired coal bed temperature is reached, the O_2 content of the inlet gas mixture is gradually reduced to the desired value, and the afterburning air stream is shut off. The combustion temperature of the coal bed is controlled at the desired level by regulating both the O_2 content of the inlet gas mixture and the induction heating energy input.

The success of the standard experimental procedures in eliminating the condensation of undesirable tar and/or soot on the cold trap was shown by a two-part test run designed to burn two batches of coal, one immediately after the other, under the same experimental conditions. This test run was also designed to test the capability of obtaining reproducible experimental conditions for the two batches by controlling the operational characteristics. This is a necessary capability because two or more batches of coal have to be burned under the same experimental conditions in order to collect enough condensate on the cold trap for analysis.

In each part of this test run, 50 g of -20 +40 mesh Herrin No. 6 coal from Montgomery County, Illinois, was burned. Neither the hot filter nor the cold trap was removed from the combustor during loading of the second batch of coal. The analyses of effluent gas compositions and the coal bed temperature for the entire course of the experiment are shown in Fig. 83 (batch 1) and Fig. 84 (batch 2). The experimental controls used for the two batches differed: a preheated inlet gas mixture was used in the batch 2 experiment but not in the batch 1 experiment, and the afterburning air was shut off earlier in the batch 2 experiment than in the batch 1 experiment. As shown in both figures, the first peak in the CO_2 concentration curve was a result of the sudden increase in flow rate caused by introduction of the inlet gas mixture. The second sharp peak in the CO_2 curve (which ran over-scale on the graph) and the corresponding sharp drop in the O_2 curve shows that the volatile matter evolved during this stage burned rapidly. No carbon monoxide was detected, indicating that volatile matter was combusted completely.

This rapid combustion of volatile matter also resulted in a rapid rise of the coal bed temperature. The bed temperature was controlled stably at 855°C (on this average) for both batches. The effluent gas compositions for both batches were also observed to be nearly identical, indicating that the rate of combustion of coal was the same for both batches. This test run has demonstrated the capability of controlling the burning of coal under a single set of experimental conditions in this combustor system. The cold trap was stably controlled at 150°C in this test run. It was dry and completely free of tar and/or soot.

On the basis of the rate of CO_2 formation, the rate of burning of coal at the experimental conditions has been calculated and found to be 10 to 15 g/hr. This rate decreased with a decrease in the particle size of the coal used. A possible explanation for this is that finer coal particles form a more packed bed that offers more resistance to the diffusion of oxygen into the bed. When the oxygen content in the inlet combustion mixture of oxygen and nitrogen was plotted against the oxygen consumption and also against the formation of carbon dioxide, straight lines were obtained (Fig. 85). This linear relationship indicates that burning of coal in this batch system is controlled by the rate of diffusion of oxygen into the bed.

The cold trap is made of 304 stainless steel. At the end of each coal combustion experiment, bluish condensates were always collected on the surface of the cold trap. They were identified as iron sulfates by X-ray diffraction.* It was shown in subsequent experiments that the bluish condensates were products formed by the attack of sulfuric acid on the stainless steel cold trap. To solve this acidic corrosion problem, the cold trap was electroplated with a very thin layer of rhodium metal (about 0.00005 in.). No thicker layer was possible because, without special treatment, stress cracking would occur in an electroplated layer thicker than 0.00005 in. The choice of rhodium (instead of platinum) is based on its inertness (as compared with platinum) in corrosive environments, lower price, hardness (three times

---

*Done by B. Tani.

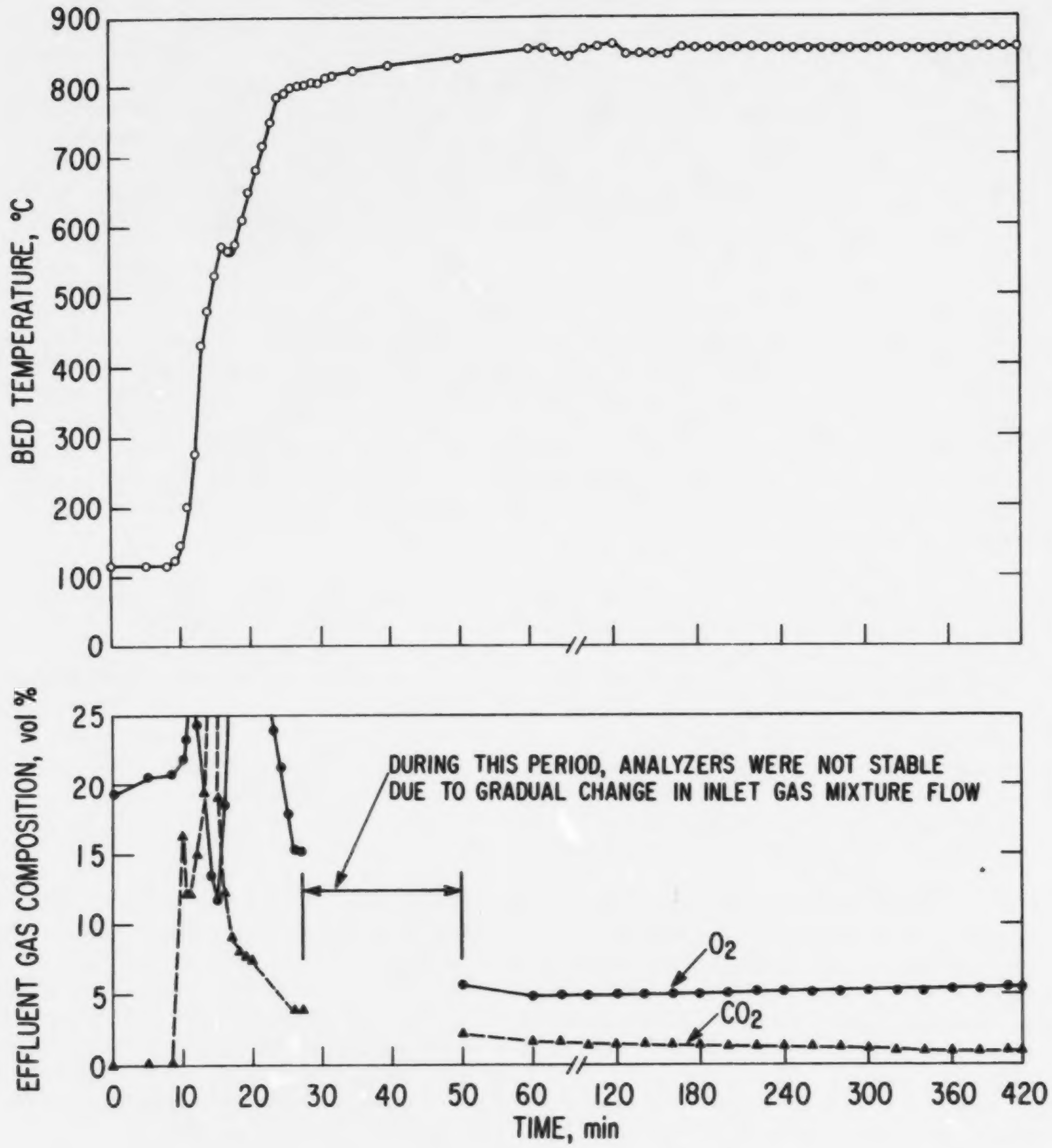

Fig. 83. Bed Temperature and Effluent Composition in a Typical Continuous Two-Batch Coal Combustion Experiment. Batch No. 1.

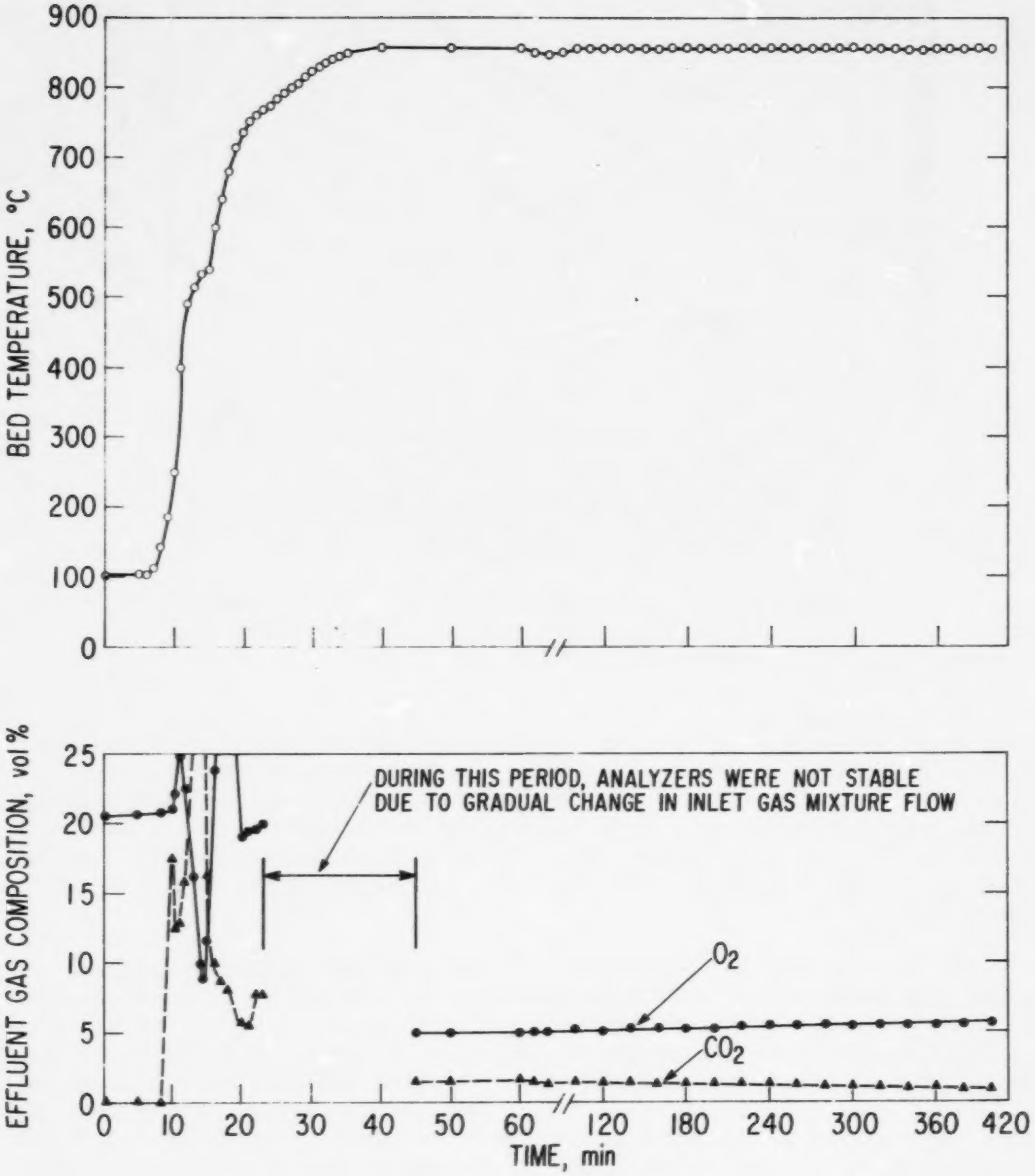

Fig. 84. Bed Temperature and Effluent Composition in a Typical Continuous Two-Batch Coal Combustion Experiment. Batch No. 2.

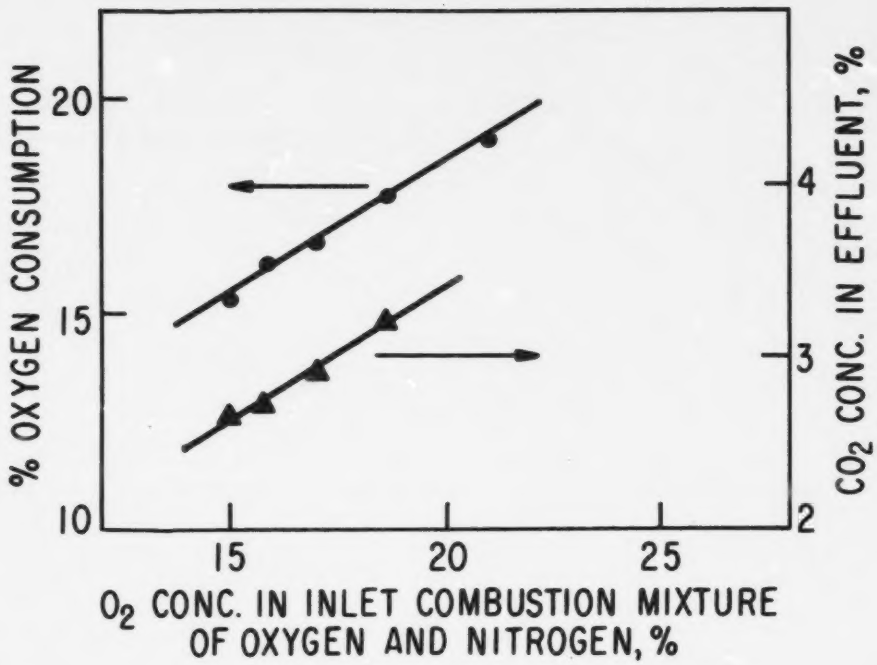

Fig. 85. Relationship of O_2 Content of Inlet Combustion Mixture to O_2 Consumption and CO_2 Formation in Combustion of Coal

harder than platinum at room temperature), and its technical availability for electroplating. After several runs of experiments using this electroplated cold trap, however, the rhodium metal was found to peel off gradually from the surface of the cold trap, resulting in the acidic attack on the surface of the cold trap again. This acidic corrosion problem was finally solved by coating the surface of the cold trap with a layer of porcelain enamel (about 0.01 cm).

In a series of systematic studies completed in this reporting period, the transport of alkali metals from the combustion of high-chlorine coal was examined. Study of high-chlorine coal is of interest because of past findings obtained from the operation of boiler furnaces, that is, the chlorine content of coal is closely related to its fouling and corrosive effects on the fire-side of a boiler furnace. Data has been obtained showing that the rate of deposition in boiler furnaces does not become significant until the chlorine content exceeds about 0.3%.[33] Because naturally occurring high-chlorine coal was not available in this laboratory, a simulated high-chlorine coal was used in this study. The simulated high-chlorine coal was synthesized by impregnating coal with NaCl, using waster solution. The choice of NaCl instead of other chlorine compounds to increase the chlorine content of the coal to the desired concentration is based on a general agreement that chlorine in coal is largely present as a chloride, especially as a sodium chloride. The NaCl used was 99.5% purity A.C.S. reagent.

The first series of experiments (SL-1 series) was carried out to burn 0.5% by wt NaCl-impregnated Herrin No. 6 seam coal from Montgomery County, Illinois. It is a high-volatile bituminous B coal containing 3.68 % S, 0.135% Na, 0.195% K, and about 0.1% Cl[34] on a dry basis. The proximate analysis on a dry basis of this coal is 38.22% volatile matter, 45.13% fixed carbon, and 16.54% ash. In this series of experiments, five batches of -20 +40 mesh coal were burned at the same experimental conditions--850°C atmospheric pressure, and a flow of 8% O_2 in N_2 mixture at a flow rate of 6.0 L/min. The cold trap and the Al_2O_3 filter were not removed until all five batches of coal had been burned. A total of 215 g of coal was combusted in this series of experiments.

To obtain quantitative information on sodium transport during combustion, the cold trap was carefully rinsed with distilled water after this series of experiments to collect all deposits on the surface for analysis. The Al_2O_3 filter was leached, first with distilled water, and then with 5% HCl solution at a gentle boiling temperature for two hours. Both leaching solutions were collected for analysis. (Before it was used in the combustor, this Al_2O_3 filter had been new and had been first treated as described above for 15 hr to remove both water- and acid-soluble salts, and then it had been heated in a muffle furnace at 900°C in an air flow to completely remove the absorbed HCl.) The combustion residues left in the combustion boat after each experiment were also collected for analysis. All analyses were done by atomic absorption.*

The material balance for sodium element collected on the Al_2O_3 filter, collected on the cold trap, and retained in the ash bed has been computed. Results show that the total sodium in the "output" is about 23% higher than that in "Input." This wide spread may be compared with ±5%, the analytical error obtained when analyzing sodium by the atomic absorption method. Since this analytical error can not account for the discrepancy in the material balance, possible sources of error verified later are: (1) nonhomogeneity of the coal sample and (2) contamination of the combustion ash residue by the mortar and by both "Joy" and "Comet" detergents used for cleaning purposes during the experiments. In contrast, the total amount of sodium collected from the cold trap and the Al_2O_3 filter shows only 0.2% of the sodium vaporized from the coal bed.

To study whether some trace elements in coal vaporized at the experimental conditions (850°C and atmospheric pressure) and to obtain the chemical compositions of the Al_2O_3 filter, (1) condensates collected on the cold trap and (2) Al_2O_3 filter powder scraped from the filter element before and after the SL-1 series of experiments were analyzed, using emission spectrometry.† The analytical results show that aluminum and silicon are the major constituents of all filter scrapings. The source of other elements present at a trace level is the chemical binder used in the manufacture of the filter. Within the analytical accuracy and the possible inhomogeneity of the filter, the results show that except for possible volatilization of manganese and lead, the composition of the filter generally remains the same upon exposure to the flue gases. Several elements were also found in trace amounts in the condensates collected on the cold trap. Since all elements found in the condensates were also found in the Al_2O_3 filter scrapings, these elements might have volatilized from the Al_2O_3 filter, instead of the coal bed. Further study is required to verify this.

---

*Done by R. Bane.

†Work done by J. Faris.

The combustion temperature is known to be an important factor affecting the evolution of alkali metals during coal combustion. To investigate this effect, the same 0.5% NaCl-impregnated Illinois Herrin No. 6 coal as was used in the SL-1 series was combusted at 900°C and atmospheric pressure. Two series (SL-2 and SL-3 series) of experiments were carried out at these experimental conditions. The only difference between SL-2 and SL-3 series was that a porcelain enamel-coated cold trap was used in the SL-3 series, whereas an uncoated stainless steel cold trap was used in the SL-2 series. In each series of experiments, five batches (a total of 237 g in SL-2 and 228 g in SL-3) of coal were burned in a flow of 8% O_2 in N_2. The flow rate was 6.0 L/min. The Al_2O_3 filter, the condensates collected on the cold trap, and the ash residues left in the combustion boat were treated the same as were those in the SL-1 series.

At the end of the SL-3 series of experiments, the entire cold trap was completely free of bluish products which, in previous work of this study, had been formed by the attack of acids on the uncoated stainless steel cold trap. The cold trap was observed to be intact. These observations indicate that the porcelain enamel coating was effective in preventing acidic attack on the stainless steel under the experimental conditions. The surface of the cold trap finger appeared to be substantially clean, and no condensate and/or ash could be collected mechanically; however, scattered liquid drops were observed on the surface. They showed both strong acidic reactions when tested with pH paper and the presence of SO_4^{2-} and Cl^- when tested with solutions of $BaCl_2$ and $AgNO_3$, respectively. These results indicate that the liquid condensates on the cold trap finger very likely were H_2SO_4 and HCl.

The material balances for sodium and potassium for the SL-2 and the SL-3 series of experiments are shown in Tables 27 and 28. As noted in these tables, fairly good agreement is observed for both series of experiments, indicating the reproducibility of the experiments. However, the totals of sodium and potassium in the "Output" are again higher than those in the "Input," especially for potassium. As discussed in a previous paragraph, it is believed that nonhomogeneity of the coarse coal samples used in these experiments and contamination of the ash residues by the mortar and by both "Joy" and "Comet" detergents used for cleaning purposes account significantly for the errors observed in the tables. However, because of the large discrepancy in the material balance for potassium, there may be unknown sources of potassium contamination.

Tables 27 and 28 indicate that about 1% of the sodium and 2% of the potassium evolve from the coal bed and that most of the sodium and potassium evolved is captured by the Al_2O_3 filter. Upon comparison with 0.2% Na evolution observed in the SL-1 series of experiments, these results show

Table 27. A Material Balance of Sodium from Combustion of Illinois Herrin No. 6 Coal Impregnated with 0.5 wt % NaCl. Combustion was at 900°C and atmospheric pressure.

	mg[a]	
	SL-2 Series	SL-3 Series
Input		
In Coal	312.5	312.5
Added as NaCl	492.0	492.0
Total	804.5	804.5
Output		
Collected on Cold Trap	0.3	0.6
Captured by Al_2O_3 Filter		
(a) Water Leaching Solution	4.7	1.7
(b) Acid Leaching Solution	3.6	3.3
	8.6	5.6
Left in the Combustion Residue		
(a) Water Leaching Solution	92.4	100.7
(b) Acid Dissolution	740.9	742.5
	833.3	843.2
Total	841.9	848.8

[a] Obtained by an atomic absorption method; estimated precision is ±5%. Analyses done by Ralph Bane.

only a slight effect of combustion temperature on the evolution of alkali metals from the combustion of Herrin No. 6 coal from Montgomery County, Illinois. Tables 27 and 28 also show that both sodium and potassium are essentially retained in the ash bed, especially in compound forms that are not soluble in water. Results similar to these were also reported by the Combustion Power Co. in California when a mixture of 221 samples of Illinois No. 6 coal was combusted in their CPU-400 fluidized-bed combustor at 870°C.[35]

The reactions that cause NaCl to be retained in the ash may be very complicated. Possible chemical reactions are those in which NaCl, silica, and metal oxides (such as CaO, Al_2O_3, or Fe_2O_3) react to form end products with high melting points. Examples of these products are devitrite ($Na_2O \cdot 3CaO \cdot 6SiO_2$), Acmite ($Na_2O \cdot Fe_2O_3 \cdot 4SiO_2$), and sodium aluminum silicates ($Na_2O \cdot Al_2O_3 \cdot 2SiO_2$). Some of the reactions involved are:

$$2\ NaCl + S + 1\ 1/2\ O_2 + H_2O \rightarrow Na_2SO_4 + 2\ HCl$$

$$Na_2SO_4 + 3\ SiO_2 \rightarrow Na_2O \cdot 3SiO_2 + SO_2 + 1/2\ O_2$$

$$2\ NaCl + 3\ SiO_2 + H_2O \rightarrow Na_2O \cdot 3SiO_2 + 2\ HCl$$

Table 28. A Material Balance of Potassium from Combustion of Illinois Herrin No. 6 Coal Impregnated with 0.5% NaCl. Combustion was at 900°C and atmospheric pressure.

		mg[a]	
		SL-2 Series	SL-3 Series
Input			
In Coal		475.0	475.0
	Total	475.0	475.0
Output			
Collected on Cold Trap		0.1	0.4
Captured by Al_2O_3 Filter			
(a) Water Leaching Solution		1.3	1.9
(b) Acid Leaching Solution		2.3	7.6
		3.7	9.9
Left in the Combustion Residue			
(a) Water Leaching Solution		4.7	5.0
(b) Acid Dissolution		577.9	584.3
		582.6	589.3
	Total	586.3	599.2

[a] Obtained by an atomic absorption method; estimated precision is ±5%. Analyses done by Ralph Bane.

$$Na_2O \cdot 3SiO_2 + 3SiO_2 + 3\ CaO \rightarrow Na_2O \cdot 3CaO \cdot 6SiO_2$$

$$Na_2O \cdot 3SiO_2 + Fe_2O_3 + SiO_2 \rightarrow Na_2O \cdot Fe_2O_3 \cdot 4SiO_2$$

$$Na_2O \cdot 3SiO_2 + Al_2O_3 \rightarrow Na_2O \cdot Al_2O_3 \cdot 2SiO_2 + SiO_2$$

$$2\ NaCl + H_2O + Al_2O_3 \cdot 2SiO_2 \rightarrow Na_2O \cdot Al_2O_3 \cdot 2SiO_2 + 2\ HCl$$

Mineral matter in coal is the source of silica and metal oxides for all these reactions.

b. Charcoal Combustion Experiments

Sodium chloride has a significant vapor pressure at both 850°C (1.55 mm Hg[36]) and 900°C (3.39 mm Hg[36]). Significant amounts of NaCl are expected to vaporize if silica and metal oxides are not available or are available in inadequate quantity to fix NaCl by the reactions shown above. This appeared to be the case when a mixture of NaCl and coconut charcoal was combusted. A mixture of 20 g of 8 to 12 mesh activated charcoal and 1 g NaCl has been burned under the same experimental conditions as those of the SL-1 series. At the end of the experiment, substantial amounts of NaCl (which was identified by X-ray diffraction) were collected on the cold trap, indicating that NaCl had vaporized at the experimental conditions and was condensed on the cold trap. Since the charcoal has low sulfur (0.4%) and ash (1.3%) contents for retaining the NaCl in the bed, NaCl vaporized, as would be expected on the basis of its vapor pressure.

In the experiment with activated charcoal, the combustor pipe for the combustion and filtration sections was maintained at 800°C throughout the experiment. The purpose was to keep NaCl vapor from condensing on the pipe before it reached the cold trap. At the end of this experiment, all stainless steel sheaths of the thermocouples exposed to hot flue gases were observed to be severely corroded, and substantial amounts of black scale had spalled off the combustion and filtration sections. These phenomena had not been observed when charcoal alone or coal was burned under similar experimental conditions. Apparently, the severe corrosion observed in this experiment resulted from attack of the NaCl vapor on the metal surfaces of the thermocouple sheaths and the combustor pipe. The corrosive property of NaCl vapor has also been reported in the technical literature.[37-39] Alexander[39] proposed that NaCl destroys the normally protective chromium-iron spinel oxide layer by the reaction:

$$24\ NaCl + 10\ Cr_2O_3 + 9\ O_2 \rightarrow 12\ Na_2CrO_4 + 8\ Cr_2Cl_3$$

In a fluidized-bed coal combustion system, the addition of a small amount of NaCl to the bed has been shown to improve the SO_2 absorption characteristics of limestones.[21] However, the experimental results reported above show that the use of NaCl may also dangerously increase the potential of the flue gases to corrode the metal surfaces of components located downstream from the combustion system.

As shown in the preceding paragraphs, the samples in the SL-2 and SL-3 series of experiments were believed to be contaminated in the mortar used for grinding (*i.e.*, from the commercial detergents used for cleaning). To investigate this contamination, another set of experiments has been carried out using activated coconut charcoal in place of coal. This set of experiments was also designed to study quantitatively the performance of the cold trap and the characteristics of the Al_2O_3 filter with respect to its ability to retain alkali metal compounds.

Two experiments were performed: SL-4 and SL-5. For both experiments, the charcoal was impregnated with 0.5 wt % NaCl, using a water solution, and then combusted at 900°C and 3-psig pressure using an inlet combustion gas of 30% O_2 in N_2 at a flow rate of 3.2 L/min. A section of glass wool was packed inside the flue gas exhaust line right at the end cap of the combustor. This was used as a second filter trap, called a downstream filter, to collect any alkali metal compounds not captured by the upstream Al_2O_3 filter and cold trap. The cold trap was air-cooled in this set of experiments; the temperature at the tip of the cold trap was controlled at about 200°C. The Al_2O_3 filter was used in the SL-5 experiment but not the SL-4.

The material balances for sodium for both experiments are given in Table 29. Within the limits of analytical and experimental errors, very good material balances were obtained for both experiments. No commercial detergents were used, and the ash residues were not ground in the mortar;

Table 29. Material Balance of Sodium from Combustion of Activated Coconut Charcoal Impregnated with 0.5 wt % NaCl. Combustion was at 900°C and atmospheric pressure.

	Sodium, mg[a]	
	SL-4	SL-5
Input		
(1) in Charcoal	13	13
(2) Added as NaCl	39	39
Total	52	52
Output		
(3) Collected on Cold Trap	5 (10%)	2 (4%)
(4) Captured by Al_2O_3 Filter		
(a) Water Leaching Solution	-	1
(b) Acid Leaching Solution	-	6
	5 (10%)	9 (17%)
(5) Retained in Combustion Residue		
(a) Water Leaching Solution	26	30
(b) Acid Dissolution	14	13
	40 (77%)	43 (83%)
(6) Collected by Downstream Filter	6 (11%)	1 (2%)
Total	51	53

[a] Obtained by an atomic absorption method; estimated precision is ±5%.

therefore, these results appear to support the findings that the samples in both the SL-2 and the SL-3 series of experiments were contaminated by detergents from the mortar and pestle.

It may be seen that the quantities of sodium retained in the combustion residue in compound form that dissolved only in acid solution (item 5b in the table) are about the same as those in the charcoal (item 1); therefore, the sodium vaporized during the experiments (items 3 + 4 + 6) was from the NaCl added (item 2). In the SL-4 experiment, in which no Al_2O_3 filter was used, about 21% of the NaCl (items 3 + 4 + 6) was vaporized, and the cold trap captured slightly less than 50% of the NaCl vaporized.

When the Al_2O_3 filter was placed upstream from the cold trap (experiment SL-5), 74% of the NaCl vaporized was captured by the Al_2O_3 filter [item 4/(item 3 + item 4 + item 6)]; the sodium captured by the filter was essentially in compound forms not soluble in water, but soluble in 5% HCl solution. The Al_2O_3 filter was maintained at about 800°C during this experiment. These results indicate that the Al_2O_3 filter reacts with the NaCl to (probably) form sodium alumina silicates, most of which are known to be insoluble in water but soluble in acid. The small amount of sodium compounds soluble in water (item 4a) is possibly in the form of simple sodium silicates or sodium aluminate ($NaAlO_2$).

Results of X-ray diffraction analysis of the condensates collected on the cold trap finger (from SL-4) showed that a significant amount of KCl, in addition to NaCl, was present. In order to determine the source of the KCl and also to look into the chemical behavior of KCl during the combustion of charcoal, all samples collected from these two experiments were also analyzed for potassium. The material balances for potassium in both SL-4 and SL-5 are given in Table 30.

Table 30 shows significantly different potassium contents in two different samples of the activated coconut charcoal. They were obtained from analyses of two 20-g charcoal samples collected from the same bottle of sample. The great variation observed in potassium concentrations in the charcoal samples indicates the nonhomogeneity of the charcoal (-8 +12 mesh) used in these experiments.

Table 30. Material Balance of Potassium from Combustion of Activated Coconut Charcoal Impregnated with 0.5 wt % NaCl. Combustion was at 900°C and atmospheric pressure.

	Potassium, mg[a]	
	SL-4	SL-5
Input		
(1) In charcoal (one analysis for each of two 20-g samples)	130;171	130;171
Output[b]		
(2) Collected on Cold Trap	13 (12%)	2 (2%)
(3) Captured by Al_2O_3 Filter		
(a) Water Leaching Solution	c	1
(b) Acid Leaching Solution	c	12
		13 (12%)
(4) Retained in Ash Residue		
(a) Water Leaching Solution	75	77
(b) Acid Dissolution of Ash	13	16
	88 (78%)	93 (85%)
(5) Collected by Downstream Filter	11 (10%)	1 (1%)
Total	112	109

[a] Obtained by an atomic absorption method; estimated precision is ±5%. Analysis by Ralph Bane.

[b] A separate 20 g sample of charcoal was combusted in each experiment.

[c] No Al_2O_3 filter was used.

To obtain a more homogeneous sample, the particle size must be reduced. The activated coconut charcoal is a product of MCB (Metheson Coleman & Bell Manufacturing Chemists), Norwood, Ohio. The information provided by MCB indicates that the potassium is an inherent element in the charcoal. The exact compound form in which the potassium exists in the charcoal is not known; however, X-ray diffraction results showed that potassium was present as chloride vapor in the combustion gas.

As for the material balances of sodium (Table 29), the reproducibility obtained for the material balances for potassium was good (Table 30). Table 30 also shows a possible loss of potassium in the combustor system, which needs to be further investigated. Despite this, it is noticeable that the material balances of potassium are very similar to those of sodium insofar as the distribution of potassium in the various "Output" categories is concerned. This similarity shows that the chemical behavior of KCl during combustion is similar to that of NaCl. The potassium captured by the Al_2O_3 filter was essentially in compound forms not soluble in distilled water but soluble in 5% HCl solution. This indicates that the Al_2O_3 filter material reacts with KCl similarly to the way it reacts with NaCl, probably forming potassium alumina silicates.

As mentioned above, the Al_2O_3 filter shows high reactivity with the KCl and NaCl vapors under the experimental conditions. This suggests that solid material with a chemical composition similar to that of the Al_2O_3 filter would be a good solid sorbent for removing alkali compounds from hot combustion gas of coal. However, in this study, the material removed in this Al_2O_3 filter consists not only of particulates but also of most of the NaCl vapor (and probably other alkali compounds too); as a consequence, with the Al_2O_3 filter in place, the quantity of condensation collected by the cold trap is hardly enough for analysis. A filter that captures only particulates from flue gas must be fabricated from another type of filter material.

c. Lignite Combustion Experiments

Experimental results so far obtained for the combustion of Illinois Herrin No. 6 coal (Tables 27 and 28) and of activated coconut charcoal (Tables 29 and 30) have shown that vaporization of alkali metals during combustion is related to the ash content of the coal. In order to investigate this relationship and the transport behavior of the alkali metals from the combustion of low-rank coal, this study has been extended to the burning of lignite from the Glen-harold seam of North Dakota. The proximate analysis on a dry basis of this lignite is 38.93% volatile matter, 52.97% fixed carbon, and 8.10% ash. Lignite with a particle size range of -20 +40 mesh was used in this study. It was dried at 110°C in a nitrogen flow before being combusted.

Three series of experiments were completed. In all of these experiments, lignite was combusted with air at a flow rate of 3.5 L/min. Each series of experiments consisted of five batch combustion runs, and in each run 50 g of dry lignite was burned. In two of the three series of experiments (SL-6 and SL-8), lignite was impregnated with 0.5% by weight NaCl, using water solution to increase the chlorine content of the lignite and thereby simulating high-chlorine coal. To allow comparison, plain lignite was burned in the third series of experiments (series SL-9). The material balances for sodium for these experiments are tabulated in Table 31.

Table 31. Material Balance of Sodium from Combustion of Glen-harold Lignite, North Dakota

Lignite was combusted in air at atmospheric pressure.

Experimental Series	SL-8	SL-6	SL-9
Combustion Temp, °C	850	900	900
Amount of Coal Combusted, g	250	250	250
Amount of NaCl added, g	1.25	1.25	None
Input per Series of Experiments	Sodium, mg[a]		
(1) In Lignite	1670	1670	1670
(2) Added as NaCl	490	490	--
Total:	2160	2610	1670
Output per Series of Experiments			
(3) Left in Ash Residue			
(a) Water Leaching Solution	1180	1020	910
(b) Acid Dissolution of Ash	730	850	690
	1910	1870	1600
(4) Collected on Cold Trap	57	71	N.A.[b]
(5) Captured by Downstream Filter	30	26	N.A.
Total:	1997	1967	
(6) Lost	163	193	
(7) Total Vaporized [(4)+(5)+(6)]	250 (11.5%)	290 (13.5%)	70 (4.2%

[a] Obtained by an atomic absorption method; estimated precision is ±5%; done by Ralph Bane.

[b] Not determined due to tar and soot condensation.

In series SL-6 and SL-8, combustion of lignite was complete, and substantial amounts of condensates were collected on the cold trap finger and in the downstream filter; however, in Series SL-9, in which lignite had not been impregnated with NaCl solution, significant amounts of tar and soot were condensed on the cold trap finger. For this reason, no condensates could be collected for analysis, as shown in Table 31. Condensation of tar and soot was due to incomplete combustion of volatile matter, which rapidly evolved during the early stage of combustion. Since all three series of experiments were conducted under the same operational controls during combustion, the observed tar and soot condensation in the SL-9 series indicates the effect of NaCl on the combustion characteristics of lignite.

NaCl appears to suppress the evolution of volatile matter from lignite during the early stage of combustion—possibly by blocking of the pores in lignite by NaCl.

As shown in Table 31, when untreated lignite was combusted at 900°C (series SL-9), sodium essentially remained in the ash residue, mostly in compound forms that are soluble in distilled water. Sodium has been shown to be present in lignite primarily as salts of humic acids,[40] to be uniformly distributed within lignite,[41] and not to be readily removed by washing with distilled water.[42] Apparently, the combustion results for lignite show that most of the sodium in lignite was converted to compound forms that can be readily leached out with distilled water after combustion. Among those compounds are (possibly) sodium sulfates, chlorides, simple silicates, and aluminates.

Also shown in Table 31 is the vaporization of 11.5 wt % and 13.5 wt % of the sodium, respectively, when lignite impregnated with a 0.5 wt % NaCl was combusted at 850°C (SL-8) and 900°C (SL-6). Comparison with the results for series SL-9 shows that sodium vaporized essentially from the NaCl added.

The condensates, which were primarily collected on the hemispheric surface of the cold trap finger, were gray-white. X-ray diffraction analysis of the condensate indicated that the sodium was presently mostly as NaCl and to a smaller extent as Na_2SO_4. The relative quantities of NaCl and Na_2SO_4 are being determined by wet chemistry methods and will be reported.

d. Relation of Coal Ash Content to Sodium Vaporization

Figure 86 is a plot, as a function of the percent ash in each coal, of the percent sodium vaporized from the combustion of 0.5% by wt NaCl-impregnated Herrin No. 6 coal, lignite, and coconut charcoal at 900°C. It can be seen that a fairly good linear relationship exists between the ash content of coal and the quantity of sodium vaporized during combustion. The greater the amount of mineral matter in coal, the more the NaCl is tied up in the ash and, therefore, the less NaCl is vaporized. The amount and form of mineral matter vary widely from one coal to another. Mineral matter in Illinois Herrin No. 6 coal consists of more than 50 wt % clay minerals and about 15 wt % SiO_2.[43] On the other hand, lignite is estimated to contain 20 to 40 wt % clay and SiO_2.[41] It is believed that clay minerals are responsible for tieing up the sodium in the ash. This needs to be further investigated.

Work continues on study of the transport of alkali metals from the combustion of other coals of different ranks. The effect of operating variables on the transport of alkali metals and the effectiveness of some clay minerals on the retention of alkali metals will be quantitatively evaluated. Among the operating variables are combustion temperatures, ratio of coal to additive (limestone or dolomite), and type of additive.

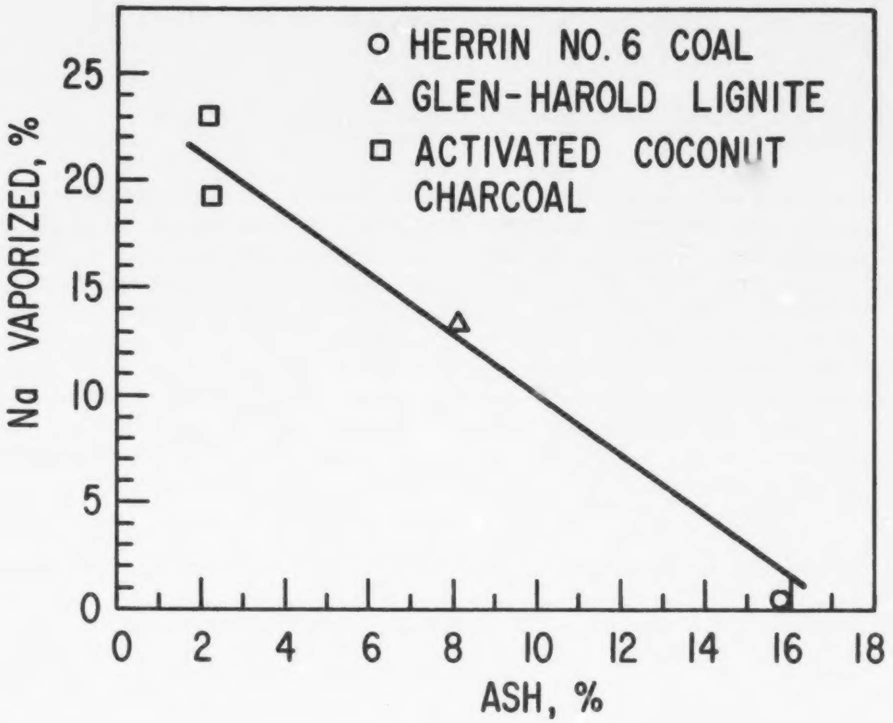

Fig. 86. Relationship between Ash Content of Coal and Sodium Vaporized during Combustion at 900°C of Coal Impregnated with 0.5% NaCl.

TASK F. FLUE-GAS CLEANING STUDIES

1. Evaluation of On-Line Light-Scattering Particle Analyzers

(J. Montagna, G. Smith, G. Teats, H. Lautermilch, and S. Smith)

In the development of pressurized fluidized-bed combustion systems, a continuous on-line particle analyzer for the flue gas would be useful (1) in measuring the efficiency of particulate-removing devices (cyclones and filters), (2) for evaluating particulate gas loading characteristics to establish gas turbine performance with different particulate loadings, and (3) to protect turbines in an industrial-size plant. In a pressurized FBC system, the flue gas will be at ∿900°C and ∿1000 kPa (∿10 atm) between the boiler and the turbine. If no on-line particle analyzer is available, routine batch sampling of the hot gas (using inertial impactors, for example) will be necessary. Batch sampling from a pressurized hot flue gas environment is difficult; another disadvantage is the long time lag between sampling and analysis of samples.

Two on-line light-scattering particle analyzers are to be evaluated in the ANL fluidized-bed combustion system under ERDA sponsorship. Both instruments use a laser light source. The experiments with the Spectron Development Laboratory (SDL) split laser beam particle morphokinetometer (PM) have been completed, and the instrument has been returned to the manufacturer. Preliminary results are reported comparing (1) measurements with the PM analyzer, (2) Coulter counter measurements of steady state samples, and (3) cascade impactor analyses. A meeting of representatives of ANL and SDL was held on January 27, 1977, to discuss the results. Final analysis of the results is being performed.

The Leeds and Northrup single laser beam analyzer was due to arrive at ANL in February 1977; however, because of final adjustments being made by Leeds and Northrup, its shipment has been delayed.

a. Principles of the SDL Particle Morphokinetometer

The particle morphokinetometer (PM) measures the sizes of particles and their velocities by measuring the light scattered from each particle as it crosses an interference pattern generated by the intersection of two laser beams. A schematic of a typical PM instrument is given in Fig. 87. The laser beams are directed radially into the flue-gas duct of the ANL PDU combustion system through specially designed windows. The region of measurement, called the PM probe volume or sample space, is at the center of the duct where the two coherent beams intersect and generate the interference pattern. The light scattered from the sample space is detected and changed to an electric signal of the type shown in Fig. 87. The light may be detected in either a forward or backward observation mode. Forward-scattered light is being detected in the ANL evaluation.

The parameter measured to determine particle velocity is the time period (see Fig. 87) of the scattered light signal.

$$\nu = \frac{\delta}{\tau} \qquad (1)$$

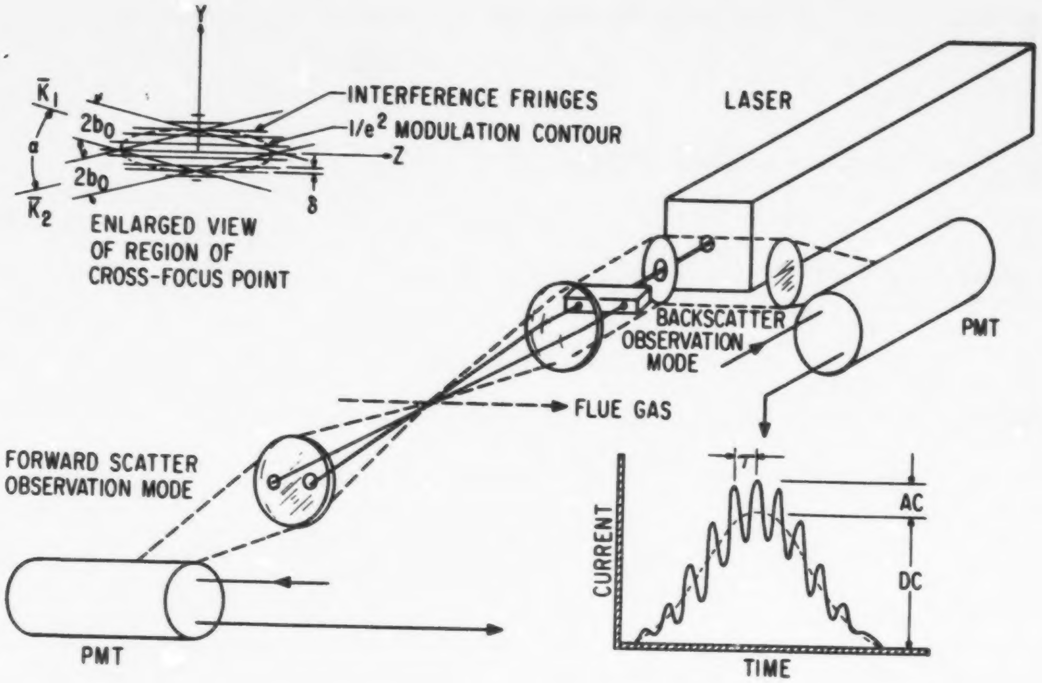
Y
$\bar{K}_1$
$2b_0$
α
$2b_0$
$\bar{K}_2$
INTERFERENCE FRINGES
$1/e^2$ MODULATION CONTOUR
Z
δ
ENLARGED VIEW OF REGION OF CROSS-FOCUS POINT
LASER
BACKSCATTER OBSERVATION MODE
PMT
FLUE GAS
FORWARD SCATTER OBSERVATION MODE
PMT
τ
AC
DC
CURRENT
TIME

Fig. 87. Spectron Development Laboratory's PM Analyzer System for Velocity and Particle Size Measurement

where

ν = particle velocity
δ = distance between fringes in the sample space (fringe period)
τ = time period of the scattered light

As the size of the scattering particle increases relative to δ (which is controlled by the intersection angle of the laser beams), the illumination of the particle becomes less uniform, and it is averaged over the cross-sectional area of the particle. Nonuniform illumination of the particle results in a reduction in the contrast or visibility of the scattered light signal. Visibility, V, is defined as:

$$V = \frac{I_{max} - I_{min}}{I_{max} + I_{min}} \qquad (2)$$

where I_{max} is the maximum value of intensity in a period of the scattered light from a particle, and I_{min} is the next successive minimum. It has been shown that V can be equivalently expressed as the ratio of the AC amplitude divided by the DC amplitude of the scattered signal (see Fig. 87).

By imposing some geometric limitations on the particles (D is the particle diameter) that will be measured in terms of the radius of the laser beams, b

$$D < 0.2\ b \tag{3}$$

and on the distance between fringes, δ

$$\delta < 0.2\ b \tag{4}$$

a simplified analytic expression of visibility, V, has been obtained for spherical particles.

$$V \simeq 2[J_1(\pi D/\delta)]/(\pi d/\delta) \tag{5}$$

where J_1 is a first order Bessel function of the first kind.

The visibility, V, for a cylindrical particle has been obtained as:

$$V \simeq \sin\ (\pi D^*/\delta)/(\pi D^*\delta) \tag{6}$$

where D^* is the length of the major axis of the cylindrical particle. Equations 5 and 6 are plotted in Fig. 88 to illustrate the features of the visibility in particle size measurement. From this plot, it is apparent that particle size cannot be unambiguously determined unless $V \geq 0.15$ for spherical particles and $V \geq 0.23$ for cylinders. This imposes an upper bound on the size of particles than can be measured for a given fringe period. The interference fringe periods and their respective detectable spherical particle size ranges that will be used in this evaluation are given in Table 32. A more detailed description of the principles of a Spectron PM analyzer is available in the literature.[44]

Table 32. Selected Interference Fringe Spacings and the Corresponding Measurable Spherical Particle Size Ranges

Fringe Period, μm	Min. Particle, Diameter, μm	Max. Particle Diameter, μm
71.4	4.9	74
22.3	1.5	23
2.94	0.2	3.1

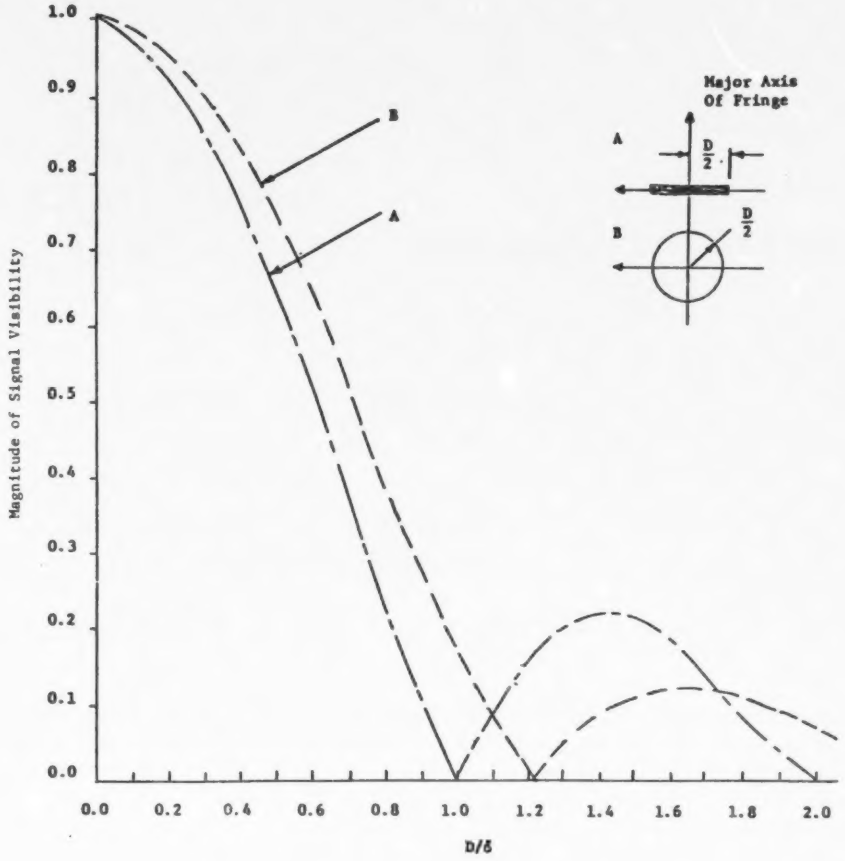

Fig. 88. Visibility as a Function of Particle Size and Fringe Period for Two Particle Shapes

b. Procedure for Comparative Flue-Gas Particle Measurements

The flue gas system in the ANL fluidized-bed combustion system (PDU system) has been modified for these evaluations, as shown in Fig. 89. Windows for particle analyzers have installed in two locations; one pair is upstream from the primary cyclone. The other windows are near the system's outlet, and there is the capability of routing the flue gas past these windows, either upstream or downstream from the metal filters. With this arrangement, the coarse entrained particles from the combustor, the smaller particles escaping the two cyclones, and the smallest particles leaving the metal filters (representative of particles that might enter turbines) were sized. Downstream from each window location, sampling ports have been installed that allow particle size analysis of representative samples with cascade impactors. Also, steady state particle samples were obtained from the cyclones and test filter.

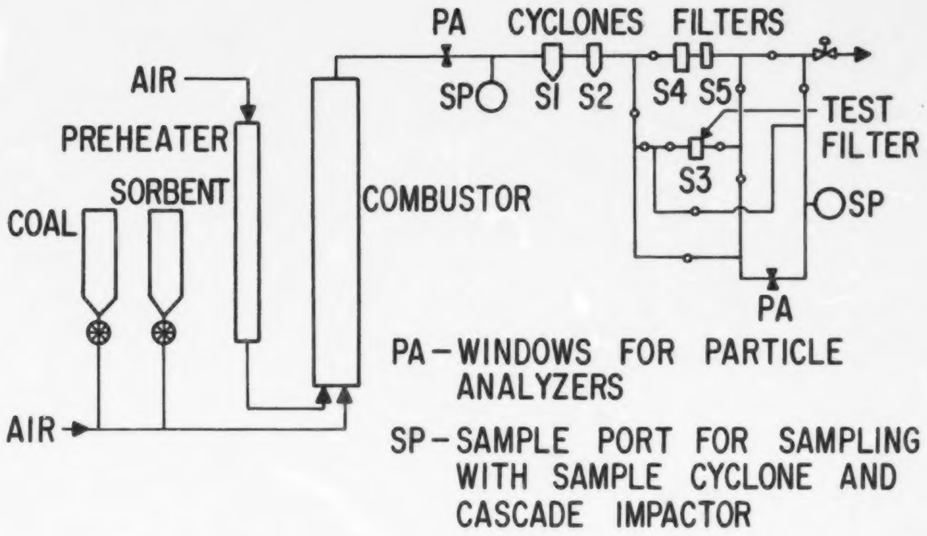
PA
CYCLONES
FILTERS
AIR
PREHEATER
SORBENT
COAL
SP
S1
S2
S4
S5
TEST FILTER
S3
SP
COMBUSTOR
PA
AIR
PA - WINDOWS FOR PARTICLE ANALYZERS
SP - SAMPLE PORT FOR SAMPLING WITH SAMPLE CYCLONE AND CASCADE IMPACTOR

Fig. 89. Schematic of FBC System with Modified Flue-Gas System

The particle size measurements were obtained (1) with the on-line Spectron PM Analyzer, (2) using an Anderson impactor, and (3) from steady state samples obtained from the cyclones and/or the test filter. The steady state samples were analyzed by sieve anlaysis and a Coulter counter. Hereafter, samples analyzed by this method are referred to as Coulter counter samples. It was assumed that all observed particles were spheres of equal density (apparent particle density, 1 g/cm^3, for Anderson impactor) and that the particles observed with the on-line instrument (PM) were identical to those that were mechanically removed from the system and later analyzed. The validity of these assumptions will be discussed in subsequent reports as more results are compared. Since the density is assumed to be constant for all particle diameters, the fractional volume and mass distributions are equivalent.

Cascade impactors are the devices used most often for obtaining airborne particle size distributions from process or ambient air in the size range, 0.3-30 μm. In this study, an Anderson cascade impactor was used to obtain combustor flue gas particle size distribution data for flue gas samples. Each stage of the impactor consists of equidiameter orifices followed by a target plate for collecting the particles. Smaller orifices are used in successive stages, and thus the size of the particles collected in successive stages becomes smaller. The particle size distributions are calculated from experimental data by relating the mass collected on each stage to the corresponding stage diameter. The impactor designs (including the design of the Anderson impactor) are based on the theoretical development of Ranz and Wong.[45]

The sampling system in the FBC system for the cascade impactor is illustrated in Fig. 90. The particle-laden flue gas flows by the optical windows (located in the line downstream from the combustor or cyclones or metal filter) where the particles are sized with a light-scattering particle analyzer (Spectron PM). Next, the off-gas is expanded to reduce the velocity to that required for isokinetic sampling by the cascade impactor. The tip of the sampling probe (0.78-cm ID) is machined to enhance aerodynamic stability near the probe entrance. The sample line is electrically heated to maintain the temperature of the gas sample above its water dew point. The cascade impactor is contained in a heated pressure shell to permit sampling from the pressurized (3 to 8 atm) combustion system. After passage of the gas sample through the impactor, its volumetric flow rate is measured with rotameter, after which the gas is depressurized. The gas velocities are based on the measured gas flows and temperatures.

c. Experimental Evaluation of the PM Particle Analyzer

Some results of particle size measurements obtained with the PM analyzer for several combustion experiments have been compared with size distributions obtained for steady state particle samples. The measurements with the laser instrument were made in the PDU combustion system's off-gas duct between the combustor and the primary cyclone, where all particles leaving the combustor were observed. Also, measurements between the secondary cyclone and the metal filters are reported.

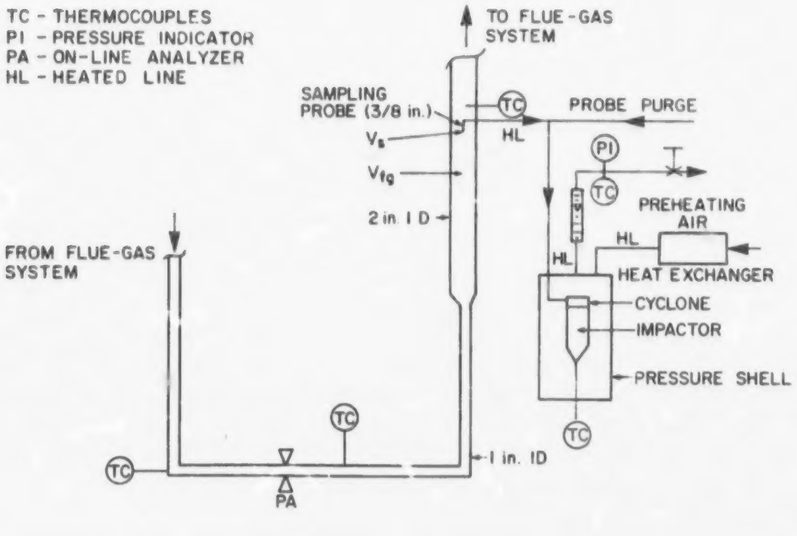
TC - THERMOCOUPLES
PI - PRESSURE INDICATOR
PA - ON-LINE ANALYZER
HL - HEATED LINE
TO FLUE-GAS SYSTEM
SAMPLING PROBE (3/8 in.)
V_s
V_{fg}
2 in. I D
FROM FLUE-GAS SYSTEM
TC
PROBE PURGE
HL
PI
TC
PREHEATING AIR
HL
HL
HEAT EXCHANGER
CYCLONE
IMPACTOR
PRESSURE SHELL
TC
TC
TC
1 in. ID
PA

Fig. 90. Sampling System for Flue Gas Particles

The conditions for the first combustion experiment (SGL-1) for this evaluation are given in Table 33. In this experiment, the distribution of particles leaving the combustor was measured. This experiment was performed in two one-day segments. Two fringe periods were used on Spectron's PM analyzer in the reported experiment, 71.4 μm and 22.3 μm, on separate day segments of this experiment. With a fringe period of 71.4 μm, the measurable spherical particle diameter range is ∿5-74 μm, and with a fringe period of 22.3 μm, the range is ∿1.5-23 μm. In this experiment, Sewickley coal was combusted in a fluidized bed of Greer limestone at 805°C, and the measured particles consisted of limestone fragments, coal ash, and unburned coal.

Table 33. Experimental Conditions for a Combustion Experiment in the Evaluation of the SDL Particle Morphokinetometer (PM)

Location of PM Windows: Between PDU combustor and cyclones, SGL-1.
Between second cyclone and filter, SGL-2C.
Sorbent: Greer limestone Coal: Sewickley
System Pressure, kPa: 308 (3 atm)
Fluidizing Gas Velocity, m/s: 1.0

		Conditions at PM Windows		Conditions Near Probe at Sampling Duct		
Exp	Combustor Temp, °C	Gas Velocity, m/s	Temp, °C	Gas Velocity V_{fg}, m/s	Temp, °C	Ratio of Duct Velocity to Probe Gas Velocity, V_{fg}/V_s
SGL-1	850	5.2	350	-	-	-
SGL-2C	855	11.76	123	3.26	110	0.99

In the first comparison, only the mass distributions inside each measurable particle size range (1.5-23 μm and 5-74 μm) of the Spectron PM analyzer were compared with the corresponding distributions obtained with the Coulter counter. Comparisons of the partial cumulative mass distributions by the two methods for the small (1.5-23 μm) and the large (5-74 μm) PM size ranges are given in Figs. 91 and 92, respectively. The mass mean particle diameter obtained was 8.5 μm with the Coulter counter and 20 μm with the PM analyzer for the small particle size range. For the large particle size range, the mass means of the partial distribution were found to be 26 μm with the Coulter counter and 70 μm with the PM analyzer. From these early results, it is apparent that the difference between the two measurements is greater for larger particles. Some reasons for the difference are given below:

a. The mass loading downstream from the combustor was ∿14 grains/scfm (20 grains/acf), which is quite high. Thus, the chance that there would be more than one particle in the sample space of the PM analyzer was high. Over 98% of the signals

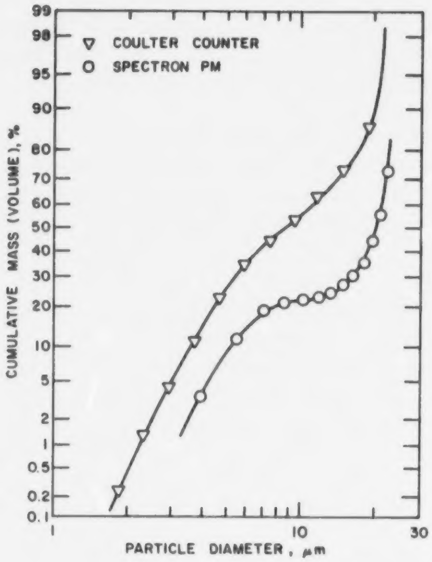

Fig. 91. Partial (1.5-23 μm) Cumulative Mass Distribution Obtained On-Line with the Spectron PM Analyzer Compared with that Obtained with a Coulter Counter (SGL-1)

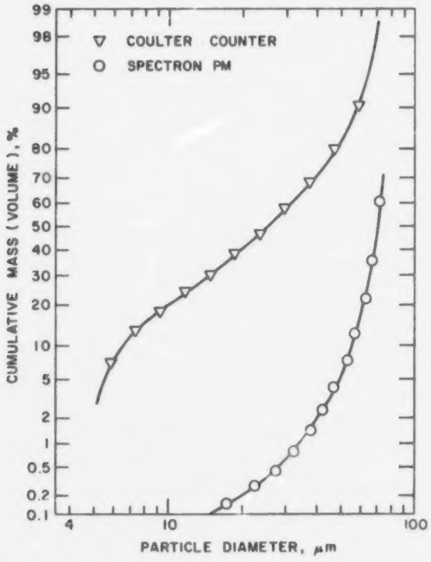

Fig. 92. Partial (5-74 μm) Cumulative Mass Distribution Obtained On-Line with the Spectron PM Analyzer Compared with that Obtained with a Coulter Counter (SGL-1)

were rejected by the PM analyzer because of particle coincidence interference. (Signal rejection rates between 97 and 90% are considered acceptable by Spectron.)

b. The assumption that the measured particles are spherical would bias the PM measurements towards large diameters if the particles are actually nonspherical; the bias would become more pronounced for large measured particles (see Fig. 89).

c. The fragile particles might have broken up as the particle samples were collected in the cyclones and test filter and as they were prepared for Coulter counter analysis (dispersed in an electrolyte). This effect could impose a bias towards small diameters in the Coulter counter measurements.

These possible sources of the discrepancies in the two particle measurements will be discussed in a subsequent report upon completion of this evaluation.

The total particle distribution leaving the combustor, in combustion experiment SGL-1, was characterized. The fractional mass distribution of all particles between 1 μm and 1000 μm was obtained by combining Coulter counter measurements and sieve analyses. They are presented in Fig. 93. The elutriated-particle distribution is trimodal, with peaks at 750 μm (elutriated sorbent), 70 μm, and 6.4 μm. A similar distribution was obtained by combining the measurements made with the Spectron PM analyzer with sieve analysis; it also is presented in Fig. 93. This distribution is also trimodal, but the mass contributions of the small-diameter fractions are much smaller because of the possible measurement biases discussed above. The cumulative mass distributions obtained from these fractional distributions are compared in Fig. 94. The mass mean obtained with the Coulter counter and sieve analysis was 54 μm, and the one obtained with the PM analyzer and sieve analysis was 58 μm.

On-line particle analyzers are intended to be used downstream from FBC particle removal devices to monitor particle distributions and loading in the flue gas entering gas turbines. The results obtained in this first experiment, in which there were large (∿14 grains/scf) particle loadings (upstream from particle-removal devices), are not representative of those at a turbine inlet. It is encouraging that the characteristics of the fractional distributions obtained by the two different methods were the same and that the discrepancy between the two measurements (PM *vs* Coulter counter) became smaller for smaller particles (<20 μm). The smaller particles <10 μm and >1 μm are expected to erode turbine blades.

The conditions for combustion experiment SGL-2C in which the sizes of particles between the secondary cyclone and metal filters of the PDU combustion system were measured are given in Table 33. In this experiment, Sewickley coal was combusted in a fluidized bed of Greer limestone at 855°C, and the measured particles consisted of limestone fragments, coal ash, and unburned coal. Particles with diameters between 1.5 and 23.8 μm were sized with the Spectron PM.

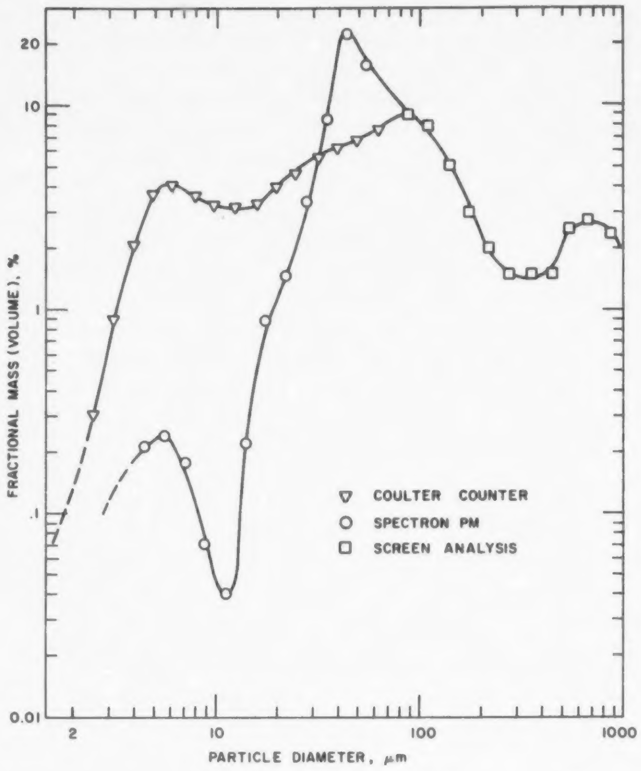

Fig. 93. Fractional Mass Distribution of All Elutriated Particles from the ANL PDU Combustor During a Combustion Experiment (SGL-1)

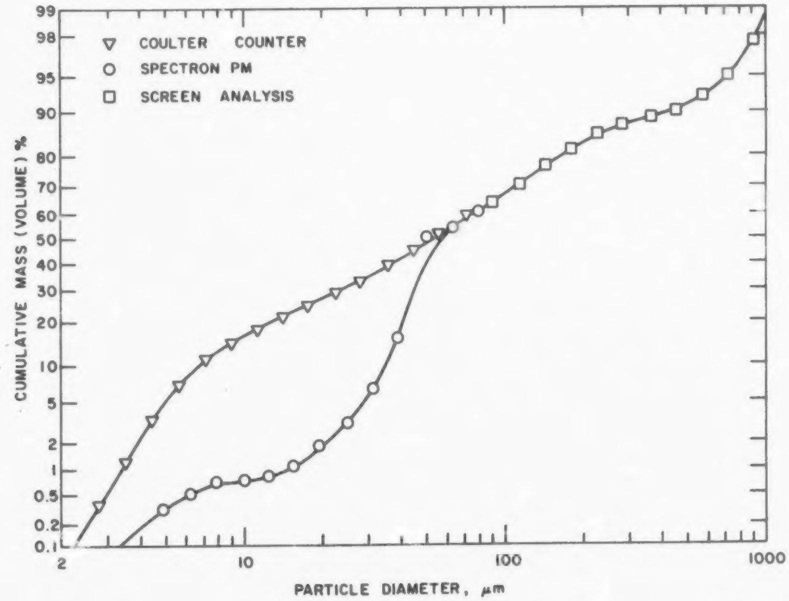

Fig. 94. Cumulative Mass Distribution of All Elutriated Particles from the ANL PDU Combustor During a Combustion Experiment (SGL-1)

In the first comparison, only that part of the mass distribution within the measurable size range of the Spectron PM analyzer was compared with the corresponding distribution obtained with the Coulter counter. Particles outside the Spectron PM range were ignored. The resulting partial cumulative mass distributions for particles contained in the flue gas exiting from the secondary cyclone are given in Fig. 95. The mass means of these distributions are 3.5 μm (Coulter counter) and 17 μm (Spectron PM). In the distribution obtained with the Spectron PM, the particle mass population increases sharply above 15 μm. Since at this point, the flue gas has passed through two cyclones, most particles larger than 10 μm should have been removed. Hence, the distribution obtained by Coulter counter analysis appears to be more representative. The total (0.5 μm-100 μm) fractional mass distribution obtained with the Coulter counter of the solids in the flue gas downstream from the secondary cyclone is given in Fig. 96. The largest mass fraction was found to be between 3.0 and 3.8 μm (3.38 μm, geometric mean), which contained 22.5 wt % of the total (0.2 grains/scf) particulate mass loading.

The total cumulative mass distributions obtained for two consecutive measurements of suspended particles from SGL-2 with the Anderson cascade impactor are given in Fig. 97. Aerodynamic mass mean diameters of 2.7 μm and 3.0 μm were obtained, with the assumption that the apparent density of all particles was 1.0 g/cm^3. (The measured apparent density of sulfated dolomite is ∿1.9 g/cm^3, and literature values for devolatilized coal and coal ash are ∿0.6-0.9 g/cm^3.) The sampling conditions for the Anderson impactor samples are given in Table 33. The ratio of duct velocity to inlet sample probe velocity was 0.99, indicative of isokinetic conditions.

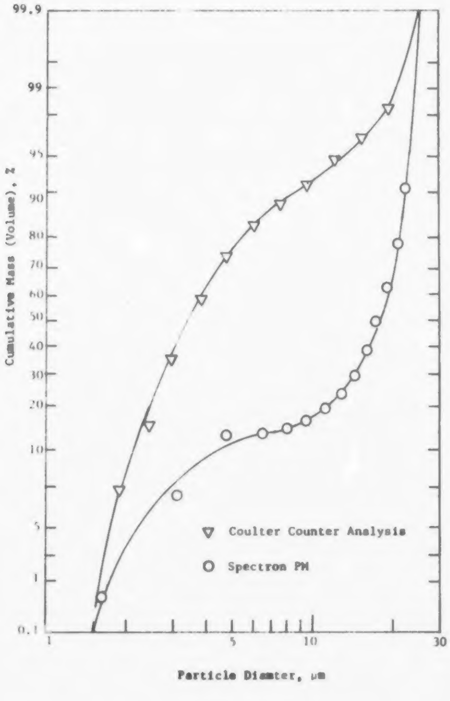

Fig. 95. Comparison of the Partial (1.5-23.9 μm) Cumulative Distribution Obtained On-Line with the Spectron PM Analyzer with that Obtained by Coulter Counter Analysis of a Particle Sample (SGL-2C)

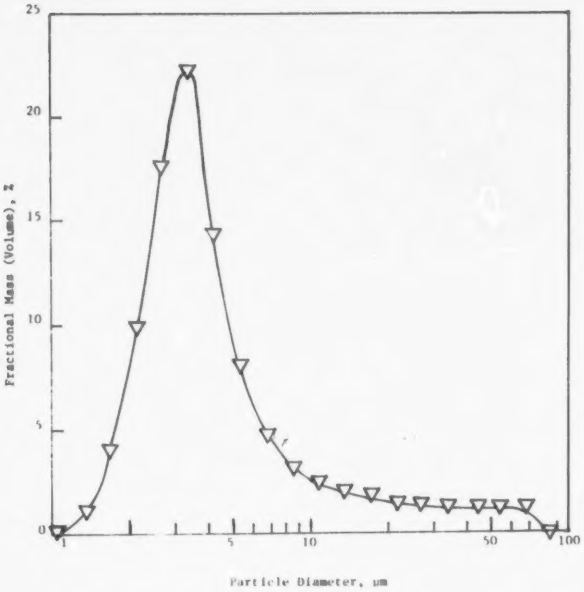

Fig. 96. Fraction Mass Distribution of Particles Contained in the Flue Gas Between the Secondary Cyclone and the Filter (SGL-2C) Obtained by Coulter Counter Analysis

The total cumulative mass distribution obtained with the Coulter counter is also given in Fig. 97. The mass mean diameter was found to be 3.5 µm, which compares favorably with the distribution means obtained with the Anderson cascade impactor.

From the above results, it appears that the Spectron PM analyzer with originally supplied calibration is biased towards large diameters.

d. The Effect of the PM Particle Analyzer Calibration on Particle Measurements

A discussion by ANL and SDL representatives disclosed two possible effects that would lead to bias in the PM measurements:

a. Large particles could block the response of the electronics to small particles at relatively high particulate loadings.

b. The original calibration for spherical particles, which was obtained with low number densities of mists and aerosols by microscopic measurements, is greatly influenced by particle shape and orientation in the sample space.

Because of the difficulties in evaluating these and other effects, an empirical correlation of the experimental data was used to obtain a best fit for the calibration curve. In this analysis, it was assumed that the Coulter counter and inertial impaction measurements were correct. The particle distribution measurements obtained with the Coulter counter and cascade impactor were expressed as histograms with intervals equivalent to the PM analyzer increments. The diameter-dependent factor necessary to force the fractional contributions of the histogram intervals from the PM analyzer into agreement with those from the Coulter counter and impactor measurements was

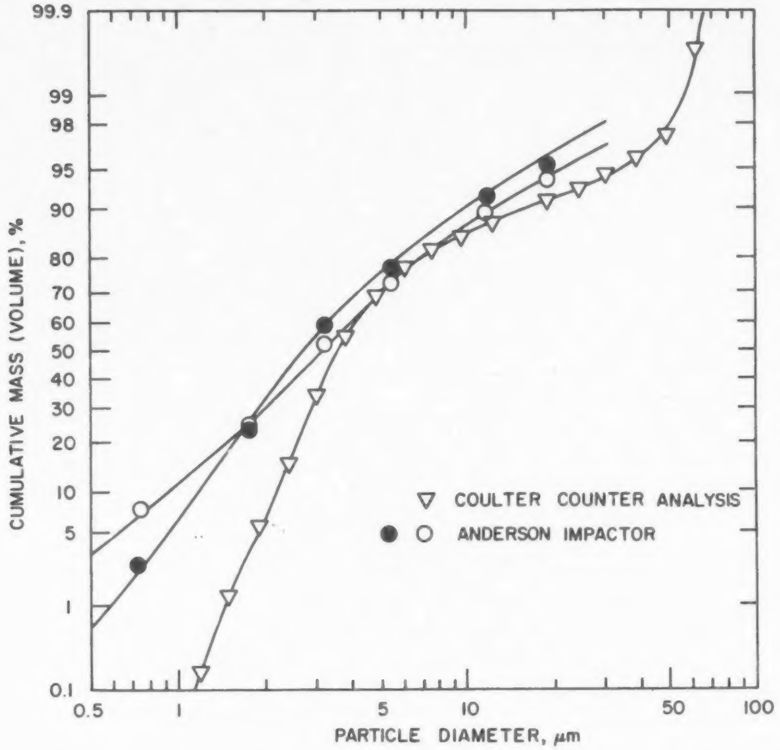

Fig. 97. Cumulative Mass Distribution of Particles in the Flue Gas Between the Secondary Cyclone and the Metal Filter (SGL-2C)

obtained. The ratios of the fractional contributions obtained from the Coulter counter and impactor measurements to those obtained from the PM analyzer for a considerable number of measurements were correlated with the reduced diameter of the interval, D/δ. (D is the particle diameter and δ is the fringe period of the laser probe volume.) By use of least squares techniques, the following correlation was obtained:

$$\ln (K) = -4.91 \ln\left(\frac{D}{\delta}\right) - 2.5 \left[\ln \left(\frac{D}{\delta}\right)\right]^2 \qquad (7)$$

where K is the ratio of the expected mass concentration in the diameter interval to the measured number of particles within the PM interval. This correlation gives a fair fit (a correlation coefficient of ∿0.88) for the relationship between K and the reduced diameter, D/δ.

The previously discussed experiments (SGL-1 and SGL-2C, see Table 33) were reanalyzed using this empirical calibration.

The measurements from these experiments were adjusted using the calibration function (Eq. 7). The resulting truncated distributions (actual particle distributions were wider than the range of the analyzer) are compared with the corresponding truncated distributions obtained by Coulter analysis in Figs. 98 and 99. These figures also contain the previously reported distributions which were based on Spectron's originally supplied calibration function,

$$K \propto 1/D \qquad (8)$$

The mass means of the truncated particle size distribution were calculated to be 26 μm (using the Coulter counter measurement) and 47 μm (with the PM analyzer) for the large PM particle size range. (A 70-μm mass mean was previously obtained with the PM analyzer using the Spectron supplied calibration.) For the small PM particle size range, the Coulter counter analysis produced a mass mean of 8.5 μm; that from the PM analyzer was 5.2 μm.

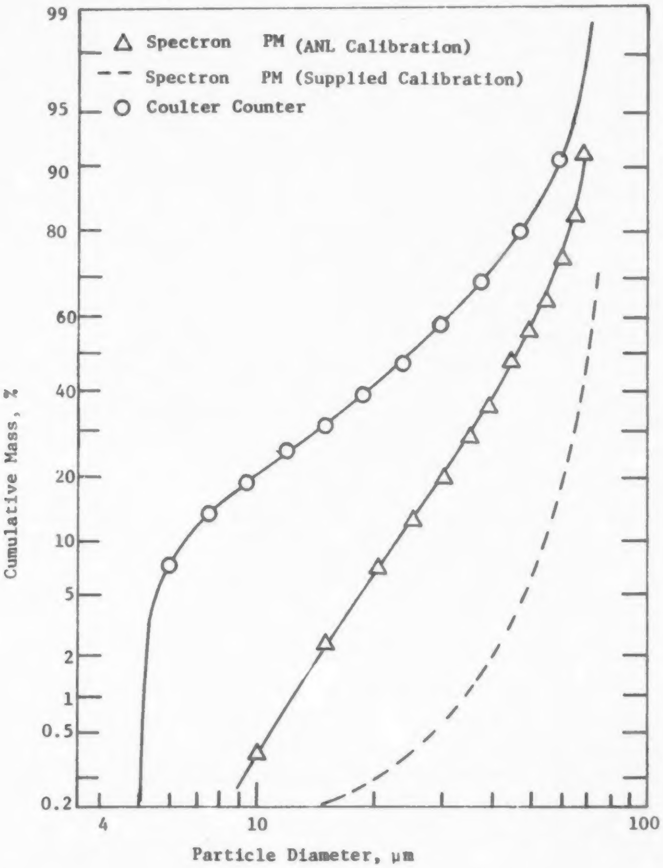

Fig. 98. Comparison of the Partial (5-73 μm) Cumulative Mass Distribution Obtained On-Line with the Spectron PM Analyzer with that Obtained with a Coulter Counter (SGL-1)

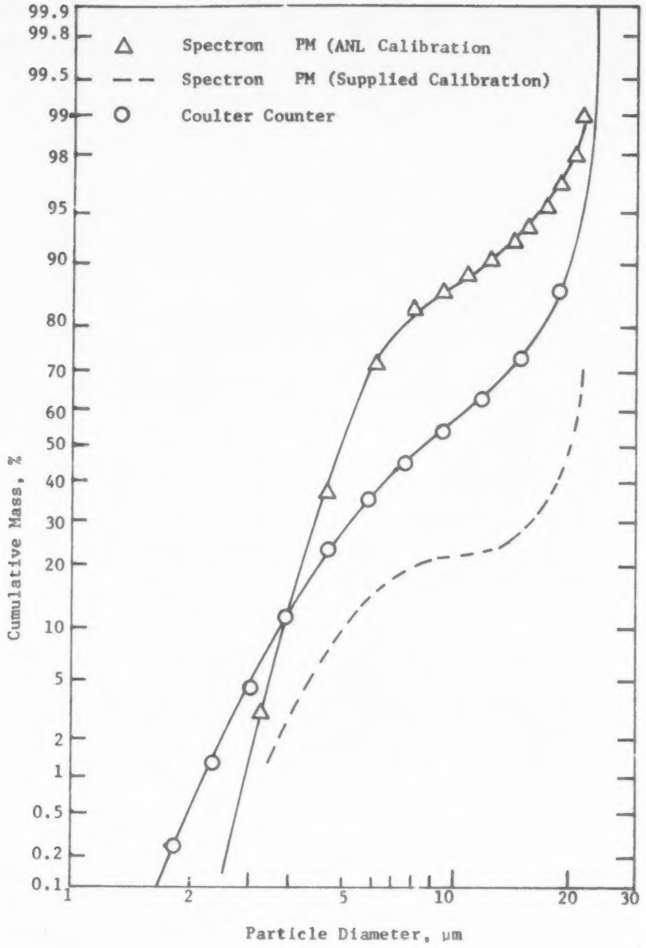

Fig. 99. Comparison of the Partial (1.5-23 μm) Cumulative Mass Distribution Obtained On-Line with the Spectron PM Analyzer with that Obtained with a Coulter Counter (SGL-1)

The results of experiment SGL-2C, in which the particle measurements were performed on material upstream from the final filters, are presented in Fig. 100. A fringe period of 23.0 μm was set in the PM analyzer, which corresponds to the approximate size range 1.5-23.8 μm. The mass mean particle diameter obtained by the PM analyzer was 8.8 μm and that by the Coulter counter was 3.5 μm.

Although these adjusted analyses continue to show some deviation between the different measuring techniques, the agreement between the measurements has improved considerably. Further analysis of the remaining experiments is being performed which will help determine the usefulness of the experimentally obtained calibration. Included in the experiments to be reported

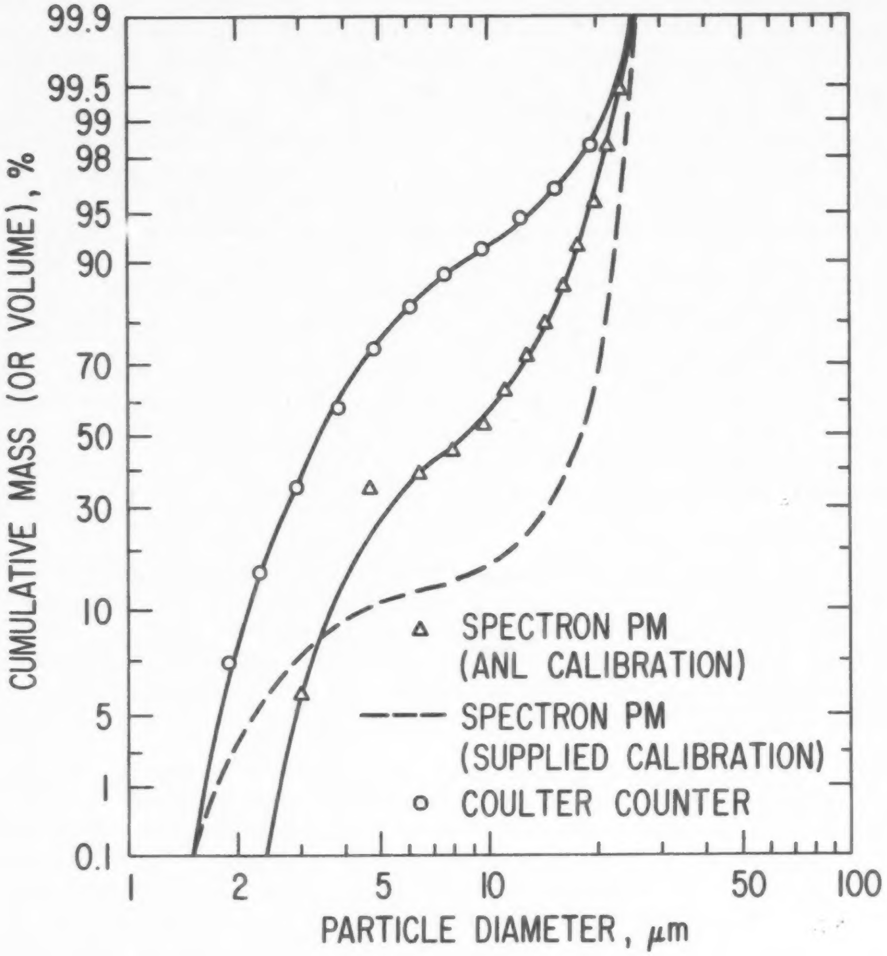

Fig. 100. Comparison of the Partial (1.5-23.8 μm) Cumulative Mass Distribution Obtained On-Line with the Spectron PM Analyzer to that Obtained by Coulter Counter Analysis of a Particle Sample (SGL-2C)

are measurements made on suspended virgin limestone particles which were generated by fluidizing a bed of virgin Greer limestone in the 6-in.-dia combustor (no coal was combusted). These experiments were performed to evaluate the effect of different particle densities and chemical compositions on the measurements of suspended particles in the off-gas from combustion experiments.

2. Particle Removal From Flue Gas

(W. Swift, G. Teats, S. Smith, and H. Lautermilch)

In pressurized fluidized-bed combustion, the hot flue gas from the combustor must be expanded through a gas turbine. To prevent erosion of the turbine blades by particulate matter entrained in the flue gas, the particulate loading must be reduced to acceptably low levels. What constitutes "acceptably low levels" of particulate loading for a gas entering a gas turbine is, however, still not fully understood. Estimates of acceptable loadings range from 0.05 to 0.0005 g/m^3 (0.02 to 0.0002 grain/scf). If it is assumed that the loading in the flue gas as it leaves the combustor is ∿50 g/m^3 the particle removal efficiency required to meet the estimated allowable loadings for the turbine would be between 99.9 and 99.999%.

The critical factor in defining an acceptable loading for gas turbines is the particulate size distribution. Obviously, the finer the particles entering the gas turbine, the higher the permissible mass loading. Westinghouse, for example, has estimated an acceptable loading of 0.002 grain/scf (∿0.005 g/m^3) provided that ∿80% wt % of the particulate is smaller than 10 μm in diameter and that ∿40 wt % is smaller than 2 μm. If 100 wt % of the particulate is smaller than 10 μm and ∿40 wt % is smaller than 2 μm, Westinghouse estimates the tolerable particulate loading to be ∿0.03 grain/scf (∿0.07 g/m^3).[46]

Existing devices readily adaptable to high-temperature, high-pressure particulate removal (*e.g.*, conventional cyclones) are not very efficient. in removing particulate matter with diameters smaller than ∿10 μm. Achieving the "acceptable loading" necessary for PFBC requires. therefore, the development of highly efficient methods for removing from flue gas the particulate solids having diameters between 2 and 10 μm.

Prior to our undertaking an experimental program on removing small (<10 μm) particles from a flue gas, a literature survey was made of the existing technology. The history of particulate agglomeration and separation at high temperatures and pressures was examined, with particular emphasis on the unique features of the direct-cycle application of fluidized-bed combustion. The basic long-range mechanisms of aerosol separation were examined, and the effect of high temperature and high pressure upon usable collection techniques was assessed. Primary emphasis was placed on those avenues that are not currently attracting widespread research. This survey is being published as a separate report.[47]

An experimental program is under way at ANL to test and evaluate promising flue gas cleaning methods in the off-gas system of the 6-in.-dia fluidized-bed combustor. Two techniques which have been identified for investigation are acoustic agglomeration and granular-bed filtration. A third approach, the use of high-efficiency, controlled-vortex cyclones, is also being considered; installation and testing are planned. The high-efficiency cyclone, in addition to being independently evaluated, would be used in measuring the effectiveness of (upstream) acoustic flue gas conditioning for increasing the removal of fine particulate matter from the flue gas.

a. Granular-Bed Filter

Granular-bed filters currently under development can be generally classified by the condition of the granular bed during filtration as fixed-bed moving-bed, or fluidized-bed collectors. The concept of collection to be investigated at ANL is the use of fresh or sulfated limestone or dolomite as granular-bed material in a fixed-bed collector with periodic bed replacement. Use of sorbent from the combustion process as the collection medium has the advantage of eliminating the need to "backflush" the filter to remove the ash material that has been trapped during the forward filtration cycle. As is done with fixed granular beds employing backflush cleaning, several granular bed modules would be operated in parallel. Periodically, each module would be taken off line, and sorbent plus trapped particulate matter would be replaced with fresh bed material. The sorbent containing the trapped particulate matter could then be transferred either to the combustor (if fresh sorbent had been used as the filter material) or to the regenerator or disposed of (if sulfated sorbent was used as the filter material). This scheme would eliminate the need for inventorying and disposing of an additional solid material if some other material was used in the granular-bed filter.

The test filter itself is illustrated in Fig. 101. The dirty flue gas enters through the centrally located pipe in the top flange of the filter housing. Inside the housing, the gas passes downward through the granular filter chamber suspended from the top flange of the filter housing. The filter chamber is circular in cross section and has an inside diameter which can be changed to be either 3 or 6 in. The fixed, horizontal granular-bed filter at the lower end of the filter chamber is supported by a wire mesh screen over a perforated plate. After the gas passes through the granular bed, the gas, now cleaned, exits through a port in the side of the granular bed filter housing. Pressure taps are located just above the top surface of the granular bed and below the support plate to measure the pressure drop across the bed. A thermocouple just below the bed support plate will monitor the gas temperature during each test.

Tymochtee dolomite has been selected for initial testing. By appropriate selection of bed cross section and bed depth during a series of runs, the particle size of the granular bed sorbent, the superficial velocity of the gas being filtered, and the ΔP of the clean bed at the start of filtration can each be varied while the other two variables are constant. The principal response variables of interest are the overall gas cleaning efficiency and the efficiency of cleaning as a function of flue gas particulate size.

Initially, testing of the granular-bed filter was carried out at ambient conditions to determine under what conditions testing of the filter in the flue gas system of the ANL combustor would be warranted. Specifically, tests were run:

1. To determine a relationship for the pressure drop of gas flowing through the sorbent in a fixed bed as a function of the mean particle diameter of the sorbent, the superficial gas velocity, and the bed depth. The tests were made with the bed material screened to -6 +14 or -14 +30 U.S. mesh.

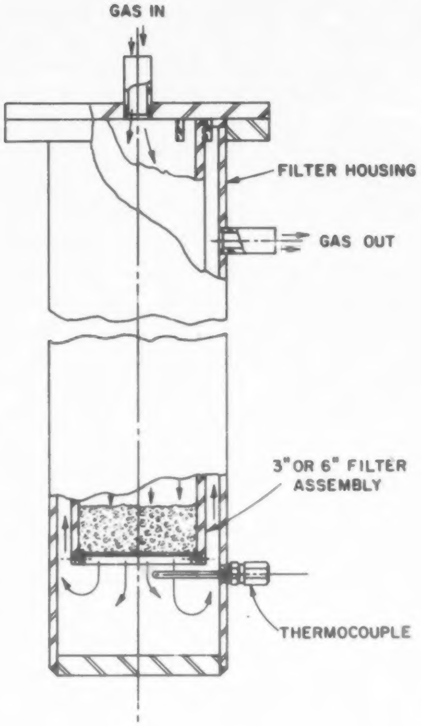

Fig. 101. Granular-Bed Filter Assembly

2. To determine any contribution of dust from the sorbent to the dust loading in the effluent gas from the filter. These tests were made to determine what treatments (such as washing) would be required if the natural dustiness of the as-screened sorbent material was found to contribute to the dust loading in the effluent gas from the filter. These tests included a comparison of unsulfated and sulfated sorbent.

It is well known that the pressure drop through a granular bed is proportional (1) to the gas velocity at low flow rates and (2) to the product of the gas density and the square of the velocity at high flow rates

$$\frac{\Delta P g_c}{L} = aU + b\rho U^2 \qquad (1)$$

where $\Delta P/L$ is the pressure drop per unit length of bed, U is the superficial gas velocity, ρ is the gas density, g_c is the gravitational constant, and a and b are constants which are functions of the granular bed geometry and gas viscosity. Dividing by the gas velocity gives a linear expression:

$$\frac{\Delta P g_c}{UL} = a + bG \qquad (2)$$

where G equals ρU, the mass velocity through the bed. According to the correlation of Ergun,[48] the factors a and b can be expressed by:

$$a = 150 \frac{(1 - \varepsilon)^2}{\varepsilon^3} \frac{\mu}{D_p^2} \tag{3}$$

$$b = 1.75 \frac{(1 - \varepsilon)}{\varepsilon^3} \frac{1}{D_p} \tag{4}$$

where ε equals the fractional void-volume in the bed, μ is the gas viscosity and D_p is the diameter of a sphere having the same specific surface area, S_v, as a bed particle. If d_p is defined as the diameter of a sphere having the same volume as that of a bed particle, D_p can be expressed by

$$D_p = \phi_s d_p \tag{5}$$

where ϕ_s represents the sphericity of the particle and is the ratio of the surface area of a sphere having the same volume as a bed particle to the surface area of the bed particle. Thus, ϕ_s is less than or equal to unity.

For nonspherical particles of a wide size distribution, a mean equivalent particle diameter, $\bar{d}_p$, can be approximated from the following relation:

$$\bar{d}_p = \frac{1}{\sum_i \frac{X_i}{d_{p_i}}} \tag{6}$$

where X_i equals the weight percent of particles with particle diameter d_{p_i}. Thus the Ergun correlation for fluid flow through packed columns can be expressed as:

$$\frac{\Delta P g_c}{L} = 150 \frac{(1 - \varepsilon)^2}{\varepsilon^3} \frac{\mu}{(\phi_s \bar{d}_p)^2} + 1.75 \frac{(1 - \varepsilon)}{\varepsilon^3} \frac{G}{(\phi_s \bar{d}_p)} \tag{7}$$

The characterization tests were made by measuring the pressure drop across the granular-bed filter as a function of mass flow through the bed at several bed levels and with two different particle size distributions (-6 +14 and -14 +30 U.S. mesh) of Tymochtee dolomite. For each experiment, the quantity $\Delta P g_c/UL$ was plotted as a function of the mass flow G. Values of a and b were then determined by a linear regression analysis of the data. Using a value for $\bar{d}_p$ calculated from screen analysis data for the two particle size distributions, the expressions for a and b (Eqs. 3 and 4) were then solved simultaneously for the parameters ε and ϕ_s.

Figures 102 and 103 are pressure drop curves obtained for -6 +14 and -14 +30 U.S. mesh Tymochtee dolomite as a function of mass flow and taken at different bed levels. Variations in the curves for a given particle size distribution at different bed levels would be expected, due to minor random

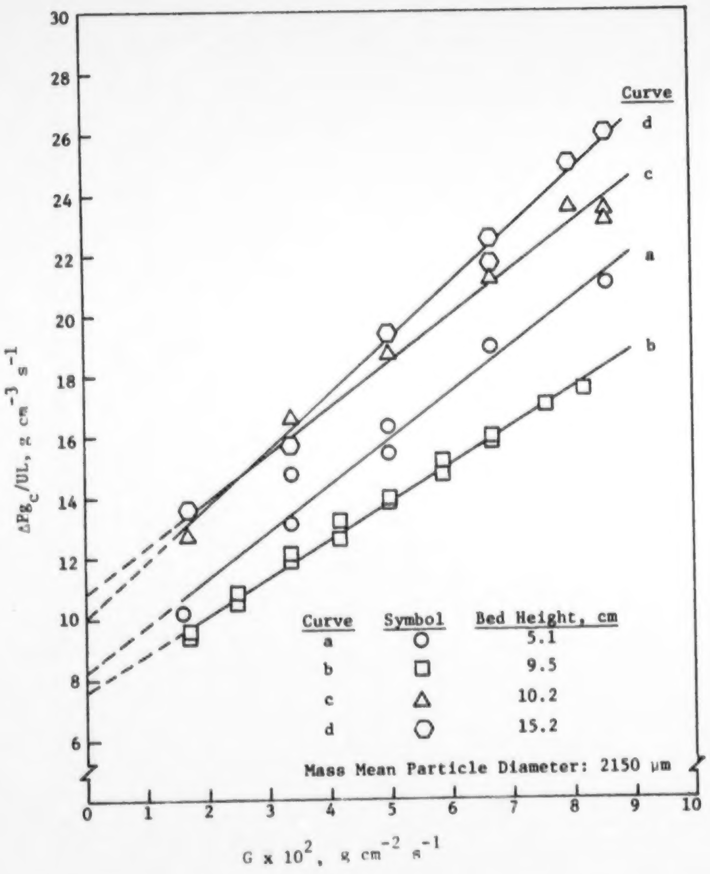

Fig. 102. Pressure Drop Across a Fixed Bed of -6 +14 Mesh Tymochtee Dolomite as a Function of Mass Flow Rate Through the Bed

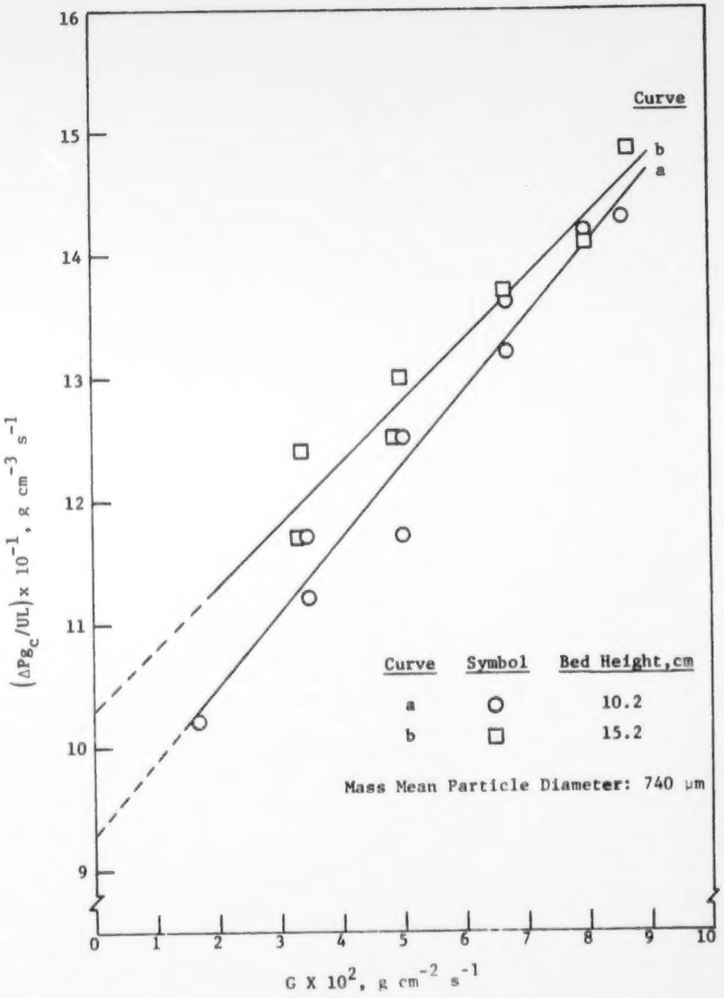

Fig. 103. Pressure Drop Across a Fixed Bed of -14 +30 Mesh Tymochtee Dolomite as a Function of Mass Flow Rate, Through the Bed

variations in ε, the fractional void volume of the bed, for each experiment. The pressure drop curves are very sensitive to this parameter (see Eq. 7).

The results of the linear regression analysis to determine the parameters, ε and ϕ_s, are presented in Table 34. For both particulate size distributions, there was considerable variation in the calculated values for both the ε and ϕ_s parameters. The variations in ϕ_s are measures of the experimental error in making the measurements.

Average values of ε and ϕ_s for the -6 +14 mesh dolomite were 0.36 and 0.78, respectively. For the -14 +30 mesh dolomite, average values of ε and ϕ_s were 0.34 and 0.78, respectively. The calculated bed voidages agree fairly well with the measured bed voidage of 0.38 for both particle size distributions based on apparent particle density (2.4 cm^{-3}) and bulk density (1.5 g cm^{-3}) measurements. The calculated value for ϕ_s of 0.78 also agrees favorably with the value of 0.8 reported by Saxena,[49] who used the Ergun correlation to correlate the incipient fluidization velocity of Tymochtee dolomite.

Table 34. Experimental Determinations of ε and ϕ_s in the Ergun Correlation for the Flow of Gas Through a Fixed Bed of Tymochtee Dolomite

Test No.	U.S. Mesh	$\bar{d}_p$, μm	Bed Height, cm	Intercept, a, g cm^{-3} s^{-1}	Slope, b, cm^{-1}	ε	ϕ_s
1	-6 +14	2150	5.1	8.23	153	0.34	0.88
2	-6 +14	2150	9.5	7.62	124	0.38	0.72
3	-6 +14	2150	10.2	10.8	152	0.38	0.63
4	-6 +14	2150	15.2	10.1	183	0.33	0.87
					Average	0.36	0.78
5	-14 +30	740	10.2	92.8	598	0.31	0.93
6	-14 +30	740	15.2	103	497	0.36	0.64
					Average	0.34	0.78

A second series of tests was performed at ambient conditions with essentially clean gas fed to the filter to measure the dust loading in the gas leaving the filter. The tests were performed using three different granular-bed materials, two bed heights, two particle size ranges, and two superficial gas velocities through the bed.

The test arrangement is illustrated in Fig. 104. The filter was charged with the material to be tested and then inserted in the filter housing in the test arrangement. Flow of compressed air to the filter and sampling of the effluent gas from the filter for the determination of entrained

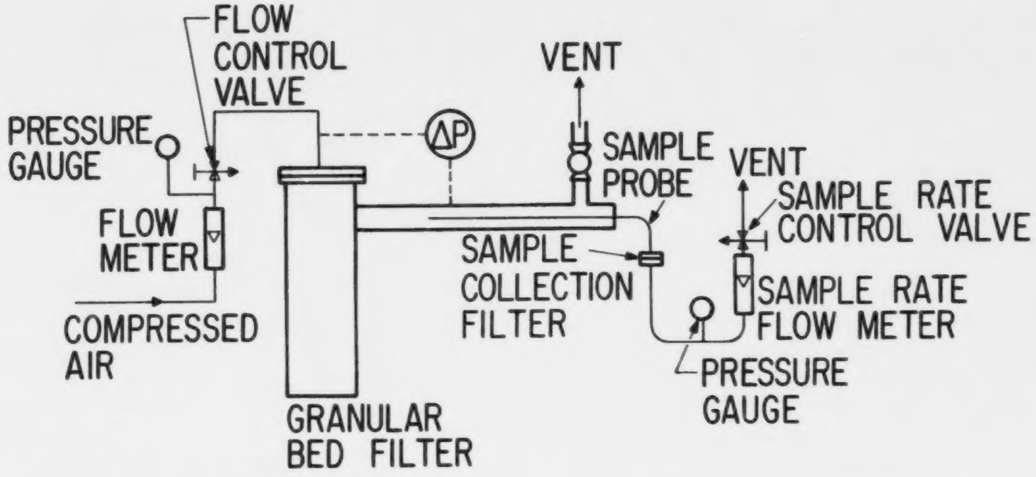

Fig. 104. Test Arrangement for the Determination of Particulate Loadings in the Effluent Gas from the Granular-Bed Filter

particulate matter were then initiated at time zero. At the conclusion of the dust sampling period, the sample collection filter was weighed and the average dust loading over the sampling period was determined.

The results of the tests are presented in Table 35. The particulate loadings in all tests were quite low, less than 0.004 g m^{-3} (<0.002 grain/scf). In tests 1 and 9, in which sampling was done during a 4-hr period, the particulate loadings were <0.0002 and 0.0007 g m^{-3}, respectively.

Test 1, made with a 5.1-cm bed of -6 +14 mesh Tymochtee dolomite and a gas velocity of 0.61 m/s, served as a baseline experiment. In subsequent tests (tests 2 and 9), changes in the baseline test conditions were made to check the possible effect on the particulate loading in the filter effluent of (1) sampling time interval, (2) bed height, (3) bed particle size, (4) gas velocity, and (5) bed material (sulfated and unsulfated). Evan at the unreasonably high bed velocity of 2.4 m/s in tests 5 and 6, the loadings were quite low (0.0037 and 0.0021 g/m^3, respectively).

Thus, these tests indicate the feasibility of using sorbent materials in fixed granular-bed filters with no necessity of washing or air classification to control fines in the screened bed material.

The granular-bed test filter has been installed in the flue gas system of the ANL PDU combustor. Testing is scheduled to begin shortly.

A schematic diagram of the granular bed test system is given in Fig. 105. The particulate-laden flue gas from the secondary cyclone of the FBC system will be directed through the granular-bed test loop once the system is operating at steady state conditions. Initially, the dirty gas in the test loop will bypass the granular bed filter and the porous metal cartridge filters for sampling in the cascade impactor sampling system

Table 35. Measured Particulate Loadings in Effluent Gas from Granular-Bed Filter when Passing a "Clean" Gas through the Filter

		Normal Test Conditions					Particulate Loading		
Test	Bed Material	U.S. Mesh	Time Interval, min	Gas Vel, m/s	Bed Height, cm	ΔP, kPa	$g\ m^{-3}$	grains/scf	Variable Tested
1	Tymochtee	-6 +14	0-240	0.61	5.1	2.24	<0.0002	0.0001	Baseline Test
2-A	Tymochtee	-6 +14	0-30	0.61	5.1	0.50	0.0002	0.0001	Loadings During 30-min Intervals Over 2-hr Sampling Period
2-B			30-60				0.0023	0.0010	
2-C			60-90				0.0007	0.0003	
2-D			90-120				0.0037	0.0003	
3	Tymochtee	-6 +14	0-30	0.61	10.2	1.00	0.0009	0.0004	Increase Bed Ht
4	Tymochtee	-14 +30	0-30	0.61	5.1	4.18	0.0021	0.0009	Decrease Bed Part. Size
5	Tymochtee	-14 +30	0-30	2.44	5.1	18.7	0.0037	0.0016	Increase Gas Velocity
6	Tymochtee	-6 +14	0-30	2.44	5.1	5.23	0.0021	0.0009	Increase Gas Velocity
7	1337 Dolomite	-14 +30	0-30	0.61	5.1	1.24	0.0016	0.0007	Different Bed Material
8	Sulfated 1337 Dolomite	-14 +30	0-30	0.61	6.4	5.85	0.0018	0.0008	Sulfated Bed Material
9	1337 Dolomite	-14 +30	0-240	0.61	5.1	1.24	0.0007	0.0003	Increase Sample Time

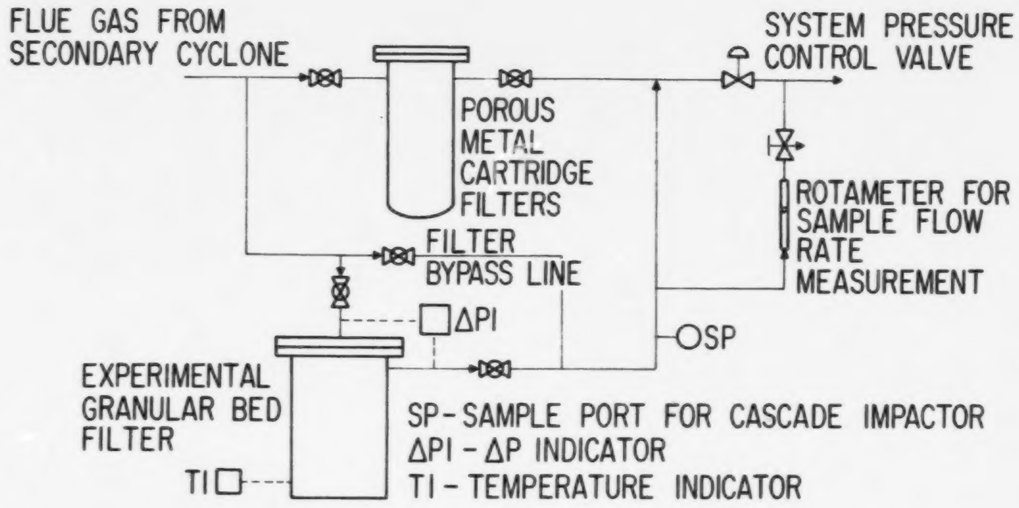
FLUE GAS FROM
SECONDARY CYCLONE
POROUS
METAL
CARTRIDGE
FILTERS
SYSTEM PRESSURE
CONTROL VALVE
ROTAMETER FOR
SAMPLE FLOW
RATE
MEASUREMENT
FILTER
BYPASS LINE
ΔPI
SP
EXPERIMENTAL
GRANULAR BED
FILTER
TI
SP - SAMPLE PORT FOR CASCADE IMPACTOR
ΔPI - ΔP INDICATOR
TI - TEMPERATURE INDICATOR

Fig. 105. Modified Flue Gas System for Granular-Bed Filter Tests

located downstream from the filter. Thereby, the particle size distribution and the mass loading of the inlet gas to the granular bed filter can be determined. To assess the efficiency of the filter as a function of particulate size and test conditions in the filter, the dust-laden gas will then be directed through the granular bed filter, with the clean effluent gas from the filter again sampled in the cascade impactor sampling system.

Variables considered for study include particle size of the granular bed sorbent, face velocity of the gas being filtered (acfm of gas being cleaned per sq ft of granular bed surface area), and bed starting ΔP (as determined by bed height). Response variables include efficiency of cleaning as a function of particulate size and the energy loss per cubic foot of gas cleaned.

b. Acoustic Agglomeration

The general objective of this agglomerating technique is to enhance the natural tendency of polydispersed particulates to impact upon each other. Thus, the use of acoustics in controlling fine particle emissions is a process whereby the mean size of the effluent particles is significantly increased (and correspondingly their number is decreased) by exposure to finite amplitude acoustic fields. As described here, sonic agglomeration is a conditioning process designed to increase the collection efficiency of downstream dust collectors.

As a result of visits made to laboratories currently investigating acoustical agglomeration of aerosols, Dr. David S. Scott, Chairman of the Department of Mechanical Engineering at the University of Toronto, Canada, has been retained as a consultant for testing and evaluating the use of acoustic agglomeration to condition the flue gas (from the ANL 6-in.-dia combustor) to increase particulate removal efficiency. Professor Scott has been investigating the fundamentals of acoustic-aerosol interactions for several years and has been a proponent of acoustic conditioning to help control industrial aerosol emissions.[50]

Discussions with Dr. Scott have led to the following understanding of acoustic-aerosol interactions and its proposed application to PFBC.

(1) The use of nondimensional groups in the description of finite-amplitude sound propagation through aerosols. Acoustic-aerosol interactions can be studied from two viewpoints. The first consideration is the effect of the particulate matter upon the sound propagating through the aerosol, and the second is the effect of the acoustic field on the particulate matter. In the latter case, the effect that is of interest is an increase in the aerosol agglomeration rate resulting from an increase in particle-particle collision frequency. In different situations, it is possible for either the sound or the particulate matter to dominate the interaction.

The important parameters in characterizing the aerosol are the momentum relaxation time and the mass loading ratio. The momentum relaxation time is essentially a fundamental description of the "type" of aerosol; the relaxation time is directly proportional to the particle density and the particle diameter squared and is inversely proportional to the gas viscosity. The mass loading ratio can be considered the "how much" parameter in the characterization of the aerosol.

The corresponding "type" and "how much" parameters which characterize the acoustic field are its frequency and its acoustic Mach number (essentially the amplitude of the acoustic wave form), respectively.

In a comparison of the "what type" parameters for the aerosol and the acoustic field, the following observations can be intuitively made. If the particle relaxation time is very short with respect to the acoustic cycle time, the particles will behave as elements of the fluid. There will be little attenuation of the acoustic field, and particle-particle collisions may not be enhanced because no significant differential motion is induced in the particulate matter. If the particle relaxation time is long with respect to the acoustic cycle time, the particles will essentially remain stationary, with no enhancement of particle-particle collisions. Thus, for enhanced coagulation of the entrained particulate matter, the optimum coupling of particle relaxation time (for particles in the size range of interest) and the reciprocal of the acoustic frequency occurs when both are of approximately the same order of magnitude.

Coupling of the "how much" parameters is equally important. If the amount of aerosol is large relative to the amount of sound, the sound is rapidly attenuated and there is insufficient energy for enhanced coagulation. If the amount of aerosol is very small relative to the amount of sound, enhanced coagulation becomes less likely due to the large interparticle distances in the aerosol.

(2) Applicability of acoustic agglomeration to the removal of fine particulate (2 to 10 μm) from high-temperature high-pressure flue gases. The conditions, mass loading, and particle-size distributions expected in the flue gases from pressurized, fluidized-bed combustors have been discussed with Dr. Scott. The relatively high loadings expected from a PFBC, coupled with a relatively low mass contribution from particulate matter below 2 μm, appear favorable to the use of acoustical conditioning of the flue gas. In work done at the Ontario Research Foundation, Mississauga, Canada, and reported by Scott,[50] a very fine aerosol (∿85 wt % below 15 μm) of ZnO dust was exposed for 2.5 s to either a 160-dB or a 165-dB acoustic field. With exposure to 160-dB sound, the mass mean diameter of the ZnO increased to ∿4 μm from ∿1 μm. At 165 dB, the mean diameter increased to ∿6 μm. When a cyclone having a poor efficiency was intentionally used downstream, the collection efficiency increased from ∿30-40% for untreated aerosol to as high as 80% for acoustically treated aerosol at the highest dust loading investigated.

(3) Capital cost and power requirements. The limited commercial application of finite-amplitude sound for agglomerating aerosols has resulted primarily from the consideration of high capital cost and high specific power requirements. Scott, however, cites (1) the potential cost advantages of progressive saw-tooth waves for acoustic agglomeration (as compared with standing-wave fields conventionally used) and (2) the advantages of pulse-jet sound generation that indicate economic feasibility in comparison with other gas cleaning systems.[50]

Dr. Scott has submitted to ANL a suggested procedure for the development of a resonant manifold system for the evaluation of acoustic dust conditioning (ADC) in the FBC system at ANL. The principal components of the proposed system are (1) pulse-jet sound generation, (2) a resonant manifold for "splitting" the resultant acoustic power, and (3) an acoustic treatment section.

There appear to be several promising features of pulse jet acoustic dust conditioning. For instance, the heat of combustion of the pulse jet fuel simply adds to the overall process heat. Furthermore, due to the elevated pressures of PFBC, the pulse jet will run at higher power levels than if it were at ambient conditions and should in principle, therefore, be a more effective sound generator.

The pulse jet will be designed to operate with a frequency of 400-500 Hz. Although flexibility in the choice of the ultimate design is being retained, a flap-valve unit utilizing gasoline as the fuel now appears most feasible.

A problem in the use of the pulse jet is that of scaling. A pulse jet, which is a quarter wave-length device, cannot be scaled up or down without changing the acoustic characteristics. A resonant manifold system is required, therefore, to split the resultant pulse-jet acoustic power and off-gas into a waste stream and one or two process streams.

A tentative schematic design for the resonant manifold system is given in Fig. 106. The manifold will be designed as a "length resonator." In this configuration, the ends of the diameter will become pressure antinodes for standing waves set up within the resonant manifold. The acoustic field will be drawn from the flat end walls.

The inlet to the vent will be a distance λ/8 (λ equals acoustic wave length) from the end wall, to minimize leakage of sound through this orifice. However, the depth to which the vent is immersed in the resonant manifold will be adjustable to control the amount of acoustic energy wasted, and thereby control the sound levels transmitted to the process sound ducts (see Fig. 106) which will carry the sound to the acoustic treatment section.

The acoustic treatment sections will be interchangeable sections of pipe of various configurations which can be installed in the PDU flue gas system between the combustor and the primary dust collector. It is in these sections that the sound and aerosol will interact and agglomeration of the aerosol will occur.

The design and development of the pulse jet, the resonant manifold, and the acoustic treatment sections will be performed by Dr. Scott at the University of Toronto. As soon as the components have been fabricated and tested for acoustic performance, they will be transported to ANL for installation and testing in the ANL flue gas system. It is anticipated that delivery of the pulse jet-resonant manifold system to ANL will be in the first quarter of 1978.

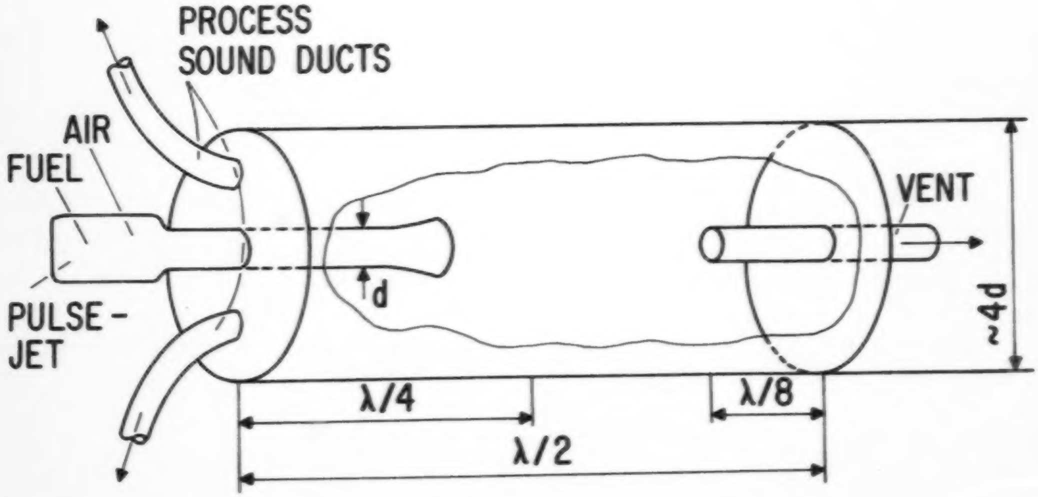

Fig. 106. Schematic of Resonant Manifold System

Notes: (a) estimate λ/2 ≅ 75 cm
(b) estimate 4d ≅ 30 cm
(c) all dimensions involving λ to be adjustable

c. High Efficiency Cyclones

The third method of particulate control being considered for investigation is the TAN-JET high-efficiency cyclone. Similar high-efficiency cyclones will also be installed with granular bed filter systems as control systems in the ANL Component Test and Integration Unit and the Curtiss-Wright PFBC pilot plant. Installation of such a unit would also be used in testing and evaluating acoustic conditioning as a pretreatment step in the control process.

The two most frequently mentioned high-efficiency cyclones for use in PFBC flue gas cleaning systems are the TAN-JET (Donaldson Co.) and the Aerodyne SV (Aerodyne Development Corporation). These devices are similar in that each employs injection of auxiliary (secondary) air to create a constant controlled vortex at the cyclone wall. Collection efficiencies of 90% for 1-μm dust for the Aerodyne cyclone and 90% for 2-μm dust for the Donaldson cyclone have been reported.

In discussions with representatives of Donaldson Co., it was determined that the TAN-JET cyclone can be adequately scaled and tested on the flue gas effluent from the ANL 6-in.-dia combustor. It is planned, therefore, to proceed with the design, procurement, and installation of a Donaldson TAN-JET cyclone as a part of the flue gas cleaning studies. This effort will proceed in parallel with design and installation of acoustic agglomeration equipment.

ACKNOWLEDGMENTS

Many people have contributed to the progress made in these studies. We gratefully acknowledge the help given by Mr. L. Burris and Mr. D. Webster in directing the program. Operation and maintenance of the PDU equipment was ably done by Messrs. H. Lautermilch, S. Smith, R. Mowry, R. Beaudry, and J. Stockbar.

We also appreciate the analytical services support given us by Dr. P. Cunningham and his associates, Messrs. R. Bane, K. Jensen, B. Tani, R. Meyer, N. Johnson, H. Goodspeed, R. Telford, W. Shinn, Ms. C. Blogg, and Ms. A. Engelkemeir.

Design and drafting services were provided by Mr. R. Stimac and Mr. R. Frank and secretarial services by Ms. M. Sobczak.

REFERENCES

1. W. F. Bischoff, Jr. and Peter Steiner, *Coal Converts SO_2 to S*, Chem. Eng., 74 (January 1975).

2. D. A. Martin, F. E. Brantley, and D. M. Yergensen, *Decomposition of Gypsum in a Fluidized-Bed Reactor*, U.S. Bureau of Mines Report of Investigation 6286 (1963).

3. T. D. Wheelock and D. R. Boyland, *Reductive Decomposition of Gypsum by Carbon Monoxide*, Ind. Eng. Chem. 52, 215 (March 1960).

4. John C. Montagna, John F. Lenc, Gerhard J. Vogel, and Albert A. Jonke, *Regeneration of Sulfated Dolomite from a Coal-Fired FBC Process by Reductive Decomposition of Calcium Sulfate in a Fluidized Bed*, Ind. Eng. Chem., Process Des. Dev. 16 (2), 230 (April 1977).

5. R. C. Hoke *et al.*, *A Regenerative Limestone Process for Fluidized-Bed Coal Combustion and Desulfurization*, EPA-650/2-74-001 (January 1974).

6. A. Skopp, J. T. Sears, and R. R. Bertrand, *Fluid Bed Studies of the Limestone Based Flue Gas Desulfurization Process*, Report No. GR-9-FGS-69, Esso Research and Engineering Company, Government Research Div., Linden, N.J. (August 1969).

7. J. S. Gordon *et al.*, *Study of the Characterization and Control of Air Pollution from a Fluidized-Bed Boiler - The SO_2 Acceptor Process*, Pope, Evans and Robbins Report, EPA-R2-72-021 (1972).

8. W. M. Swift and T. D. Wheelock, *Decomposition of Calcium Sulfate in a Two-Zone Reactor*, Ind. Eng. Chem. Process Design Develop. 14(3), 323 (1975).

9. Pope, Evans and Robbins, Inc., *Multicell Fluidized-Bed Boiler Design, Construction and Test Program*, Quarterly Program Status Report, FE-1237-Q76-2, October-December 1975.

10. Westinghouse Research Laboratories, *The Influence of Limestone Calcination on the Utilization of the Sulfur-Sorbent in Atmospheric Pressure Fluid-Bed Combustion*, Quarterly Progress Report for EPRI, 76-5E3-FBCAL-R3, August 1-October 31, 1976.

11. M. J. Gluckman, J. Yerushalmi, and A. M. Squires, *Defluidization Characteristics of Sticky or Agglomerating Beds*, Proceedings of the International Fluidization Conference, Pacific Grove, California, June 15-20, 1975.

12. J. C. Montagna, W. M. Swift, G. W. Smith, G. J. Vogel, and A. A. Jonke, *Fluidized Bed Regeneration of Sulfated Dolomite Via Reductive Decomposition with Coal*, Presented at 69th Annual AIChE Meeting in Chicago, December 1, 1976.

13. C. W. Zielke *et al.*, *Sulfur Removal During Combustion of Solid Fuels in a Fluidized Bed of Dolomite*, J. Air Pollution Contr. Assoc., 164 (March 1970).

14. M. G. Nagier, *The Theory of Recycle Processing in Chemical Engineering*, Vol. 3, International Series of Monographs on Chemical Engineering, MacMillan, New York (1964).

15. M. Hartman and R. W. Coughlin, *Reactions of Sulfur Dioxide with Limestone and the Influence of Pore Structure*, Ind. Eng. Chem. 13(3), 248 (1974).

16. G. A. Hammond and A. Skopp, *A Regeneration Limestone Process for Fluidized Bed Coal Combustion and Desulfurization*, Final Report, Esso Research and Engineering Co., Gov. Res. Div., Linden, N.J. (February 1971).

17. N. P. Phillips, *Thermodynamics Screening of Dry Metal Oxides for High Temperature SO_2 Removal*, Radian Corporation Technical Note 200-045-10-01 (September 1974).

18. R. B. Snyder, W. I. Wilson, G. J. Vogel, and A. A. Jonke, *Sulfation and Regeneration of Synthetic Additives*, Proceedings of the Fourth International Conference on Fluidized-Bed Combustion, McLean, Virginia, Dec. 9-11, 1975.

19. D. L. Keairns *et al.*, *Fluidized Bed Combustion Process Evaluation*, Annual Report, EPA-650/2-75-027-C (September 1975).

20. R. H. Borgwardt and R. D. Harvey, Environ. Sci. Technol. 6(4), 350 (1972).

21. Pope, Evans and Robbins, Inc., *Multicell Fluidized-Bed Boiler Design, Construction, and Test Program*, Combustion Systems Division, Monthly Progress Report No. 39, December 1975.

22. E. Bagdoyan, Kennedy Van Saun Corp., private communication to R. Snyder, ANL (October 1976).

22a. D. L. Graf, Amer. Miner. 37(1), 1 (1952).

23. T. Noda, J. Chem. Ind. Soc. Japan 42, 265B (1939).

24. J. Ryba *et al.*, Zb. Pr. Chemickotechnol. Fak SVST 1969-1970, 115-21 (1971).

25. J. Krajci *et al.*, Zb. Pr. Chemickotechnol. Fak SVST 1969-1970, 131-143 (1971).

26. J. A. Murray, *Summary of Fundamental Research on Lime*, National Lime Association, Washington, D.C. (1956).

27. K. P. Kacher *et al.*, Zem. Kalk-Gips 25(1), 37-41 (1972).

28. P. S. Mamykin and A. V. Ivanova, Ogneupory 36(10), 32-36 (1971).

29. D. R. Glasson, J. Appl. Chem. 17, 91-96 (1967).

30. W. R. Bandi and G. Krapf, Thermochimica Acta 146, 221-243 (1976).

31 A. E. Potter, Am. Ceram. Soc. Bull. 48, 855 (1969).

32. M. Hartman and R. W. Coughlin, Ind. Eng. Chem., Process Des. Develop. 13(3), 248-53 (1974).

33. W. T. Reid, External Corrosion and Deposits - Boiler and Gas Turbines, American Elsevier Publishing Company, N.Y., p. 140, 1971.

34. H. J. Gluskoter and O. W. Rees, *Chlorine in Illinois Coal,* Circular 372, Illinois State Geological Survey, Urbana, Illinois (1964).

35. K. E. Phillips, *Energy Conversion from Coal Utilizing CPU-400 Technology,* Quarterly Report, July-Sept., 1976, FE-1536-Q7, Combustion Power Co., Inc., California.

36. N. H. H. Small, H. Strawson, and A. Lewis, *Recent Advances in the Chemistry of Fuel Oil Ash,* Proceedings of the Conference on Mechanism of Corrosion by Fuel Impurities, Butterworths, Scientific Publications, London, p. 240, 1963.

37. P. D. Miller, H. H. Krause, J. Zupan, and W. K. Boyd, *Corrosive Effects of Various Salt Mixtures under Combustion Gas Atmospheres,* Corrosion 28(6), 222 (1972).

38. A. J. B. Cutler, W. D. Halstead, J. W. Laxton, and C. C. Stevens, *The Role of Chloride in the Corrosion Caused by Flue Gases and Their Deposits,* Trans. ASME, J. Eng. Power 93, 37 (1971).

39. P. A. Alexander, *Laboratory Studies of the Effects of Sulfates and Chlorides on the Oxidation of Superheater Alloys,* Proceedings of the Conference on Mechanism of Corrosion by Fuel Impurities, Butterworths, Scientific Publications, London, paper 40, p. 571, 1963.

40. L. E. Paulson and W. W. Fowkes, *Changes in Ash Composition of North Dakota Lignite Treated by Ion Exchange,* Bur. Mines RI 7176, 1968, 18 pp.

41 P. H. Tufte and W. Beckering, *A Proposed Mechanism for Ash Fouling Burning Northern Great Plains Lignites,* J. Power, Trans. ASME, 405 (1975).

42. G. H. Gronhovd, W. Beckering, and P. H. Tufte, *Study of Factors Affecting Ash Deposition from Lignite and Other Coals,* ASME Winter Annual Meeting, Los Angeles, Calif. Nov. 16-20, 1969, 9 pp.

43. C. P. Rao and H. J. Gluskoter, *Occurrence and Distribution of Minerals in Illinois Coals,* Illinois State Geological Survey, Circular 476 (1973).

44. W. M. Farmer, *Measurement of Particle Size, Number Density, and Velocity Using a Laser Interferometer*, Applied Optics 10, 2603 (1972).

45. W. E. Ranz and J. B. Wong, *Impaction of Dust and Smoke Particles*, Ind. Eng. Chem. 44(6), 1371 (1952).

46. D. L. Keairns *et al.*, *Fluidized Bed Combustion Process Evaluation*, Environmental Protection Agency Report No. EPA-650/2-75-027-C (1975).

47. R. Razgaitis, *An Analysis of the High Temperature Particulate Collection Problem*, Argonne National Laboratory, Argonne, Ill., ANL-77-14 (in preparation).

48. S. Ergun, *Fluid Flow through Packed Columns*, Chem. Eng. Prog. 48(2), 89 (1952).

48. S. Saxena, private communication (1977).

50 S. D. Scott, *A New Approach to the Acoustic Conditioning of Industrial Aerosol Emissions*, J. Sound Vib. 43(4), 607-618 (1975).

APPENDIX A

PHYSICAL AND CHEMICAL PROPERTIES OF COALS AND SORBENTS USED IN SORBENT REGENERATION STUDIES

Table A-1. Particle Size Distribution and Chemical and Physical Characteristics of Arkwright Coal

Sieve Analysis

U.S. Sieve No.	% on Sieve
+14	0.0
-14 +25	8.0
-25 +35	14.2
-35 +45	12.3
-45 +80	24.7
-80 +170	17.9
-170	23.0

Mean Particle Dia: 323 μm

	Proximate Analysis, wt %	
	As Received	Dry Basis
Moisture	2.89	--
Volatile Matter	38.51	39.66
Fixed Carbon	50.92	52.43
Ash	7.68	7.91
	100.00	100.00
Sulfur, wt %	2.82	2.90
Heating value, Btu/lb	13,706	14,114

	Ultimate Analysis, wt %
Carbon	77.14
Hydrogen	5.23
Sulfur	2.90
Nitrogen	1.66
Chlorine	0.19
Ash	7.91
Oxygen (by difference)	4.97

	Fusion Temperature of Ash	
	Reducing Atm, °C	Oxidizing Atm, °C
Initial deformation	1104	1160
Softening (H = W)	1177	1216
Softening (H = 1/2W)	1193	1243
Fluid	1232	1271

Table A-2. Particle Size Distribution and Chemical and Physical Characteristics of Triangle Coal

Sieve Analysis	
U.S. Sieve No.	% on Sieve
+14	0.0
-14 +25	25.0
-25 +35	22.0
-35 +45	26.0
-45 +80	24.0
-80 +170	2.0
-170	0.3

Mean Particle Dia: 576 μm

	Proximate Analysis, wt %	
	As Received	Dry Basis
Moisture	3.46	--
Volatile Matter	31.47	32.60
Fixed Carbon	55.69	57.68
Ash	9.38	9.72
	100.00	100.00
Sulfur, wt %	0.98	1.02
Heating value, Btu/lb	13,053	13,521

	Ultimate Analysis, wt %
Carbon	76.11
Hydrogen	4.99
Sulfur	1.02
Nitrogen	1.30
Chlorine	0.22
Ash	9.72
Oxygen (by difference)	6.64

	Fusion Temperature of Ash	
	Reducing Atm, °C	Oxidizing Atm, °C
Initial deformation	1383	1430
Softening (H = W)	1444	1480
Softening (H = 1/2 W)	1485	1510+
Fluid	1510+	1510+

Table A-3. Particle Size Distribution and Chemical Characteristics of Tymochtee Dolomite

Sieve Analysis

U.S. Sieve No.	% on Sieve
+14	0.4
-14 +25	48.6
-25 +35	19.9
-35 +45	18.8
-45 +80	11.7
-80 +170	0.4
-170	0.4

Average Particle Dia: 750 μm

Constituent	Chemical Analysis, wt %
Ca	20.0
Mg	11.3
CO_2	38.5
Si	2.3
Al	0.87
Fe	0.29
H_2O	0.2

Derived Composition	wt %
$CaCO_3$	50.0
$MgCO_3$	39.1

Table A-4. Chemical and Physical Characteristics of Sewickley Coal

	Proximate Analysis, wt %	
	As Rec'd	Dry Basis
Moisture	1.08	--
Ash	12.73	12.87
Volatile	39.02	39.45
Fixed Carbon	47.17	47.68
	100.00	100.00
Sulfur, wt %	4.33	4.38
Heating value, Btu/lb	13,018	13,610

	Ultimate Analysis, wt %	
	As Rec'd	Dry Basis
Moisture	1.08	--
Carbon	70.75	71.52
Hydrogen	4.93	4.98
Nitrogen	1.10	1.11
Chlorine	0.01	0.01
Sulfur	4.33	4.38
Ash	12.73	12.87
Oxygen (dif)	5.07	5.13
	100.00	100.00

	Fusion Temperature of Ash	
	Reducing Atm, °C	Oxidizing Atm, °C
Initial deformation	1115	1185
Softening (H = W)	1170	1250
Softening (H = 1/2W)	1240	1320
Fluid	1295	1360

Table A-5. Analysis of Greer Limestone, As Fed

	wt %
CaO	44.80
MgO	1.90
Fe_2O_3	0.80
SiO_2	10.50
Al_2O_3	3.60
S	0.17
Others	0.71
Loss on calcination	37.52